

Equalization, windowing and zero restoration for OFDM and single-carrier block transmission

Gert Cuypers

Supervisor:
Prof. dr. ir. M. Moonen

Dissertation presented in partial fulfillment
of the requirements for the degree of
Doctor in Engineering Science:
Electrical Engineering

October 2015

Equalization, windowing and zero restoration for OFDM and single-carrier block transmission

Gert CUYPERS

Examination committee:

Prof. em. dr. A. Bultheel, chair

Prof. dr. ir. M. Moonen, supervisor

Prof. dr. ir. B. Preneel

Prof. dr. ir. M. Steyaert

Prof. dr. ir. MS B. Nauwelaers

Dissertation presented in partial

fulfillment of the requirements for

the degree of

Doctor in Engineering Science (PhD):

Electrical Engineering

Prof. dr. ir. L. Vandendorpe

(U.C.L)

Prof. dr. ir. G Leus

(T.U. Delft)

October 2015

© 2015 KU Leuven – Faculty of Engineering Science
Uitgegeven in eigen beheer, Gert Cuypers, Kasteelpark Arenberg 10, B-3001 Heverlee (Belgium)

Alle rechten voorbehouden. Niets uit deze uitgave mag worden vermenigvuldigd en/of openbaar gemaakt worden door middel van druk, fotokopie, microfilm, elektronisch of op welke andere wijze ook zonder voorafgaande schriftelijke toestemming van de uitgever.

All rights reserved. No part of the publication may be reproduced in any form by print, photoprint, microfilm, electronic or any other means without written permission from the publisher.

This document was typeset using \LaTeX

Voorwoord

Toen ik in 1999 aan het doctoraat begon was er niets dat erop wees dat die onderneming uiteindelijk 16 jaar zou duren, twee eeuwen zou beslaan, drie decennia en 40 % van mijn leven tot dusver. Met de eindmeet in zicht is het tijd om enkele mensen te bedanken. Zonder jullie hulp was dit nooit gelukt.

In de eerste plaats bedank ik mijn promotor, Prof. Marc Moonen. We kennen elkaar intussen al lang: op het moment van de verdediging ben ik ouder dan Marc was toen hij me als doctoraatsstudent aannam.

Het adagium wil dat promotor en doctorandus tegelijk elkaars sterkste bondgenoten en meest geduchte vijanden zijn. Ik twijfel er niet aan dat hij af en toe heeft gevloekt. Samen hebben we echter mooie resultaten geboekt.

Marc's redactie van artikels verdient daarbij zeker een bijzondere vermelding: ik kan me geen promotor voorstellen die teksten grondiger naleest, met oog voor zowel een elegante formulering als elegante wiskunde. Onze gesprekken leidden vaak tot nieuwe inzichten, waarbij ik regelmatig versteld stond van het gemak waarmee hij uit obscure referenties een ontbrekend puzzelstukje kon opdiepen dat het plaatje compleet maakte. Dat staat in schril contrast met verhalen die ik over sommige andere promotoren heb gehoord -binnen onze faculteit en daarbuiten- die amper weten waarmee hun studenten bezig zijn.

Daarnaast wens ik de leden van de begeleidingscommissie, Prof. Bart Preneel, Prof. Michiel Steyaert en Prof. Bart Nauwelaers te bedanken voor hun steun en advies doorheen de jaren. I also thank Prof. Geert Leus en Prof. Luc Vandendorpe for accepting to be in the jury and for the interesting discussion during the preliminary defense. De feedback op het proefschrift werd erg gewaardeerd! Tenslotte prijs ik mezelf gelukkig met een alerte juryvoorzitter, Prof. Adhemar Bultheel, waarvoor dank.

Recente collega's die me vragen naar de samenstelling van de jury zijn daar doorgaans van onder de indruk. Een van de voordelen van een... eh *grondig* doctoraat is dat ik die mensen heb kunnen vragen "before they were famous".

Ik dank het IWT voor de financiering gedurende de eerste vier jaar, Alcatel voor de leerzame samenwerking, en de medewerkers van SCD, in het bijzonder Ida en P ela voor de aanmoediging en hulp.

Daarnaast bedank ik ook graag mijn collega-doctoraatsstudenten, wat er in mijn geval nogal veel zijn. De meesten van hen zijn intussen doctor, enkelen professor, en allen vergeven ze mij hopelijk dat ik de titels even achterwege laat.

In de eerste plaats zijn dat de mensen waarmee ik een bureau heb gedeeld: Jerre, Maarten, Geert Y, Koen V, Deepak en Toon, en diegenen die ongeveer in dezelfde periode actief waren: Piet, Geert L, Katleen, Koen E, Geert R, Simon, Ann, Hilde, Raphael, Imad, Olivier en Geert VM. Het opmerkelijkste resultaat van de samenwerking tussen deze mensen was een schilderij dat intussen door Marc in een kluis wordt bewaard -hetzij omwille van de waarde, dan wel uit g ene. Ook aan Peter D, Bart V, Axel, Pancho, Jeroen V, Tom B en Tom S bewaar ik goede herinneringen.

Sinds ik in 2004 vrij wetenschappelijk medewerker werd, was er minder tijd om fysiek op Esat te verschijnen. Het was telkens een aangenaam weerzien met Paschalis, Jan, Alex, Beier, Sam, Bram, Kim, Romain, Sylwec, Prabin, Pepe, Bruno, Rodrigo en Joe, die mij overigens met de bijnaam *The legend* bedachten (could have been worse). Het was een toffe groep, vooral de vrijgezellenavond van Beier zal ik niet snel vergeten.

Een bijzonder woord van dank gaat uit naar enkele mensen die op praktische wijze hebben bijgedragen aan dit werk. Patrick V en Steven T, voor de brainstormsessie bij Huub thuis op een moment dat de inspiratie ontbrak. Koenraad voor het nalezen van de tekst en de nooit aflatende aanmoedigingen in de afgelopen jaren. Mijn zus, Leen voor het herinneren aan milestones (uh-oh...) en het maken van illustraties. In de afgelopen jaren werd het leeuwendeel van mijn verlofdagen benut voor het doctoraatswerk. Dat voltrok zich grotendeels in Leuven, maar het was prettig om af en toe van omgeving te kunnen wisselen, met dank aan Cecile (Cevennes) en Wim (Dubai).

Door de lange tijd die eroverheen is gegaan was het doctoraat niet enkel een academische opleiding, maar tevens een soort *coming-of-age story*, en heeft als dusdanig een grote invloed gehad op mijn persoonlijkheid. Wie tegen monsters vecht moet er voor zorgen dat hij zelf geen monster wordt. En als je te lang in een afgrond kijkt, kijkt de afrond ook in jou.

Ik dank daarom ook de mensen in mijn omgeving, die jarenlang gezaag en vertwijfeling hebben doorstaan. In het bijzonder Leen en Maarten, Barbara en Jo, Kathleen en Kristof (en Dani el), Jappe en Nathalia, Klaas en Katja, Dag, Svekke, Frans, Luc P, Luk U, Karl, Bart V, Beire, Greet en Dirk, Steve, JP en Patrick, Kaat en Leon, Geert V, Bart G, Katrien H, Jonathan, Dieter en Lemmens. Sommigen ken ik al een kwarteeuw, zoals Wim en Liesbet, Filip en Elisabeth, Tom en Adia, Bart en Kristel en David en Tiny. Anderen, zoals Tosca, Stefan, Sabine en Kurt, Dirk, Pieter, Wendi, Olivia en Tanguy zijn recentere, maar daarom niet minder gewaardeerde supporters.

Petrus (Isabel en Felix), Lander (Liesbet en Huub) en vooral hun ouders zijn bedankt om mijn petekindjes te willen zijn. Ik beloof niet te zullen voorlezen uit dit boekje.

Bij mijn huidige werkgever bestond veel interesse voor het curiosum dat de eeuwige doctoraatsstudent is. In het bijzonder bedank ik Wim, Jean-Marie, Pieter, Philip, Kristof en Patrick voor de vele aanmoedigingen, Danny voor de flexibiliteit in de afgelopen maanden en Kristl, die me zowel bij Septentrio als op Esat wegwijs kon maken wanneer ik verdwaald was.

De laatste woorden, en tevens de belangrijkste, gaan uit naar mijn familie. Ik prijs me gelukkig met ouders die me bij elke onderneming hebben gesteund, onvoorwaardelijk en tot op heden. Alles wat ik tot dusver heb bereikt is ook hun succes.

Helaas ging dat niet altijd even makkelijk. In de loop der jaren werd het doctoraat mijn eigen persoonlijke *Moby Dick*, die ik niet kon loslaten, maar lange tijd evenmin kon temmen. De wanhoop is vaak nabij geweest, maar de troost gelukkig ook. Wanneer ik dit hoofdstuk eindelijk kan afsluiten, is dat dus meer dan wat dan ook te danken aan de nooit aflatende steun en liefde van mijn ouders, Leen en Kris, en de rest van de familie.

Heel erg bedankt!

Gert Cuypers
oktober 2015

Dit werk is opgedragen aan mijn grootmoeder, Ida Ghoos, die zelf nooit de gelegenheid heeft gehad om te studeren, Het vooruitzicht om op een dag voor haar deze opdracht te kunnen schrijven, is een belangrijke motivatie geweest om het niet op te geven.

Abstract

This work treats some aspects of *multi-carrier modulation* (MCM) and *single-carrier frequency-domain equalization* (SC-FDE), which are closely related *block transmission* schemes. In both cases, the equalization of a frequency-selective channel is done by dividing the total occupied bandwidth into a large number of narrow bands (tones) which experience a flat fading. The algorithms involved rely heavily on the *discrete Fourier transform* (DFT). In the case of MCM, the transmitted data is encoded into blocks in the frequency domain, by using an inverse DFT (IDFT) at the transmitter. The receiver then consists of a DFT, followed by a one-tap complex equalizer for each tone. In SC-FDE the information is encoded into blocks in the time domain. At the receiver, the DFT and one-tap equalizer are followed by an extra IDFT. To avoid the loss of orthogonality between the tones, a *guard interval* (GI) is inserted between each two blocks. If the channel order doesn't exceed the GI length, zero-forcing equalization is possible. For longer channels, a *Per-Tone equalizer* (PTEQ) can be used, which minimizes the mean square error of the received symbols.

In practice, the individual bands are orthogonal but overlap, due to the slow roll-off of the DFT's side lobes. This has an undesirable effect both for the ingress and egress of the signal. Traditionally this problem is solved by applying window functions. Unfortunately, at the transmitter, window functions disturb the orthogonality between the tones. Therefore, a special class of window functions was developed, for which the loss of orthogonality is predictable, such that it can be restored at the receiver. These window functions have a beneficial influence on the egress and make it easier to meet regulatory standards.

There is also a need for window functions at the receiver, to avoid the contamination of a whole range of tones by one narrow-band interferer. For short channels, this can be easily done. However, combining window functions and the PTEQ is nontrivial. For two classes of windows, namely the trapezoidally tapered and the raised cosine window, an efficient equalization scheme was developed, combining these windows with the PTEQ. This technique was also patented by an industrial partner.

Some channels exhibit one or more spectral zeros, i.e. tones where the channel response is zero or close to zero. For the case of a MCM with feedback from the receiver to the transmitter, it can be decided to discard that tone and not to encode any information on it. For all other cases, the loss of the information which was stored at the spectral zero should be dealt with using some form of coding. For the case of SC-FDE using a zero pad for a GI, we have developed a method to estimate the content of a spectral zero, making use of redundancy in the time domain. This technique was called *zero-restoration* (ZR) because it allows to restore information which was lost in spectral zeros. Finally, a combination of the PTEQ and ZR was proposed.

Beknopte samenvatting

Dit proefschrift behandelt enkele aspecten van *multi-carrier-modulatie* (MCM) en *single-carrier-frequentiedomeinegalisatie* (SC-FDE). Deze twee systemen van bloktransmissie zijn nauw gerelateerd. In beide gevallen gebeurt de egalisatie van het frequentieselectieve kanaal door het totale beschikbare spectrum op te delen in een groot aantal smalle banden (tonen). Binnen deze smalle banden is het kanaal nagenoeg vlak. De algoritmes maken intensief gebruik van de *discrete Fouriertransformatie* (DFT). In het geval van MCM wordt de data door de zender geëncodeerd in blokken in het frequentiedomein door middel van een inverse DFT (IDFT). De ontvanger bestaat uit een DFT, gevolgd door een complexe één-taps-egalisator voor elke toon. Bij SC-FDE wordt de informatie geëncodeerd in blokken in het tijdsdomein. Aan de ontvangtzijde worden de DFT en de één-taps-egalisator gevolgd door een extra IDFT. Om de orthogonaliteit tussen de tonen te bewaren wordt tussen elke twee blokken een zgn. *guard-interval* (GI) voorzien. Indien de orde van het kanaal niet groter is dan de lengte van het GI, is *zero-forcing*-egalisatie mogelijk. Voor langere kanalen kan een zogenaamde *per-toon egalisator* (PTEQ) worden gebruikt, die de *mean squared error* van de ontvangen symbolen minimaliseert.

In de praktijk zijn de afzonderlijke banden weliswaar orthogonaal, maar overlappen, omwille van de trage *roll-off* van de zijlobben van de DFT. Dit heeft een nadelig effect op zowel de *ingress* als de *egress*. Traditioneel wordt dat probleem opgelost door middel van vensterfuncties. Helaas veroorzaakt het gebruik van vensterfuncties aan de zender het verlies van de orthogonaliteit tussen de tonen. Daarom werd een speciale klasse van vensterfuncties ontwikkeld waarbij dat verlies van orthogonaliteit voorspelbaar is, zodat de ontvanger het weer ongedaan kan maken. Deze vensterfuncties hebben een gunstige invloed op de *egress* en helpen zo aan emissiestandaarden te voldoen.

Ook aan ontvangtzijde kunnen vensterfuncties nuttig zijn, om te verhinderen dat een smalbandige interferentie een groot aantal tonen zou contamineren. In het geval van korte kanelen is dat makkelijk te doen. Het is echter niet zo eenvoudig om vensterfuncties te combineren met de PTEQ. Voor twee klassen van vensterfuncties, namelijk die met een lineaire taper en de *raised cosine* vensterfuncties,

werd een egalisatieschema ontwikkeld, waarin deze vensterfuncties efficiënt worden gecombineerd met de PTEQ. Deze techniek werd gepatenteerd voor een industriële partner.

Sommige kanalen vertonen één of meerdere spectrale nullen. Dat zijn tonen waarvoor de frequentierespons van het kanaal zeer klein is. In het geval van MCM met een terugkoppeling van de ontvanger naar de zender kan worden besloten om de bewuste tonen niet te gebruiken voor de transmissie van informatie. In alle andere gevallen moet het verlies aan informatie die was opgeslagen in de toon, worden opgevangen door een of andere vorm van codering. Voor het geval van SC-FDE met *zero pad* als GI hebben we een methode ontwikkeld om de inhoud van een toon met spectrale nul te schatten, gebruik makende van redundantie in het tijdsdomein. Deze techniek noemen we *zero-restauratie (ZR)*, aangezien die toelaat informatie te herwinnen die aanvankelijk verloren was gegaan in de spectrale nul. Tenslotte wordt een combinatie van de PTEQ en ZR voorgesteld.

Glossary

Acronyms and Abbreviations

ADSL	asymmetric digital subscriber loop
AFE	analog front-end
AWGN	additive white Gaussian noise
BER	bit error rate
CDMA	code division multiple access
CO	central office
CP	customer premises
CP	cyclic prefix
DA	digital to analog
DAB	digital audio broadcasting
DCT	discrete cosine transform
DFE	decision feedback equalizer
DFT	discrete Fourier transform
DMT	discrete multitone
DSL	digital subscriber line
DSLAM	digital subscriber line access multiplexer
DSSS	direct sequence spread spectrum
DVB	digital video broadcast

DVB-S	terrestrial digital video broadcast
DVB-T	digital video broadcast over satellite
ETSI	European telecommunications standards institute
FD	frequency domain
FDE	frequency-domain equalization
FEC	forward error correction
FEQ	frequency domain equalizer
FEXT	far-end crosstalk
FFT	fast Fourier transform
FHSS	frequency hopping spread spectrum
FIR	finite impulse response
FTTB	fiber-to-the-building
FTTC	fiber-to-the-curb
FTTH	fiber-to-the-home
FTTN	fiber-to-the-node
GFSK	Gaussian frequency shift keying
GI	guard interval
GMSK	Gaussian minimum shift keying
GPS	global positioning system
GSM	global system for mobile communications
ICI	inter carrier interference
IDFT	inverse discrete Fourier transform
ISDN	integrated services digital network
ISI	inter symbol interference
ISM	industrial, scientific and medical
IW	iterative water filling

KSP	known signal pad
LC	linear combiners
LMS	least-mean-squares
LNA	low noise amplifier
LS	least-squares
LTE	long term evolution
MCM	multi-carrier modulation
MIMO	multiple-input, multiple output
MMSE	minimum mean squared error
MSE	mean squared error
NEXT	near-end crosstalk
OFDM	orthogonal frequency division multiplexing
OLA	overlap-add
OLS	overlap-save
OSB	optimal spectrum balancing
PAM	pulse amplitude modulation
PAPR	peak-to-average power ratio
PLL	phase locked loop
POTS	plain old telephone system
PSD	power spectral density
PSK	phase shift keying
PTEQ	per-tone equalizer
PTS	partial transmit sequence
QAM	quadrature amplitude modulation
RFI	radio frequency interference
RLS	recursive least squares

RTTY	radio-teletypes
SAGE	semi-automatic ground environment
SC	single-carrier
SNR	signal to noise ratio
TD	time domain
TEQ	time domain equalizer
UMTS	universal mobile telecommunication system
UW	unique word
VCO	voltage controlled oscillator
VDSL	very high-bitrate digital subscriberline
VOD.	video-on-demand
ZFE	zero-forcing equalizer
ZR	zero-restoration

Contents

Abstract	v
Glossary	ix
Contents	xiii
List of Figures	xix
List of Tables	xxiii
1 Introduction	1
1.1 Multi-carrier communication	2
1.1.1 General philosophy	2
1.1.2 Cyclic prefix	4
1.2 Wireless modems	5
1.2.1 Digital broadcasting	5
1.2.2 Computer networks	6
1.2.3 Mobile phones	6
1.3 Digital subscriber loop	7
1.3.1 History of DSL	7
1.3.2 The DSL Spectrum	8

1.3.3	The copper installation	9
1.3.4	Interference	10
1.4	Outline of the thesis and contributions	12
2	Basic concepts	15
2.1	Multicarrier modulation	15
2.1.1	The CP	15
2.1.2	Zero padding and known signal padding	20
2.2	Discrete multi-tone	21
2.2.1	Transmitter and modulation	21
2.2.2	Bit loading	23
2.2.3	Peak to average power ratio	26
2.2.4	Receiver and equalization	27
2.2.5	Windowing	30
2.3	Single-carrier block transmission with frequency domain equalization	32
2.3.1	Motivation	32
2.3.2	Single carrier frequency division multiple access	33
3	Receiver windowing	35
3.1	Introduction and motivation	36
3.2	Mathematical derivation	38
3.2.1	Per tone equalization	38
3.2.2	PTEQ and window functions	41
3.3	Complexity	51
3.3.1	DFT complexity	51
3.3.2	RLS update complexity	53
3.3.3	Total complexity	55
3.3.4	Memory consumption	56

3.4	Simulation results	57
3.4.1	MMSE simulations	57
3.4.2	RLS simulations	60
3.5	Conclusions	61
4	Transmitter windowing	63
4.1	Introduction	64
4.2	DMT transmit signal spectrum	65
4.3	Transmitter windowing	68
4.3.1	Derivation of the window structure	69
4.3.2	Determining the window parameters	72
4.3.3	Modification of the equalizer	74
4.4	Simulation results	75
4.4.1	Influence on the egress	75
4.4.2	Influence on the transmission	78
4.5	Conclusion and further work	78
4.6	Addendum: an alternative application of the window	79
4.6.1	Definitions	80
4.6.2	Known signal padding	80
4.6.3	Intra-symbol windowing	81
4.6.4	Decoding	81
4.6.5	Channel equalization	83
5	Zero restoration	85
5.1	Introduction	86
5.2	System model and equalizers	87
5.2.1	Time domain equalization	88
5.2.2	Frequency domain equalization based on matrix folding	89

5.2.3	Frequency domain equalization based on matrix extension . . .	90
5.3	Improved frequency-domain equalization	91
5.3.1	Frequency-domain ZFE with zero restoration	92
5.3.2	Frequency-domain MMSE-like equalization with zero restoration	95
5.4	Theoretical analysis of the performance	96
5.4.1	ZFE	96
5.4.2	MMSE	97
5.4.3	Remarks	101
5.5	Simulations and discussion	103
5.6	Conclusion	107
6	Combining zero restoration and per-tone equalization	111
6.1	Introduction	111
6.2	System model	113
6.2.1	Short channels	114
6.2.2	Long channels	115
6.3	Per-tone equalization (PTEQ)	115
6.4	Spectral zero restoration PTEQ (ZR-PTEQ)	119
6.4.1	Motivation	119
6.4.2	Mathematical derivation	120
6.4.3	Selection of the spectral zeros	121
6.5	Simulation results	122
6.6	Conclusion	123
6.7	Acknowledgments	124
7	Chebyshev interpolation for DMT modems	125
7.1	Introduction	125
7.2	Chebyshev interpolation theory	127

7.3	Implementation	129
7.4	Simulation results	132
7.5	Conclusions	133
8	Conclusions and future work	135
8.1	Conclusions	135
8.1.1	Intruductory material	135
8.1.2	Own contributions	136
8.2	Future work	137
A	A brief overview of the history of electronic communication	139
A.1	Nineteenth century: the age of invention	139
A.1.1	Telegraphy	139
A.1.2	Telephony	140
A.1.3	Dispelling dispersion	140
A.2	Twentieth century: the age of information theory	141
A.2.1	Bandwidth and sampling	141
A.2.2	Information and channel capacity	142
A.3	Voice-band modems	142
A.3.1	Early modems: 110-300 bps	143
A.3.2	Dispelling dispersion II: 9600 bps	143
A.3.3	Trellis encoding: 33k6 bps	144
	Bibliography	145
	Curriculum vitae	165
	List of publications	167

List of Figures

1.1	The IDFT converts a complex vector representing the individual carrier modulation data into a superposition of modulated carriers	3
1.2	Modulation using the DFT leads to a sinc-shaped spectrum for each carrier. The spectrum goes through zero at the frequencies of the other carriers	4
1.3	Edge effects of the convolution lead to the loss of orthogonality. Adding a CP preserves the orthogonality, as shown for two different tone frequencies.	5
1.4	The DSL spectrum.	9
1.5	A bridged tap and a splice both generate reflections	10
1.6	NEXT and FEXT in a cable binder. While interference from other users used to be a limiting factor for DSL, it can now be exploited by coordinating the transmissions.	11
2.1	The OFDM modulation scheme. The transformation with DFT and IDFT matrices and the insertion and removal of the CP decomposes the dispersive channel into a collection of flat-fading channels.	18
2.2	Comparison of the CP (a), ZP (b) and KSP (c).	22
2.3	The DMT transmitter. Only the lowest half of the tone vector can be chosen freely. The higher half is a complex conjugate symmetrical copy of the lower half.	23
2.4	The subchannels can be considered as flat-fading (a). The water-filling algorithm for the single-user case (b).	24

2.5	A practical example of the SNR and bitloading in a DSL system. . . .	25
2.6	The TEQ+FEQ-based DMT receiver. The TEQ shortens the channel impulse response and the FEQ corrects the tones' amplitude and phase.	29
2.7	The PTEQ-based DMT receiver. The TEQ is moved behind the DFT, which becomes a <i>sliding DFT</i> . Each tone is equalized based on an individual linear combination of the sliding DFT outputs at that tone. .	29
2.8	The PTEQ based on difference terms. The sliding DFT is replaced by one full DFT and difference terms. Each tone is equalized based on an individual linear combination of the DFT output at that tone and the difference terms.	30
2.9	To maintain the orthogonality between the tones, the window should extend beyond the DFT size and the head and tail should be complimentary.	31
2.10	By moving the IDFT from the transmitter to the receiver, OFDM (a) can be transformed into SC-FDE (b), combining a low PAPR with inexpensive equalization.	33
3.1	Classical receiver block scheme with a time domain equalizer, serial-to-paraller converter, removal of the cyclic prefix DFT and one-tap complex frequency domain equalizer	37
3.2	Side lobe decay of the rectangular (<i>Dirichlet</i>), <i>raised cosine</i> and <i>trapezoidal</i> window. The window taper length μ equals 16.	38
3.3	Receiver block scheme with PTEQ using successive DFTs. In practice, these are calculated using one DFT and difference terms.	39
3.4	<i>RLS PTEQ implementation</i> . The top triangle corresponds to the shared (real) difference terms. For each tone, an individual (complex) input is added. The scheme is updated for every DMT symbol.	40
3.5	Windowing: weighting of samples and folding of the edges	41
3.6	Signal flow graph when using <i>trapezoidal</i> window (unconstrained). The top triangle corresponds to the shared real difference terms. For each tone individually, this is extended with two complex tone-dependent inputs.	47
3.7	Extending D_{rc} to a sinusoidal window	48
3.8	Butterfly scheme for the second FFT. Nonzero numbers are represented as dots. Operations on zeros are represented by dotted lines.	52

3.9	Complexity of PTEQ and <i>trapezoidal</i> windowing scheme ($\mu = 16$) . . .	56
3.10	Comparison between PTEQ and the WiPTEQ ($\mu = 16$, trapezoidal window) in absence and presence of RFI	58
3.11	Influence of taper length μ in the absence and presence of RFI (please notice the difference in scale)	59
3.12	RLS simulations: PTEQ vs WiPTEQ with trapezoidal window and raised cosine window. RFI emerges at time 300	60
4.1	Basic DMT system (refer to text for α to γ)	66
4.2	The first (DC only) symbol as a sampled rectangular window, and a possible next symbol.	67
4.3	Spectrum of the continuous and sampled rectangular window	68
4.4	The cyclic prefix in DMT systems leads to a toothed spectrum exhibiting valleys in between the tones	69
4.5	Transmitter windowing translates to symbol precoding	70
4.6	In approach-1 (left) the linear combiners (LC) of the PTEQ and the decoder are separated. In approach-2 (right) they are combined.	75
4.7	The shape of the rectangular window as well as $\mathbf{W}_{1,opt}$, $\mathbf{W}_{2,opt}$ and \mathbf{W}_{opt}	76
4.8	Spectrum of the rectangular window, $\mathbf{W}_{3,opt}$, $\mathbf{W}_{5,opt}$ and \mathbf{W}_{opt}	77
4.9	Spectrum of the rectangular window, $\mathbf{W}_{3,opt}$, $\mathbf{W}_{5,opt}$ and \mathbf{W}_{opt} (detail of amateur radio band)	77
4.10	Comparison between the rectangular window using an ordinary PTEQ and the $\mathbf{W}_{3,opt}$ window using approach-2.	79
4.11	The window \mathbf{g} is the inverse of a raised cosine	82
5.1	The originally transmitted signal and the equalized received signal, assuming one sub-carrier was discarded. The phase and amplitude of the missing sub-carrier can be estimated by inspecting the zero-pad.	92
5.2	The noise contribution to the MSE for different spectral responses λ_{e_i} . For high SNR (right hand side) the MSE is dominated by the noise contribution of the sub-carriers with the lowest spectral response (close-to-zeros).	99

5.3	Example of the MSE contributions from inexact channel equalization and noise enhancement for the MMSE-FD-EXT and the MMSE-ZR	100
5.4	Magnitude response for $h_1(n)$ (from [115]) and $h_2(n)$ (from [204])	104
5.5	Performance comparison for channel $h_1(n)$	105
5.6	Performance comparison for channel $h_2(n)$	106
5.7	Mean square error for channel $h_2(n)$	107
5.8	Performance comparison for Rayleigh fading channels	108
5.9	Comparing several existing methods for IEEE802.11a dimensions and ITU channels.	109
6.1	The TEQ+FEQ (a) and the PTEQ (b)	116
6.2	A simple example of a binary signal with zero pad, which has been passed through a channel with a spectral zero and through an MMSE equalization. The tone corresponding to the spectral zero is discarded by the equalizer and shows itself as a complex exponential error in the ZP (only real component shown here).	119
6.3	Frequency response of a typical Rayleigh fading channel. This example exhibits a spectral zero on tone 61.	122
6.4	The PTEQ and the ZR-PTEQ for the channel from Fig.6.3. The DFT-size $M=80$, the ZP length P is varied from 0 to 20 and the number of coefficients T ranges from 1 to 19.	123
7.1	Cosines on a uniform grid in the θ -plane correspond to Chebyshev polynomials on a nonuniform grid in the XZ-plane	129
7.2	L output samples at \tilde{t}_k interpolated from P input samples at t_k	130
7.3	The Chebyshev interpolator block diagram	131
7.4	The modified Farrow structure	131
7.5	Comparison of Chebyshev and Lagrange interpolation. Fractional delay is $1/2$ sample	132

List of Tables

3.1	DFT complexity when using the <i>trapezoidal</i> window	53
3.2	RLS update complexity when using the <i>trapezoidal</i> window	54
3.3	RLS update complexity when using the <i>raised cosine</i> window	55
3.4	Total complexity of PTEQ and <i>trapezoidal</i> windowing scheme, ADSL downstream, 218 tones	56
3.5	Nominal RFI frequencies and power levels	57
5.1	Comparing the complexity for block size N , ZP-length P and K spectral zeros ($M = N + P$).	102

Chapter 1

Introduction

This chapter gives an introduction to *multi-carrier modulation* (MCM) and its application to *digital subscriber line* (DSL) technology. While different implementations have been proposed over time, the distinguishing property of MCM is that the available spectrum is divided into a large number of narrow sub-bands, which are individually modulated. Because the symbol rate in these sub-bands is lower and the dispersion is smaller, the equalization can be much simpler than for the original large band.

The idea of dividing the band into smaller sub-bands is naturally associated with an individual modulation of each sub-band, but can also be beneficial for the equalization of a wide-band signal, referred to as *single-carrier frequency domain equalization* (SC-FDE).

The chapter is organized as follows: in section 1.1 we provide a brief overview of MCM. The application to wireless communication is highlighted in section 1.2. The application of MCM to DSL, and the challenges faced in the DSL-environment are treated in section 1.3. Finally, section 1.4 provides an overview of the contributions in this work.

In this chapter we have avoided formulas. For a more rigorous description of the mathematics involved, we refer to chapter 2, which also explains SC-FDE in more detail. For a short history of telecommunications prior to MCM, and an overview of how the current twisted pair infrastructure came to be, we refer to Appendix A.

1.1 Multi-carrier communication

1.1.1 General philosophy

There are two approaches for the utilization of a dispersive channel with large bandwidth. One approach fills the complete band with a *single-carrier* (SC) transmission at high symbol rate and relies on equalization to avoid *inter symbol interference* (ISI). The other approach, now known as *multi-carrier modulation* (MCM), divides the large band into a number of narrower sub-channels or sub-bands or *tones*. As a result, the symbol period increases, leading to a relatively lower ISI.

Dividing the available band into multiple channels incurs the risk of *inter-channel interference* (ICI). This can be prevented by avoiding spectral overlap of adjacent channels using strong filtering and a large spectral distance between the carriers. Unfortunately, this leads to a less efficient spectrum use.

A first implementation which allowed the bands to *overlap*, while avoiding ICI, was the 1958 *Collins Kineplex system* -so called because it combines kinematic filters at the receiver and used multiplexing [130]. This wireless system operated in the HF-band and had a carrier spacing of 110 Hz [84]. Each of 20 tones is modulated by differential *phase shift keying* (PSK) without filtering. The spectra of the sub-bands are therefore *sinc-shaped* and strongly overlap. However, similar to modern MCM-implementations, the tones are spaced at frequency intervals almost equal to the signaling rate and can be separated at the receiver [10].

While the Kineplex system had some remarkably modern properties, it also had disadvantages. First of all, it was very complex and bulky. Secondly, some spectrum was lost above the highest tone and below the lowest, to allow for a proper roll-off of their slowly decaying sinc spectrum.¹ It would be interesting to have at least *some* filtering to limit the overlap to the nearest neighbours, while maintaining the orthogonality between the tones. In the 1960's it was realized that it is possible to shape filters such that the transmitted signals are still orthogonal to each other [25]. Later on *Saltzberg* proposed a system with base band signals meeting this condition [160], and deemed it promising enough to be patented [161].

A drawback of these early systems was their complexity, resulting from the analog implementation using individual oscillators, mixers and the shaping filters for each tone. The discovery of the *fast Fourier transform* (FFT) algorithm in 1965 [32] (which was actually already conceived by *Gauss* in 1805 [85]) opened up a completely new approach. Considering that the Fourier transform of a complex exponential signal yields a single pulse in the frequency domain (FD), and the inverse Fourier transform

¹Note that this same issue of slow roll-off still exists in modern MCM systems and makes it more difficult to meet egress masks. Chapter 4 is dedicated to this issue

of a single pulse yields a complex exponential in the time domain (TD), it is obvious that the inverse Fourier transform of a superposition of impulses yields a superposition of complex exponentials. Applied to the *discrete Fourier transform* (DFT), this means that the sum of a large number of modulated carriers can be obtained through the *inverse DFT* (IDFT) of a complex vector representing the phases and magnitudes of the individual carriers, as shown in **Fig. 1.1**. This coding scheme is called *orthogonal frequency division multiplexing* (OFDM). The first DFT-based system was proposed by *Weinstein and Ebert* in 1971 [208].

A fully digital implementation has the significant benefit that the design is much simpler and cheaper because there is no need for individual oscillators and mixers. Because of the orthogonality of the DFT, no base band filters are needed either. The spectrum occupied by each carrier has the shape of a sinc function (like the Kineplex system), which goes through zero at the center frequency of the other bands, as shown in **Fig. 1.2**.

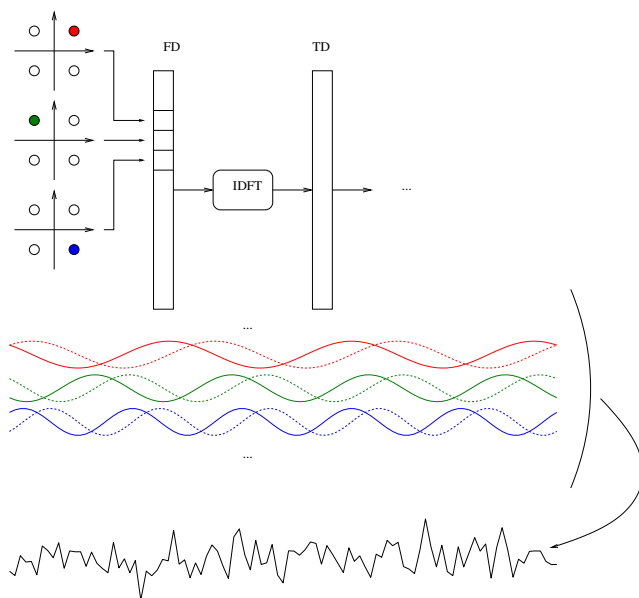


Figure 1.1: The IDFT converts a complex vector representing the individual carrier modulation data into a superposition of modulated carriers

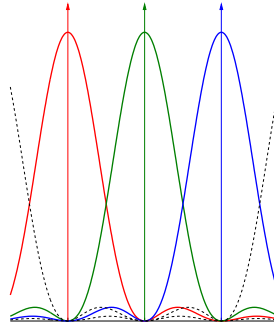


Figure 1.2: Modulation using the DFT leads to a sinc-shaped spectrum for each carrier. The spectrum goes through zero at the frequencies of the other carriers

1.1.2 Cyclic prefix

A naive approach to DFT-based modulation would be to simply group transmit symbols together in blocks, compute the IDFT and serialize this result for transmission over the channel. There are two problems with this approach. Firstly, there is obviously ISI, because the received symbols are overlapping. This can be avoided by inserting some kind of *guard interval* (GI) in between successive blocks. Secondly, the orthogonality between the tones is lost. This implies that energy from one tone will be transferred to other tones, resulting in ICI.

The fundamental reason for this loss of orthogonality is found in the *edge effects* of the convolution with the channel. This observation leads to a solution for the problem, which is to somehow extend the duration of the transmitted symbol, and selecting only a part of it at the receiver, discarding the edge effects. It was therefore proposed to copy the last ν samples of the transmitted block and insert these in front of the block [145]. This block of copied samples is referred to as a *cyclic prefix* (CP). **Figure 1.3** shows in a graphical way how the CP indeed leads to the preservation of the orthogonality between the tones. In the mean time, alternatives for the CP have been proposed, which are discussed in chapter 2.

In spite of the advantages, no commercial voice-band telephone modems ever used a modern MCM-scheme and wireline communication were even late to adopt it. The first use of OFDM took place in wireless modems.

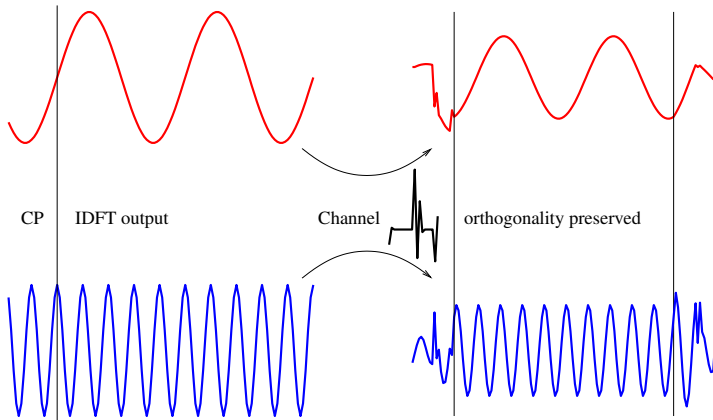


Figure 1.3: Edge effects of the convolution lead to the loss of orthogonality. Adding a CP preserves the orthogonality, as shown for two different tone frequencies.

1.2 Wireless modems

We divide the evolution of digital wireless communication into three domains: digital broadcasting, computer networks, and mobile telephony.

1.2.1 Digital broadcasting

The possibility of OFDM for mobile communication was already studied in the 1980's [29]. This coding scheme offers some significant advantages, in particular for *digital audio broadcasting* (DAB). Not only does the digital implementation allow for a good audio quality, it also offers the advantage that all transmitters can operate at the same frequency, known as a *single-frequency network* [15]. In such a single-frequency network, the signals of other transmitters can be modeled as echo or multi path. The delay spread of the equivalent channel is related to the distances between the transmitters. It is therefore necessary to implement very long symbols (about 1 ms), with a guard interval able to eliminate echoes from 100 km distant transmitters [153]. DAB was standardized by the *European Telecommunications Standards Institute* (ETSI) and was the first standard ever to adopt OFDM [50].

The same advantage of a single-frequency network is also exploited for *digital video broadcast* (DVB). More specifically, in 1997 OFDM was adopted for *terrestrial*²

²Note that *DVB over satellite* (DVB-S) uses a simple M-PSK modulation.

broadcasting (DVB-T) [56]. Single-frequency networks require a good synchronization, typically based on precision *global positioning system* (GPS) timing receivers [55].

1.2.2 Computer networks

It took a bit longer for computer networks to adopt OFDM. The first equipment for digital wireless communication were radio-teletypes (RTTY), which were introduced around 1922 and used a simple *frequency shift keying* (FSK) modulation. In the 1950's, PSK was developed and offered a higher spectral efficiency [34]. In the mid-1960's, data packet technology was developed, and in 1970, the ALOHANET, based at the University of Hawaii, was the first large-scale packet radio project [3].

The first modern wireless digital communication network standard was HiperLAN (High Performance Radio Local Area Network), which was approved in 1996 [53]. This system operated at 5 GHz and delivers 23.5 Mbps using FSK and Gaussian minimum shift keying (GMSK). Its successor, HiperLAN 2 *used OFDM* to deliver 54 Mbps [52]. Neither of them were successful, because the competing IEEE802.11 standards were released around the same time. Even though the performance of both competitors was comparable [47], the IEEE was already better known by manufacturers and therefore their standard got the upper hand [136].

Indeed, ubiquitous as Wi-Fi³ networks are now, it is hard to imagine that the IEEE802.11 standard dates back to only 1997 [92]. This system works in the industrial, scientific and medical (ISM) band around 2.4 GHz, and offers a throughput of 2 Mbps, using direct sequence spread spectrum (DSSS) and frequency hopping spread spectrum (FHSS). Two years later it was supplemented by the IEEE802.11b standard, offering a rate of 11 Mbps using DSSS [94].

In 2003, the IEEE802.11g promised up to 54 Mbps, *finally using OFDM* [95]. The first support for multiple-antenna communication appeared in 2009, with the IEEE802.11n standard, theoretically capable of delivering 150 Mbps [97].

In 1999 the first Bluetooth specification was released. This system also operated in the ISM band; it uses *Gaussian frequency shift keying* (GFSK) and has a transmission speed of 1 Mbps [18].

1.2.3 Mobile phones

Also in cellular mobile telephony and data, it took a long time for OFDM to be adopted. The first cellular communication systems -now referred to as *1G*- were deployed in the

³Note that the term "Wi-Fi" is not an abbreviation, but a mere wordplay on "Hi-Fi", without meaning.

beginning of the 1980's and used analog modulation in the 900 MHz band. The second generation (2G), known in Europe as *Global system for mobile communications* (GSM) uses a digital modulation, more specifically GMSK. It became the most successful ETSI-standard ever [57], with deployment starting in 1992 at 900 MHz and in 1994 also at 1800 MHz. Its American counterpart D-AMPS aka IS-54 used a PSK modulation and is no longer operational.

Both the European *Universal Mobile Telecommunication System* (UMTS), and the American *CDMA2000* implementations of 3G use a code division multiple access (CDMA)-coding [188], [2]. The more recent Wimax standard, approved in 2005, however uses OFDM [96].

Finally, the 4G *long term evolution* (LTE)-standard uses OFDM for the downlink, and single-carrier FDMA for the uplink [58]. We come back to this in more detail in section 2.3.2.

1.3 Digital subscriber loop

A development which remained unmentioned so far was the laser, invented in 1960. After the initial excitement about this cool device, it dawned that the practical applications were limited, and for years, lasers were considered *a solution in search of a problem* [81]. By 1966 the problem had finally arrived, when it was proposed to use *optical fiber* as a means of communication [104], which became a reality when Corning developed the first low-loss optical fiber in 1970 [106].

From then on, fiber optic communication became the method of choice between telecom centers. However, there was still a need to deliver the so-called *last mile* from the telco to the customer. Ideally, this would also be done optically, referred to as *fiber-to-the-home* (FTTH), but this has a prohibitive cost of installation. Practical options for the last-mile were re-use of the existing coax television network and the telephony network [65]. It is against this backdrop that DSL was developed.

1.3.1 History of DSL

Although the theory was sufficiently elaborated, it still took quite a while before MCM for wireline communication really took off [17], [110]. The first step towards a DSL was the *Integrated Services Digital Network* (ISDN) offering a 144 kbps link using pulse amplitude modulation (PAM), a nice improvement over the 56 kbps speed of voice-band modems, but not nearly enough for *video-on-demand* (VOD).

The breakthrough of MCM occurred when *John Cioffi* developed a variant of OFDM, called *discrete multitone* (DMT) for communication over the telephone twisted pair [30], and proposed this for the upcoming standard of *asymmetric digital subscriber line* (ADSL). The "asymmetric" derives from the observation that for typical domestic use, required speed in downstream is much larger than upstream. The upcoming standardization of ADSL again intensified the old debate between MCM and SC, here represented by a QAM-solution. To decide which one was to be used in the upcoming ADSL-standard, Bellcore organized a technical contest, called the *DSL-Olympics* in 1993. The supremacy of the, at that time, unproven DMT was overwhelming in terms of speed, efficiency and flexibility. The main strength of DMT over the SC system was its capability to avoid expending power in parts of the spectrum characterized by very large noise or a deep channel null, a capability difficult to achieve for single-carrier systems [207]. On March 10, 1993 DMT was selected by ANSI [69, p.450], with the ITU and ETSI following later. Since then, Cioffi is known as the *father of DSL*.

Newer standards based on DMT followed, such as ADSL2, ADSL2+, very-high-bitrate DSL (VDSL), VDSL+ and so on.

1.3.2 The DSL Spectrum

DSL operates in the frequency band above 30 kHz, and is completely separated from the *plain old telephone service* (POTS) by means of a diplexer called a *POTS-splitter*. This allows uninterrupted operation of the POTS, regardless of DSL.

The distance between the carriers is 4.3125 kHz for all DSL flavours, with a symbol rate of 4000 symbols/s. The initial ADSL system used 256 tones to occupy a bandwidth of 1.1 MHz. The low tones are used for upstream communication, the high ones for downstream. Later DSL systems kept the same tone spacing, but used a larger number of tones [86], [186], [122], as illustrated in **Fig. 1.4**.

Because the attenuation of the copper pair increases with the frequency, the more advanced flavours of DSL only work on shorter loops. This implies that the *DSL access multiplexer* (DSLAM), basically a rack of DSL modems, where the interfacing with the optical network is located, is steadily moving closer to the subscriber, from *fiber-to-the-node* (FTTN), where the fiber is terminated in a street cabinet, possibly miles away from the customer, over *fiber-to-the-curb* (FTTC) to *fiber-to-the-building* (FTTB) etc.

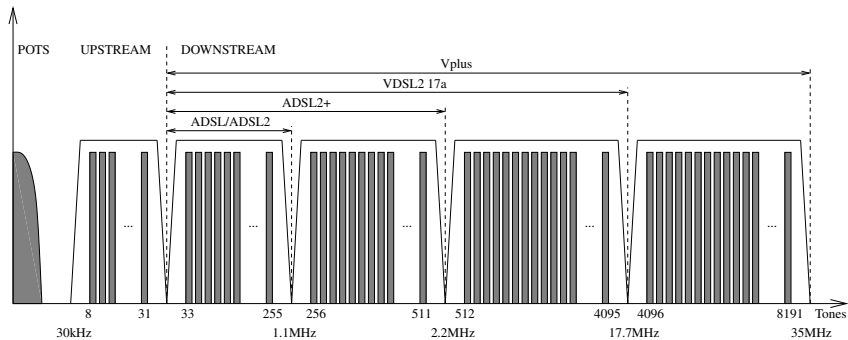


Figure 1.4: The DSL spectrum.

1.3.3 The copper installation

The twisted pair

Each cable pair consists of two twisted insulated conductors. They are packed together in feeder cables. Older feeder cables may contain as many as 100 wire pairs per binder, most newer distribution cables consist of 25-pair binders [180]. Neighbouring pairs in a given 25 pair group have a different twist length, varying from two to six inches, to further reduce the crosstalk between them [155, p.307].

Bridged taps

A bridged tap is a length of wire pair that is connected to the loop on one end and unterminated on the other. They originate from the re-use of a telephone cable pair for a new customer without disconnecting the previous one from the loop, as shown in **Fig. 1.5**. The DSL signal enters the decommissioned branch of twisted pair and is reflected at the end. This reflected signal is added out of phase to the original signal, leading to a reflection to the transmitter and an attenuation towards the receiver.

Bridged taps behave like an open stub, and will therefore have an especially nefarious effect for frequencies for which they are of quarter wavelength. Approximately 80% of the loops in the U.S. have bridged taps, sometimes more than one [31].

Splices and gauge changes

Because of the limited length of the spools on which telephone cables are delivered, splices are necessary. Moreover, different wire gauges (diameters) are used, depending on the length of the loop, to keep the total resistivity under control. These splices, especially between different wire gauges, generate reflections, as shown in **Fig. 1.5**.

The DSL standard defines several test loops to evaluate the performance of DSL modems. The test loops have various lengths and have several bridged taps and wire gauge changes [101]. These test loops can be used by manufacturers and researchers to evaluate their design and algorithms.

Loading coils

At the beginning of the twentieth century, telephone loops were periodically loaded with series inductances to create a flatter frequency response in the voice band. As a side-effect, this also created a sharp cut-off around 3 kHz. For DSL to be possible on such lines, the coils need to be removed.

1.3.4 Interference

Crosstalk

By using slightly different twist rates for all pairs, the crosstalk can be minimized. However, it is not completely gone, and it is an important source of interference. The crosstalk can be divided into several types: *far-end crosstalk* (FEXT) results from signals traveling in the same direction on twisted pairs, while *near-end crosstalk*

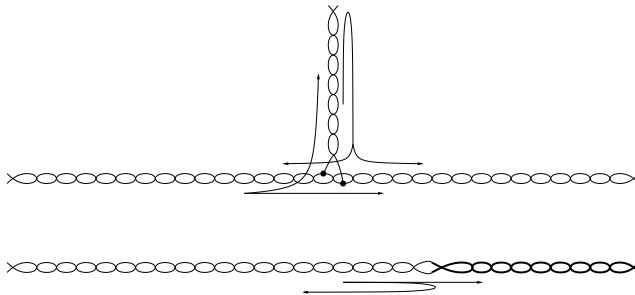


Figure 1.5: A bridged tap and a splice both generate reflections

(NEXT) is crosstalk between signals traveling in opposite directions. This is illustrated in **Fig. 1.6**. The coupling between telephone pairs, from the point of view of digital communications, was first studied by *Salz* in 1985 [162]. In the early days of DSL, this crosstalk used to be the primary limitation for DSL [67]. Due to advances in coordination between the users in a multiple-input, multiple output (MIMO) fashion, this is no longer the case, the dominant disturbance now being home-generated noise. This coordination is further discussed in section 2.2.2

Echo

On top of the crosstalk from other communications, the echo of the own transmitted signal also interferes with the reception. A substantial amount of this echo energy comes from the impedance mismatching at the *hybrid*, a duplexing device that separates the transmitted and received signals. The echo can be mitigated using adaptive filters.

RF ingress and egress

The loop acts as an antenna for HF signals, e.g. from AM broadcast stations and radio amateurs. In principle the balanced structure and the twisting of the line should prevent this, but especially at higher frequencies this is not sufficient. If there is any unbalance, the pickup on each wire will be different in amplitude and phase, resulting in a differential-mode signal [78, Chapter 9]. For typical installations, this unbalance has been estimated, to be about -35 dB with a worst case of about -30 dB [16].

The bandwidth of AM broadcast station is 10 kHz, that of amateur radio stations around 4 kHz. In principle, this narrow-band interference should only affect a few tones. However, because of the rather high side lobes of the DFT, the interference is smeared out over a much wider frequency range. This can be prevented by using

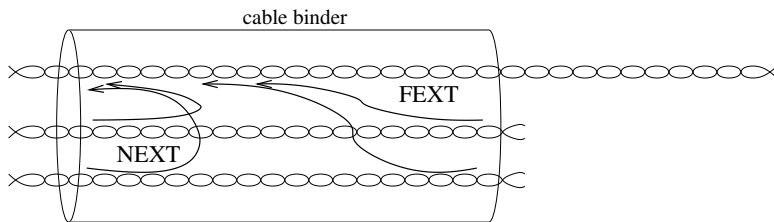


Figure 1.6: NEXT and FEXT in a cable binder. While interference from other users used to be a limiting factor for DSL, it can now be exploited by coordinating the transmissions.

windowing functions to make the DFT more spectrally contained [79]. Unfortunately, this generally leads to a loss of orthogonality between the tones, and adds complexity to the equalizer. In chapter 3 we present a technique of combined windowing and equalization to reduce the spectral leakage at the receiver side. This research was carried out in cooperation with *Alcatel* and patented by them [38], [35].

The dual problem also exists: emanation of radio waves that interfere with radio communication. And again, because of the side lobes of the DFT, it does not suffice to turn off the tones overlapping with the victim band. To reduce the egress from the telephone loop to radio receivers, windowing at the transmit side can be used. Generally this will disturb the orthogonality between the tones. The orthogonality can be maintained by making the symbols longer [117], but this would lower the transmission efficiency. In chapter 4 a special class of windowing functions is presented, for which the recovery of the orthogonality between the tones can be done with very limited complexity [39].

Impulse noise

Impulse noise is the non-stationary crosstalk from temporary electromagnetic events in the vicinity of phone lines, such as refrigerators turning on. It is difficult to eliminate, and with improving solutions for the mitigation of NEXT and FEXT, may become the limiting factor for DSL.

1.4 Outline of the thesis and contributions

The thesis is mainly composed of journal articles. Chapters 3, and 4 and 7 are related to the DSL context, while chapters 5 and 6 treat the frequency-domain equalization of SC systems.

Chapter 2 provides the introductory mathematical foundations of OFDM and SC-FDE systems.

Chapter 3 describes a combination of equalization and windowing functions for DMT-receivers to offer an improved protection against narrow-band interference. A general windowing function would interfere with the equalizer used, which is a so-called *per-tone equalizer* (PTEQ), explained in more detail in chapter 2. The method, described in chapter 3 uses both a *trapezoidal window* and a *raised cosine* window, and explains how these can be integrated with the PTEQ.

Chapter 4 considers the opposite problem: how can egress, from the DSL-system to other communications be prevented. With the increasing bandwidth of DSL

communication, they overlap more and more with existing protected radio spectrum where no energy may emanate from the twisted pair. Unfortunately it does not suffice to "turn off" the tones overlapping with this forbidden zone of the spectrum. Also in this case will the high side lobes of the DFT lead to a leakage, even from tones which are not neighbouring the forbidden zone. Again, it is possible to solve this problem by applying a windowing function, but this time at the *transmitter* side. This is even more influential, because it implies that the tones already lose their orthogonality right from the start. In chapter 4 we therefore develop a special class of windows with the property that they can easily be compensated for at the receiver. We also show how this special class of windows can be helpful for OFDM based on *known signal padding* (KSP).

Chapter 5 deals with the frequency-domain equalization of *zero-padded single-carrier* (ZP-SC) transmissions, more specifically in the presence of *spectral zeros*, i.e. tones for which the channel frequency response dips to zero. Simple equalizers react to this situation by strongly amplifying these tones, leading to a blowup of noise. One of the advantages of the ZP over the CP is that a ZP-based transmission can always be equalized, regardless of the presence of spectral zeros. To lower the complexity of the equalization, it can be done in the frequency domain, in a fashion very similar to OFDM. However, this *frequency-domain equalization* (FDE) brings the risk of re-introducing the problem of spectral zeros, and the possible loss of the information that was modulated onto these tones. In chapter 5 we show how the lost information can be recovered by exploiting the redundancy, offered by the ZP, in the time domain.

Chapter 6 combines the strong elements of the *zero-restoration* from chapter 5 and the PTEQ into a powerful equalizer.

Finally, in chapter 7 we cover an interpolation technique for DSL receivers, based on Chebyshev polynomials.

Chapter 2

Basic concepts

In this chapter we give a mathematical description of multicarrier modulation and equalization, applied to the case of DMT and OFDM. Frequency domain equalization for SC will also be highlighted.

2.1 Multicarrier modulation

2.1.1 The CP

In chapter 1 we mentioned that the CP is needed to maintain the orthogonality between the tones. This was intuitively clear from **Fig. 1.3**, but will now be explained more rigorously.

Assume we transmit samples x_0, x_1, \dots , grouped in blocks $\bar{\mathbf{x}}^k$ of length M with time index k . The channel is modeled as a *finite impulse response* (FIR) filter \mathbf{h} of order L . The received samples are also grouped in blocks $\bar{\mathbf{y}}^k$ of length M . They are contaminated by white noise $\bar{\mathbf{n}}^k$, but also by ISI from the preceding transmitted block

$\bar{\mathbf{x}}^{k-1}$. In matrix form, this looks as follows:

$$\underbrace{\begin{bmatrix} y_{kM} \\ \vdots \\ y_{(k+1)M-1} \end{bmatrix}}_{\bar{\mathbf{y}}^k} = \underbrace{\begin{bmatrix} h_0 & & & & \\ \vdots & \ddots & & & \\ & h_L & & \ddots & \\ & & & & h_0 \end{bmatrix}}_{\mathbf{H}_{0,(M \times M)}} \underbrace{\begin{bmatrix} x_{kM} \\ \vdots \\ x_{(k+1)M-1} \end{bmatrix}}_{\bar{\mathbf{x}}^k} \quad (2.1)$$

$$+ \underbrace{\begin{bmatrix} & & h_L \dots h_1 \\ & & \vdots \\ & & h_L \end{bmatrix}}_{\mathbf{H}_{1,(M \times M)}} \underbrace{\begin{bmatrix} x^{(k-1)M} \\ \vdots \\ x_{kM-1} \end{bmatrix}}_{\bar{\mathbf{x}}^{k-1}} + \bar{\mathbf{n}}^k,$$

where \mathbf{H}_0 represents the linear channel convolution matrix of \mathbf{h} and \mathbf{H}_1 expresses the ISI contribution of $\bar{\mathbf{x}}^{k-1}$.

With the current structure of \mathbf{H}_0 and the annoying \mathbf{H}_1 , equalization is a difficult task. To improve this, we insert a cyclic prefix of length ν . Mathematically this can be described by the multiplication with a matrix \mathbf{P} ,

$$\mathbf{P}_{M \times N} = \left[\begin{array}{c|c} \mathbf{O}_{(N-\nu) \times \nu} & \mathbf{I}_\nu \\ \hline \mathbf{I}_N & \end{array} \right]. \quad (2.2)$$

Because the CP occupies ν samples, and we want to keep the transmitted block size equal to M , we now start from smaller input blocks of length N , called \mathbf{x}^k and name the received blocks \mathbf{y}_{CP}^k such that we can now write

$$\underbrace{\begin{bmatrix} y_{kM} \\ \vdots \\ y_{(k+1)M} \end{bmatrix}}_{\mathbf{y}_{\text{CP}}^k} = \mathbf{H}_0 \mathbf{P} \underbrace{\begin{bmatrix} x^{kN} \\ \vdots \\ x^{(k+1)N-1} \end{bmatrix}}_{\mathbf{x}^k} + \mathbf{H}_1 \mathbf{P} \underbrace{\begin{bmatrix} x^{(k-1)N} \\ \vdots \\ x_{kN-1} \end{bmatrix}}_{\mathbf{x}^{k-1}} + \mathbf{n}^k, \quad (2.3)$$

The elaboration of Eq. (2.3) depends strongly on the relation between L and ν . More specifically, we can distinguish the case of a *short channel* ($L \leq \nu$) and a *long channel* ($L > \nu$).

If we define \mathbf{s}^k and \mathbf{r}^k such that $\mathbf{s}^k = \mathcal{F}_M \mathbf{x}^k$ and $\mathbf{r}^k = \mathcal{F}_M \mathbf{y}^k$, we can write

$$\mathbf{r}^k = \mathcal{F}_M (\mathbf{C} \mathbf{x}^k + \mathbf{Q} \mathbf{n}^k) \quad (2.8)$$

$$= \mathcal{F}_M \mathcal{F}_M^H \mathbf{\Lambda} \mathcal{F}_M \mathbf{x}^k + \mathcal{F}_M \mathbf{Q} \mathbf{n}^k \quad (2.9)$$

$$= \mathbf{\Lambda} \mathbf{s}^k + \tilde{\mathbf{n}}^k \quad (2.10)$$

The dispersive channel is now decomposed into a collection of flat-fading channels. The practical application to OFDM systems is straightforward and is illustrated in **Fig. 2.1**: the tone vector \mathbf{s}^k is modulated using the IDFT and a CP is appended. The result is then serialized and transmitted over the channel where it is filtered and contaminated with Gaussian noise. At the receiver, the incoming samples are grouped in a block, the CP is discarded, and the block is demodulated using the DFT, resulting in the tone vector \mathbf{r}^k .

The channel equalization is now trivial: all we have to do is multiply \mathbf{r}^k with the inverse of $\mathbf{\Lambda}$ to obtain an estimate for \mathbf{s}^k , i.e.

$$\hat{\mathbf{s}}^k = \mathbf{\Lambda}^{-1} \mathbf{r}^k \quad (2.11)$$

$$= \mathbf{s}^k + \mathbf{\Lambda}^{-1} \tilde{\mathbf{n}}^k. \quad (2.12)$$

Unfortunately the term $\mathbf{\Lambda}^{-1} \tilde{\mathbf{n}}^k$ looks rather ominous. Keeping in mind that the diagonal of $\mathbf{\Lambda}$ contains the channel frequency response, $\mathbf{\Lambda}^{-1}$ may contain very large values at frequencies for which the channel response dips towards zero, leading to *noise enhancement* [59]. This is an important problem, which we will come back to in section 2.2.4 and also in much more detail in chapter 5.

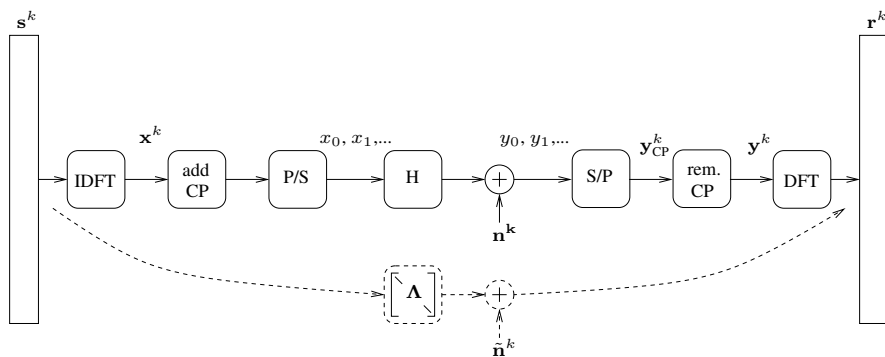


Figure 2.1: The OFDM modulation scheme. The transformation with DFT and IDFT matrices and the insertion and removal of the CP decomposes the dispersive channel into a collection of flat-fading channels.

equalization, regardless of channel zero locations [164]. Indeed, the *tall thin matrix* of Eq. (2.17) is always of full column rank and therefore a left inverse always exists,¹ while the circular matrix \mathbf{C} is not necessarily of full rank. This issue will be covered in much more detail in chapter 5.

Known signal padding

A KSP, also called a *unique word* (UW) [211], is a predefined sequence of samples, known by the transmitter and the receiver, which is inserted in between the transmitted blocks. Because the KSP is fixed, its contribution can be predicted at the receiver, and be subtracted from the incoming signals. At that point, the system behaves like a ZP-based system and the mathematics are comparable [178]. Alternatively, it can be considered as a cyclic extension which is shared between successive symbols, leading to a solution based on a DFT-size of $(N + \nu)$ [211].

A disadvantage of the KSP, with respect to the ZP, is that it consumes power which does not contribute to the useful signal. However, it is very useful for channel estimation and synchronization [91].

Note that, because the data is encoded in the frequency domain, and the KSP is defined in the time domain, it is nontrivial to generate. The typical way to do so, is to assign so-called *pilot tones* in the frequency domain. These pilot tones don't carry information, but are modulated such that the KSP appears in the time domain. In general, determining the required modulation of the pilot tones is rather complex [90], [88]. In chapter 4.6, we will present a cheaper alternative method.

For comparison, the CP, ZP and KSP are illustrated in **Fig. 2.2**.

2.2 Discrete multi-tone

Discrete multi-tone (DMT) is the standard which was adopted for ADSL, and that has been in use ever since for the next generations of DSL systems.

2.2.1 Transmitter and modulation

Because DMT is a base-band system, the vector \mathbf{x}^k needs to be real-valued, introducing a symmetry condition on s^k . In practice this means that only the first half of the tone vector s^k is used for data transmission and the second half is a complex conjugate

¹Note that this left inverse is not unique.

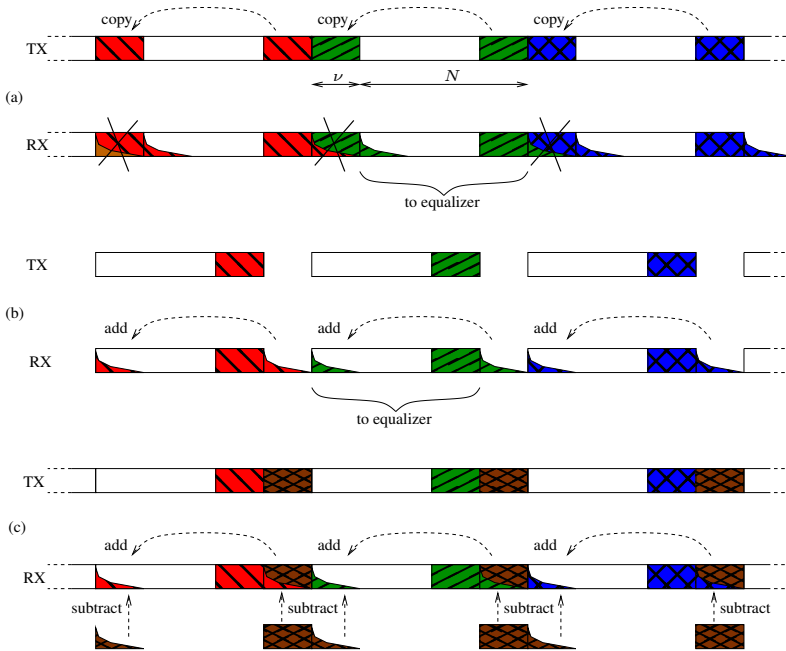


Figure 2.2: Comparison of the CP (a), ZP (b) and KSP (c).

symmetrical copy of the first half. For the case of ADSL, the DFT-size $N = 512$, CP length $\nu = 32$ and the tone spacing is 4.3125 kHz, leading to a total bandwidth of 1.104 MHz. More advanced DMT schemes, like VDSL keep the same tone spacing, but use a larger number of tones.

This is shown in **Fig. 2.3**. We have also included the *mapper*, which converts the binary stream of data to constellation points for each tone, the digital-to-analog converter and the analog front-end (AFE), which includes the analog filtering and the line driver.

Note that DMT uses *pilot tones*, which have a fixed modulation and cannot be used to convey information. The pilots assist in synchronization and equalization at the receiver size. Tone 64 is such a pilot for ADSL, and has constant, non-varying modulation. Because 64 is an integer multiple of 16, the ratio between the DFT size and the CP length, the pilot tone signal has no discontinuity at the symbol edges in the time domain.

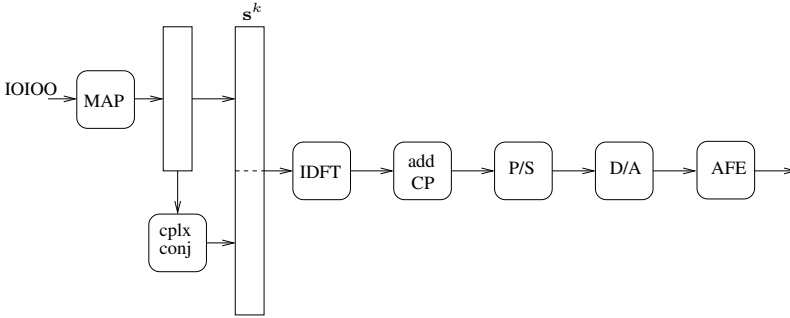


Figure 2.3: The DMT transmitter. Only the lowest half of the tone vector can be chosen freely. The higher half is a complex conjugate symmetrical copy of the lower half.

Gap and margin

It is well known that the channel capacity is given by the formula of Shannon and Hartley (see appendix, Eq. (A.3)). Note that this is a theoretical result for an *ideal* system. For practical systems, the actual rate will be lower than the channel capacity. For any given coding scheme and a target probability of error P_e , the rate R can be expressed as

$$R = B \log_2 \left(1 + \frac{\text{SNR}}{\Gamma} \right), \quad (2.18)$$

with Γ the so-called *gap*. The gap is an indication of the quality of the coding scheme, where smaller is better. An ideal coding scheme has a gap of 1 (i.e. 0 dB). The gap from an uncoded modulation e.g. QAM can be lowered by using coding, e.g. trellis coding or forward error correcting coding. The key obstacle to practically approaching channel capacity was not the construction of good codes, rather it was the problem of decoding complexity [63]. For DSL the attainable gap is close to 1 or 2 dB [31].

2.2.2 Bit loading

An interesting advantage of DMT over OFDM is that the variations over time of the channel characteristic are limited, and the connections are always point-to-point. This allows to estimate the channel characteristic and use this knowledge to distribute the available power over the different carriers in an intelligent way. This has two advantages. Firstly, it is possible to assign more energy, and therefore bits, to high quality carriers and to discard carriers with a spectral response close to zero, or with a large interference due to noise. Secondly, it allows to coordinate between different users in a cable binder, minimizing the mutual interference and maximizing the throughput.

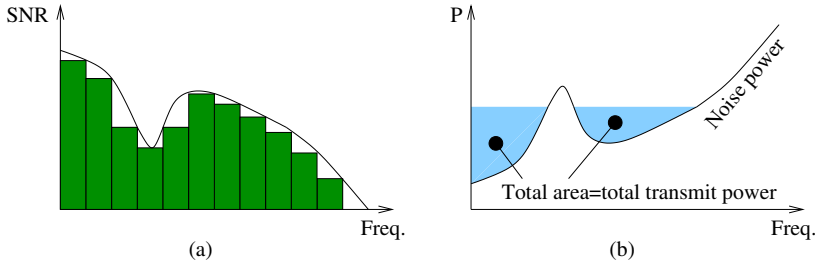


Figure 2.4: The subchannels can be considered as flat-fading (a). The water-filling algorithm for the single-user case (b).

In the single-user case, the bit-allocation is rather simple. The multi-user case is much more complex.

Single user scenario

The variation in the spectral response within one subchannel is typically small enough to consider it as flat fading. We can therefore apply Shannon's formula or, more precisely, Eq. (2.18) to each subband, as shown in **Fig. 2.4a**.

The rate of a DMT system in the presence of white noise equals the sum of the rates of the individual flat-fading subchannels. Obviously this will be dependent on the power which is assigned to each carrier, so how should this be done? This question was answered by Shannon, who proved that for each subband the sum of the noise power and the signal power should be equal [166]. This is known as the *water-filling* algorithm, because it looks as if the noise power curve should be 'filled' with water to obtain the signal power distribution, as illustrated in **Fig. 2.4b**. Obviously also more elaborate algorithms have been developed, taking into account the granularity of the power distribution over the tones [28]. In general, the most crucial aspect of loading algorithms is determining which subchannels to turn off and which ones to turn on. Turning on a subchannel which should actually be off increases the probability of error in that subchannel which then dominates the overall probability of error [112], [113].

After startup the receiver measures the signal quality on each subchannel and calculates the optimal bit loading, which is then fed back to the transmitter [101]. The bit-loading is subject to power spectral density constraint masks. To ensure widespread deployment, these masks are based on worst case scenarios [6].

A practical result of this bit-loading for the case of ADSL2+ is shown in **Fig. 2.5**. Note that this figure also shows the pilot tones.

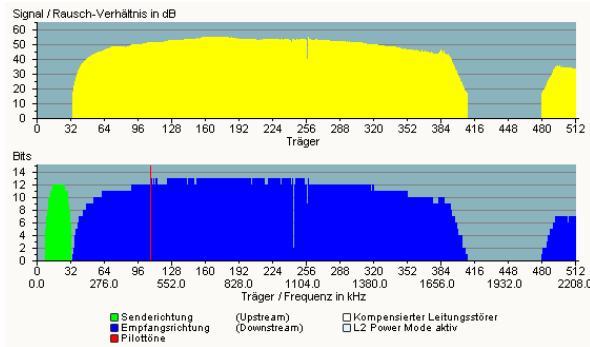


Figure 2.5: A practical example of the SNR and bitloading in a DSL system.

Dynamic spectrum management

In the multi-user context, where we not only need to take into account the thermal noise, but also the crosstalk from other users, the problem of bit-allocation is significantly more complex, and has been a topic of intensive research [22], [189], [129]. It is the most significant factor in the performance of DSL systems and has the potential to severely limit the performance of the system if it is not dealt with [89].

The adaptive approach, based on a coordination between the individual DSL links is known as *dynamic spectrum management* [177, chap. 11], [174]. Four levels of coordination are distinguished, with level 0 being the absence of coordination, level 1 and 2 using spectrum coordination, and level 3 using a coordination at signal level.

One of the first algorithms for level 1 DSM was *iterative water filling* (IW) [216]. Like the name suggests, this algorithm tries to find the optimal power allocation by sequentially applying the water filling algorithm for each user individually, taking into account interference from other users. Each user selfishly maximizes its own data-rate. Not only does this lead to a suboptimal result because of the inefficient use of the frequency spectrum, moreover, it isn't fair, e.g. because users that are far away from the DSLAM will be at a disadvantage.

For level 2 DSM, the transmit spectra are controlled by a spectrum management center. A centralized algorithm called *Optimal Spectrum Balancing* (OSB) was developed to solve for the globally optimal power allocation. While OSB is not computationally tractable for many users, it serves as an upper bound on the performance of other DSM algorithms for cases with few users [24]. Later on, cheaper suboptimal algorithms were introduced. A good overview of such algorithms is given in [89].

In DSM level 3, also known as *vectoring* [70], the users are coordinated on a *signal*

level, using techniques developed for wireless multi-input multi-output (MIMO) communication. A MIMO transmitter and receiver have multiple -say N - antennas, leading to N^2 interactions between these antennas. These interactions can be represented in a matrix. By using a precoding at the transmitter and a postcoding at the receiver, this matrix can be decomposed into a diagonal form, resulting in N virtual channels² *at the same frequency* [64]. Something similar can be done for DSL, where the binder effectively becomes a multi-user communication system [180]. The coordination requires estimates of all crosstalk channels and can only happen at a location where all user pairs are available. It therefore typically happens in the DSLAM, where all downstream transmitters and upstream receivers are co-located. The crosstalk channel estimates can be used to cancel the crosstalk of the received upstream signals and to do a precompensation to eliminate the crosstalk of the downstream signals at the CPE.

The results are impressive: where crosstalk once was the limiting factor for DSL, it has now become an advantage which can be exploited. On very short loops, spectacular results can be achieved, e.g. 10 Gbps over 30 m [33]. For vectoring to work it is essential that everyone plays nicely and that sudden changes in the crosstalk channels are avoided, e.g. because of a change in the termination impedance when a user suddenly powers off his modem [126].

2.2.3 Peak to average power ratio

The DSL signal consists of a summation of complex exponentials (in case of OFDM) or cosines (in case of DMT) with phases and amplitudes that differ from block to block. Consequently, each sample in the time domain is made up of a large sum of essentially random numbers. The *central limit theorem* therefore predicts a *Gaussian* distribution for the sample magnitude. This implies that there is a large difference between the *average* magnitude and the *peak* of the magnitude, which is expressed by the peak-to-average power ratio (PAPR),

$$PAPR = \frac{\max_n(\|x_n\|^2)}{\mathcal{E}(\|x_n\|^2)}. \quad (2.19)$$

It can be shown that for DMT or OFDM using M-PSK, the $PAPR \leq N$ [182]. Mathematically there is no objection against this, but in the real world it implies either that amplifiers should be dimensioned to handle the peaks without distortion, leading to a low efficiency, or work efficiently, leading to non-linear distortion for high magnitudes. This distortion cannot be compensated for by linear equalizers and leads to a reduced SNR.

²Note that this situation is comparable to traditional electronic beam-forming in arrays, where one array of N antennas can also maintain N independent links.

This problem has been known for a long time, and many techniques to solve it have been proposed already. Most of these are rather ad-hoc. The simplest solution is to just clip the signal in the time domain, followed by a filtering to avoid out-of-band signals.

It is better to go to the root of the problem and try to avoid the peaks themselves. Most efforts to do so boil down to providing alternative representations for the same data, or providing pilot tones that carry no information, but can be modulated to give a favourable result. These alternative representations can either be at the tone level [75], at block level [11] or in between, like in the partial transmit sequence (PTS) technique [132]. For PTS, the tone vector is divided into blocks of modulated tones; each of these blocks gets a rotation (common for all tones in the block) which is chosen to optimize the total PAPR.

Another approach is to do an exhaustive search of all possible tone vectors with a low PAPR and only encode the data on one of these [103]. As mentioned before, numerous solutions and refinements have been proposed. A good overview of solutions in the digital domain can be found here [76], [102], [114]. Alternatively, it is possible to work on the hardware itself [146].

2.2.4 Receiver and equalization

Frequency domain equalizer

From Eq. (2.10), repeated here for convenience, we know that the CP converts the dispersive channel into a collection of flat-fading channels:

$$\mathbf{r}^k = \mathbf{\Lambda} \mathbf{s}^k + \tilde{\mathbf{n}}^k. \quad (2.20)$$

The amplitude and phase of each tone is modified by multiplication with the complex channel response at the frequency of that tone.

A *frequency domain equalizer* (FEQ) aims to undo this channel influence by adjusting the phase and amplitude of each tone individually. It is therefore a *parallel one-tap complex filter*, operating at the block rate; it can be implemented as a multiplication of the tone vector \mathbf{r}^k by a complex diagonal matrix.

An obvious choice for the FEQ is the one used in Eq. (2.11), i.e.

$$\mathbf{W}_{\text{ZFE}} = \mathbf{\Lambda}^{-1}. \quad (2.21)$$

This particular FEQ is a *zero-forcing equalizer* (ZFE). The expected value of its output equals the transmitted signal:

$$\mathcal{E} \left\{ \mathbf{W}_{\text{ZFE}} \mathbf{r}^k \right\} = \mathbf{s}^k. \quad (2.22)$$

At first sight this is what we want. However, Eq. (2.22) gives no information about the *deviation* from the expected value, which may be very large. This is a well-known weakness of ZFEs [59].

Instead of using the expected value of the equalized output as a criterion, it is better to use the expected value of the error. More specifically, the *minimum mean squared error* (MMSE) FEQ is the one that minimizes the following cost function:

$$J(\mathbf{W}) = \mathcal{E} \left\{ \text{tr} \left\{ (\mathbf{W}\mathbf{r}^k - \mathbf{s}^k) (\mathbf{W}\mathbf{r}^k - \mathbf{s}^k)^{\mathcal{H}} \right\} \right\}. \quad (2.23)$$

Assuming that the transmitted signal and the noise have a variance of 1 and σ_n respectively, \mathbf{W}_{MMSE} is given by

$$\mathbf{W}_{\text{MMSE}} = (\sigma_n^2 \mathbf{I} + \mathbf{\Lambda} \mathbf{\Lambda}^{\mathcal{H}})^{-1} \mathbf{\Lambda}^{\mathcal{H}}. \quad (2.24)$$

Note that for high values of the SNR, \mathbf{W}_{MMSE} approaches \mathbf{W}_{ZFE} .

Time domain equalizer

In case the channel order exceeds the prefix length, ISI and ICI are unavoidable, regardless of the FEQ design [87], [149]. Instead of increasing the CP length, which incurs a loss in transmission efficiency, the *time domain equalizer* (TEQ) was invented to remedy this problem [198]. The TEQ is an FIR filter \mathbf{t} , operating in the time domain at the sample rate. After the TEQ, the part of the block corresponding to the CP is removed, and the symbol is further equalized using a FEQ, as shown in **Fig. 2.6**.

Ideally, the TEQ is designed such that the cascade of the channel impulse response and the TEQ has an extension in time which is shorter than the CP. In practice this is often not possible, and other criteria are used, e.g. maximization of the bit rate [8], [202]. More TEQ designs are discussed in [200].

Per-Tone equalizer

The TEQ+FEQ can be replaced by a combined structure called a *per-tone equalizer* (PTEQ) [194]. The PTEQ moves the TEQ behind the DFT, offering each tone its own multi-tap equalizer, based on the output of a sliding DFT. Each tone i is equalized based on a linear combination \mathbf{w}_i of the outputs of the sliding DFT at that tone i , as shown in **Fig. 2.7**.

Moreover, the sliding DFT can be replaced by one full DFT and difference terms, such that each tone i can now be equalized based on a linear combination \mathbf{v}_i of the output of the DFT at tone i and the difference terms. This is illustrated in **Fig. 2.8**. Because these

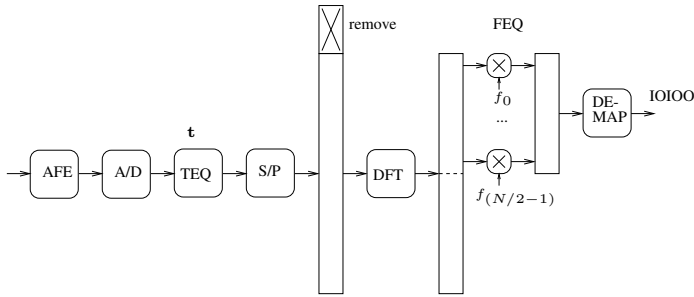


Figure 2.6: The TEQ+FEQ-based DMT receiver. The TEQ shortens the channel impulse response and the FEQ corrects the tones' amplitude and phase.

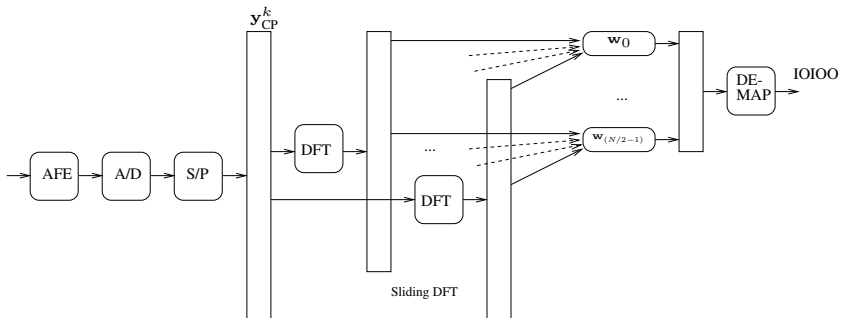


Figure 2.7: The PTEQ-based DMT receiver. The TEQ is moved behind the DFT, which becomes a *sliding DFT*. Each tone is equalized based on an individual linear combination of the sliding DFT outputs at that tone.

equalizers now run at the block rate instead of the sample rate and because only one DFT needs to be calculated, the complexity is comparable to that of the TEQ+FEQ.

A problem with TEQ+FEQ-designs is the nontrivial relation between the filter coefficients and the eventual equalizer performance. The advantage of the PTEQ is that it optimizes the capacity for each tone individually -each tone has its own v_i , whereas the TEQ t is common for all tones- and therefore also optimizes the overall capacity [148]. It is an important building block, which is used as a starting point for more complex equalizers in chapters 3 and 6.

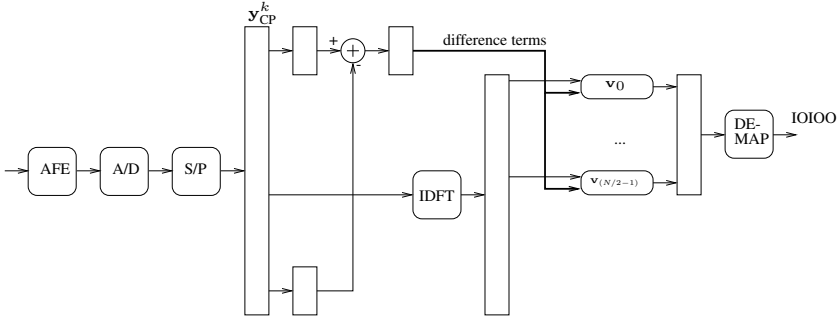


Figure 2.8: The PTEQ based on difference terms. The sliding DFT is replaced by one full DFT and difference terms. Each tone is equalized based on an individual linear combination of the DFT output at that tone and the difference terms.

2.2.5 Windowing

As mentioned before, the spectrum used by DSL overlaps with the spectrum of possibly powerful narrow-band transmitters, leading to RFI ingress. At first sight this need not be such a big problem because the RFI only overlaps with a limited number of tones.

Unfortunately, the RFI does not only interfere with the tones that overlap directly. The DSL receiver only considers a frame of N samples, on which the DFT is performed, and because of the slow side-lobe roll-off of the sinc-function, neighbouring tones are also affected. More specifically, if we consider one interferer, modeled in the frequency domain as a single impulse at ω_{RFI} , its contribution to the interference at tone i will be proportional to [214]:

$$\sigma_{\text{RFI},i} \sim \frac{\sin^2 \left(N \left(\frac{2\pi i}{N} - \omega_{\text{RFI}} \right) / 2 \right)}{\left(N \left(\frac{2\pi i}{N} - \omega_{\text{RFI}} \right) / 2 \right)^2}. \quad (2.25)$$

In case the frequency of the interferer is placed exactly on the frequency grid of the DMT system, interference is limited to the one particular tone it coincides with. Otherwise, the energy of the interferer leaks to a large number of tones -theoretically all of them. This effect is most severe if the interferer is located exactly in the middle of two tones [71].

How can this spreading out of interference over all tones be limited? It is well-known that applying a window function prior to the DFT has a strong influence on the decay of the side-lobes [150, chapter 7]. However, this cannot be just any window function. Simply applying a window to the received symbol will destroy the orthogonality

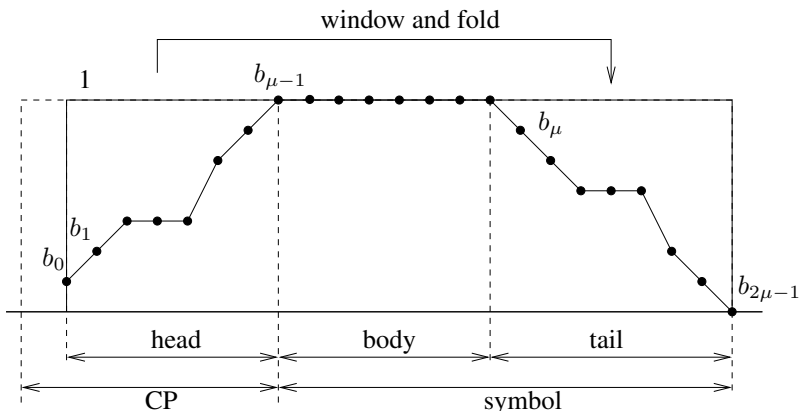


Figure 2.9: To maintain the orthogonality between the tones, the window should extend beyond the DFT size and the head and tail should be complementary.

between the tones, resulting in ICI [176]. In some cases this can be overcome by trying to cancel this (predictable) ICI [105].

A way to maintain the orthogonality is to let the window extend μ samples beyond the DFT-size N , into the CP and fold back these extensions after the multiplication with the time-domain samples [176]. If we divide the window function into three parts: the head, body and tail, then the body should be of unity value, and the head and tail should be complementary, as illustrated in **Fig. 2.9**.

It is trivial to combine the use of windowing functions with a TEQ+FEQ design. The windowing function can be chosen freely, and can be combined with the TEQ design itself [215]. However, the combination of windowing functions and the PTEQ is not so straightforward. More specifically, without any constraint on the windowing function, it is not possible to replace the sliding DFT by a single DFT and difference terms. In chapter 3 we show the PTEQ can be combined efficiently with two types of windows, a trapezoidally tapered window and a raised cosine window.

Note that there are also other methods for the mitigation of RFI, be it in the analog or digital domain, e.g. using notch filters. Alternatively, instead of canceling the RFI or avoiding the leakage of the DFT, it has been proposed to estimate the influence of the RFI on some unmodulated pilot tones and to use this information to cancel the influence of the RFI on the modulated tones [172].

2.3 Single-carrier block transmission with frequency domain equalization

2.3.1 Motivation

After an initial hesitation to adopt OFDM, it has been embraced as a powerful technique to handle channel dispersion and make optimal use of the available spectrum. However, it also has drawbacks, such as intolerance to amplifier nonlinearities and a high sensitivity to carrier frequency offsets [144]. A very important one, especially for portable devices, is the high PAPR.³

In contrast, the PAPR problem is far less pronounced in *single-carrier* (SC) transmissions, because these either use a PSK-based encoding with constant modulus, or a QAM-based constellation which typically also has a modest PAPR. It would therefore be interesting to combine the advantages of OFDM's simple FDE and the low PAPR of SC.

The key to this problem is the realization that the equalizer at the receiver "*doesn't know*" what the data in the frequency domain represents. Instead of tones carrying individual OFDM-data, it can also be e.g. the DFT of a SC block transmission. By moving the IDFT operation from the transmitter to the receiver, it is therefore possible to benefit from the low-PAPR of SC, while exploiting the low complexity of FDE, leading to a *single carrier block transmission with frequency domain equalization* (SC-FDE), as illustrated in **Fig. 2.10**.

The SC-FDE represents the ideal marriage between a good PAPR and ease of equalization. Because of this lower PAPR, it has a higher power efficiency than OFDM [190]. Interestingly, the idea of what is now called SC-FDE dates back to 1973 [203], but was laid to rest until years later. Even though frequency-domain techniques to implement FIR filters were very well known in digital signal processing [170], it lasted until 1995 before the resemblance with OFDM was observed and SC-FDE was proposed [163]. Since then, SC-FDE has been picked up as a viable competitor for OFDM and is becoming increasingly important [60]. For more details on the demodulation of zero-padded transmissions we refer to chapter 5.

While the original proposal of 1973 used a ZP in between the blocks [203], it is also possible to use another GI, like a CP or KSP [211], [46], [210]. One particular advantage of SC block transmission over OFDM is the easy integration of a KSP within the length of the DFT size. With respect to **Fig. 2.2**, this means that the equalization

³Note that a high PAPR may be an inherent property of efficient communication. The one-dimensional continuous distribution function that maximizes the entropy for a fixed average power, is the Gaussian distribution [7, p.225]. Or, as the adage goes: "Any sufficiently advanced modulation scheme is virtually indistinguishable from noise" [169].

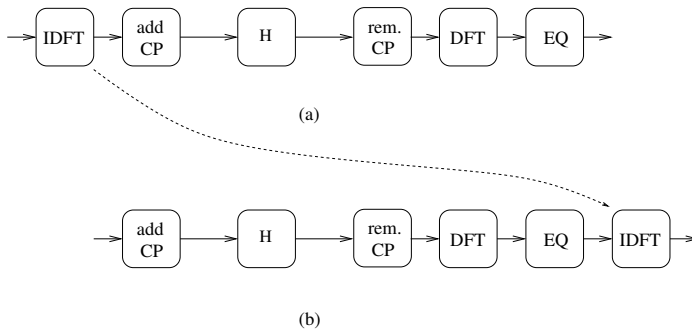


Figure 2.10: By moving the IDFT from the transmitter to the receiver, OFDM (a) can be transformed into SC-FDE (b), combining a low PAPR with inexpensive equalization.

will be based on a DFT-size of $(N + \nu)$ instead of N , and the KSP will also be equalized. In the case of OFDM it is much more difficult to achieve a certain KSP in the time domain [90], as mentioned before. This topic is elaborated in section 4.6.

Note that OFDM and SC can be elegantly described under one unifying theory of *transmultiplexers*, together with e.g. code division multiple access (CDMA) and wavelet encoding [4].

2.3.2 Single carrier frequency division multiple access

Note that the high PAPR of OFDM signals is mostly problematic for transmitters, because of the linearity requirements and the consequent limited efficiency of power amplifiers. At the receiving side it is less dramatic because a low noise amplifier (LNA) has a lower power consumption, even if the linearity requirements are strict. It is therefore possible to combine individual SC transmissions (each with low PAPR) into one OFDM signal. This is exactly what happens in single carrier frequency division multiple access (SC-FDMA), which has been selected as the encoding for the uplink in *long term evolution* (LTE), aka 4G [159], [58].

Conceptually, all users simultaneously transmit an OFDM signal in which only a few exclusive tones are active for that user and the others are set to zero. Because of the smart choice of the assigned tones, this individual OFDM signal is equivalent to a SC transmission, which has the advantageous low PAPR and which explains the name of the encoding schema. In practice the assignment of the tones to each user varies over time to level out the good and bad tones. The uplink receiver at the base station can process the sum of all individual SC signals simultaneously as one large OFDM block.

Chapter 3

Receiver windowing

This chapter is based on the article *Combined per tone equalization and receiver windowing in DSL receivers: WiPTEQ* [42], as published in *Elsevier Signal Processing*. Only the layout and the numbering of the references, equations and figures have been changed to accommodate for the different page size and to improve consistency. The research in this chapter was done in collaboration with *Alcatel* and was patented [38], [35].

List of symbols

Lower case bold-faced letters are used to denote vectors and upper case bold-faced letters to denote matrices. In addition, the following notation is used throughout the text:

\mathbf{A}^T	the transpose of \mathbf{A}
$\mathbf{A}(k, :)$	row k of matrix \mathbf{A}
$\mathbf{I}_{r \times c}$	unity matrix of size $r \times c$
$\mathbf{O}_{r \times c}$	zero matrix of size $r \times c$
J	cost function
$\min_{\mathbf{x}} J$	the minimization of J over \mathbf{x}
$\mathcal{E}\{\cdot\}$	expected value

Number of pages: 42 (including figures and tables)

Number of figures: 12

Number of tables: 5

Keywords: DSL, equalization, window functions, interference, PTEQ

Abstract

A novel technique is described for the combination of per-tone equalization (PTEQ) with receiver windowing. The PTEQ is an equalization technique for discrete multitone modulation (DMT) based modems, such as asymmetric digital subscriber line (ADSL) modems and very high bitrate digital subscriber line (VDSL) modems, optimizing the SNR (and thus capacity) of each carrier separately. Windowing functions are very useful in multitone communications systems, to prevent a narrow band noise source from causing wide band interference. Combining both techniques in a windowed PTEQ (referred to as WiPTEQ) leads to a robust communication system. The described technique is especially useful in case of a trapezoidal or raised cosine window, and when the window taper length is large compared to the number of equalizer filter taps.

3.1 Introduction and motivation

Asymmetric Digital Subscriber Loop (ADSL) makes use of *discrete multitone modulation* (DMT): the spectrum is divided into a large number of bands. Carriers (tones) in these bands are (de)modulated in the digital domain, through a (*inverse*) *Discrete Fourier Transform* (DFT), in practice carried out using the *Fast Fourier Transform* (FFT) algorithm [31]. Equalization is facilitated by a *cyclic prefix* (CP) preceding each symbol [145]. As long as the channel impulse response length does not exceed the CP length the equalization of each tone can be done easily through a one-tap frequency domain equalizer (FEQ), consisting of a multiplication and phase shift for each tone individually.

Since the prefix does not carry any useful information, it is kept as short as possible, implying that often the channel impulse response length exceeds the cyclic prefix, such that the aforementioned condition for easy equalization does not hold, and inter carrier interference (ICI) results ([149], [165], [87], [21]). Classical DMT receiver schemes (e.g. for ADSL) make use of a time domain equalizer (TEQ) to shorten the channel such that the cascade of the channel and TEQ is shorter than the CP, shown in **Fig.3.1**. This TEQ is mostly implemented as a finite impulse response (FIR) filter of length T taps. Many algorithms have been developed to initialize the TEQ using training sequences. The final result depends on the optimization criterion used, but in general the resulting capacity is suboptimal (although there are exceptions, e.g. [5], [201]).

In [196] a new receiver structure, based on so-called *per tone equalization* (PTEQ), has been developed as an alternative to the classical TEQ. For each tone separately, a T -taps FEQ is constructed that maximizes the SNR on that tone. In [196], it is shown that the PTEQ of length T offers a performance upper bound for any TEQ design of the same length.

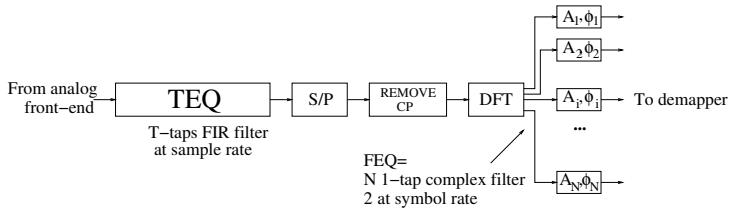


Figure 3.1: Classical receiver block scheme with a time domain equalizer, serial-to-parallel converter, removal of the cyclic prefix DFT and one-tap complex frequency domain equalizer

The spectrum occupied by high speed digital subscriber line (DSL) modems overlaps with the bands used for radio communications. AM broadcast stations and amateur radio transmitters introduce radio frequency interference (RFI) impairing the DSL-receiver. For discrete multitone (DMT) based *Very high-bitrate Digital Subscriber Loop* (VDSL) modems, *receiver windowing* is used to reduce the effect of spectral leakage of such narrow band RFI. However, also for ADSL, the use of windowing functions is important in order to sustain high rates under RFI conditions, as will be shown later. In [154], a procedure is given to calculate an optimal window, given an existing TEQ.

In [197] it was shown that applying a time domain window is equivalent to applying a fixed per-tone equalizer, be it with different equalizer coefficients for different tones. However, the straightforward implementation of the windowing operation as a per tone equalization is computationally demanding.

In the presence of RFI, the PTEQ effectively behaves as a windowing function for each tone separately, but obviously only if the RFI is also present during equalizer training. In case RFI emerges only after the training phase, neither the classical TEQ nor the PTEQ handle this interference satisfactory. We describe a novel method for combining windowing with per tone equalization. The windowing operation stays in place and is done before the FFT. The PTEQ is modified to take windowing into account, hence the name window incorporating PTEQ (WiPTEQ). More specifically, a new scheme is developed, based on the efficient implementation of a sliding windowed FFT (as opposed to the simple sliding FFT formula used by the PTEQ when no windowing is applied). We will consider two specific choices for the window functions to be applied, namely the trapezoidal window [44] and the raised cosine window [41], as these correspond to practical choices in view of e.g. implementation complexity. In **Fig.3.2**, the side lobe behaviour of these windows is compared to the classical rectangular (*Dirichlet*) window.

In section 3.2, a mathematical derivation is presented, section 3.3 covers the complexity

analysis followed by performance simulation results in section 3.4. Finally in section 3.5 conclusions are drawn.

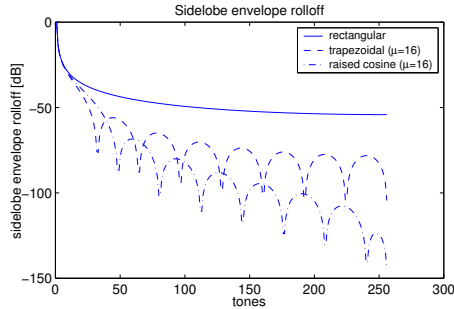


Figure 3.2: Side lobe decay of the rectangular (*Dirichlet*), *raised cosine* and *trapezoidal* window. The window taper length μ equals 16.

3.2 Mathematical derivation

Because the WiPTEQ is truly a generalization of the PTEQ ([196], [197]), this latter equalization structure will briefly be reviewed first. Our notation is as follows: N is the symbol size, expressed in samples, ν the cyclic prefix length, k the time index of a symbol, $X_i^{(k)}$ is a complex subsymbol for tone i , $i \in [1, N]$ to be transmitted at symbol period k . The received time domain samples are grouped in a column vector $\mathbf{y}^{(k)}$ of length $N + T - 1$, where T is the equalizer length. The data model is adopted from [196].

3.2.1 Per tone equalization

The TEQ filter and the DFT block (in Fig.3.1) are both linear operations, so their order can be reversed. This results in a T -taps filter $\bar{\mathbf{w}}_i$ for each tone output i , as shown in **Fig.3.3**. For each tone i , the PTEQ coefficients $\bar{\mathbf{w}}_i$ are obtained by solving the

following minimization problem (see [196] for details):

$$\min_{\bar{\mathbf{w}}_i} J(\bar{\mathbf{w}}_i) = \min_{\bar{\mathbf{w}}_i} \mathcal{E} \left\{ \bar{\mathbf{w}}_i^T \cdot \underbrace{\begin{bmatrix} \mathcal{F}_N(i, :) & 0 & \dots \\ & \ddots & \ddots \\ 0 & \dots & \mathcal{F}_N(i, :) \end{bmatrix}}_{\mathbf{F}_i^w} \cdot \mathbf{y}^{(k)} - X_i^{(k)} \right\}^2 \quad (3.1)$$

with $\mathcal{E}\{\cdot\}$ the expected value operator, $\bar{\mathbf{w}}_i^T = [w_{i,T-1} \dots w_{i,0}]$ and $\mathcal{F}_N(i, \cdot)$ the i^{th} row of the DFT matrix, i.e.

$$\mathcal{F}_N(i, \cdot) = [1 \ \alpha_i \ \dots \ \alpha_i^{N-1}], \alpha_i = e^{-\frac{j2\pi(i-1)}{N}}$$

This form is directly equivalent to a TEQ implementation, but has the major drawback that T consecutive DFTs (FFTs) need to be calculated.

A more efficient implementation is based on the use of difference terms, and requires only one DFT. The optimization problem from equation (3.1) is transformed into :

$$\min_{\bar{\mathbf{v}}_i} J(\bar{\mathbf{v}}_i) = \min_{\bar{\mathbf{v}}_i} \mathcal{E} \left\{ \bar{\mathbf{v}}_i^T \cdot \underbrace{\begin{bmatrix} \mathbf{I}_{T-1} & \mathbf{O} & -\mathbf{I}_{T-1} \\ \mathbf{O} & \mathcal{F}_N(i, \cdot) & \end{bmatrix}}_{\mathbf{F}_i^v} \cdot \mathbf{y}^{(k)} - X_i^{(k)} \right\}^2 \quad (3.2)$$

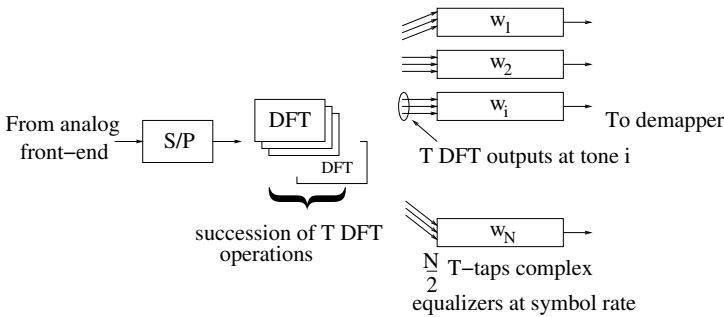


Figure 3.3: Receiver block scheme with PTEQ using successive DFTs. In practice, these are calculated using one DFT and difference terms.

This involves a transformation from $\bar{\mathbf{w}}_i$ to $\bar{\mathbf{v}}_i$ ([196]), such that $\bar{\mathbf{w}}_i^T \cdot \mathbf{F}_i^w = (\bar{\mathbf{w}}_i^T \cdot \mathbf{P}_i) \cdot (\mathbf{P}_i^{-1} \cdot \mathbf{F}_i^w) = \bar{\mathbf{v}}_i^T \cdot \mathbf{F}_i^v$, with

$$\mathbf{P}_i = \begin{bmatrix} 1 & \alpha_i & \dots & \alpha_i^{(T-1)} \\ 0 & 1 & \ddots & \ddots \\ \vdots & \ddots & \ddots & \alpha_i \\ 0 & \dots & 0 & 1 \end{bmatrix}.$$

Apart from the advantage that the number of DFTs needed is reduced to only one, the processing of the difference terms (all but the last row of the matrix \mathbf{F}_i^v) can be shared for all tones. In a recursive least squares (RLS) implementation, this leads to a huge computational saving. In an implementation based on RLS processing with inverse updating ([83]), as shown in **Fig.3.4**, the bulk of the RLS operations are shared by all tones (triangular part at the top). The tone-specific part has complexity $\mathcal{O}(N)$. For more details, we refer to [195]

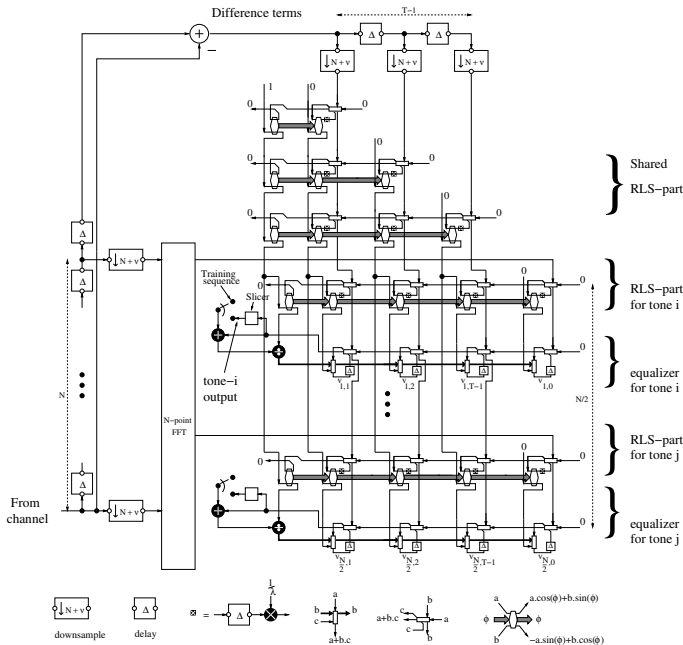


Figure 3.4: *RLS PTEQ implementation*. The top triangle corresponds to the shared (real) difference terms. For each tone, an individual (complex) input is added. The scheme is updated for every DMT symbol.

3.2.2 PTEQ and window functions

As stated before, receiver windowing makes the receiver more spectrally contained. The operation consists of a weighting of the input samples with the window function, followed by a folding of the edges, such that again a (weighted) sample vector of length N is obtained. Indeed, limiting the window size to the FFT size N would inevitably lead to the loss of orthogonality between the tones ([176], [105]). This can be overcome by extending the window size with a length μ . The windowing operation is graphically represented in **Fig.3.5**. A general windowing function can be written as:

$$\left[\underbrace{b_0 \ b_1 \ \dots \ b_{\mu-1}}_{\mu} \ \underbrace{1 \ \dots \ 1}_{N-\mu} \ \underbrace{b_{\mu} \ \dots \ b_{2\mu-1}}_{\mu} \right], \tag{3.3}$$

assuming the following symmetry property:

$$b_x + b_{x+\mu} = 1, \text{ for } 0 \leq x \leq (\mu - 1) \tag{3.4}$$

Just as the PTEQ was obtained by reversing the order of the TEQ filter and the DFT operation, the same can be done in the case of a windowed DFT. Taking into account that $\mathbf{y}^{(k)}$ now has length $(\mu + N + T - 1)$, the new optimization problem can be formulated as:

$$\min_{\bar{\mathbf{w}}_i} J(\bar{\mathbf{w}}_i) = \min_{\bar{\mathbf{w}}_i} \mathcal{E} \left\{ \left| \bar{\mathbf{w}}_i^T \mathbf{F}_{win,i}^w \mathbf{y}^{(k)} - X_i^{(k)} \right|^2 \right\}, \text{ with} \tag{3.5}$$

$$\mathbf{F}_{win,i}^w = \begin{bmatrix} \boxed{\mathcal{F}_{win}(i, :)} & \dots & 0 \\ & \ddots & \ddots \\ 0 & \dots & \boxed{\mathcal{F}_{win}(i, :)} \end{bmatrix},$$

with

$$\mathcal{F}_{win}(i, :) = [b_0 \ b_1 \alpha_i \ \dots \ b_{\mu-1} \alpha_i^{\mu-1} | \alpha_i^{\mu} \ \dots \ \alpha_i^{N-1} | b_{\mu} \alpha_i^N \ \dots \ b_{2\mu-1} \alpha_i^{\mu+N-1}].$$

Equation (3.5) is similar to equation (3.1) and involves the computation of T windowed DFTs. A cheaper formulation, based on difference terms is again needed.

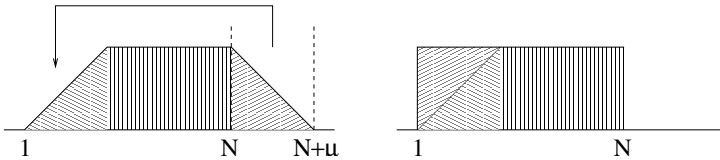


Figure 3.5: Windowing: weighting of samples and folding of the edges

A straightforward way to do so, would be to extend the normal PTEQ with μ extra difference terms (further referred to as the ' $T + \mu$ ' solution). Indeed, as shown in [197], the window can also be generated by a per-tone equalizer, if we increase the number of taps T to $(T + \mu)$. Because of the symmetry condition (3.4), the row-space of $\mathbf{F}_{\text{win},i}^w$ is fully contained in the row space of the matrix

$$\mathbf{F}_i^{T+\mu} = \left[\begin{array}{c|c} \mathbf{I}_{T+\mu-1} & \mathbf{O} \\ \hline \mathbf{O} & \mathcal{F}_N(i, :) \end{array} \right]^{-1} \mathbf{I}_{T+\mu-1}, \quad (3.6)$$

corresponding to the matrix \mathbf{F}_i^v from equation 3.2, in case μ additional difference terms are used. In short, incorporating a window function in this straightforward manner introduces μ additional difference terms, bringing the total number of taps per tone to

$$T^{\mu+T} = T + \mu. \quad (3.7)$$

Because generally $\mu \gg T$, the increase in complexity is significant, and we look for an alternative way to implement equation (3.5).

We will first derive an intermediate result, valid for all windowing functions satisfying the symmetry condition (3.4). This result will be further elaborated for the case of the trapezoidal window and the raised cosine window. Extensions to other windowing functions will be treated briefly.

General derivation

Because of the window symmetry, the following relation holds:

$$(b_x - b_{x-1}) \equiv -(b_{x+\mu} - b_{x+\mu-1}), \text{ for } x \in [1, \mu - 1].$$

Further define the differences of the window taper as:

$$D_{\text{win}} = [d_0 \quad d_1 \quad \dots \quad d_{\mu-1}], d_x = \begin{cases} b_0 & x = 0 \\ b_x - b_{x-1} & 1 \leq x \leq \mu - 1 \end{cases}$$

and, for tone i , modulated differences as:

$$D_{\text{win}_i} = [d_0 \quad d_1 \alpha_i \quad \dots \quad d_{\mu-1} \alpha_i^{\mu-1}].$$

Applying the transformation \mathbf{P}_i^{-1} on $\mathbf{F}_{\text{win},i}^w$ has the following effect: from each row $\mathbf{F}_{\text{win},i}^w(s, :)$ except the last one ($1 \leq s < T$), the next row $\mathbf{F}_{\text{win},i}^w(s+1, :)$, multiplied by α_i is subtracted. The result is called $\mathbf{M}_i = \mathbf{P}_i^{-1} \mathbf{F}_{\text{win},i}^w$. The 'flat' parts in the middle of the window will be canceled out and the tapers are converted to the modulated taper differences. More specifically

$$\mathbf{M}_i = \begin{bmatrix} \boxed{D_{win_i}} & 0 & \cdots & 0 & \boxed{-D_{win_i}} & \cdots & 0 \\ & \ddots & & & \ddots & & \\ 0 & \cdots & \boxed{D_{win_i}} & 0 & \cdots & 0 & \boxed{-D_{win_i}} & 0 \\ 0 & \cdots & & \underbrace{\hspace{10em}}_{\mathcal{F}_{win}(i, :)} & & & & \end{bmatrix}.$$

Now the matrix $\mathbf{F}_{win,i}^w$ can be rewritten as

$$\mathbf{F}_{win,i}^w = \mathbf{P}_i \mathbf{M}_i, \quad (3.8)$$

and we can again substitute $\bar{\mathbf{w}}_i^T$ by $\bar{\mathbf{v}}_i^T$, defined as $\bar{\mathbf{v}}_i^T = \bar{\mathbf{w}}_i^T \cdot \mathbf{P}_i$, such that (3.5) can be rewritten as a function of $\bar{\mathbf{v}}_i$

$$\min_{\bar{\mathbf{v}}_i} J(\bar{\mathbf{v}}_i) = \min_{\bar{\mathbf{v}}_i} \mathcal{E} \left\{ \left| \bar{\mathbf{v}}_i^T \mathbf{M}_i \mathbf{y}^{(k)} - X_i^{(k)} \right|^2 \right\} \quad (3.9)$$

So the matrix $\mathbf{F}_{win,i}^w$ from eq. (3.5) can be replaced by the sparser matrix \mathbf{M}_i . To simplify this even further, difference terms will be used such that the D_{win_i} and $-D_{win_i}$ -boxes can be smashed together. At the same time we isolate them from the last row of \mathbf{M}_i , i.e. we split $\bar{\mathbf{v}}_i^T$ into $\bar{\mathbf{u}}_i = \bar{\mathbf{v}}_i(1 : T - 1)$ and $\bar{\mathbf{v}}_i(T)$, leading to

$$\min_{\bar{\mathbf{v}}_i} J(\bar{\mathbf{v}}_i) = \min_{\bar{\mathbf{v}}_i} \mathcal{E} \left\{ \left| \bar{\mathbf{u}}_i^T \begin{bmatrix} \boxed{D_{win_i}} & \cdots & 0 \\ & \ddots & \\ 0 & \cdots & \boxed{D_{win_i}} \end{bmatrix} \underbrace{[\mathbf{I} \mid \mathbf{O} \mid -\mathbf{I} \mid \mathbf{0}]}_{\Delta} \mathbf{y}^{(k)} + R - X_i^{(k)} \right|^2 \right\}, \quad (3.10)$$

where \mathbf{I} are unity matrices of size $\mu + T - 2$, \mathbf{O} is a zero matrix of size $(\mu + T - 2) \times (N - \mu - T + 2)$, $\mathbf{0}$ is a zero column vector of size $\mu + T - 2$, and $R = \bar{\mathbf{v}}_i(T) \mathcal{F}_{win}(i, :) \mathbf{y}(T - 1 : N + T - 1 + \mu - 1)$, i.e. the contribution of the last row of \mathbf{M}_i .

If we define the vector of difference terms

$$\Delta = [\Delta_1 \quad \cdots \quad \Delta_{T+\mu-2}]^T, \quad \Delta_x = (y_x^{(k)} - y_{x+N}^{(k)}),$$

we can rewrite the $\bar{\mathbf{u}}_i$ -part of (3.10) resulting in:

$$\min_{\bar{\mathbf{v}}_i} J(\bar{\mathbf{v}}_i) = \min_{\bar{\mathbf{v}}_i} \mathcal{E} \left\{ \left\| \bar{\mathbf{u}}_i^T \begin{bmatrix} \boxed{D_{win_i}} & \cdots & 0 \\ \vdots & \ddots & \vdots \\ 0 & \cdots & \boxed{D_{win_i}} \end{bmatrix} \begin{bmatrix} \Delta_1 \\ \Delta_2 \\ \vdots \\ \Delta_{T+\mu-2} \end{bmatrix} + R - X_i^{(k)} \right\|^2 \right\} \quad (3.11)$$

The simplification of this expressing now depends on the shape of the window, two examples of which are elaborated.

Trapezoidal window

The trapezoidal windowing function is defined by:

$$b_x = \begin{cases} \frac{x+1}{\mu} & 0 \leq x \leq (\mu - 1) \\ \frac{2\mu - x - 1}{\mu} & \mu \leq x \leq (2\mu - 1) \end{cases} \quad (3.12)$$

Note that the symmetry condition (3.4) holds, and more specifically $b_{\mu-1} = 1$, and $b_{2\mu-1} = 0$. Because of the constant slope at the window edges, all differences are equal to μ^{-1} , and the modulated differences are equal to a scaled version of the first μ elements of the i^{th} row of the DFT matrix. We can substitute this explicitly, such that (3.11) becomes:

$$\min_{\bar{\mathbf{v}}_i} J(\bar{\mathbf{v}}_i) = \min_{\bar{\mathbf{v}}_i} \mathcal{E} \left\{ \left\| \frac{\bar{\mathbf{u}}_i^T}{\mu} \underbrace{\begin{bmatrix} \boxed{\mathcal{F}_N(i, 1 : \mu)} & \cdots & 0 \\ \vdots & \ddots & \vdots \\ 0 & \cdots & \boxed{\mathcal{F}_N(i, 1 : \mu)} \end{bmatrix}}_{\mathbf{A}} \underbrace{\begin{bmatrix} \Delta_1 \\ \Delta_2 \\ \vdots \\ \Delta_{T+\mu-2} \end{bmatrix}}_{\mathbf{\Delta}} + R - X_i^{(k)} \right\|^2 \right\} \quad (3.13)$$

Each row in the rightmost matrix-vector product $\mathbf{A} \cdot \mathbf{\Delta}$ may be viewed as a windowed DFT of difference terms. Instead of straightforwardly performing this matrix-vector product, one can also perform the DFT on the last row only, and derive the others by making use of this one DFT and some correction terms, similar to, but slightly different from (3.8). For a row s and a tone i , we can write that:

$$\mathbf{A}(s-1, :)\mathbf{\Delta} = \mathbf{A}(s, :)\alpha_i \mathbf{\Delta} + \underbrace{\Delta_{s-1} - \Delta_{\mu+s-1} \alpha_i^\mu}_{\text{correction term}}$$

By recursing this formula \mathbf{A} can be made sparser. Going back to the formulation of the optimization problem in terms of $\mathbf{y}^{(k)}$ and defining a new transformation matrix

\mathbf{R}_i ,

$$\mathbf{R}_i = \left[\begin{array}{c|c} \mu \mathbf{P}_i^{-1}(1:T-1, 1:T-1) & \mathbf{O}_{T-1 \times 1} \\ \hline \mathbf{O}_{1 \times T-1} & 1 \end{array} \right],$$

we can write

$$\bar{\mathbf{v}}_i^T \cdot \mathbf{M}_i = (\bar{\mathbf{v}}_i^T \cdot \mathbf{R}_i^{-1}) \cdot (\mathbf{R}_i \cdot \mathbf{M}_i) = \bar{\mathbf{t}}_i^T \cdot \mathbf{F}_{trap,i},$$

with

$$\mathbf{F}_{trap,i} = \left[\begin{array}{ccccccc} \mathbf{I}_{T-2} & \mathbf{O}_A & -\alpha^{-\mu_i} \cdot \mathbf{I}_{T-2} & \mathbf{O}_B & -\mathbf{I}_{T-2} & \mathbf{O}_A & \alpha^{-\mu_i} \cdot \mathbf{I}_{T-2} & \mathbf{0} \\ 0 \cdots & \boxed{\mathcal{F}_N(i, 1 : \mu)} & & \cdots & & \boxed{-\mathcal{F}_N(i, 1 : \mu)} & & 0 \\ 0 & \cdots & \boxed{\mathcal{F}_{trap}(i, :)} & & & & & \end{array} \right],$$

and $\mathbf{O}_A = \mathbf{O}_{T-2, \mu-T+2}$, $\mathbf{O}_B = \mathbf{O}_{T-2, N-\mu-T+2}$ (The index *win* has been replaced by *trap* to indicate this is the special case of the trapezoidal window function and the variable).

The optimization problem of eq.(3.9) can now be written as

$$\min_{\bar{\mathbf{t}}_i} J(\bar{\mathbf{t}}_i) = \min_{\bar{\mathbf{t}}_i} \mathcal{E} \left\{ \left| \bar{\mathbf{t}}_i^T \mathbf{F}_{trap,i} \mathbf{y}^{(k)} - X_i^{(k)} \right|^2 \right\}, \quad (3.14)$$

It is seen that the correction terms are tone-dependent, such that they cannot be processed for all tones together, as could be done with the PTEQ. For an RLS implementation, it might be computationally more interesting to break them into common (tone-independent) terms, i.e. difference terms Δ_x , which can then again be shared. In matrix form, the optimization criterion can then be represented as follows:

$$\min_{\bar{\mathbf{t}}_{i,u}} J(\bar{\mathbf{t}}_{i,u}) = \min_{\bar{\mathbf{t}}_{i,u}} \mathcal{E} \left\{ \left| \bar{\mathbf{t}}_{i,u}^T \mathbf{F}_{trap,i,u} \mathbf{y}^{(k)} - X_i^{(k)} \right|^2 \right\}, \quad (3.15)$$

with

$$\mathbf{F}_{trap,i,u} = \left[\begin{array}{cccc|cccc|c} \mathbf{I}_{T-2} & \mathbf{O}_x & \mathbf{O}_{T-2} & \mathbf{O}_y & -\mathbf{I}_{T-2} & \mathbf{O}_x & \mathbf{O}_{T-2} & 0 \\ \mathbf{O}_{T-2} & \mathbf{O}_x & \mathbf{I}_{T-2} & \mathbf{O}_y & \mathbf{O}_{T-2} & \mathbf{O}_x & -\mathbf{I}_{T-2} & \vdots \\ 0 \cdots & \boxed{\mathcal{F}_N(i, 1 : \mu)} & & 0 \cdots 0 & & \boxed{-\mathcal{F}_N(i, 1 : \mu)} & & 0 \\ 0 \cdots & 0 & \boxed{\mathcal{F}_{trap}(i, :)} & & & & & \end{array} \right],$$

where \mathbf{O}_x is size $(T-2, \mu-T+2)$ and \mathbf{O}_y is size $(T-2, N-\mu)$.

The rows (from bottom to top) correspond to the original windowed DFT output, the DFT corresponding to the last row of $\mathbf{A} \cdot \mathbf{\Delta}$ in (3.13), and the $2(T-2)$ difference terms needed to generate the other rows of $\mathbf{A} \cdot \mathbf{\Delta}$, i.e. $\Delta_1, \dots, \Delta_{T-2}, \Delta_{1+\mu}, \dots, \Delta_{T+\mu-2}$. The

indices u are added because the equation (3.14) can be viewed as a *constrained* version of the *unconstrained* optimization problem of (3.15). If one denotes the number of rows in matrix $\mathbf{F}_{\text{trap},i,u}$ as $T_{\text{trap},u}$, the following relationship holds:

$$T_{\text{trap},u} = 2(T - 2) + 2 = 2T - 2.$$

This implies that the amount of taps needed roughly doubles in going from (3.14) to (3.15). However, this result should be compared to the straightforward ' $T + \mu$ '-implementation. We are able to decrease the required number of difference terms from $T + \mu - 1$ to only $2T - 3$, at the cost of an extra tone-dependent term. Obviously, this method is interesting in case

$$\begin{aligned} 2T - 3 &\ll T + \mu - 1, \text{ or} \\ T &\ll \mu - 2. \end{aligned} \quad (3.16)$$

In summary, for the WiPTEQ using the trapezoidal window, the inputs for the equalizer on tone i at symbol time k are:

- the i^{th} output of the windowed DFT of the received symbol
- the i^{th} output of the DFT of a vector of difference terms $[\Delta_1 \dots \Delta_\mu \ 0 \dots 0]$ (padded with zeroes)
- difference terms $\Delta_1 \dots \Delta_{T-2}$, and $\Delta_{1+\mu} \dots \Delta_{T+\mu-2}$.

As stated before, (3.15) corresponds to the *unconstrained* version of (3.14). The latter can be derived from the former by premultiplication of the matrix $\mathbf{F}_{\text{trap},i,u}$ by a (tone dependent) *constraint matrix* \mathbf{C}_i :

$$\mathbf{C}_i = \left[\begin{array}{c|c|c} \mathbf{I}_{T-2} & -\alpha_i^\mu \cdot \mathbf{I}_{T-2} & \mathbf{O}_2 \\ \hline \mathbf{O}_{2 \times (T-2)} & \mathbf{O}_{2 \times (T-2)} & \mathbf{I}_2 \end{array} \right],$$

i.e.

$$\mathbf{F}_{\text{trap},i} = \mathbf{C}_i \mathbf{F}_{\text{trap},i,u}. \quad (3.17)$$

Obviously, enforcing the constraint will reduce the number of taps needed from $2T - 2$ to T , so this looks rather appealing. However, we reiterate that when using a standard RLS implementation, one will benefit more from the use of common difference terms than one would gain when using the constraint, thereby reducing the number of taps.

A *signal flow graph* of such an RLS implementation of this (unconstrained) algorithm is presented in **Fig.3.6**.

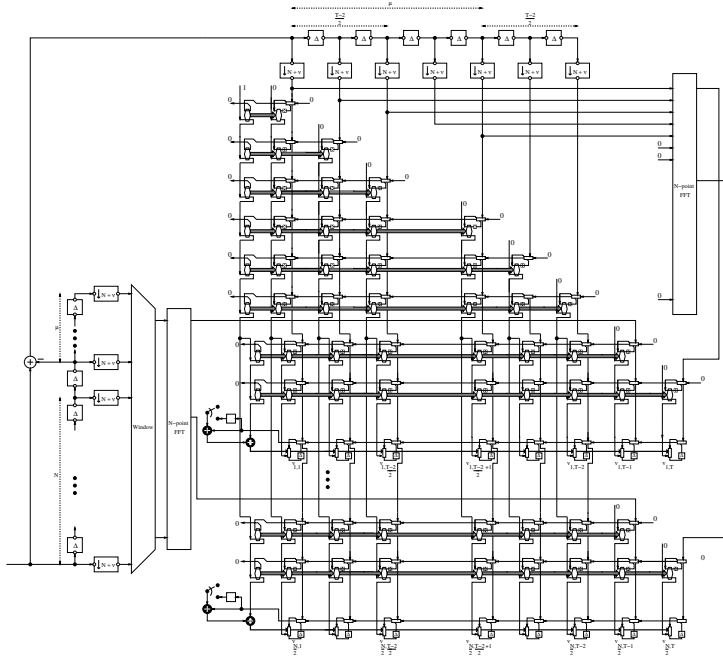


Figure 3.6: Signal flow graph when using *trapezoidal* window (unconstrained). The top triangle corresponds to the shared real difference terms. For each tone individually, this is extended with two complex tone-dependent inputs.

Raised cosine window

The raised cosine windowing function is defined by:

$$b_x = \frac{1}{2} \left(1 - \cos \left(\frac{2\pi(x+1)}{2\mu} \right) \right).$$

Again, $b_{\mu-1} = 1$, and $b_{2\mu-1} = 0$.

Equation (3.11) will be repeated here (with the index *win* replaced by *rc*, for raised cosine), and from there on the rest of the derivation will be shown.

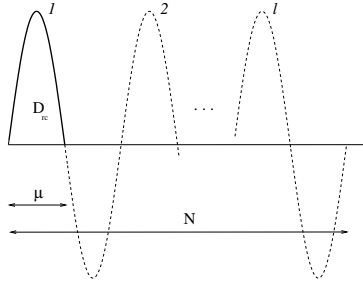


Figure 3.7: Extending D_{rc} to a sinusoidal window

$$\min_{\bar{\mathbf{v}}_i} J(\bar{\mathbf{v}}_i) = \min_{\bar{\mathbf{v}}_i} \mathcal{E} \left\{ \left| \bar{\mathbf{u}}_i^T \begin{bmatrix} \boxed{D_{rc_i}} & \cdots & 0 \\ \vdots & \ddots & \vdots \\ 0 & \cdots & \boxed{D_{rc_i}} \end{bmatrix} \begin{bmatrix} \Delta_1 \\ \Delta_2 \\ \vdots \\ \Delta_{T+\mu-2} \end{bmatrix} + R - X_i^{(k)} \right|^2 \right\} \quad (3.18)$$

Being the differences of (half) a cosine function, the differences D_{rc} correspond to half a period of a sine function. Accordingly, D_{rc_i} can be seen as the first μ elements of the i^{th} row of the DFT-matrix, with a sinusoidal window applied. Under the condition that the DFT size N is an even integer multiple of the window taper length μ , i.e.

$$N = 2l\mu, \quad (3.19)$$

with l integer (in practice this means that μ is a power of 2), the sinusoidal window can be extended to full length (see **Fig.3.7**) yielding $D_{rc_i,ext}$

$$D_{rc_i,ext} = \underbrace{[D_{rc} \quad -D_{rc} \quad D_{rc} \quad \cdots \quad -D_{rc}]}_{l \text{ repetitions}} \odot \mathcal{F}_N(i, :),$$

with \odot the componentwise multiplication.

We can now rewrite (3.18) as:

$$\min_{\bar{\mathbf{v}}_i} J(\bar{\mathbf{v}}_i) = \min_{\bar{\mathbf{v}}_i} \mathcal{E} \left\{ D_{rc_i, ext} \begin{bmatrix} \Delta_1 & \Delta_2 & \cdots & \Delta_{T-1} \\ \Delta_2 & \Delta_3 & \cdots & \Delta_T \\ \vdots & \vdots & & \vdots \\ \Delta_\mu & \Delta_{\mu+1} & \cdots & \Delta_{T+\mu-2} \\ & & O & \\ & & \vdots & \\ & & O & \end{bmatrix} \bar{\mathbf{u}}_i + R - X_i^{(k)} \right\}^2 \quad (3.20)$$

The matrix-vector product with $D_{rc_i, ext}$ represents a series of sinusoidally weighted DFTs. The output of a windowed DFT for which the window is a sinusoid with an integer number of repetitions can be written as a linear combination of outputs of the corresponding non-windowed DFT [121]. More specifically,

$$D_{rc_i, ext} = -j \frac{\mathcal{F}_N(\text{mod}_N(i-l), :) - \mathcal{F}_N(\text{mod}_N(i+l), :)}{2},$$

with $\text{mod}_N(\cdot)$ the modulo-operator, yielding a result in $[1 \cdots N]$. In other words, instead of calculating another windowed DFT and use its output at tone i as an input for the equalizer, we can also calculate a non-windowed DFT, and use the outputs at tones $\text{mod}_N(i-l)$ and $\text{mod}_N(i+l)$. Moreover, the series of DFTs can be calculated recursively, as was done in the previous paragraph (trapezoidal window). This leads to the following optimization problem (unconstrained case, see §3.2.2):

$$\min_{\bar{\mathbf{t}}_{i,u}} J(\bar{\mathbf{t}}_{i,u}) = \min_{\bar{\mathbf{t}}_{i,u}} \mathcal{E} \left\{ \left| \bar{\mathbf{t}}_{i,u}^T \mathbf{F}_{rc,i,u} \mathbf{y}^{(k)} - X_i^{(k)} \right|^2 \right\}, \text{ with} \quad (3.21)$$

$$\mathbf{F}_{rc,i,u} = \begin{bmatrix} I_{T-2} & \begin{array}{c|c} 0_x & 0_{T-2} \\ \hline 0_x & I_{T-2} \end{array} & \begin{array}{c|c} 0_y & -I_{T-2} \\ \hline 0_y & 0_{T-2} \end{array} & \begin{array}{c|c} 0_x & 0_{T-2} \\ \hline 0_x & -I_{T-2} \end{array} & \begin{array}{c} \vdots \\ \vdots \\ 0 \\ 0 \\ 0 \end{array} \\ \hline 0 \cdots & \boxed{\mathcal{F}_N(\text{mod}_N(i - \frac{N}{2\mu}), 1 : \mu)} & 0 \cdots 0 & \boxed{-\mathcal{F}_N(\text{mod}_N(i - \frac{N}{2\mu}), 1 : \mu)} & 0 \\ 0 \cdots & \boxed{\mathcal{F}_N(\text{mod}_N(i + \frac{N}{2\mu}), 1 : \mu)} & 0 \cdots 0 & \boxed{-\mathcal{F}_N(\text{mod}_N(i + \frac{N}{2\mu}), 1 : \mu)} & 0 \\ \hline 0 \cdots & \boxed{0} & \boxed{\mathcal{F}_{rc}(i, :)} & \boxed{0} & \vdots \end{bmatrix} \quad (3.22)$$

The rows of the matrix $\mathbf{F}_{win,i,u}$ correspond (from bottom to top) to the original windowed DFT output at tone i , the two additional DFT outputs at frequencies symmetric around i , and the $2(T-2)$ Δ 's needed to compute the other (sliding)

DFT's, namely $\Delta_1, \dots, \Delta_{T-2}$, and $\Delta_{\mu+1}, \dots, \Delta_{T+\mu-2}$. If one denotes the number of rows in matrix $\mathbf{F}_{rc,i,u}$ as $T_{rc,u}$, the following relationship holds:

$$T_{rc,u} = 2(T - 2) + 3 = 2T - 1.$$

Notice that one more row (equalizer tap) is required as compared to the *trapezoidal* window case, because two outputs of the non-windowed DFT of difference terms are needed to compute one output of the corresponding windowed DFT of difference terms.

In summary, for the WiPTEQ using the raised cosine window, the inputs for the equalizer on tone i at time k are:

- the i^{th} output of the windowed DFT of the received symbol
- two outputs of the DFT of a vector of difference terms $[\Delta_1 \dots \Delta_\mu \ 0 \dots 0]$ (padded with zeroes), symmetrical around i . The distance to i is determined by the length of the head (tail) of the window and the size of the DFT.
- the difference terms $\Delta_1 \dots \Delta_{T-2}$, and $\Delta_{\mu+1} \dots \Delta_{T+\mu-2}$.

A *signal flow graph* of an RLS implementation of this algorithm would look very much like Fig.3.6, but would use two outputs of the righthmost FFT per tone. This leads to an additional row for each tone (3 tone-dependent inputs instead of 2).

Extension to other window functions

The previous mathematical derivation was based on two principles. First of all, the window function was divided into the bulk part (amplitude 1) and the taper, as in formula (3.3). This latter is seen to give rise to the calculation of a new sliding windowed DFT. The new 'window' is the taper differences padded with zeros. In the case of the trapezoidal window, the taper differences are constant, i.e. correspond to a DC-term only. For the raised cosine function, the taper differences correspond to a sinusoid, i.e. two frequency components. A sinusoidal weighted DFT output can then be calculated from two other outputs of the corresponding non-weighted DFT, resulting in a significant computational saving. In general, the technique is applicable to window functions for which the DFT of the taper differences only has a low number of nonzero frequency components. The optimization problem can generally be transformed to:

$$\min_{\bar{\mathbf{t}}_{i,u}} J(\bar{\mathbf{t}}_{i,u}) = \min_{\bar{\mathbf{t}}_{i,u}} \mathcal{E} \left\{ \left| \bar{\mathbf{t}}_{i,u}^T \mathbf{F}_{win,i,u} \mathbf{y}^{(k)} - X_i^{(k)} \right|^2 \right\}, \text{ with} \quad (3.23)$$

$$\mathbf{F}_{win,i,u} \left[\begin{array}{c|c|c|c|c|c|c|c}
 I_{T-2} & O_x & O_{T-2} & O_y & -I_{T-2} & O_x & O_{T-2} & 0 \\
 O_{T-2} & O_x & I_{T-2} & O_y & O_{T-2} & O_x & -I_{T-2} & \vdots \\
 0 \cdots & \boxed{} & & 0 \cdots 0 & & \boxed{} & & 0 \\
 0 \cdots & \boxed{} & & 0 \cdots 0 & & \boxed{} & & 0 \\
 0 \cdots & \boxed{} & & 0 \cdots 0 & & \boxed{} & & 0 \\
 0 \cdots & 0 & \boxed{} & \mathcal{F}_{win}(i, \cdot) & \boxed{} & & & 0
 \end{array} \right] \left. \vphantom{\mathbf{F}_{win,i,u}} \right\} \begin{array}{l} \text{\# of freq.} \\ \text{comp.} \end{array}$$

3.3 Complexity

When comparing the complexity of Fig.3.6 (trapezoidal window case) with the PTEQ scheme of [195], the most apparent difference is the presence of an additional DFT, however with only few non-zero elements. Furthermore, there are one (trapezoidal window) or two (raised cosine window) additional tone dependent inputs. Additionally, the number of common difference terms almost doubles as compared to the PTEQ, but is still well beyond the number of taps needed in [197], whenever $\mu \gg T$

3.3.1 DFT complexity

Trapezoidal window

In general, to evaluate a windowed DFT, a real multiplication with the window function is needed, followed by additions due to the folding back. This amounts to $2(\mu - 1)$ real multiplications and $(\mu - 1)$ real additions. The calculation of the N point real DFT itself is implemented as a complex $\frac{N}{2}$ point FFT, requiring $\frac{1}{2} \frac{N}{2} \log_2(\frac{N}{2})$ complex multiplications and $\frac{N}{2} \log_2(\frac{N}{2})$ complex additions. To compute the original N point DFT from this result (only the first $\frac{N}{2}$ bins), another $\frac{N}{2}$ mixed real-complex multiplications and $\frac{N}{2}$ complex additions are needed.

Since there are only μ (successive) non-zero elements (eq. 3.20), the calculation of the second DFT (of difference terms) can be simplified. This N point real DFT can also be calculated as an $\frac{N}{2}$ point complex FFT having only $\frac{\mu}{2}$ non-zero elements. When implementing the FFT algorithm, the first $\log_2(\frac{N}{\mu})$ butterfly columns can be replaced by (complex) multiplications with a lookup table (see **Fig.3.8**). This requires $\frac{N}{2}$ complex multiplications, and no additions. The remaining $\left[\log_2(\frac{N}{2}) - \log_2(\frac{N}{\mu}) \right] = \log_2(\frac{\mu}{2})$ butterfly columns need to be fully calculated, requiring $(\frac{N}{4}) \log_2(\frac{\mu}{2})$ complex multiplications and $\frac{N}{2} \log_2(\frac{\mu}{2})$ complex additions. In [175] a variant to scheme was presented. With L the number of non-zero elements, and $P(> L)$ a freely chosen power of 2, this method leads to $N \log_2(P) - 3N + 4 \frac{N}{P} + 4NH - 4L$ multiplications

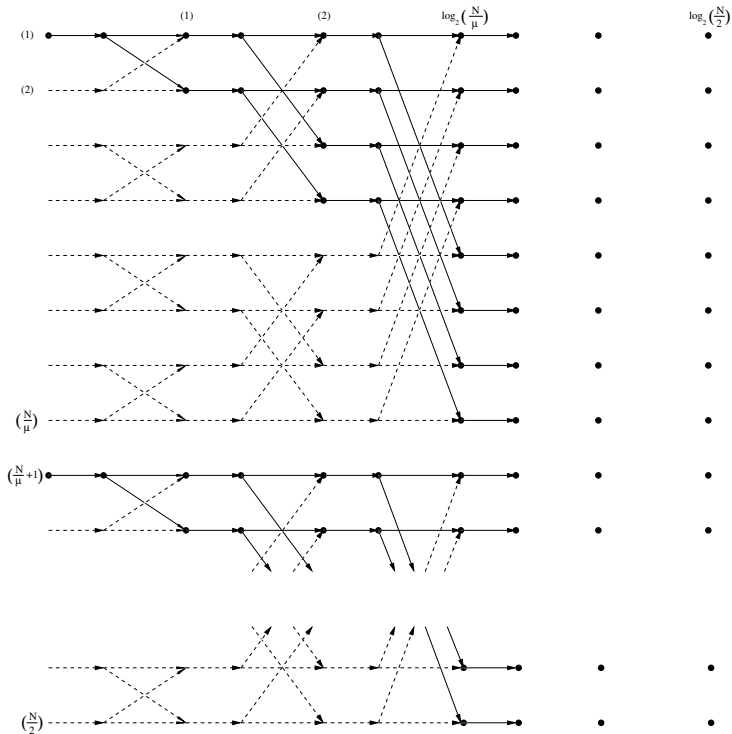


Figure 3.8: Butterfly scheme for the second FFT. Nonzero numbers are represented as dots. Operations on zeros are represented by dotted lines.

and $3N\log_2(P) - 3N + \frac{N}{P} + 2\frac{LN}{P} - 2L$ additions. However, the gain of this method is not very high, and hence it is only interesting when the number of non-zero elements is not a power of 2. Again, we still need to compute the original N point DFT (only lowest $\frac{N}{2}$ bins) from this $\frac{N}{2}$ point DFT. This requires an additional $\frac{N}{2}$ complex multiplications and $\frac{N}{2}$ complex additions.

These calculations have been put together in **Table 3.1**. It is assumed that a complex-complex multiplication requires four real multiplications and two real additions, a complex-complex addition gives rise to two real additions and a complex-real operation requires half of the corresponding fully complex operations.

Table 3.1: DFT complexity when using the *trapezoidal* window

	# multiplications	# additions
weighted DFT	$2(\mu - 1) + 4\frac{N}{4}\log_2(\frac{N}{2}) + 2\frac{N}{2}$	$(\mu - 1) + 2\frac{N}{4}\log_2(\frac{N}{2}) + 2\frac{N}{2}\log_2(\frac{N}{2}) + 2\frac{N}{2}$
partial DFT	$4\frac{N}{2} + 4(\frac{N}{4})\log_2(\frac{\mu}{2}) + 4\frac{N}{2}$	$2\frac{N}{2} + 2(\frac{N}{4})\log_2(\frac{\mu}{2}) + 2(\frac{N}{2})\log_2(\frac{\mu}{2}) + 2\frac{N}{2} + 2(\frac{N}{2} + \frac{N}{\mu})$
total DFT	$2(\mu + 1) + N [3 + \log_2(\mu N)]$	$\mu - 1 + N \left[\frac{3}{2}\log_2(\mu N) + 1 + \frac{2}{\mu} \right]$

Raised cosine window

The previous complexity calculation also holds for the *raised cosine* window, except that for the second DFT (of difference terms), one needs to compute more output terms than just the lowest N frequencies. Indeed, because all tones are equalised based upon (among others) the outputs of this DFT at two frequencies that lie symmetrically around the tone itself, one needs to compute a few outputs at 'negative frequencies'. In total, $\frac{N}{2} + \frac{N}{\mu}$ outputs need to be calculated.

3.3.2 RLS update complexity

Trapezoidal window

A significant computational advantage is obtained by jointly processing the common difference terms and dealing with the tone dependent inputs afterwards. In the case of the *trapezoidal* window, there are two tone specific inputs, being the windowed DFT output and the output of the DFT of difference terms. Assuming the number of taps of the original (*constrained*) problem was T , now $T_{t,u} = 2T - 2$ taps will be needed, of which $2T - 4$ are used for the difference terms. If one makes use of the QR-RLS scheme with inverse updating [83], as in Fig.3.6, the difference terms will make up for $2T - 4$ rows (of linearly increasing length). In each row k , a fully real vector-vector product will be executed, requiring k multiplications, followed by $k + 1$ Givens rotations, which require 4 multiplications each.

After these (real) operations on difference terms, each tone is treated individually. The additional tone dependent inputs are complex. This implies that the first new vector-vector product will consist of $2T - 4$ complex-real multiplications, and one complex-complex multiplication. These are followed by real-complex Givens rotations, requiring 9 real multiplications per rotation with one real and one complex input. The

second tone dependent input introduces an additional complex-complex multiplication in the matrix-vector product, and an additional Givens rotation. By now, the Givens rotations are fully complex, requiring 12 real multiplications per rotation. After these operations, the entire update of the \mathbf{R}^{-T} -matrix (from the mentioned algorithm) is complete. Finally, the filter output needs to be calculated, requiring $2T - 4$ real-complex multiplications (weighting of difference terms), 2 complex multiplications (tone dependent gain inputs), a complex division and $2T - 2$ complex multiplications for the *Kalman gain vector* update. In case the adaptation is stopped (upon convergence), only the calculation of the filter output is necessary, requiring only $2(2T - 4) + 8$ real multiplications per tone.

These results are brought together in **Table 3.2**.

Table 3.2: RLS update complexity when using the *trapezoidal* window

		# Multiplications
Common	matrix vector product	$\frac{(2T-4)(2T-4+1)}{2}$
Common	(real) rotations	$4 \left[\frac{(2T-4)(2T-4+1)}{2} + 2T - 4 \right]$
Common	total common	$10T^2 - 27T + 14$
per tone	individual matrix vector products	$8T - 4$
per tone	individual rotations	$42T - 30$
per tone	filter update	$2(2T - 4) + 8 + 4 + 4(2T - 2)$
per tone	total per tone	$62T - 38$

Raised cosine window

The *trapezoidal* and *raised cosine* windowing RLS scheme only differ in the number of tone specific inputs. In case of the *raised cosine* window, there are three tone specific inputs, being the windowed DFT output and two outputs of the DFT of difference terms. Assuming the number of taps of the original (*unconstrained*) problem was T , now $T_{rc,u} = 2T - 1$ taps are needed, of which $2T - 4$ are used for the difference terms. If one again makes use of the QRD-RLS scheme with inverse updating, the difference terms will make up for $2T - 4$ rows (of linearly increasing length). In each row k , a matrix-vector product will be executed, requiring k multiplications, followed by $k + 1$ Givens rotations, of which it is assumed that they require 4 multiplications each. Again, after these (real) operations on difference terms, each tone is treated individually.

The first new matrix-vector product will consist of $2T - 4$ complex-real multiplications, and one complex-complex multiplication. These are again followed by a real-complex Givens rotations. The second and third tone dependent input each have an increase of one complex multiplication in the matrix-vector product, and an additional Givens rotation (both fully complex)). Calculating the output requires $2T - 4$ real-complex multiplications (weighting of difference terms), 3 complex multiplications (tone dependent inputs), a complex division and $2T - 1$ complex multiplications for the *Kalman gain vector* update.

These results are brought together in **Table 3.3**.

Table 3.3: RLS update complexity when using the *raised cosine* window

		# vermenigvuldigen
Common	matrix vector product	$\frac{(2T-4)(2T-4+1)}{2}$
Common	(real) rotations	$4 \left[\frac{(2T-4)(2T-4+1)}{2} + 2T - 4 \right]$
Common	total common	$10T^2 - 27T + 14$
per tone	individual matrix vector products	$12T$
per tone	individual rotations	$66T - 30$
per tone	filter update	$2(2T - 4) + 12 + 4 + 4(2T - 2)$
per tone	total	$90T - 30$

3.3.3 Total complexity

If we assume an ADSL downstream simulation with RLS updating, the total resulting complexity (for the case of the *trapezoidal* window) is shown in **Table 3.4**, as compared to a PTEQ under the same conditions. This complexity included calculation of the FFT's, common difference term processing and individual tone processing. The PTEQ complexity results are derived from [195]. The table also shows the complexity figures assuming that no updating is done, i.e. after convergence. These results have also been plotted against the number of taps of the constrained optimization problem T in **Fig.3.9**.

Table 3.4: Total complexity of PTEQ and *trapezoidal* windowing scheme, ADSL downstream, 218 tones

ADSL down	PTEQ	<i>trapezoidal</i> windowing
updating	$N \log_2\left(\frac{N}{2}\right) + N + \frac{5}{2}T^2 + \frac{7415}{2}T + 3702$	$2\mu - 8268 + N(3 + \log_2(\mu N)) + 13489T + 10T^2$
convergence	$N \log_2\left(\frac{N}{2}\right) + N + 436T + 436$	$2\mu + 2 + N(3 + \log_2(\mu N)) + 872T$

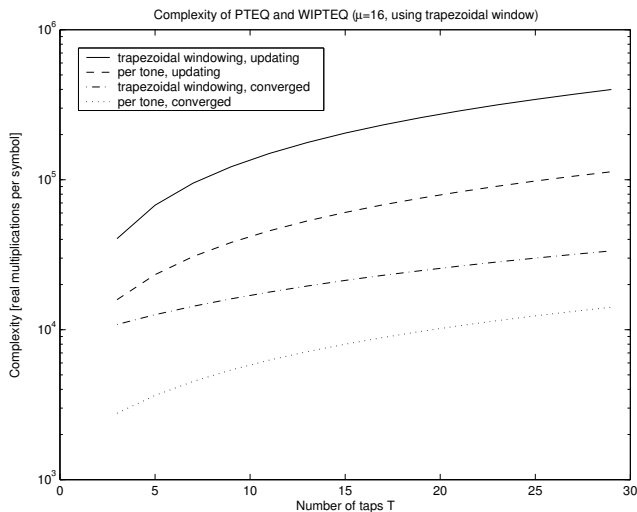


Figure 3.9: Complexity of PTEQ and *trapezoidal* windowing scheme ($\mu = 16$)

3.3.4 Memory consumption

The total number of parameters stored is also an important issue. It can be divided into a tone-independent and a tone-dependent portion.

The first one corresponds to the top triangle in the signal flow graphs (fig. 3.4 and fig. 3.6). For the PTEQ, it contains $\frac{T \cdot (T-1)}{2}$ real coefficients, for the *trapezoidal* window $\frac{(T-1)(T-2)}{2}$, and for the *raised cosine* window $\frac{(T-2)(T-3)}{2}$ real coefficients.

The second, tone-dependent portion however is dominant: for the PTEQ it contains $2T$ complex coefficients per tone. For the *trapezoidal* window this amounts to $3T - 1$, and for the *raised cosine* window $4T - 3$ complex coefficients per tone. At first sight, it

appears that the number of coefficients in going from the PTEQ to the *raised cosine* windowed implementation is doubled. However, one should take into account that the number of taps needed is significantly lower: if one combines the PTEQ with a windowing function (such as in [197]), the PTEQ requires μ additional taps. This is in accordance with the previously made statement that the proposed methods are especially interesting in case $T \ll \mu$.

3.4 Simulation results

To verify the validity of the technique, first of all *minimum mean square* (MMSE) simulations have been done, based on formula (3.14). Because in such simulations all tones are processed individually, it is rather easy to use the *trapezoidal* windowing scheme with tone-dependent difference terms, such that effectively the *constrained* rather than the *unconstrained* optimization problem is solved. The computational complexity of this MMSE method is however too high for a practical application. Therefore, also a *Recursive Least Squares* (RLS) implementation has been studied. Because this method benefits from equalizer inputs common for all tones, these simulations have been done based on equation (3.15) such as shown in Fig.3.6 (unconstrained case), and (3.21).

3.4.1 MMSE simulations

Environment

The performed MMSE simulations are off-line simulations for an ADSL setup, offering an upper bound of the performance that can be expected of recursive schemes. To make a fair comparison, the same loop and noise conditions have been used throughout. The standard loop used is a T1.601#13 line. The crosstalk environment consists of additive white gaussian noise (AWGN) at -140 dBm/Hz, and 24 *near-end crosstalk* (NEXT) sources. In case RFI is taken into account, its frequencies and nominal power levels are indicated in **Table 3.5**. Notice that the last RFI interferer was originally located at 1900kHz, but effectively appears at 308kHz due to aliasing.

Table 3.5: Nominal RFI frequencies and power levels

frequency [kHz]	620	740	800	980	1100	1160	308
power [dBm/Hz] in 4312.5 Hz band	-92.2	-90.5	-59.9	-59.6	-95.5	-79.8	-112.7

The first result presented compares the behaviour of the PTEQ and the WiPTEQ as a function of the number of equalizer taps per tone. A *trapezoidal* window was chosen, because this allows for the tone dependent combination of difference terms (3.14). The taper length is kept constant: $\mu = 16$.

Constant RFI conditions

Figure 3.10 shows the bit rate for both equalisation techniques, in the absence and presence of RFI interference. The results for the case where RFI is present were derived with an equalizer that was also designed in the presence of RFI. Although the performance gain over the PTEQ is negligible in the absence of RFI, the WiPTEQ significantly outperforms the PTEQ when RFI is present, especially when the number of taps is relatively small. It should come as no surprise that the PTEQ will approach the result of the WiPTEQ very closely when the number of taps is higher. When using a high number of equalizer taps, the equivalent window to which the PTEQ (as well as the combined technique) adapts, becomes far more important than the fixed *trapezoidal* window. Note that results are shown for T up to 29. The results for $T > \mu$ should be regarded as outside the usefull operation area of the algorithm, and are only given for extended comparison with the PTEQ. Indeed, after all, with $\mu = 16$, the taper only has a rather modest length as compared to the DFT size N .

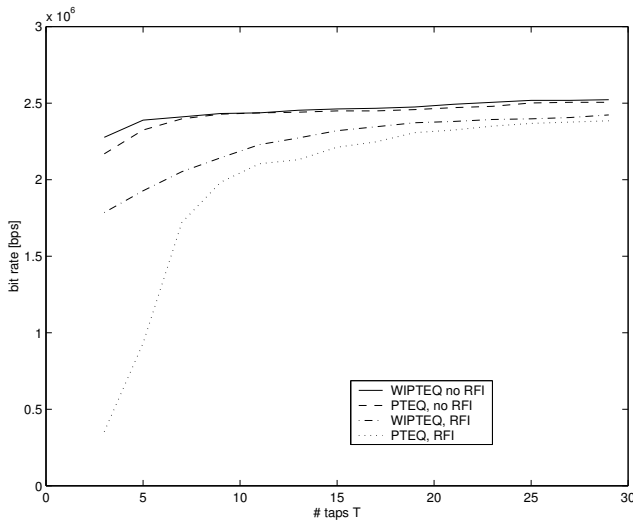


Figure 3.10: Comparison between PTEQ and the WiPTEQ ($\mu = 16$, trapezoidal window) in absence and presence of RFI

Taper length influence

Another simulation shows the influence of the taper length μ . Increasing μ leads to an interesting tradeoff. On the one hand, the window becomes more important, thus reducing the side lobe height, reducing *inter carrier interference* (ICI) and RFI. On the other hand, the taper will extend further into the cyclic prefix, requiring more channel shortening from the difference terms to minimise *inter symbol interference* (ISI). For a taper length exceeding 32 samples, ISI is unavoidable. The simulation results have been brought together in **Fig.3.11**. On the left-hand side, an RFI-less scenario is depicted. All window lengths perform roughly the same, although one notices that the window with taper length $\mu = 32$ has the lowest bit rate, because of the mentioned ISI problem. On the right-hand side, RFI has been taken into account. As seen before, the window is beneficial especially for small numbers of taps. Therefore, it comes as no surprise that in this region, the performance increases with μ . At higher tap numbers, the window becomes less important, an can even counteract the optimal window the PTEQ tries to compose.

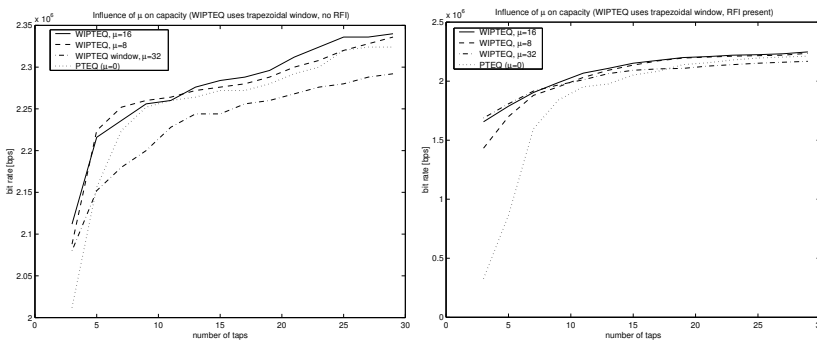


Figure 3.11: Influence of taper length μ in the absence and presence of RFI (please notice the difference in scale)

3.4.2 RLS simulations

The results of the MMSE simulations are also reflected in RLS simulations: in the absence of RFI, the combination of windowing ($\mu = 16$) and equalization does not have a big impact. In case RFI emerges, the use of the window is beneficial. In **Fig.3.12**, the dynamic behaviour of the three techniques is compared. Because the RLS algorithm greatly benefits from common terms, the *unconstrained* problem of eq.(3.15) was used for the combination of PTEQ and trapezoidal window, with $T_{trap,u} = 12$. Also, for the combination of PTEQ and the raised cosine window, the unconstrained formulation of eq.(3.21) was used, with $T_{rc,u} = 11$. The number of taps used for the PTEQ, was $T = 12$, such that "in the regime", the three methods have a comparable complexity.

The simulated scenario used the same ADSL standard loop, T1.601#13 and AWGN at -140dBm/Hz . After a training based adaptation (250 symbols) all equalizer coefficients are frozen, and at time $t = 300$ RFI disturber emerges at 740kHz. While the classical PTEQ capacity halves, the two techniques combining PTEQ and windowing clearly do better. If further decision directed equalizer adaptation were used, the PTEQ scheme may diverge because of the large number of decision errors. The WiPTEQ will experience less decision errors and will give significant improved performance.

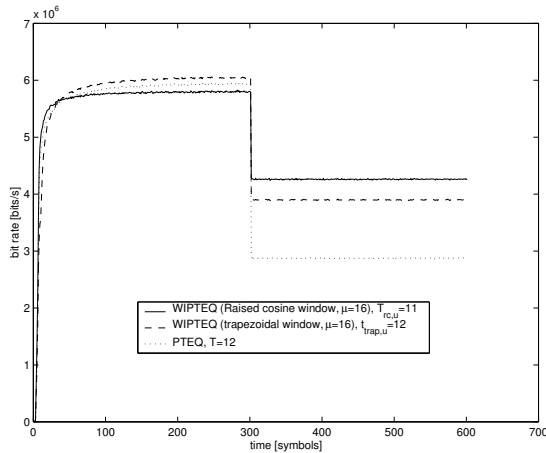


Figure 3.12: RLS simulations: PTEQ vs WiPTEQ with trapezoidal window and raised cosine window. RFI emerges at time 300

3.5 Conclusions

The presented method combines the benefits of per tone equalization and windowing functions. Two special cases of windowing functions are considered, the trapezoidal and raised cosine window. In the most common case that the window extension $\mu \gg T$, where T is the number of equalizer taps the method significantly reduces the computational complexity with respect to [197], which requires equalization with $\mu + T$ taps.

Chapter 4

Transmitter windowing

This chapter consists mostly of a copy of the article *Intra-symbol windowing for egress reduction in DMT transmitters* [40], as published in *EURASIP J. Appl. Signal Process.* Only the layout and the numbering of the references, equations and figures has been changed to accommodate for the different page size and to improve consistency.

In section 4.6 a further application of these windowing functions is proposed. This section is added here for completeness, but was not included in the original article.

Abstract

Discrete multitone (DMT) uses an inverse discrete fourier transform (IDFT) to modulate data on the carriers. The high side lobes of the IDFT filter bank used can lead to spurious emissions (egress) in unauthorised frequency bands. Applying a window function within the DMT symbol can alleviate this. However, window functions either require additional redundancy or will introduce distortions that are generally not easy to compensate for. A special class of window functions is constructed that corresponds to a precoding at the transmitter. These do not require any additional redundancy and need only a modest amount of additional processing at the receiver. The results can be used to increase the spectral containment of DMT-based wired communications such as ADSL and VDSL (i.e. asymmetric resp. very-high-bitrate digital subscriber loop).

4.1 Introduction

Discrete Fourier Transform (DFT) based modulation techniques [208] have become increasingly popular for high speed communications systems. In the wireless context, e.g. for the digital transmission of audio and video, this is usually referred to as orthogonal frequency division multiplexing (OFDM). Its wired counterpart has been dubbed discrete multitone (DMT), and is employed e.g. for digital subscriber loop (DSL) systems, such as asymmetric DSL (ADSL) and very-high-bitrate DSL (VDSL).

A high bandwidth efficiency is achieved by dividing the available bandwidth into small frequency bands centered around carriers (tones). These carriers are individually modulated in the frequency domain, using the inverse DFT (IDFT). A cyclic prefix (CP) is added to the resulting block of time-domain samples by copying the last few samples and putting them in front of the symbol [145]. This extended block is parallel-to-serialized, passed to a digital to analog (DA) convertor and then transmitted over the channel. At the receiver, the signal is sampled and serial-to-parallelized again. The part corresponding to the CP is discarded, and the remainder is demodulated using the DFT.

In case the order of the channel impulse response does not exceed the CP length by more than one, equalization can be done easily using a one-tap frequency domain equalizer (FEQ) for each tone, correcting the phase shift and attenuation at each tone individually. When the channel impulse response is longer than the CP, the transmission suffers from inter carrier interference (ICI) and inter symbol interference (ISI), requiring more complex receivers e.g. a per-tone equalizer (PTEQ) [196]. The windowing technique presented in this document is irrespective of the equalization technique used but can be combined with the PTEQ in a very elegant way.

In addition to a CP VDSL systems can also use a cyclic suffix (CS). The difference between the CP and CS is irrelevant for our purpose, therefore they will be treated as one (larger) CP. More importantly, the presence of the CP influences the spectrum of the transmit signal, as will be shown later.

While DMT seems attractive because of its flexibility towards spectrum control, the high side lobe levels associated with the DFT filter bank form a serious impediment, resulting in an energy transfer between in-band and out-of-band signals. This contributes to the crosstalk, e.g. between different pairs in a binder, especially for next-generation DSL systems using dynamic spectrum management (DSM), where the transmit band is variable [174]. Moreover, because the twisted pair acts as an antenna [179], there exists a coupling with air signals. The narrow band signals from, e.g., an AM broadcast station can be picked up by the receiver and, due to the side lobes, be smeared out over a broad frequency tone range. This problem has been recognised, and various schemes have been developed to tackle it ([154], [105], [44]). On the other hand, the same poor spectral containment of transmitted signals makes it difficult to meet egress norms, e.g.

the ITU-norm [51] specifies that the transmit power of VDSL should be lowered by 20dB in the amateur radio bands. Controlling egress is usually done in the frequency domain by combining neighbouring IDFT-inputs (such as in [123]), or equivalently, by abandoning the DFT altogether and reverting to other filter banks, such as e.g. in [26].

Another approach would be to apply an appropriate time-domain window (see [79] for an overview) at the transmitter. Unfortunately, the application of nonrectangular windows destroys the orthogonality between the tones, resulting in ICI. In [173], a windowed VDSL system is proposed, where the window is applied to additional cyclic continuations of the DMT symbol to prevent distorting the symbol itself.

The technique proposed in this contribution avoids the overhead resulting from such additional symbol extension by applying the window directly to the DMT symbol, i.e. without adding additional guard bands. This windowing is observed to correspond to a pre-coding operation at the transmitter. Obviously, this alters the frequency content at each carrier, such that a correction at the receiver is needed. While this compensation is generally nontrivial [116], we construct a class of windows that can be compensated for with only a minor amount of additional computations at the receiver.

When investigating transmit windowing techniques, it is important to have an accurate description of the transmit spectrum of DMT/OFDM signals. Although DMT and OFDM are commonplace, a lot of misconception and confusion seem to exist with regard to the nature of their transmit signal spectrum. When working on sampled channel data, the continuous-time character of the line signals is transparent, and therefore usually neglected. However, it is important to realize that the behaviour in between the sample points can be of great importance [128]. The analog signal will generally exceed the sampled points' reach, possibly leading to unnoticed clipping, and hence out-of-band radiation.

Therefore, section 4.2 starts by describing the spectrum of the classical DMT signal. The novel windowing system is then presented in section 4.3. Section 4.4 covers the simulation results. Finally, in section 4.5, conclusions are presented.

4.2 DMT transmit signal spectrum

Consider the DMT system of **Fig. 4.1**, with (I)DFT-size N and a CP length ν , resulting in a symbol length $L = N + \nu$. The symbol index is k and $\mathbf{X}^{(k)} = [X_0^{(k)} \dots X_{N-1}^{(k)}]^T$ holds the complex subsymbols at tones $i, i = 0 : N - 1$. In a baseband system, such as ADSL, the time-domain signal is real-valued, requiring that $X_i^{(k)} = X_{N-i}^{(k)*}$. The corresponding discrete time-domain sample vector (at point α in fig.4.1) is equal to

$$\mathbf{x}^{(k)} = \left[x^{(k)}[0], \dots, x^{(k)}[L - 1] \right]^T, \quad (4.1)$$

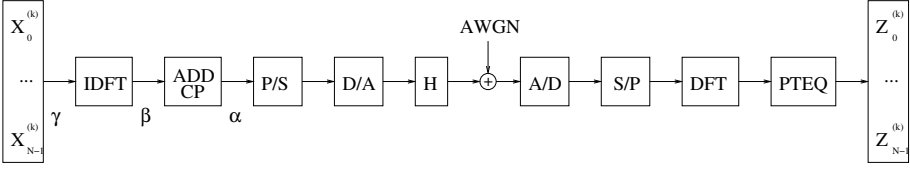


Figure 4.1: Basic DMT system (refer to text for α to γ)

$$x^{(k)}[n] = \frac{1}{\sqrt{N}} \sum_{i=0}^{N-1} X_i^{(k)} e^{j \frac{2\pi i}{N} (n-\nu)}, \quad n = 0 \dots L-1. \quad (4.2)$$

Note that the CP is automatically present, due to the periodicity of the complex exponentials. The total discrete time-domain sample stream $x[n]$ is obtained as a concatenation of the individual symbols $\mathbf{x}^{(k)}$. Interpolation of these samples yields the continuous time-domain signal $s(t)$, given by:

$$s(t) = \int_{\tau=-\infty}^{\infty} v(\tau-t) \left[\sum_{n=-\infty}^{\infty} \delta(t-nT)x[n] \right] d\tau, \quad (4.3)$$

$$x[n] = \frac{1}{\sqrt{N}} \sum_{k=-\infty}^{\infty} \sum_{i=0}^{N-1} X_i^{(k)} e^{j \frac{2\pi i}{N} (n-\nu-kL)} w_{r,s}[n-kL], \quad (4.4)$$

with $\delta(t)$ the *dirac impulse* function, T the sampling period, $w_{r,s}[n]$ a (*rectangular, sampled*) discrete time-domain window, $w_{r,s}[n] = 1$ for $0 \leq n \leq L-1$ and zero elsewhere, and $v(t)$ an interpolation function.

The shape of the DMT spectrum will now be derived by construction, starting from a single symbol with only one active carrier at DC. This result will be extended to a succession of symbols with all carriers excited. After this, the influence of time-domain windowing will be investigated in section 4.3.

Assume a single DMT symbol, having a duration $L = N + \nu$ in which only the DC component is excited (e.g. with unit value), in other words:

$$X_i^{(k)} = \begin{cases} 1 & i = 0, k = 0 \\ 0 & \text{elsewhere.} \end{cases} \quad (4.5)$$

The corresponding discrete-time-domain signal is a sequence of L identical pulses, which is equivalent to a multiplication of a rectangular window and an impulse train (**Fig. 4.2**). A rectangular window $w_r(t)$ extending from $t = 0$ to $t = L$ has a modulated sinc as its Fourier transform

$$W_r(f) = \frac{\sin(\pi L f)}{\pi f} \cdot \exp(-j\pi L f). \quad (4.6)$$

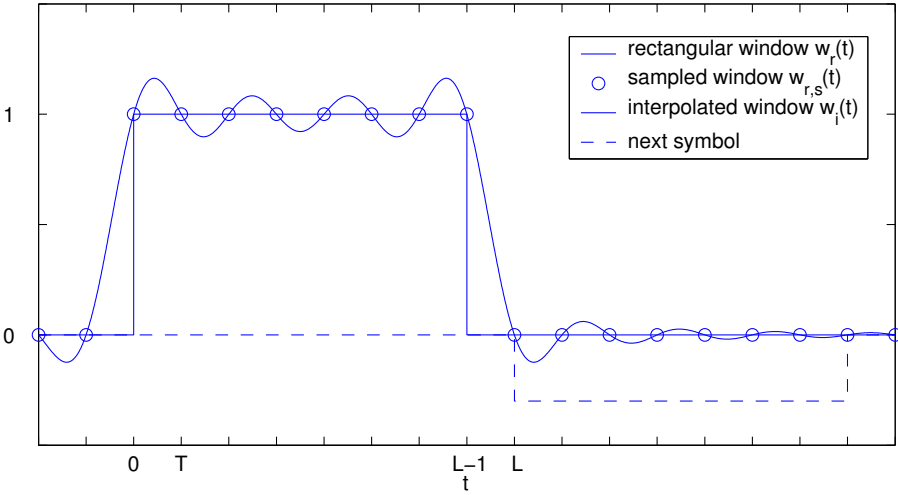


Figure 4.2: The first (DC only) symbol as a sampled rectangular window, and a possible next symbol.

The multiplication of this $w_r(t)$ with a sequence of pulses with period T results in the spectrum $W_r(f)$ being convolved with a pulse train with period $\frac{2\pi}{T}$. The original sinc spectrum $W_r(f)$ and the convolved spectrum $W_{r,s}(f)$ are represented in **Fig. 4.3**. Here, $W_{r,s}(f)$ is periodic with a period $\frac{1}{T}$. Surprisingly, this can be expressed analytically as [150, p.3.14]

$$W_{r,s}(f) = \frac{\sin(\pi L T f)}{\sin(\pi T f)} \exp(-j\pi L f). \quad (4.7)$$

In literature, $W_{r,s}(f)$ is sometimes approximated by a sinc. While this approximation is suitable for some applications, it leads to an underestimate of the (possible egress-) energy in non-excited frequency bands. More specifically, from (4.7), it is clear that this leads to a maximum error of 3.9dB around $f = \pm \frac{1}{2T}$.

The final DA conversion consists of a lowpass filtering with $v(t)$, such that only the frequencies between $-\frac{1}{T}$ and $\frac{1}{T}$ are withheld. In the case of an ideal lowpass filter, this is equivalent to a time-domain interpolation with a sinc function, resulting in $w_i(t)$, as shown in fig.4.2. Note that the continuous behaviour in between the sampled values is far from constant.

This result can now be extended to describe a succession of multiple symbols ($k = 0, 1, \dots$), with all tones ($i = 0, 1, \dots, N-1$) excited. Assume that the $X_i^{(k)}$ have a variance $\mathcal{E}|X_i^{(k)}|^2 = \sigma_i^2$, and are uncorrelated. The power spectral density (PSD) $S(f)$

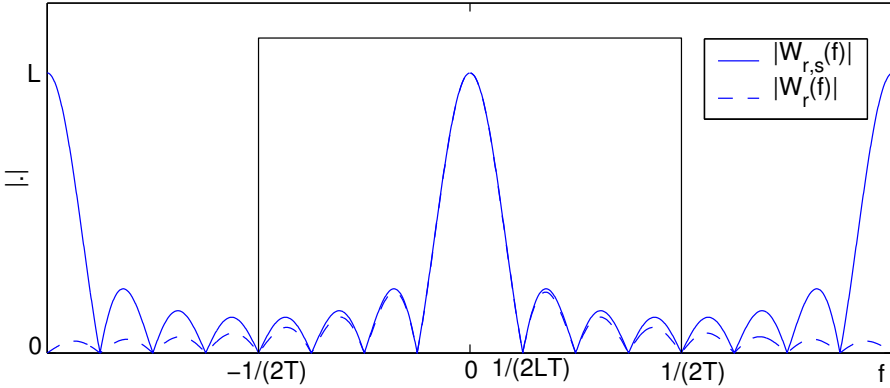


Figure 4.3: Spectrum of the continuous and sampled rectangular window

of $s(t)$ can then be described as

$$S(f) = \sum_{i=0}^{N-1} \sigma_i^2 |W_{r,s}(f - \frac{i}{NT}) \cdot V(f)|^2, \quad (4.8)$$

with $V(f)$ the frequency characteristic of the interpolation filter $v(t)$ (an example of this is shown in section 4.4).

Only in the case where the prefix is omitted ($\nu = 0$) and the variances $\sigma_i^2 = \sigma^2$ are equal for all tones (except DC and the nyquist frequency, having only $\frac{\sigma^2}{2}$), this spectrum is more or less flat. In general, the CP results in a toothed spectrum. Indeed, because the symbols are lengthened by the CP, the PSD of the individual tones is narrowed compared to the intertone distance, such that 'valleys' (or 'teeth') appear in between the tone frequencies. This is demonstrated in **Fig. 4.4**, where a detail of the spectrum of a prefixless DMT system ($\nu = 0$) is compared to a system using a prefix.

4.3 Transmitter windowing

Practical lowpass filters are not infinitely steep, such that some small signal components above the Nyquist frequency will remain. The out-of-band performance is then largely dependent on the quality of these filters (and possible clipping in further analog stages). On the other hand, the in-band transitions (e.g. for suppression of VDSL in the amateur radio bands) can only be sharpened by the application of a window function on the entire time-domain symbol. To achieve this, the rectangular window $w_{r,s}[n]$ is replaced by another one having faster decaying side lobes. This new window

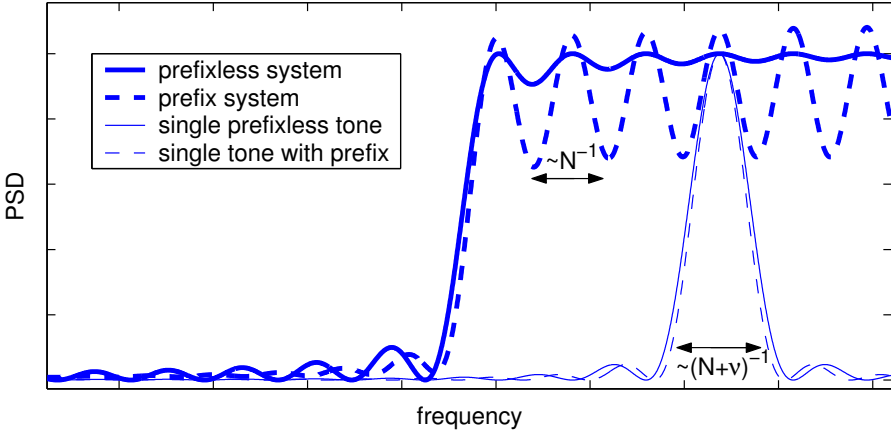


Figure 4.4: The cyclic prefix in DMT systems leads to a toothed spectrum exhibiting valleys in between the tones

$$\mathbf{w} = [w(0) \dots w(L - 1)]^T \tag{4.9}$$

is applied at point α in fig.4.1. In the next paragraph we impose constraints on \mathbf{w} to construct a class of window functions that are easy to compensate for at the receiver.

4.3.1 Derivation of the window structure

To preserve the cyclic structure of the transmitted symbols, needed for an easy equalization, we impose the cyclic constraint:

$$w(n) = w(n + N), n = 0, \dots, \nu - 1. \tag{4.10}$$

As a result, instead of applying the window \mathbf{w} at point α (fig.4.1), one can also apply the window

$$\mathbf{g} = [g(0) \dots g(N - 1)]^T \tag{4.11}$$

$$= [w(\nu) \dots w(N + \nu - 1)]^T \tag{4.12}$$

at point β . Let \mathbf{G} be a diagonal matrix with \mathbf{g} as its diagonal. After defining \mathcal{I}_N the IDFT-matrix of size N , the vector of windowed samples $\mathbf{x}_w^{(k)}$ at point β (before the

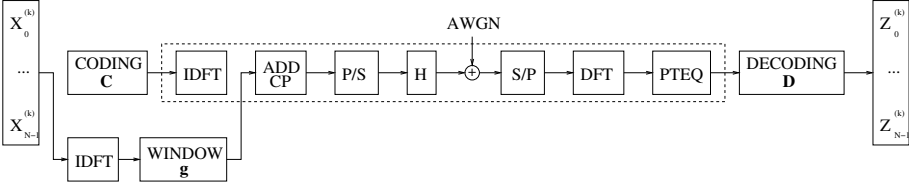


Figure 4.5: Transmitter windowing translates to symbol precoding

application of the CP) can be written as:

$$\mathbf{x}_w^{(k)} = \underbrace{\begin{bmatrix} g(0) & 0 & \dots & 0 \\ 0 & g(1) & \ddots & 0 \\ \vdots & & \ddots & \vdots \\ 0 & \dots & 0 & g(n-1) \end{bmatrix}}_{\mathbf{G}} \mathcal{I}_{\mathbf{N}} \cdot \mathbf{X}^{(k)}. \quad (4.13)$$

As the product of a diagonal matrix and the IDFT-matrix is equal to the product of the IDFT-matrix and a circulant matrix, we can rewrite (4.13) as:

$$\mathbf{x}_w^{(k)} = \mathcal{I}_{\mathbf{N}} \underbrace{\begin{bmatrix} c(0) & c(1) & \dots & c(N-1) \\ c(N-1) & c(0) & \ddots & c(N-2) \\ \vdots & & \ddots & \vdots \\ c(1) & \dots & & c(0) \end{bmatrix}}_{\mathbf{C}} \cdot \mathbf{X}^{(k)}. \quad (4.14)$$

The circulant matrix \mathbf{C} ("C" for coding) is fully defined by its first row \mathbf{c}^T , with

$$\mathbf{c} = [c(0) \dots c(N-1)]^T = \mathcal{I}_{\mathbf{N}} \cdot \mathbf{g} \quad (4.15)$$

i.e. IDFT of \mathbf{g} . The transition from (4.13) to (4.14) is more than mathematical trickery. Looking at the DMT-scheme incorporating transmitter windowing of **Fig. 4.5**, it becomes clear that the windowing operation in the time-domain is equivalent to the multiplication of the subsymbol vector $\mathbf{X}^{(k)}$ with a (pre-)coding matrix \mathbf{C} . Compensating for the window at the receiver is now identical to a decoding in the frequency domain, which is done by multiplication with the decoding matrix $\mathbf{D} = \mathbf{C}^{-1}$ ("D" for decoding), leaving the rest of the signal path (equalization etc.) unaltered. Thus, appealing windows should not only satisfy the constraint (4.10), but preferably also give rise to a sparse decoding matrix \mathbf{D} . We will now further investigate the nature of such windows.

Being the inverse of a circulant matrix, \mathbf{D} is also circulant. We denote the first row of \mathbf{D} as

$$\mathbf{d}^T = [d(0) \dots d(N-1)]. \tag{4.16}$$

Define \mathcal{F}_N the DFT-matrix of size N , and

$$\mathbf{f} = [f(0), \dots, f(N-1)] = \mathcal{F}_N \cdot \mathbf{d}. \tag{4.17}$$

It is now possible to associate to \mathbf{D} a diagonal matrix \mathbf{F} , having on its diagonal the elements of \mathbf{f} . The following relations now hold:

- \mathbf{C} and \mathbf{D} are circular, with $\mathbf{C}^{-1} = \mathbf{D}$, and have as a first row \mathbf{c}^T and \mathbf{d}^T respectively.
- \mathbf{G} and \mathbf{F} are diagonal, with diagonals \mathbf{g} and \mathbf{f} .
- $\mathbf{c} = \mathcal{I}_N \cdot \mathbf{g}$
- $\mathbf{d} = \mathcal{I}_N \cdot \mathbf{f}$

From this, we can conclude that $\mathbf{F} = \mathcal{I}_N \cdot \mathbf{D} \cdot \mathcal{F}_N = \mathcal{I}_N \cdot \mathbf{C}^{-1} \cdot \mathcal{F}_N = (\mathcal{I}_N \cdot \mathbf{C} \cdot \mathcal{F}_N)^{-1} = \mathbf{G}^{-1}$. In other words,

$$g(n) = f(n)^{-1}, n = 0, \dots, N-1. \tag{4.18}$$

Since \mathbf{g} is real-valued, so is \mathbf{f} . Consequently \mathbf{d} is the IDFT of a real-valued vector. Because of the IDFT's symmetry properties, the first and middle element of \mathbf{d} are real-valued, and all other nonzero elements appear in complex conjugate pairs.

We can now distinguish between three cases:

- (i) a general \mathbf{d} (non-sparse)
- (ii) a maximally sparse \mathbf{d} (with only three non-zero elements) is as follows

$$d(n) = \begin{cases} a & n=0 \\ b \cdot e^{j\phi} & n=l \\ b \cdot e^{-j\phi} & n=N-l \\ 0 & n \notin \{0, l, N-l\} \end{cases}, \tag{4.19}$$

with

$$\begin{aligned} a, b & \text{ real} \\ \phi & \text{ real} \in [-\pi \quad \pi] \\ l & \text{ integer} \in [1 \quad N-1] \end{aligned}, \tag{4.20}$$

so that

$$\mathbf{D} = \begin{bmatrix} a & & b.e^{j\phi} & & b.e^{-j\phi} & & \\ & \ddots & & & & & \\ b.e^{-j\phi} & & & & & & \\ & \ddots & & & & & \\ b.e^{j\phi} & & & & & & \\ & \ddots & & & & & \\ & & b.e^{j\phi} & & b.e^{-j\phi} & & a \end{bmatrix} \quad (4.21)$$

is a sparse matrix¹. In practice, this means that \mathbf{f} ($\mathbf{f} = \mathcal{F}_{\mathbf{N}}.\mathbf{d}$) takes the form of a generalized *raised cosine* function. The different parameters influencing \mathbf{f} are the pedestal height a , the frequency and amplitude of the sinusoidal part l and b , and ϕ determining the position of the peak(s).

(iii) intermediate structures

Obviously, multiple complex pairs can be included (hence 5, 7, ... non-zero elements in \mathbf{d}), possibly leading to more powerful windows. A tradeoff should be made between the window quality and the complexity of the decoding.

4.3.2 Determining the window parameters

Returning to the original goal of egress reduction, we now need to choose \mathbf{w} such that an improved side lobe characteristic is obtained. For the rectangular window, the width of the main lobe is equal to $\omega_s = \frac{2.\pi}{N+\nu}$. Note that this decreases with increasing CP length. As a general design criterion, we specify that the power outside the main lobe $\omega_s = \frac{2.\pi}{N+\nu}$ should be as low as possible. Assuming that the total energy is kept constant, this is equivalent to *maximising* the energy ρ within the main lobe [192], i.e. maximising

$$\rho = \int_0^{\omega_s} |W(e^{j\omega})|^2 \frac{d\omega}{\pi}, \quad (4.22)$$

$$\text{with } W(z) = \mathbf{w}^T \mathbf{e}(z), \quad (4.23)$$

$$\text{and } \mathbf{e}(z) = [1 \quad z \quad \dots \quad z^{N+\nu-1}]^T \quad (4.24)$$

$$(4.25)$$

¹This matrix has been made easier to interpret, compared to the originally published version

under unit-energy constraint

$$\mathbf{w}^T \cdot \mathbf{w} = 1. \quad (4.26)$$

Equation (4.22) can be written as

$$\rho = \mathbf{w}^T \left[\int_0^{\omega_s} \mathbf{e}(e^{j\omega})^* \mathbf{e}(e^{j\omega}) \frac{d\omega}{\pi} \right] \mathbf{w} \quad (4.27)$$

$$= \mathbf{w}^T \cdot \mathbf{Q} \cdot \mathbf{w}, \quad (4.28)$$

where \mathbf{Q} has (m,n)th entry

$$q_{m\ n} = \int_0^{\omega_s} \cos(m-n)\omega \frac{d\omega}{\pi}, \quad 0 \leq m, n \leq N + \nu - 1 \quad (4.29)$$

$$= \frac{\sin((m-n)\omega_s)}{(m-n)\pi}. \quad (4.30)$$

$$(4.31)$$

To enforce the cyclic structure (4.10), (4.28) is transformed into a problem in \mathbf{g} . After defining

$$\mathbf{P} = \begin{bmatrix} \mathbf{O}_{\nu \times (N-\nu)} & \mathbf{I}_{\nu \times \nu} \\ & \mathbf{I}_{N \times N} \end{bmatrix}, \quad (4.32)$$

with $\mathbf{O}_{m \times n}$ and $\mathbf{I}_{m \times n}$ the all-zero and identity matrix of size $m \times n$, (4.28) can be written as:

$$\rho = \mathbf{g}^T \cdot \mathbf{P}^T \cdot \mathbf{Q} \cdot \mathbf{P} \cdot \mathbf{g}, \quad (4.33)$$

and the unit norm constraint becomes:

$$\mathbf{g} \cdot \mathbf{P}^T \cdot \mathbf{P} \cdot \mathbf{g} = 1. \quad (4.34)$$

We can now again distinguish between three cases

(i) a general \mathbf{d} (non-sparse)

The maximization of (4.33) satisfying (4.34) can be rewritten as a generalized eigenvalue problem:

$$(\mathbf{P}^T \mathbf{Q} \mathbf{P}) \mathbf{g} = \lambda (\mathbf{P}^T \mathbf{P}) \mathbf{g}, \quad (4.35)$$

and the optimal vector \mathbf{g}_{opt} is equal to the eigenvector corresponding to the largest eigenvalue of $(\mathbf{P}^T \mathbf{P})^{-1} \mathbf{P}^T \mathbf{Q} \mathbf{P}$. The optimal \mathbf{w}_{opt} is now equal to

$$\mathbf{w}_{opt} = \mathbf{P} \cdot \mathbf{g}_{opt}. \quad (4.36)$$

Note that \mathbf{w}_{opt} is only dependent on the (chosen) width of the main lobe.

(ii) a maximally sparse \mathbf{d}

To obtain the optimal *sparse* decoding matrix \mathbf{D} , we have to determine the parameters a , b , ϕ and l from (4.19) optimizing (4.33-4.34), with $\mathbf{f} = \mathcal{F}_{\mathbf{N}} \cdot \mathbf{d}$ and $g(n) = f(n)^{-1}$, $n = 1 \dots N - 1$. We will use $l = 1$, and ϕ such that \mathbf{w} is symmetrical (i.e. $\phi = -\frac{\nu\pi}{N}$). Due to the unit-energy constraint, only one of a or b can be chosen freely. This leads to a one-dimensional optimization problem in either a or b . Because only three non-zero coefficients are present in \mathbf{d} , we denote this optimal (sparse) solution as $\mathbf{w}_{3,opt}$

(ii) intermediate structures

For the intermediate structures, multiple (5, 7, ...) nonzero elements are present in \mathbf{d} , leading to $\mathbf{w}_{5,opt}, \mathbf{w}_{7,opt}, \dots$. These structures offer a tradeoff between egress reduction and computational complexity. The corresponding optimal windows are found using numerical optimization.

4.3.3 Modification of the equalizer

In the previous sections it has been shown that the classical DMT structure can be modified to incorporate an encoding (\mathbf{C}) and a decoding (\mathbf{D}) to reduce the spectral leakage. The influence on the transmission itself was not mentioned so far and will now be investigated.

(i) Approach-1: Cascaded equalization and decoding

In case the equalization of the received (encoded) symbols is perfect and in the absence of noise (i.e. if the dashed rectangle in Fig. 4.5 is equal to a unity-matrix), it is obvious that the decoding will result in the original symbols. Because $\mathbf{D} = \mathbf{C}^{-1}$ it can be considered to be a decorrelator or *zero-forcing equalizer* (ZFE). Unfortunately in practical situations such a ZFE can enhance the noise. Moreover it is not immediately clear how the equalizer itself (e.g. a PTEQ) should be designed in this case. Clearly this approach is not optimal.

(i) Approach-2: Integrated per-tone equalization and decoding

It turns out that the PTEQ can easily be modified to overcome both of the problems mentioned. To understand this we first take a look at the structure of the original PTEQ (for details on its derivation see [196]). An ordinary T -taps PTEQ for tone i operates on received sample blocks of length $N + T - 1$ and makes a linear combination of i^{th} output bin of a DFT and $T - 1$ so-called difference terms which are common for all tones.

For the case of a maximally sparse \mathbf{d} (eq. 4.19) the subsequent decoding (\mathbf{D}) amounts to a linear combination of three of the PTEQ outputs. The result is now a linear combination of the difference terms and three output bins of the DFT.

The decoder and the PTEQ can now easily be combined by making *one* linear combination of the difference terms and *three* output bins of the DFT. This effectively increases the number of taps by two (for each tone), but solves both our problems:

- the PTEQ design criterion remains unchanged, only the number of inputs changes. Usually the PTEQ is designed to minimize the mean square error (MMSE) between the output and a known transmitted constellation point.
- the decoding is part of the equalizer and no longer represents a ZFE such that noise enhancement is avoided.

Obviously, selecting a \mathbf{d} with *additional non-zero elements* will lead to an equalizer with an increased number of inputs, but it is based on the same principle. For the remainder of the text we assume approach-2 is used.

The difference between approach-1 and approach-2 is illustrated in **Fig. 4.6**.

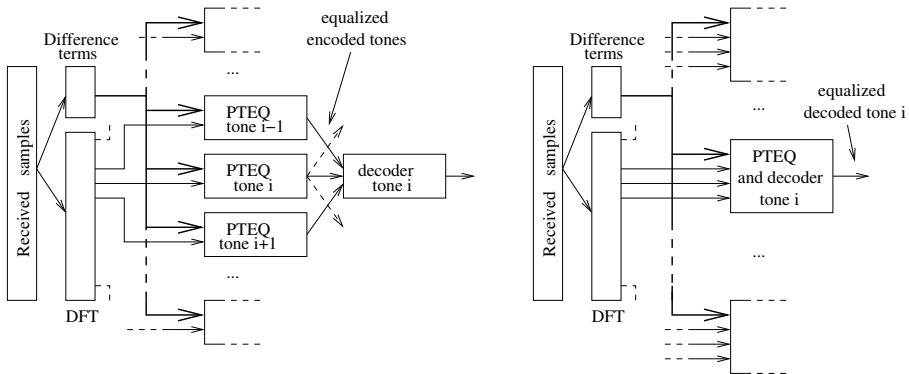


Figure 4.6: In approach-1 (left) the linear combiners (LC) of the PTEQ and the decoder are separated. In approach-2 (right) they are combined.

4.4 Simulation results

4.4.1 Influence on the gress

Three windows are presented: the minimal window $w_{3,opt}$ described by 3 non-zero coefficients in \mathbf{d} (eq. 4.19), a slightly more complex window $w_{5,opt}$, for which \mathbf{d}

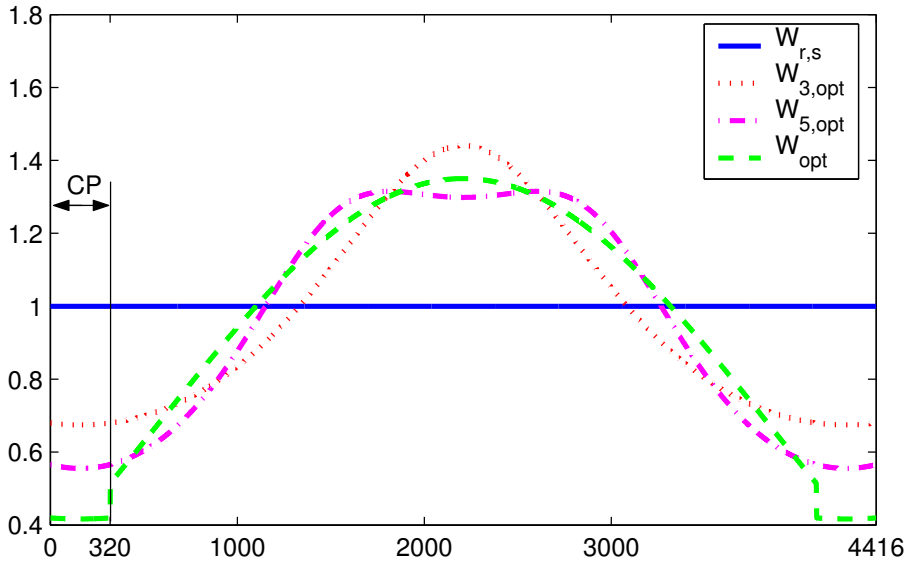


Figure 4.7: The shape of the rectangular window as well as $W_{1,opt}$, $W_{2,opt}$ and W_{opt} .

contains 5 non-zero coefficients, and the optimal window w_{opt} based on (4.35) and with non-sparse decoding.

The simulations have been done for a VDSL system. There are 2048 carriers ($N = 4096$), the prefix length is $CP = 320$ ([54], pp 22). The sampling frequency is 17664 kHz, the tone spacing is 4.3125 kHz.

In **Fig. 4.7** the shape of the rectangular window, $w_{3,opt}$, $w_{5,opt}$ and w_{opt} are shown. To illustrate the egress-reduction, the spectra are compared for a VDSL scenario based on the power spectral density mask Pcab.PM1 from [51]. The most important features are that the frequencies between 3000 kHz and 5200 kHz and above 7050 kHz are reserved for upstream communications ([54], pp 17), and that the power is lowered by 20 dB in the amateur radio bands, from 1810 kHz to 2000 kHz, and from 7000 kHz to 7100 kHz ([51], pp 35). The results are shown in **Fig. 4.8**, and **Fig. 4.9**, showing a detail around the first amateur radio band. It is interesting to note that the spectrum is less toothed (the 'valleys' in between the tones are less pronounced). Moreover, there is a significant egress reduction, especially around the band edge (about 5 dB), achieved without adding any additional (redundant) cyclic extension. Obviously it would be possible to combine this method with such extensions.

Note that the side lobe suppression of this technique in itself is not sufficient to allow

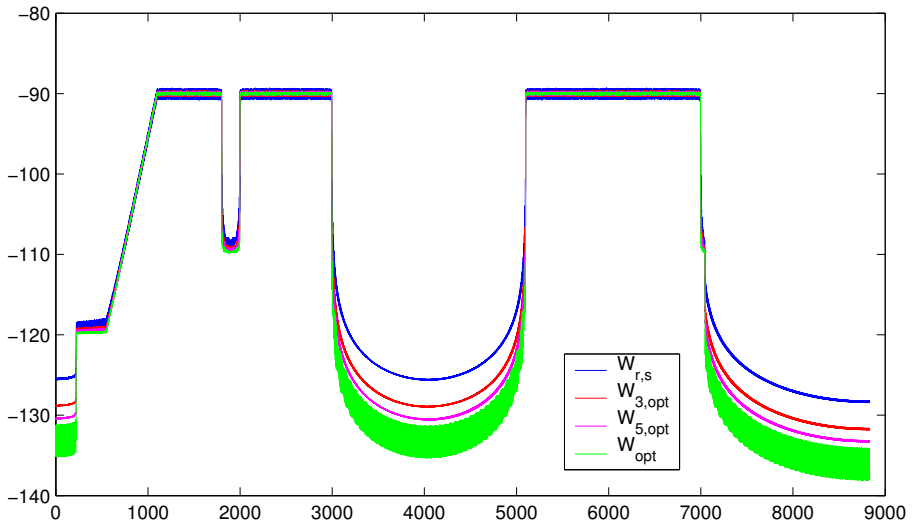


Figure 4.8: Spectrum of the rectangular window, $W_{3,opt}$, $W_{5,opt}$ and W_{opt}

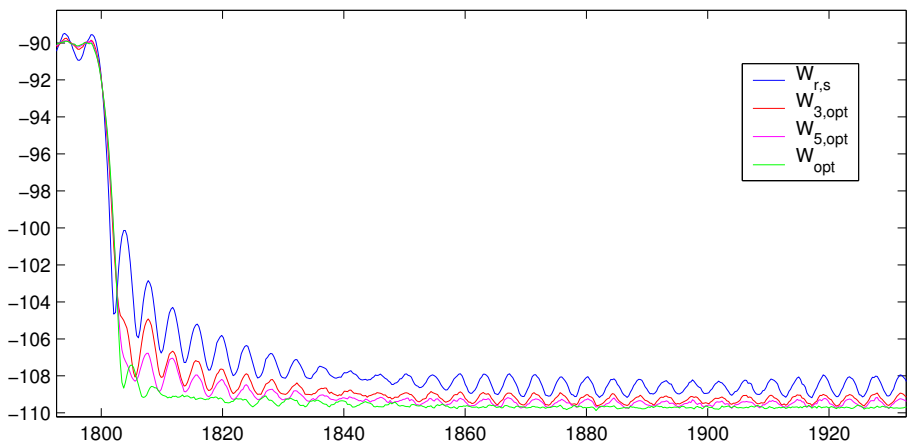


Figure 4.9: Spectrum of the rectangular window, $W_{3,opt}$, $W_{5,opt}$ and W_{opt} (detail of amateur radio band)

the use of all tones up to the forbidden band. Other measures are necessary, such as leaving some tones unused close to the band edge. Note however that the number of unused (lost) tones will be lower than in case a rectangular window is used.

4.4.2 Influence on the transmission

As mentioned before the PTEQ is usually designed according to an MMSE criterion. The exact solution to this problem requires a channel model and is very computationally demanding. Therefore practical implementations generally use an adaptive scheme and a number of training symbols.

To make a fair comparison, however we prefer the exact MMSE solution over an approach which relies on the convergence of the adaptive scheme. To reduce the simulation complexity, we then select an ADSL scenario. It can be expected that the obtained results are readily applicable to VDSL too.

More specifically the simulations are done for an ADSL downstream scenario over a standard loop T1.601#13, with $N = 512$, $\nu = 32$ and using tones 38 to 256. The transmit power is -40dBm/Hz and additive white gaussian noise of -140dBm/Hz was assumed.

A system using a rectangular window at the transmitter and an ordinary PTEQ at the receiver is compared to a system using $\mathbf{W}_{3,opt}$ (for ADSL dimensions) and approach-2 at the receiver. Note that this modified equalizer has the same number of taps as the ordinary PTEQ, implying that it uses 2 difference terms less, because these taps are assigned to the two additional DFT outputs.

The results are shown in **Fig.4.10**. For $T = 3$ the performance of the proposed technique is significantly lower than that of the rectangular window combined with an ordinary PTEq. This comes as no surprise because no taps are available for the difference terms, and the equalization is therefore poor. As the number of taps is increased both techniques are very comparable.

4.5 Conclusion and further work

A novel transmitter windowing technique for DMT has been proposed, which does not rely on an additional cyclic extension of the symbol. This inevitably introduces a distortion of the signal. For a special class of windows, this distortion can be described as a pre-coding operation for which the decoding at the receiver can be done easily. In the simplest case, the window function can be described as the pointwise inversion of a raised cosine window. More complex windows can also be described, but the advantage of the easy decoding then gradually vanishes. Furthermore, formulas are provided to calculate the optimal window, and this is illustrated for the VDSL case.

The decoding at the receiver can be combined with a per-tone equalizer in a very elegant way by taking into account additional DFT outputs. The effect on the transmission was

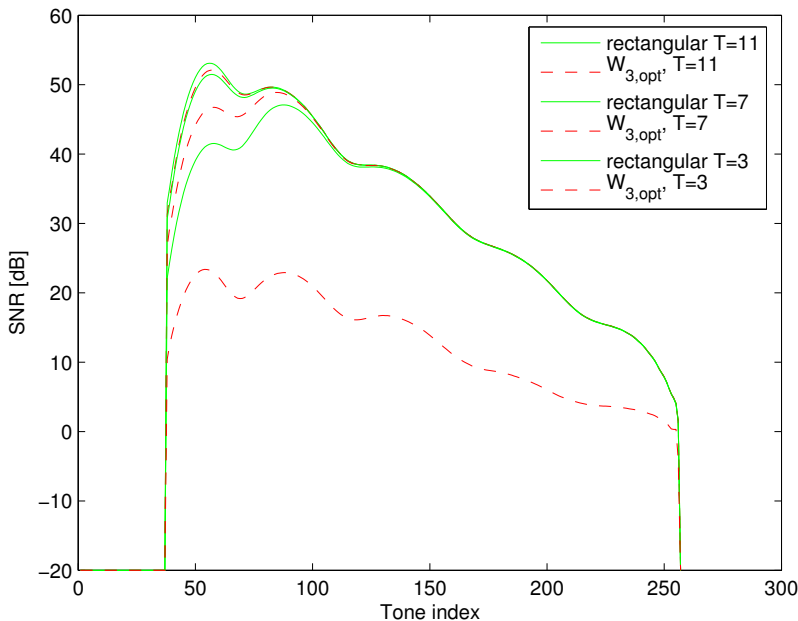


Figure 4.10: Comparison between the rectangular window using an ordinary PTEQ and the $W_{3,opt}$ window using approach-2.

illustrated for an ADSL scenario.

Future work will focus on a selective windowing of the tones in the vicinity of an unauthorised band, and the combination of the proposed technique with windowing in a cyclic extension of the symbol. Also the tradeoff between decoder complexity and egress should be further studied, as well as the interaction between the transmitter window and a channel equalizer using windowing at the receiver.

4.6 Addendum: an alternative application of the window

The windowing technique presented in this chapter can not only be used to reduce egress. It is also useful in the context of known symbol padding (KSP), which is an alternative for the cyclic prefix or zero pad. The KSP consists of a predefined sequence,

known to transmitter and receiver. While a KSP incurs an additional cost in power which does not contribute to the signal to noise ratio (SNR) of the useful signal, it can be used for channel identification and also has advantages for the synchronisation [46] as well as equalization [211].

For SC it is easy to insert the KSP, because the encoding is done in the time domain. KSP-OFDM can be implemented in two ways: either by inserting the KSP in between OFDM symbols or by incorporating the KSP in the symbols themselves. In the first case the cyclic property is lost, though this can be restored at the receiver by subtracting the contribution of the KSP and continuing the processing like in the ZP case [199], or by using a larger DFT size to take into account the KSP [181].

In the second case it is less trivial to impose constraints on the time-domain representation and reserved pilot tones are required to do so. In [23] the selection of the pilot tones led to a computationally very efficient implementation (more about this in section 4.6.2). This system has two drawbacks however, identified by [131]: the repetition of the static padding sequence at each symbol leading to peaks in the frequency spectrum, and the significant variation of the pilot tone amplitudes. In [90] the choice of pilot tones was cleverly optimised to minimise the power, at the cost of a more complex algorithm.

4.6.1 Definitions

Consider an OFDM system with DFT size N . The transmitted vector of complex symbols or *tones* in the frequency domain $\mathbf{x} = [x_0 \dots x_{N-1}]^T$ consists of an interleaving of ν equally spaced pilot tones and $U = N - \nu$ useful data symbols, i.e. $x_0, x_R, x_{2R} \dots$ are pilot tones with $R = N/\nu$. In a classic OFDM system, the time domain representation is obtained by taking the IDFT of \mathbf{x} and adding a CP, ZP or KSP. In this case however, a guard interval of length ν will be imposed based on the pilot tones. The blocks are transmitted over a linear channel of order $L \leq \nu$ with circular channel matrix $\mathbf{H}_{N \times N}$ and are corrupted by white noise \mathbf{n} .

4.6.2 Known signal padding

Define the matrices

$$\mathbf{K}_{N \times \nu} = [\mathbf{I}_\nu \quad \mathbf{I}_\nu \quad \dots \quad \mathbf{I}_\nu]^T, \text{ and} \quad (4.37)$$

$$\mathbf{Z} = \mathbf{I}_N - [\mathbf{K} \quad \mathbf{O}_{N \times U}]. \quad (4.38)$$

A known signal pad $\mathbf{t} = [t_0 \dots t_{\nu-1}]^T$ can be established on the first ν elements of the time domain block \mathbf{s} by premultiplying with \mathbf{Z} and adding the KSP multiplied by \mathbf{K} ,

$$\mathbf{s} = \mathbf{Z}\mathcal{F}^H\mathbf{x} + \mathbf{K}\mathbf{t} \quad (4.39)$$

As described in [23], this insertion of a KSP only affects the pilot tones, leaving the data symbols unchanged.

4.6.3 Intra-symbol windowing

Unfortunately the multiplication with \mathbf{Z} transfers a large amount of energy to the pilot symbols, creating undesired spikes in the frequency spectrum. This can be avoided by applying a time domain window before the multiplication with \mathbf{Z} . This window should be such that it has a low energy on its first ν elements and can easily be compensated for at the receiver. The windows presented in the previous sections are therefore excellent candidates.

Define the window vector $\mathbf{g} = [g_0 \dots g_{N-1}]$, as the piecewise inverse of a raised cosine window, i.e.

$$g_k = \left[(1 + \alpha) + \alpha * \cos \left(\frac{2\pi}{N} \left(k - \frac{\nu}{2} \right) \right) \right]^{-1}, \quad (4.40)$$

shown in **Fig. 4.11**, for $N = 64$, $\nu = 8$ and $\alpha = 5$. Indeed this window reaches its minimum in the first ν elements. Let \mathbf{G} be a diagonal matrix with \mathbf{g} as its diagonal. The received signal can now be written as:

$$\mathbf{y} = \mathbf{H} \left(\mathbf{Z}\mathbf{G}\mathcal{F}^H\mathbf{x} + \mathbf{K}\mathbf{t} \right) + \mathbf{n}. \quad (4.41)$$

4.6.4 Decoding

While the use of the window matrix \mathbf{G} lowers the excessive energy in the pilot tones, it complicates the decoding at the receiver. To explain this, we start with the trivial noiseless case of a channel $\mathbf{H} = \mathbf{I}$ and a ZP instead of a KSP, focusing only on the interaction between \mathbf{G} and \mathbf{Z} .

As explained in paragraphs 4.1 to 4.5, the application of a windowing function \mathbf{G} in the time domain is equivalent to a precoding \mathbf{C} in the frequency domain. The

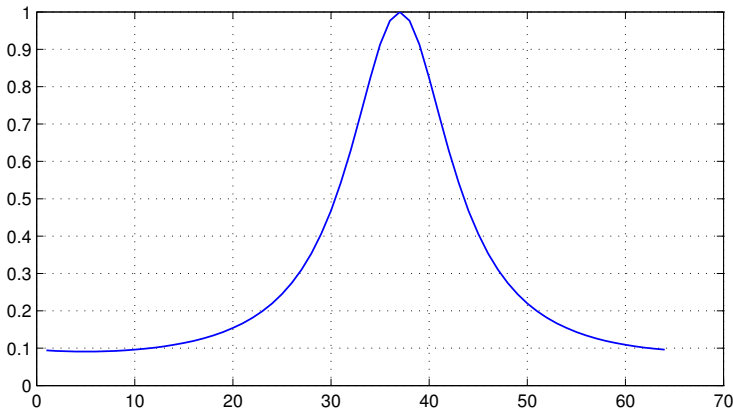


Figure 4.11: The window g is the inverse of a raised cosine

corresponding postcoding is done by multiplication with the decoding matrix

$$\mathbf{C}^{-1} = \begin{bmatrix} a & b & 0 & \dots & 0 & b^* \\ b^* & a & b & 0 & \dots & 0 \\ 0 & \ddots & \ddots & \ddots & \ddots & \vdots \\ \vdots & \ddots & & & & 0 \\ 0 & \dots & 0 & b^* & a & b \\ b & 0 & \dots & 0 & b^* & a \end{bmatrix}, \quad (4.42)$$

with $a = \alpha + 1$ and $b = \frac{\alpha}{2} \exp(j\frac{\nu\pi}{N})$. Unfortunately, due to the KSP, the information at the pilot tones is corrupted, such that the data symbols neighbouring the pilot tones cannot be reconstructed. To understand how this can be solved, assume that the KSP is simply a ZP and there is no noise. The received signal can be rewritten as

$$\mathbf{y} = \mathbf{Z}\mathcal{F}^H\mathbf{C}\mathbf{x}. \quad (4.43)$$

Because the multiplication with \mathbf{Z} only affects information at the pilot frequencies, this can be rewritten as

$$\mathbf{y} = \mathcal{F}^H(\mathbf{C}\mathbf{x} + \mathbf{p}), \quad (4.44)$$

with $\mathbf{p} = [p_0 \dots p_{N-1}]^T$ a vector of which we know that it only has non-zero elements at the pilot tones. The value of \mathbf{p} can be determined by noting that $\mathbf{C}^{-1}\mathcal{F}\mathbf{y} = \mathbf{x} + \mathbf{C}^{-1}\mathbf{p}$ has no contributions from \mathbf{x} at the pilot tone positions. The vector \mathbf{p} can therefore be calculated as

$$\mathbf{p} = \mathbf{U}\mathcal{F}\mathbf{y}, \quad (4.45)$$

with

$$\mathbf{U} = \begin{bmatrix} 1 & \frac{b}{a} & 0 & \dots & 0 & \frac{b^*}{a} \\ 0 & 0 & 0 & 0 & \dots & 0 \\ & \ddots & \ddots & \ddots & \ddots & \vdots \\ \vdots & & \frac{b^*}{a} & 1 & \frac{b}{a} & \\ & \ddots & \ddots & \ddots & \ddots & \vdots \\ 0 & 0 & 0 & 0 & 0 & 0 \end{bmatrix} \quad (4.46)$$

in which the only non-zero rows are those corresponding to the pilot tones.

By combining eqs. (4.44) and (4.45), the decoded symbols can be written as

$$\hat{\mathbf{x}} = \mathbf{C}^{-1}(\mathbf{I} - \mathbf{U})\mathcal{F} \mathbf{y}. \quad (4.47)$$

The term $\mathbf{C}^{-1}(\mathbf{I} - \mathbf{U})$ is elaborated in eq. (4.48).

$$\mathbf{C}^{-1}(\mathbf{I} - \mathbf{U}) = \begin{bmatrix} \mathbf{0} & 0 & \dots & \mathbf{0} & 0 & 0 \\ \mathbf{0} & \frac{a^2 - b \cdot b^*}{a} & b & 0 & 0 & \frac{-b^{*2}}{a} \\ \mathbf{0} & \frac{b^*}{a} & a & b & 0 & 0 \\ \vdots & \ddots & \ddots & \ddots & \ddots & \\ & & 0 & b^* & a & b & 0 & \vdots \\ & & & 0 & b^* & \frac{a^2 - b \cdot b^*}{a} & 0 & \frac{-b^2}{a} & 0 \\ \mathbf{0} & \dots & & 0 & 0 & 0 & 0 & \dots & 0 \\ & & & 0 & \frac{-b^{*2}}{a} & \mathbf{0} & \frac{a^2 - b \cdot b^*}{a} & b & 0 \\ \vdots & & & & \mathbf{0} & b^* & a & b & 0 & \vdots \\ & & & & & & \ddots & \ddots & \ddots & 0 \\ \mathbf{0} & & & & & & & b^* & a & b \\ \mathbf{0} & \frac{-b^2}{a} & 0 & & & & & b^* & \frac{a^2 - b \cdot b^*}{a} \end{bmatrix} \quad (4.48)$$

Note that no information from the pilot tones is used, as indicated by the boldface zero columns. Keeping in mind that using a KSP instead of a ZP only affects the pilot tones, a possible KSP will therefore be completely transparent to the receiver. In practice this means that the KSP is absorbed by the vector \mathbf{p} .

4.6.5 Channel equalization

The part $\mathbf{C}^{-1}(\mathbf{I} - \mathbf{U})$ in (4.47) can be seen as a modified decoder to take into account the ZP (KSP) and the windowing by \mathbf{G} . For all tones except those neighbouring

the pilot tones, this decoder is identical to the original one, \mathbf{C}^{-1} . For those tones neighbouring a pilot tone the equalisation takes into account the pilot tone's other neighbour. If one were to reduce the matrix's dimension by leaving out all rows and columns associated to the pilot tones, all remaining tones would be decoded using only the neighbouring tones. Since a non-trivial circular matrix can be diagonalized by a DFT- and IDFT-matrix, the channel matrix \mathbf{H} can be compensated for by multiplication with a diagonal matrix $\mathbf{\Lambda}$ before the decoding. The complete equalized and decoded symbols, based on the complete model of eq. (4.41) can therefore be written as

$$\hat{\mathbf{x}} = \mathbf{C}^{-1}(\mathbf{I} - \mathbf{U})\mathbf{\Lambda}\mathcal{F}\mathbf{y}$$

$$\hat{\mathbf{x}} = \mathbf{C}^{-1}(\mathbf{I} - \mathbf{U})\mathbf{\Lambda}\mathcal{F}\mathbf{H}(\mathbf{Z}\mathbf{G}\mathcal{F}^H\mathbf{x} + \mathbf{K}\mathbf{t}) + \mathbf{n}.$$

It is clear that this is a zero-forcing equalizer for the non-pilot tones of \mathbf{x} . In practice the decoder $\mathbf{C}^{-1}(\mathbf{I} - \mathbf{U})$ and the equalizer $\mathbf{\Lambda}$ can be combined. Each symbol can now be equalized based on a linear combination of three DFT-outputs, which results in a better equalization.

Unfortunately, this zero forcing equalizer incurs a significant noise enhancement. This is intuitively clear by observing that the attenuation of the windowing function of Fig.4.11 somehow needs to be compensated for. Moreover, the decoding involves the combination of several tones, which always leads to a lowering of the average SNR, be it that this contribution is less pronounced.

Chapter 5

Zero restoration

This chapter consists of a copy of the article *Frequency-domain equalizers with zero restoration for zero-padded block transmission* [37], as submitted for publication in *EURASIP Journal on Wireless Communications and Networking*. Only the layout and the numbering of the references, equations and figures has been changed to accommodate for the different page size and to improve consistency.

Abstract

This contribution focuses on the equalization of block transmissions with zero pad (ZP). If the channel impulse response length does not exceed the ZP length, it is possible to construct zero-forcing equalizers (ZFEs). Improved performance may be achieved using a minimum mean squared error (MMSE) equalizer. However, these equalizers are computationally intensive when a time-domain implementation is used. While the frequency-domain implementation of a ZFE has a lower complexity, it is prone to -potentially infinite- noise enhancement in the presence of spectral zeros. The MMSE equalizer in the frequency domain performs better by limiting the noise enhancement but still loses all information stored at the spectral zeros. We present a method to exploit the redundancy of the padding to recover this lost information, leading to two new frequency-domain equalizers, a ZFE and an MMSE-like equalizer. These have a performance close to the time-domain equalizers, while maintaining the low complexity of the original frequency-domain equalizers. With minor modifications, the equalizers can also be applied if the ZP is replaced by a unique word (UW).

5.1 Introduction

The idea of using a discrete Fourier transform (DFT) to (de)modulate data on carriers -referred to as *tones* or *sub-carriers*- goes back a long time [208]. The transmission is organized in blocks and operates as follows: each tone is assigned a complex data symbol corresponding to a constellation point. These complex data symbols for all tones are packed together in a vector which is converted to the time domain by means of an inverse DFT (IDFT). The resulting time-domain waveform can be seen as a summation of orthogonal signals -one for each tone- hence the name orthogonal frequency division multiplexing (OFDM). This waveform is now transmitted over the channel. The received samples are stored in a vector which is converted back to the frequency domain using a DFT. Unfortunately, the channel causes inter symbol interference and destroys the orthogonality between the tones, complicating the equalization. Both problems can be solved by introducing a *cyclic prefix* (CP): a block of samples at the end of the time-domain waveform is copied and added in front of the waveform prior to transmission [145]. At the receiver side, the samples pertaining to the CP are discarded. The resulting effect is that the linear channel convolution now appears to be circular. Accordingly, the corresponding channel matrix in the frequency domain becomes a diagonal one and the received symbols on each tone only depend on the transmitted symbols on that tone. Equalization can now easily be done by multiplying with the inverse of the diagonal channel matrix. A good overview is given in [17], [111] and [207].

Later on it was realized that this equalization technique is not limited to OFDM but also applicable to single-carrier block transmissions (SC), see [163], who observes that this idea was already suggested two decades earlier [203].

Since one can be converted into the other by merely adding an orthogonal precoding, OFDM and SC have many similarities and mathematical techniques for one of them can usually be adapted for use with the other. The differences mostly concern practical implementation issues: because SC systems generally have a lower peak to average power ratio (PAPR) and a better robustness against non-linearities or carrier offset [163], [60], [144], their demands on the analog hardware are lower than those of OFDM. Adaptive OFDM, on the other hand, has the advantage of allowing bit-loading and power-loading of each sub-carrier according to its quality [144].

Furthermore, adding a CP is not the only way to convert the linear channel convolution into a circular one. This can also be obtained by adding a zero pad (ZP) or *unique word* (UW) to the waveforms in the time domain. Specifically a CP system relies on the overlap-save (OLS) technique, while a ZP system uses overlap-add (OLA) to obtain a circular convolution. Although CP and ZP systems appear to be interchangeable, there are important differences. More specifically, if the channel frequency response exhibits spectral zeros on or zeros near the unit circle, zero-forcing equalization may be

impossible for a CP system, or may lead to severe noise enhancement [135], [164]. A CP-OFDM system can take this into account by discarding the affected sub-carriers if the channel is known at the transmitter, or by using forward error correction (FEC) codes if it is not [60], [164]. The signal projection scheme from [204] offers a fundamental solution but is prohibitive in complexity, while the precoding technique from [212] requires the channel to remain constant over a period of multiple blocks. For a CP-SC system with a zero-forcing equalizer (ZFE) the presence of spectral zeros in the channel response is even worse, as the enhanced noise spreads out over the entire time-domain block. The classical solution is to limit the noise enhancement by using a minimum mean square error (MMSE) equalizer instead [115]. The information stored in the sub-carriers corresponding to the zeros, however, will still be lost.

For a ZP system on the other hand, zero-forcing equalization is always possible [164], [68]. Unfortunately, using the OLA technique to implement the ZFE in the frequency domain introduces the same vulnerability to spectral zeros in the channel response as in CP systems. This results in an ill-conditioned problem and again the need to revert to an MMSE equalizer. Again, the information stored in the sub-carriers corresponding to the zeros is still lost.

We present two new frequency-domain equalizers for ZP transmission which can recover this information lost in the spectral zeros. They are applicable to OFDM as well as SC transmissions. With minor modifications they can also be used for systems using a UW.

The text is organized as follows: in section 5.2 the system model and existing equalization techniques are presented. In section 5.3 the new frequency-domain equalizers are introduced. In section 5.4 they are analysed theoretically and in section 5.5 simulation results are presented. Finally, in section 5.6 conclusions are summarized.

5.2 System model and equalizers

The following conventions are followed: bold lowercase letters denote vectors and bold uppercase letters denote matrices. Normal uppercase letters denote constants. $(\cdot)^T$, $(\cdot)^H$, $(\cdot)^\dagger$ and $E\{\cdot\}$ denote transpose, Hermitian, pseudo-inverse and expected value respectively and $\mathbf{A}(:, [l_1 \dots l_k])$ selects columns $l_1 \dots l_k$ of \mathbf{A} . The DFT, IDFT, zero and identity matrix of size K are represented by \mathcal{F}_K , \mathcal{F}_K^H , $\mathbf{0}_K$, and \mathbf{I}_K respectively. Occasionally, for clarity the dimensions of a matrix are indicated as $[\cdot]_{K \times L}$.

Now consider a finite impulse response (FIR) channel $\mathbf{h} = [h_0 \ h_1 \ \dots \ h_L]^T$ of order L , which is known by both transmitter and receiver and which can be considered *quasi static* over one block period. The transmitted block $\mathbf{x} = [x_1 \ x_2 \ \dots \ x_N]^T$

is followed by a ZP of length P , with $P \geq L$ to avoid IBI. Without loss of generality it is assumed that the variance of \mathbf{x} equals unity, i.e. $E\{\mathbf{x}\mathbf{x}^H\} = \mathbf{I}_N$ and that $P = L$. The received signal \mathbf{y} is given as:

$$\mathbf{y} = \underbrace{\begin{bmatrix} h_0 & & & & \\ \vdots & \ddots & & & \\ h_L & & \ddots & & \\ & & & \ddots & \\ & & & & h_0 \\ & & & & \vdots \\ & & & & h_L \end{bmatrix}}_{\mathbf{H}_{(N+L) \times N}} \mathbf{x} + \mathbf{n}, \quad (5.1)$$

with \mathbf{H} the linear convolution matrix of \mathbf{h} and \mathbf{n} additive noise. Without loss of generality it is assumed that the noise is zero-mean and white with variance σ_n^2 , i.e. $E\{\mathbf{n}\mathbf{n}^H\} = \sigma_n^2 \mathbf{I}_{N+L}$.

5.2.1 Time domain equalization

An equalizer \mathbf{W} is a matrix for which $\hat{\mathbf{x}} = \mathbf{W}\mathbf{y}$ is an estimate of \mathbf{x} . Moreover, any equalizer \mathbf{W}_{ZFE} that satisfies the following constraint

$$\mathbf{W}_{\text{ZFE}} \mathbf{H}_{(N+L) \times N} = \mathbf{I}_N, \quad (5.2)$$

is referred to as a *zero forcing equalizer* (ZFE). In the absence of noise, such ZFE obviously leads to a perfect reconstruction of the transmitted block. Because \mathbf{H} is a tall Toeplitz matrix, an infinite number of equalizers exist that satisfy Eq. (5.2). Since $\hat{\mathbf{x}} = \mathbf{x} + \mathbf{W}_{\text{ZFE}}\mathbf{n}$, ZFE's only differ in the way they treat the noise. One particular ZFE is obtained as the pseudo inverse of \mathbf{H} , which then provides the *minimum-norm* solution of Eq. (5.2). It is given by¹:

$$\mathbf{W}_{\text{ZFE-TD}} = \mathbf{H}^\dagger = (\mathbf{H}^H \mathbf{H})^{-1} \mathbf{H}^H. \quad (5.3)$$

Here $\mathbf{H}^H \mathbf{H}$ is a full-rank $N \times N$ matrix and hence always invertible. This is referred to as the ZFE-TD (time-domain ZFE) where "time-domain" refers to the absence of a transformation to the frequency domain (see 5.2.2). It is the optimal ZFE because it has the smallest noise enhancement.

By dropping the perfect reconstruction constraint of Eq. (5.2) it is often possible to achieve improved performance. The MMSE equalizer also takes into account the noise

¹The minimum norm ZFE is often referred to as MMSE-ZFE. In this text it is called ZFE-TD to stress its implementation in the time domain and avoid confusion with the MMSE solution of Eq. (5.4)

statistics and performs an overall optimization by minimizing the expected value of the squared error, $E\{\|\mathbf{x} - \mathbf{W}_{\text{MMSE-TD}}\mathbf{y}\|^2\}$. It can be expressed as:

$$\mathbf{W}_{\text{MMSE-TD}} = (\mathbf{H}^H \mathbf{H} + \sigma_n^2 \mathbf{I}_N)^{-1} \mathbf{H}^H. \quad (5.4)$$

The calculation of these equalizers has a complexity of $\mathcal{O}(N^2)$ flops (using structured matrix inversion formulae) while calculating $\hat{\mathbf{x}} = \mathbf{W}\mathbf{y}$ requires no more than $\mathcal{O}(N^2)$ flops per block [206].

5.2.2 Frequency domain equalization based on matrix folding

To exploit frequency-domain techniques the linear channel convolution needs to be converted into a circular one. Accordingly the matrix \mathbf{H} needs to be transformed into a circular matrix. This can be achieved in two ways: either by folding the last L rows back to the top or by extending it with L more columns. The first method corresponds to an *overlap-add* operation: the last L samples of \mathbf{y} are added to the first L samples and then only the first N samples of the result are kept, resulting in

$$\mathbf{y}_f = \underbrace{\begin{bmatrix} \mathbf{I}_N & \mathbf{I}_L \\ \mathbf{0} & \mathbf{0} \end{bmatrix}}_{\mathbf{G}_f} \mathbf{y} = \underbrace{\begin{bmatrix} h_0 & & & h_L & \dots & h_1 \\ & \ddots & & & & \vdots \\ \vdots & & & & & h_L \\ h_L & & & & & \\ & \ddots & & & & \\ & & & h_L & \dots & h_0 \end{bmatrix}}_{\mathbf{H}_f(N \times N)} \mathbf{x} + \mathbf{n}_f. \quad (5.5)$$

Note that the multiplication with the $(N \times (N+L))$ -matrix \mathbf{G}_f reduces the number of matrix rows and hence the information in the system. The existence of a ZFE solution may therefore no longer be guaranteed. Indeed, \mathbf{H}_f is an $N \times N$ matrix which becomes rank deficient if the Z-transform of \mathbf{h} has a zero on one of the N equally spaced points $e^{\frac{2\pi i}{N}k}$, with $k = 0 \dots N-1$, referred to as *spectral zeros*. If \mathbf{H}_f has rank N , the resulting unique ZFE can be written as:

$$\mathbf{W}_{\text{ZFE-TD-FOLD}} = \mathbf{H}_f^{-1} \mathbf{G}_f. \quad (5.6)$$

To perform the equalization in the frequency domain, note that \mathbf{H}_f can be diagonalized to Λ_f , such that Eq. (5.5) becomes:

$$\mathbf{y}_f = \underbrace{\mathcal{F}_N^H \Lambda_f \mathcal{F}_N}_{\mathbf{H}_f} \mathbf{x} + \mathbf{n}_f. \quad (5.7)$$

yielding:

$$\mathbf{y} = \underbrace{\mathcal{F}_M^H \Lambda_e \mathcal{F}_M}_{\mathbf{H}_e} \mathbf{x}_{ZP} + \mathbf{n}. \quad (5.11)$$

The frequency-domain ZFE can be written as:

$$\mathbf{W}_{\text{ZFE-FD-EXT}} = [\mathbf{I}_N \mid \mathbf{O}] \mathcal{F}_M^H \Lambda_e^{-1} \mathcal{F}_M \quad (5.12)$$

The calculation of the inversion of the diagonal matrix in this equation requires $\mathcal{O}(M)$ flops, whereas the calculation of $\hat{\mathbf{x}}$ requires $\mathcal{O}(M \log(M))$ flops per block. Note that, in the absence of spectral zeros, there exists a clever method to express the optimal ZFE, $\mathbf{W}_{\text{ZFE-TD}}$ in terms of $\mathbf{W}_{\text{ZFE-FD-EXT}}$ and a correction term of low complexity [185].

In case of spectral zeros at one of the points $e^{\frac{2\pi i}{N+L}k}$, with $k = 0 \dots M - 1$, Λ_e may be a rank-deficient matrix. Again, this can be dealt with by using the MMSE equalizer,

$$\mathbf{W}_{\text{MMSE-FD-EXT}} = [\mathbf{I}_N \mid \mathbf{O}] \mathcal{F}_M^H (\Lambda_e^H \Lambda_e + \sigma_n^2 \mathbf{I}_M)^{-1} \Lambda_e^H \mathcal{F}_M \quad (5.13)$$

It is remarkable that the assured possibility of zero-forcing equalization is lost in going from Eq. (5.1) to Eq. (5.12), because the number of equations is unchanged (contrary to Eq.(5.5), where information is truly discarded). The problem arises in Eq. (5.10) when the matrix \mathbf{H}_e is not of full rank. For the solution in the time domain, however, \mathbf{H}_e does not need to be of full rank because the last L elements of \mathbf{x}_{ZP} are known to be zero. In the frequency domain this additional information is unavailable. In the next section this problem is solved by feeding back this known information and fixing the possible "gaps" in Λ_e , thereby restoring the information that was lost due to the spectral zeros.

5.3 Improved frequency-domain equalization

In section 5.2.3, the ZP part of the equalized signal is discarded by the multiplication with $[\mathbf{I}_N \mid \mathbf{O}]$ in Eqs. (5.12) and (5.13). The equalized ZP, however, contains information that can help to improve the equalization of the useful signal.

Before diving into the mathematics, the general idea will be illustrated by a graphical example. Consider a simple binary communication system with zero padding. The elements of \mathbf{x} only take two values, as shown in Fig. 5.1. Assume a channel that can be properly equalized at every sub-carrier except for one, where it exhibits a spectral zero. Any energy received at the sub-carrier exhibiting this spectral zero can therefore only be noise and the best any frequency-domain equalizer can do is to discard it. Note that this is exactly what the MMSE equalizer in Eq. (5.13) does. The resulting $\hat{\mathbf{x}}$, including the equalized ZP, is also shown in Fig. 5.1. Comparing the transmitted signal and the equalized version, a sinusoidal disturbance is immediately apparent. This disturbance is

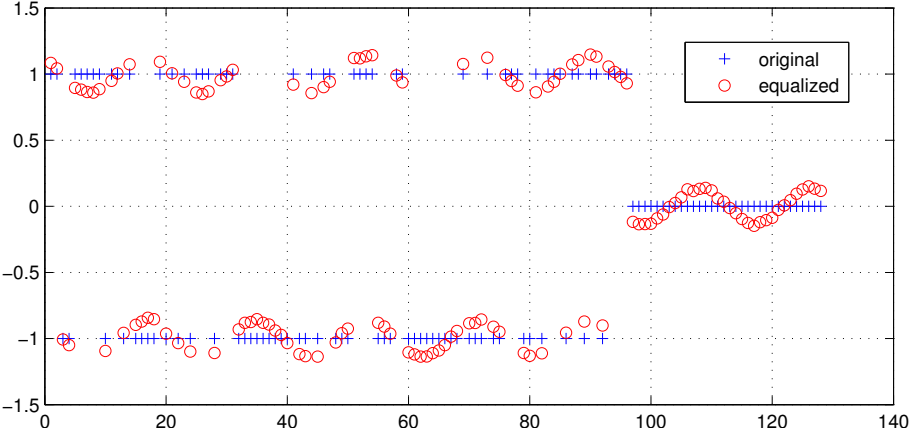


Figure 5.1: The originally transmitted signal and the equalized received signal, assuming one sub-carrier was discarded. The phase and amplitude of the missing sub-carrier can be estimated by inspecting the zero-pad.

caused by the absence of the contribution of the sub-carrier which exhibited a spectral zero. If this missing contribution would be added, the equalized useful signal points would be closer to the transmitted ones, and the equalized zero pad would be closer to zero. Exactly this last observation suggests a method to determine the contribution of the missing sub-carrier: its phase and amplitude should be chosen so as to minimize the zero pad. After determining these parameters, the contribution of this sub-carrier can be added. It is expected that this addition will also improve the quality of the useful signal. This idea will now be elaborated mathematically. To simplify the notation it is assumed that $L = P$, which can easily be obtained by padding \mathbf{h} with zeros.

5.3.1 Frequency-domain ZFE with zero restoration

If Λ_e is invertible and well-conditioned the solutions from Eqs. (5.12) or (5.13) can be used. If Λ_e is rank-deficient or ill-conditioned, assume V diagonal elements of Λ_e are non-zero while the remaining $K = M - V$ elements are zero or close to zero. Note that, because \mathbf{H}_e is at least of rank N , it follows that $K \leq P$. Now rearrange the diagonal elements of Λ_e such that the K (close-to-) zero elements are collected at the end. Rearrange the rows of the DFT-matrix \mathcal{F}_M in a likewise manner and call the

result \mathbf{F} . The matrix \mathbf{H}_e can now be diagonalized as

$$\mathbf{H}_e = \underbrace{\begin{bmatrix} \mathbf{F}_A^H & \mathbf{F}_C^H \\ \mathbf{F}_B^H & \mathbf{F}_D^H \end{bmatrix}}_{\mathbf{F}^H} \begin{bmatrix} \Lambda_{nz} & \mathbf{O} \\ \mathbf{O} & \Lambda_\epsilon \end{bmatrix} \underbrace{\begin{bmatrix} \mathbf{F}_A & \mathbf{F}_B \\ \mathbf{F}_C & \mathbf{F}_D \end{bmatrix}}_{\mathbf{F}}, \quad (5.14)$$

in which Λ_{nz} holds the non-zero diagonal elements of Λ_e , Λ_ϵ holds the (close-to-) zero elements, $\mathbf{F}_A (V \times N)$, and $\mathbf{F}_B (V \times L)$, $\mathbf{F}_C (K \times N)$ and $\mathbf{F}_D (K \times L)$ are submatrices of \mathbf{F} . Because $\mathbf{F}^H \mathbf{F} = \mathbf{I}$, specific relations hold between these submatrices, e.g. $\mathbf{F}_B^H \mathbf{F}_A = -\mathbf{F}_D^H \mathbf{F}_C$ and $\mathbf{F}_A^H \mathbf{F}_A + \mathbf{F}_C^H \mathbf{F}_C = \mathbf{I}$.

Inverting Λ_ϵ -if at all possible- would lead to a significant noise enhancement. However, by disregarding Λ_ϵ and inverting only Λ_{nz} , a first approximation of \mathbf{x}_{ZP} , can be calculated,

$$\hat{\mathbf{x}}_{ZP_{temp}} = \mathbf{F}^H \begin{bmatrix} \Lambda_{nz}^{-1} & \mathbf{O} \\ \mathbf{O} & \mathbf{O} \end{bmatrix} \mathbf{F} \mathbf{y} \quad (5.15)$$

$$= \begin{bmatrix} \mathbf{F}_A^H \\ \mathbf{F}_B^H \end{bmatrix} \Lambda_{nz}^{-1} \begin{bmatrix} \mathbf{F}_A & \mathbf{F}_B \end{bmatrix} \mathbf{y}, \quad (5.16)$$

Note that for high SNR values, this converges to the MMSE-solution of Eq. (5.13).

Because \mathbf{F}^H can be derived from \mathcal{F}^H by a simple permutation of the rows and columns, it is also an orthogonal matrix and, as such, its columns form a base onto which the eventual equalizer output $\hat{\mathbf{x}}$ can be decomposed. Most of the coefficients of this decomposition can be derived from Eq. (5.16), more specifically these are the coefficients related to the first V columns of \mathbf{F}^H and the result is $\hat{\mathbf{x}}_{ZP_{temp}}$. The coefficients related to the last K columns of \mathbf{F}^H are unknown and set to zero in (5.16). However, including these columns could potentially lead to a better approximation of \mathbf{x} . Therefore a correction term is added to $\hat{\mathbf{x}}_{ZP_{temp}}$, which lies in the column space of the last K columns of \mathbf{F}^H , and which can be written as:

$$\hat{\mathbf{x}}_{ZP_{corr}} = \begin{bmatrix} \mathbf{F}_C^H \\ \mathbf{F}_D^H \end{bmatrix} \mathbf{q}, \quad (5.17)$$

where \mathbf{q} holds the unknown coefficients related to the last V columns of \mathbf{F}^H . The correction term can be determined by taking into account that the last P elements of $\hat{\mathbf{x}}_{ZP}$ should be zero. This leads to a system of P equations in K unknowns, which can be solved exactly if no noise is present. In practice the correction term can be calculated from the following least-squares (LS) system:

$$\mathbf{F}_D^H \mathbf{q} + \begin{bmatrix} \mathbf{O} & \mathbf{I}_L \end{bmatrix} \hat{\mathbf{x}}_{ZP_{temp}} \stackrel{LS}{=} \mathbf{O}_{L \times 1}, \quad (5.18)$$

the solution of which is given by:

$$\mathbf{q} = -(\mathbf{F}_D \mathbf{F}_D^H)^{-1} \mathbf{F}_D \mathbf{F}_B^H \Lambda_{nz}^{-1} [\mathbf{F}_A \mid \mathbf{F}_B] \mathbf{y}. \quad (5.19)$$

The overall expression for $\hat{\mathbf{x}}$ therefore becomes:

$$\begin{aligned} \hat{\mathbf{x}} &= [\mathbf{I}_N \mid \mathbf{O}] (\hat{\mathbf{x}}_{ZP_{temp}} + \hat{\mathbf{x}}_{ZP_{corr}}) \\ &= \underbrace{(\mathbf{F}_A^H - \mathbf{F}_C^H (\mathbf{F}_D \mathbf{F}_D^H)^{-1} \mathbf{F}_D \mathbf{F}_B^H) \Lambda_{nz}^{-1} [\mathbf{F}_A \mid \mathbf{F}_B]}_{\mathbf{W}_{ZFE-ZR}} \mathbf{y} \end{aligned} \quad (5.20)$$

This equation defines the ZFE-ZR, where ZR refers to *zero restoration*. It can be rewritten as:

$$\mathbf{W}_{ZFE-ZR} = [\mathbf{F}_A^H \quad \mathbf{F}_C^H] \begin{bmatrix} \mathbf{I} & \mathbf{O} \\ \mathbf{Q} & \mathbf{O} \end{bmatrix} \begin{bmatrix} \Lambda_{nz}^{-1} & \mathbf{O} \\ \mathbf{O} & \mathbf{O} \end{bmatrix} \mathbf{F}, \quad (5.21)$$

with $\mathbf{Q} = -(\mathbf{F}_D \mathbf{F}_D^H)^{-1} \mathbf{F}_D \mathbf{F}_B^H = -(\mathbf{F}_D^H)^\dagger \mathbf{F}_B^H$.

It can now be shown that \mathbf{W}_{ZFE-ZR} satisfies the constraint of Eq. (5.2):

$$\begin{aligned} &\mathbf{W}_{ZFE-ZR} \mathbf{H} \\ &= \mathbf{W}_{ZFE-ZR} \mathbf{H}_e \begin{bmatrix} \mathbf{I} \\ \mathbf{O} \end{bmatrix} \\ &= [\mathbf{F}_A - \mathbf{F}_C \mathbf{Q} \quad \mathbf{O}] \begin{bmatrix} \Lambda_{nz}^{-1} \Lambda_{nz} & \mathbf{O} \\ \mathbf{O} & \mathbf{O} \Lambda_e \end{bmatrix} \begin{bmatrix} \mathbf{F}_A \\ \mathbf{F}_C \end{bmatrix} \\ &= \mathbf{F}_A^H \mathbf{F}_A + \mathbf{F}_C^H \underbrace{(\mathbf{F}_D \mathbf{F}_D^H)^{-1} \mathbf{F}_D \mathbf{F}_D^H}_{\mathbf{I}} \mathbf{F}_C \\ &= \mathbf{I}. \end{aligned} \quad (5.22)$$

So the ZFE-ZR is indeed a ZFE, capable of recovering the lost information. Note that this derivation holds even if the diagonal elements of Λ_e are not exactly equal to zero, which is more common in real-world situations.

Note that this procedure involves calculating the pseudoinverse of \mathbf{F}_D^H , which is poorly conditioned if the corresponding columns of the IDFT matrix are close to each other. In other words, the restoration of the information lost in spectral (close-to-) zeros works best if these spectral (close-to-) zeros are not clustered.

The result of Eq. (5.21) has some similarity to another ZFE proposed in [183], which indeed targets the same problem of spectral zeros, be it in the context of a *diversity*

analysis. In the current notation, this ZFE can be written as:

$$\mathbf{W} = \begin{bmatrix} \mathbf{F}_A^{-1} & \mathbf{O} \end{bmatrix} \left[\begin{array}{c|c} \mathbf{\Lambda}_{nz}^{-1} & \mathbf{O} \\ \hline \mathbf{O} & \mathbf{O} \end{array} \right] \mathbf{F}, \quad (5.23)$$

which can easily be shown to satisfy Eq. (5.2) as well. Note that Eq. (5.23) assumes that $K = P$, because \mathbf{F}_A needs to be square. Under this assumption, the solutions of Eq. (5.21) and Eq. (5.23) are mathematically identical, because of the uniqueness of \mathbf{F}_A^{-1} . Regarding the computational complexity, however, they are very different. The evaluation of Eq. (5.23) requires the inversion of \mathbf{F}_A . Taking into account the Vandermonde structure of this matrix, this requires $5N^2/2$ operations [183], which typically is much higher than the evaluation of Eq. (5.21), as will be shown later. Note that the same author also offered a similar solution, which was the first *linear* equalization scheme to achieve maximum multipath diversity over single-input single-output wireless links [184].

5.3.2 Frequency-domain MMSE-like equalization with zero restoration

As noted before, frequency-domain MMSE equalizers can avoid dramatic noise enhancement due to an ill-conditioned channel matrix. However they too do not offer any solution for the loss of information associated with a (close-to-) zero on the diagonal of $\mathbf{\Lambda}_c$. This can be solved using a structure similar to the ZFE-ZR presented in the previous section.

Using $\mathbf{\Lambda}_{nz}$ and $\mathbf{\Lambda}_\epsilon$ from Eq. (5.14), the following diagonal matrices can be defined:

$$\mathbf{\Gamma}_{nz} = (\mathbf{\Lambda}_{nz}^H \mathbf{\Lambda}_{nz} + \sigma_n^2 \mathbf{I}_V)^{-1} \mathbf{\Lambda}_{nz}^H \quad (5.24)$$

$$\mathbf{\Gamma}_\epsilon = (\mathbf{\Lambda}_\epsilon^H \mathbf{\Lambda}_\epsilon + \sigma_n^2 \mathbf{I}_K)^{-1} \mathbf{\Lambda}_\epsilon^H, \quad (5.25)$$

such that the MMSE-FD-EXT in Eq. (5.13) can be rewritten as

$$\mathbf{W}_{\text{MMSE-FD-EXT}} = \begin{bmatrix} \mathbf{F}_A^H & \mathbf{F}_C^H \end{bmatrix} \left[\begin{array}{c|c} \mathbf{\Gamma}_{nz} & \mathbf{O} \\ \hline \mathbf{O} & \mathbf{\Gamma}_\epsilon \end{array} \right] \mathbf{F}. \quad (5.26)$$

Following the same steps as in the previous section, an improved MMSE-like equalizer with zero restoration can be obtained as

$$\mathbf{W}_{\text{MMSE-ZR}} = \begin{bmatrix} \mathbf{F}_A^H & \mathbf{F}_C^H \end{bmatrix} \left[\begin{array}{c|c} \mathbf{I} & \mathbf{O} \\ \hline \mathbf{Q} & \mathbf{O} \end{array} \right] \left[\begin{array}{c|c} \mathbf{\Gamma}_{nz} & \mathbf{O} \\ \hline \mathbf{O} & \mathbf{O} \end{array} \right] \mathbf{F}, \quad (5.27)$$

with exactly the same \mathbf{Q} as in Eq. 5.21. In the following section it will be demonstrated that the ZFE-ZR and the MMSE-ZR indeed improve on the result of the ZFE-FD-EXT and the MMSE-FD-EXT

5.4 Theoretical analysis of the performance

The bit error rate (BER) of a communications system can directly be calculated from the modulation scheme and the achieved mean squared error (MSE). For any equalizer \mathbf{W} , the MSE of the equalized blocks is given by the diagonal elements of the autocorrelation matrix of the equalization error, i.e.

$$\begin{aligned} \text{MSE} &= \text{Diag} \left\{ E \{ (\mathbf{W}\mathbf{y} - \mathbf{x})(\mathbf{W}\mathbf{y} - \mathbf{x})^{\mathcal{H}} \} \right\} \\ &= \text{Diag} \left\{ (\mathbf{W}\mathbf{H} - \mathbf{I})(\mathbf{W}\mathbf{H} - \mathbf{I})^{\mathcal{H}} + \sigma_n^2 \mathbf{W}\mathbf{W}^{\mathcal{H}} \right\} \end{aligned} \quad (5.28)$$

The MSE has a contribution stemming from the inexact channel equalization and a noise contribution. The first contribution obviously equals zero for any ZFE.

5.4.1 ZFE

Bearing in mind that the ZFE-FD-EXT of Eq. (5.12) can be rewritten as

$$\mathbf{W}_{\text{ZFE-FD-EXT}} = \begin{bmatrix} \mathbf{F}_A^{\mathcal{H}} & \mathbf{F}_C^{\mathcal{H}} \end{bmatrix} \left[\begin{array}{c|c} \mathbf{\Lambda}_{\text{nz}}^{-1} & \mathbf{O} \\ \mathbf{O} & \mathbf{\Lambda}_{\epsilon}^{-1} \end{array} \right] \mathbf{F}, \quad (5.29)$$

its MSE equals

$$\begin{aligned} \text{MSE}_{\text{ZFE-FD-EXT}} &= \text{Diag} \left\{ \sigma_n^2 \begin{bmatrix} \mathbf{F}_A^{\mathcal{H}} & \mathbf{F}_C^{\mathcal{H}} \end{bmatrix} \left[\begin{array}{c|c} \mathbf{\Lambda}_{\text{nz}}^{-1} & \mathbf{O} \\ \mathbf{O} & \mathbf{\Lambda}_{\epsilon}^{-1} \end{array} \right] \right. \\ &\quad \left. \left[\begin{array}{c|c} \mathbf{\Lambda}_{\text{nz}}^{-1} & \mathbf{O} \\ \mathbf{O} & \mathbf{\Lambda}_{\epsilon}^{-1} \end{array} \right]^{\mathcal{H}} \begin{bmatrix} \mathbf{F}_A \\ \mathbf{F}_C \end{bmatrix} \right\} \\ &= \frac{\sigma_n^2}{M} \left(\text{tr} \left\{ \mathbf{\Lambda}_{\text{nz}}^{-1} \mathbf{\Lambda}_{\text{nz}}^{-1\mathcal{H}} + \mathbf{\Lambda}_{\epsilon}^{-1} \mathbf{\Lambda}_{\epsilon}^{-1\mathcal{H}} \right\} \right) \mathbf{1}_{N \times 1}, \end{aligned} \quad (5.30)$$

with $\text{tr}\{\cdot\}$ the trace operator and $\mathbf{1}_{N \times 1}$ an all-one vector. This MSE is identical for all elements in the received block. The MSE of the ZFE-ZR can be written as

$$\begin{aligned} \text{MSE}_{\text{ZFE-ZR}} &= \sigma_n \text{Diag} \left\{ \mathbf{F}_A^{\mathcal{H}} \mathbf{\Lambda}_{\text{nz}}^{-1} \mathbf{\Lambda}_{\text{nz}}^{-1\mathcal{H}} \mathbf{F}_A + \mathbf{F}_A^{\mathcal{H}} \mathbf{\Lambda}_{\text{nz}}^{-1} \mathbf{\Lambda}_{\text{nz}}^{-1\mathcal{H}} \mathbf{Q}^{\mathcal{H}} \mathbf{F}_C \right. \\ &\quad \left. \mathbf{F}_C^{\mathcal{H}} \mathbf{Q} \mathbf{\Lambda}_{\text{nz}}^{-1} \mathbf{\Lambda}_{\text{nz}}^{-1\mathcal{H}} \mathbf{F}_A + \mathbf{F}_C^{\mathcal{H}} \mathbf{Q} \mathbf{\Lambda}_{\text{nz}}^{-1} \mathbf{\Lambda}_{\text{nz}}^{-1\mathcal{H}} \mathbf{Q}^{\mathcal{H}} \mathbf{F}_C \right\}. \end{aligned} \quad (5.31)$$

This MSE has a complex dependency on the noise of the sub-carriers corresponding to $\mathbf{\Lambda}_{\text{nz}}$ and the correlation between the submatrices of \mathbf{F} . However, it is clear that it

lacks the detrimental term in Λ_ϵ^{-1} . As the diagonal elements of Λ_ϵ approach zero, the MSE of the ZFE-TD-EXT increases unboundedly while the MSE of the ZFE-ZR is not influenced. Therefore the latter has a superior performance in the presence of spectral (close-to-) zeros.

5.4.2 MMSE

The MSE of MMSE equalizers has a contribution stemming from the inexact channel equalization as well as a noise contribution. Both will now be analysed for the MMSE-FD-EXT and the MMSE-ZR.

Signal contribution

For the MMSE-FD-EXT, the signal contribution to the MSE equals

$$\begin{aligned}
 \text{MSE}_{\text{MMSE-FD-EXT}}^{\text{signal}} &= \text{Diag} \left\{ \left(\begin{bmatrix} \mathbf{F}_A^{\mathcal{H}} & \mathbf{F}_C^{\mathcal{H}} \end{bmatrix} \begin{bmatrix} \Gamma_{\text{nz}} \Lambda_{\text{nz}} & \mathbf{O} \\ \mathbf{O} & \Gamma_\epsilon \Lambda_\epsilon \end{bmatrix} \begin{bmatrix} \mathbf{F}_A \\ \mathbf{F}_C \end{bmatrix} - \mathbf{I}_N \right) \times \right. \\
 &\quad \left. \left(\begin{bmatrix} \mathbf{F}_A^{\mathcal{H}} & \mathbf{F}_C^{\mathcal{H}} \end{bmatrix} \begin{bmatrix} \Gamma_{\text{nz}} \Lambda_{\text{nz}} & \mathbf{O} \\ \mathbf{O} & \Gamma_\epsilon \Lambda_\epsilon \end{bmatrix}^{\mathcal{H}} \begin{bmatrix} \mathbf{F}_A \\ \mathbf{F}_C \end{bmatrix} - \mathbf{I}_N \right) \right\} \\
 &= \text{Diag} \left\{ \mathbf{F}_A^{\mathcal{H}} (\Gamma_{\text{nz}} \Lambda_{\text{nz}} - \mathbf{I}_V) \mathbf{F}_A \mathbf{F}_A^{\mathcal{H}} (\Gamma_{\text{nz}} \Lambda_{\text{nz}} - \mathbf{I}_V)^{\mathcal{H}} \mathbf{F}_A \right. \\
 &\quad + \mathbf{F}_A^{\mathcal{H}} (\Gamma_{\text{nz}} \Lambda_{\text{nz}} - \mathbf{I}_V) \mathbf{F}_A \mathbf{F}_C^{\mathcal{H}} (\Gamma_\epsilon \Lambda_\epsilon - \mathbf{I}_K)^{\mathcal{H}} \mathbf{F}_C \\
 &\quad + \mathbf{F}_C^{\mathcal{H}} (\Gamma_\epsilon \Lambda_\epsilon - \mathbf{I}_K) \mathbf{F}_C \mathbf{F}_A^{\mathcal{H}} (\Gamma_{\text{nz}} \Lambda_{\text{nz}} - \mathbf{I}_V)^{\mathcal{H}} \mathbf{F}_A \\
 &\quad \left. + \mathbf{F}_C^{\mathcal{H}} (\Gamma_\epsilon \Lambda_\epsilon - \mathbf{I}_K) \mathbf{F}_C \mathbf{F}_C^{\mathcal{H}} (\Gamma_\epsilon \Lambda_\epsilon - \mathbf{I}_K)^{\mathcal{H}} \mathbf{F}_C \right\} \\
 &\stackrel{\substack{\sigma_n \ll 1 \\ \Lambda_\epsilon \approx \mathbf{O}_K}}{\approx} \text{Diag} \left\{ \mathbf{F}_C^{\mathcal{H}} \mathbf{F}_C \mathbf{F}_C^{\mathcal{H}} \mathbf{F}_C \right\}, \tag{5.32}
 \end{aligned}$$

where the approximation is valid in case of spectral (close-to-) zeros and for high SNR values, i.e. small σ_n , so that the following relations hold:

$$\Gamma_{\text{nz}} \Lambda_{\text{nz}} \underset{\sigma_n \ll 1}{\approx} \mathbf{I}_V, \tag{5.33}$$

and

$$\Gamma_\epsilon \Lambda_\epsilon \underset{\Lambda_\epsilon \approx \mathbf{O}_K}{\approx} \mathbf{O}_K. \tag{5.34}$$

From Eq.(5.32) it is seen that part of the information is irrevocably *lost* due to Eq.(5.34), leading to an irreducible error. If $K = 1$ (only one spectral zero), this MSE contribution is identical for all elements of the block and equal to M^{-1} , otherwise it is dependent on the correlation between the rows of \mathbf{F}_C .

For the MMSE-ZR, the signal contribution to the MSE can be written as:

$$\begin{aligned}
\text{MSE}_{\text{MMSE-ZR}}^{\text{signal}} &= \text{Diag} \left\{ \left(\begin{bmatrix} \mathbf{F}_A^H & \mathbf{F}_C^H \end{bmatrix} \begin{bmatrix} \mathbf{I} & \mathbf{O} \\ \mathbf{Q} & \mathbf{O} \end{bmatrix} \begin{bmatrix} \Gamma_{nz} \Lambda_{nz} & \mathbf{O} \\ \mathbf{O} & \Gamma_\epsilon \Lambda_\epsilon \end{bmatrix} \begin{bmatrix} \mathbf{F}_A \\ \mathbf{F}_C \end{bmatrix} - \mathbf{I}_N \right) \times \\
&\quad \left(\begin{bmatrix} \mathbf{F}_A^H & \mathbf{F}_C^H \end{bmatrix} \begin{bmatrix} \Gamma_{nz} \Lambda_{nz} & \mathbf{O} \\ \mathbf{O} & \Gamma_\epsilon \Lambda_\epsilon \end{bmatrix} \right)^H \begin{bmatrix} \mathbf{I} & \mathbf{Q}^H \\ \mathbf{O} & \mathbf{O} \end{bmatrix} \begin{bmatrix} \mathbf{F}_A \\ \mathbf{F}_C \end{bmatrix} - \mathbf{I}_N \left. \right\} \\
&= \text{Diag} \left\{ \left(\mathbf{F}_A^H (\Gamma_{nz} \Lambda_{nz} - \mathbf{I}) \mathbf{F}_A + \mathbf{F}_C^H \mathbf{Q} \Gamma_{nz} \Lambda_{nz} \mathbf{F}_A - \mathbf{F}_C^H \mathbf{F}_C \right) \times \right. \\
&\quad \left. \left(\mathbf{F}_A^H (\Lambda_{nz}^H \Gamma_{nz}^H - \mathbf{I}) \mathbf{F}_A + \mathbf{F}_A^H \Lambda_{nz}^H \Gamma_{nz}^H \mathbf{Q}^H \mathbf{F}_C - \mathbf{F}_C^H \mathbf{F}_C \right) \right\} \\
&\approx_{\sigma_n \ll 1} \text{Diag} \left\{ \left(\begin{bmatrix} \mathbf{F}_C^H \mathbf{Q} \mathbf{F}_A \\ \equiv \mathbf{F}_C \end{bmatrix} - \mathbf{F}_C^H \mathbf{F}_C \right) \left(\mathbf{F}_A^H \mathbf{Q}^H \mathbf{F}_C - \mathbf{F}_C^H \mathbf{F}_C \right) \right\} \\
&\approx_{\sigma_n \ll 1} 0, \tag{5.35}
\end{aligned}$$

in which the approximation is valid for high SNR values, i.e. small σ_n .

Summarizing: in case the elements of Λ_ϵ are (close-to-) zero, the MSE due to inexact channel equalization decreases as the SNR increases. For the MMSE-FD-EXT this MSE hits a lower bound for low noise levels. In case of the MMSE-ZR, there is no such lower bound, implying that this equalizer has more benefit from a higher SNR. The reason for this difference is that the information stored at the corresponding sub-carriers is irrevocable lost for the MMSE-FD-EXT, while it can be recovered by the MMSE-ZR, and the quality of this recovered signal improves as the SNR increases.

Noise contribution

For the MMSE-FD-EXT, the noise contribution to the MSE equals

$$\text{MSE}_{\text{MMSE-FD-EXT}}^{\text{noise}} = \frac{\sigma_n^2}{M} \left(\text{tr} \{ \Gamma_{nz} \Gamma_{nz}^H \} + \text{tr} \{ \Gamma_\epsilon \Gamma_\epsilon^H \} \right) \mathbf{1}_{N \times 1}, \tag{5.36}$$

This MSE contribution is again identical for all elements in the transmitted block. Substituting Eqs. (5.24) and (5.25) and taking into account the definition of Λ_{nz} and

Λ_e , Eq. (5.36) can be rewritten as a function of the spectral responses λ_{e_i} :

$$\text{MSE}_{\text{MMSE-FD-EXT noise}} = \frac{1}{M} \left(\sum_{i=1}^M \sigma_n^2 \frac{\lambda_{e_i}^H}{\lambda_{e_i}^H \lambda_{e_i} + \sigma_n^2} \left(\frac{\lambda_{e_i}^H}{\lambda_{e_i}^H \lambda_{e_i} + \sigma_n^2} \right)^H \right) \mathbf{1}_{N \times 1}. \quad (5.37)$$

Spectral zeros do not contribute to the MSE here. Spectral close-to-zeros do contribute, however and dominate at high SNR values, i.e. for small values of σ_n . This follows from the behaviour of the function $\sigma_n^2 \frac{\lambda_{e_i}^H}{\lambda_{e_i}^H \lambda_{e_i} + \sigma_n^2} \left(\frac{\lambda_{e_i}^H}{\lambda_{e_i}^H \lambda_{e_i} + \sigma_n^2} \right)^H$, which is shown in Fig. 5.2. For large values of σ_n this function is small because the MMSE equalizer prevents noise enhancement. Obviously it is also small for extremely small values of σ_n . It reaches a maximum at an in between point, more specifically for $\sigma_n = |\lambda_{e_i}|$.

For the MMSE-ZR, the noise contribution to the MSE equals

$$\begin{aligned} \text{MSE}_{\text{MMSE-ZR noise}} = \sigma_n^2 \text{Diag} \{ & \mathbf{F}_A^H \Gamma_{nz} \Gamma_{nz}^H \mathbf{F}_A + \mathbf{F}_A^H \Gamma_{nz} \Gamma_{nz}^H \mathbf{Q}^H \mathbf{F}_C \\ & + \mathbf{F}_C^H \mathbf{Q} \Gamma_{nz} \Gamma_{nz}^H \mathbf{F}_A + \mathbf{F}_C^H \mathbf{Q} \Gamma_{nz} \Gamma_{nz}^H \mathbf{Q}^H \mathbf{F}_C \}. \end{aligned} \quad (5.38)$$

It is not trivial to give a quantitative description of this contribution to the MSE. Obviously, in case of a spectral zero, this MSE contribution will be larger than for the

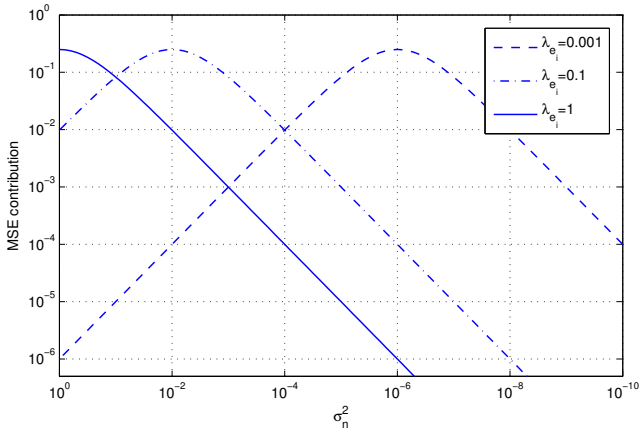


Figure 5.2: The noise contribution to the MSE for different spectral responses λ_{e_i} . For high SNR (right hand side) the MSE is dominated by the noise contribution of the sub-carriers with the lowest spectral response (close-to-zeros).

case of the MMSE-FD-EXT. However, with increasing SNR, i.e. decreasing values of σ_n , this contribution will go down rapidly. For spectral close-to-zeros the situation is even more favourable, especially at higher SNR values, because the dominant contributions from Λ_ϵ , as described above are not present here.

When looking at both the signal and the noise contributions to the MSE, it can be concluded that above a certain SNR threshold, the MMSE-ZR is expected to perform better than the MMSE-FD-EXT. Simulations have shown that for realistic scenarios this SNR threshold is typically somewhere between 10 and 30 dB.

To illustrate this with an example, Fig. 5.3 shows the value of the MSE contributions, averaged over the block, for the MMSE-FD-EXT and the MMSE-ZR, for a channel ' h_1 ' (see section 5.5 for more details). The presence of a *close-to-zero* starts dominating the MSE contribution of the noise for the MMSE-FD-EXT around SNR = 50dB. The contribution of the inexact channel equalization of the MMSE-FD-EXT tends to saturate, but eventually σ_n becomes low enough such that the approximation of Eq.(5.34) no longer holds.

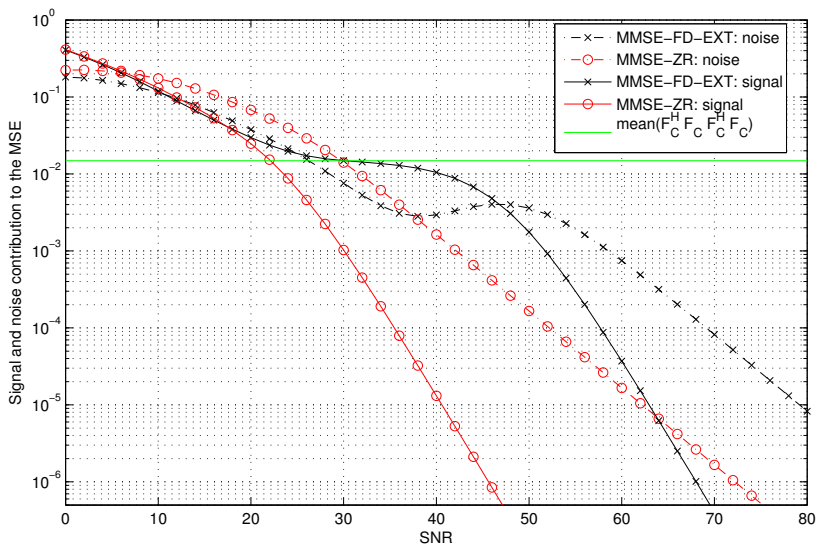


Figure 5.3: Example of the MSE contributions from inexact channel equalization and noise enhancement for the MMSE-FD-EXT and the MMSE-ZR

5.4.3 Remarks

Before proceeding to the simulation results, some additional remarks are in place:

Threshold

Practical channel knowledge is imperfect because it is based on estimates and hence spectral zeros will mostly be identified as spectral close-to-zeros. Therefore a decision needs to be made as to which elements of Λ_e should effectively be treated as zero, e.g. based on a threshold. This can be set at some percentage of the root mean square value of \mathbf{h} or through some other method. In any case it needs to be such that the number of zeros K is not larger than P . A trade-off needs to be made: setting a low threshold and identifying too few spectral close-to-zeros can lead to noise enhancement. Setting a high threshold can lead to too many spectral close-to-zeros, all of whose received information is discarded.

In case of reasonably high values of the SNR (e.g. $> 30\text{dB}$), Fig. 5.2 indicates that elements of Λ_e with an absolute value below σ_n should be treated as zeros, because they have a major contribution to the MSE. In case of non-white noise the threshold should also take into account the SNR level at each sub-carrier.

Condition

Related to the previous point, it should be avoided to assign consecutive elements of Λ_e as zeros. This would lead to an LS system based on consecutive rows of a DFT submatrix, which can be poorly conditioned.

Both points should lead to some heuristic algorithm to determine the selection of the elements which will be treated as zeros, e.g. the approach used in the simulations section is to only retain the 'lowest' of a set of consecutive zeros.

Extensive simulations have shown that treating one element of Λ_e as a zero generally does no harm and has the potential to improve the performance significantly. Keeping in mind that spectral zeros are relatively rare, and multiple spectral zeros are even rarer, designating the lowest element of Λ_e as a zero suffices for most 'difficult' channels. Even if this tone was carrying useful information, this can easily be recovered from the information in the other tones. On the other hand, in the extreme case, where $K = P$, Eq. (5.18) is no longer a LS-system and will be modeling the noise as well as reconstruct the information stored in the spectral zeros. This should only be considered for relatively high values of the SNR.

UW

The zero-restoration equalizers can also be adapted to UW-based transmission, either by subtracting the contribution of the UW at the receiver and proceeding as in the ZP case, or by replacing $\hat{\mathbf{x}}_{\text{ZP}}$ by $\hat{\mathbf{x}}_{\text{UW}}$ and modifying the LS system such that the last P samples of $\hat{\mathbf{x}}_{\text{UW}}$ equal the UW.

Implementation

Note that, while in Eq.(5.15) the last K columns of \mathbf{F}^H are effectively multiplied by coefficients equal to zero, even non-zero coefficients may be used here, because these are then absorbed by \mathbf{q} anyway. It is therefore also possible to choose coefficients equal to Λ_ϵ^{-1} . This implies that the ZFE-ZR can be implemented as a post-processing of the ZFE-FD-EXT. A practical implementation could therefore start with the evaluation of (5.12) -without the premultiplication with $[\mathbf{I}_N \mid \mathbf{O}]$ - as an alternative for $\hat{\mathbf{x}}_{\text{ZP}_{\text{temp}}}$. Next the LS system from Eq. (5.18) is solved, which is typically very small. The calculation of \mathbf{q} requires $(N + L + \frac{K}{3})K^2$ flops ([72], p. 238) and the calculation of $\hat{\mathbf{x}}_{\text{ZP}_{\text{corr}}}$ requires another $(2K - 1)N$ flops to multiply \mathbf{q} and \mathbf{F}_C^H . The overall computational complexity is thus equal to the complexity of Eq. (5.12) plus approximately $\mathcal{O}((K^2 + 2K)N)$ flops and is generally significantly smaller than the complexity of the time-domain equalizers of Eq. (5.3) and (5.4). Likewise, the MMSE-ZR can be implemented as a post-processing of the MMSE-FD-EXT. Based on the measurement of the actual channel and the SNR, it can be decided to use the post-processing step or not.

Note that the ZFE-FD-FOLD and the MMSE-FD-FOLD can *not* be used as a starting point of the ZR-algorithm because, contrary to \mathbf{H}_e , \mathbf{H}_f is not guaranteed at least of rank N and may not contain enough information to calculate N unknowns. For an easy comparison, the complexity of all equalizers has been summarized in Table.5.1.

Equalizer	Calculating \mathbf{W}	Evaluating $\hat{\mathbf{x}}$
$\mathbf{W}_{\text{ZFE-TD}}, \mathbf{W}_{\text{MMSE-TD}}$	$\mathcal{O}(N^2)$	$\mathcal{O}(N^2)$
$\mathbf{W}_{\text{ZFE-FD-FOLD}}, \mathbf{W}_{\text{MMSE-FD-FOLD}}$	$\mathcal{O}(N)$	$\mathcal{O}(N \log(N))$
$\mathbf{W}_{\text{ZFE-FD-EXT}}, \mathbf{W}_{\text{MMSE-FD-EXT}}$	$\mathcal{O}(M)$	$\mathcal{O}(M \log(M))$
$\mathbf{W}_{\text{ZFE-ZR}}, \mathbf{W}_{\text{MMSE-ZR}}$	$\mathcal{O}(M)$ $+(M + \frac{K}{3})K^2$	$\mathcal{O}(M \log(M))$ $+(2K - 1)N$

Table 5.1: Comparing the complexity for block size N , ZP-length P and K spectral zeros ($M = N + P$).

More precisely, the complexity for the MMSE-FD-EXT is:

- (per channel-update) evaluating Eq.(5.13), except for the DFT operations: $2M$ complex multiplications, M complex additions
- to evaluate $\hat{\mathbf{x}}$:
 - FFT: $\frac{1}{2}M \log(M)$ complex multiplications, $\frac{1}{2}M \log(M)$ complex additions
 - M complex multiplications
 - IFFT: $\frac{1}{2}M \log(M)$ complex multiplications, $\frac{1}{2}M \log(M)$ complex additions

In (the rather common) case only one spectral zero would be reconstructed, the MMSE-ZR would add to this:

- (per channel update) calculate $\mathbf{F}_D \mathbf{F}_D^H$, needed for \mathbf{q} : P complex multiplications, $P - 1$ complex additions
- to evaluate $\hat{\mathbf{x}}$:
 - calculating \mathbf{q} : P complex multiplications, $P - 1$ complex additions
 - scaling and adding the complex exponential pertaining to the missing zero: N complex multiplications, N complex additions.

For $N = 48$ and $P = 16$, this means that the number of complex multiplications for a channel update, assuming Λ_f is known, increases from 128 to 144 (+13%). The number of complex multiplications to evaluate $\hat{\mathbf{x}}$ it increases from 448 to 510 (+14%). The figures for the additions are nearly identical.

5.5 Simulations and discussion

To illustrate the performance of the ZR-technique, simulations have been done based on two channels found in literature as well as for the general case of Rayleigh fading. The section is concluded with a more general comparison of equalization techniques using ITU channels.

Channels $h_1(n)=[-0.3699+j0.5782 -0.4053+j0.5750 -0.0834+j0.0406 0.1587+j0.0156]$ and $h_2(n)=[0.707 0 0 0.707]$ correspond to p_2 from [115] and channel A from [204] respectively. These channels are shown in Fig. 5.4. The OFDM system in the original papers is replaced by ZP-SC with $M = 64$, $P = L$ and $N = 64 - P$. Note that $h_1(n)$ has a spectral close-to-zero at the 30th sub-carrier and $h_2(n)$ has a spectral zero as well as two spectral close-to-zeros. The noise is white Gaussian with different variances

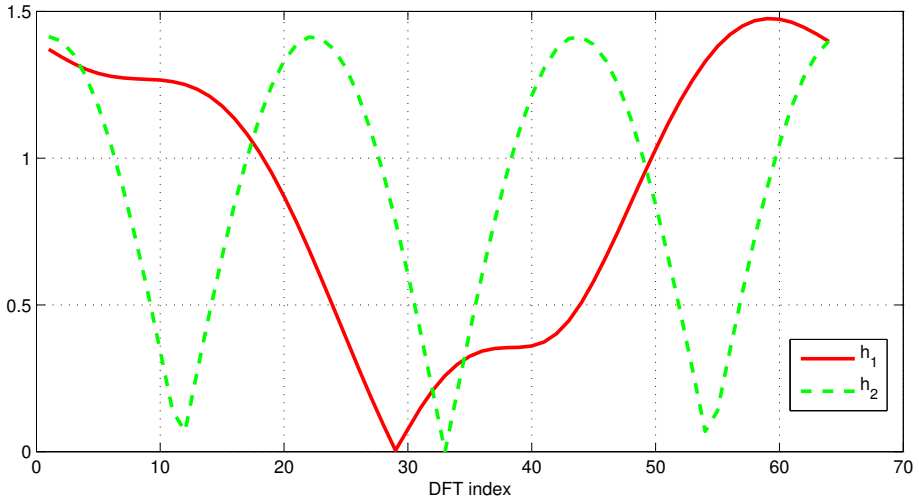


Figure 5.4: Magnitude response for $h_1(n)$ (from [115]) and $h_2(n)$ (from [204])

to match the signal-to-noise ratio (SNR). The BER performance is simulated using a Monte-Carlo method with 100000 random blocks, assuming a 16-QAM system.

For the first channel, Fig. 5.5 indicates that limiting the noise at the spectral close-to-zero frequency, as the MMSE-FD-EXT does, is a good strategy for low SNR. However, because of the noise enhancement at the spectral close-to-zero, the MMSE-FD-EXT is unable to benefit fully from increasing SNR levels and at some point the ZFE-TD starts to perform better. The ZFE-ZR equalizer manages to stay very close to the ZFE-TD, which obviously provides a performance lower bound for any ZFE. As expected, the MMSE-ZR performs better than the ZFE-ZR, especially for low SNRs, and it even outperforms the ZFE-TD. Because the channel exhibits a spectral *close-to-zero*, and therefore the noise enhancement is *finite*, even the performance of the ZFE-FD-EXT eventually improves as the SNR increases, albeit slower.

The results for channel $h_2(n)$ are shown in Fig. 5.6. Because of the spectral zero, the noise enhancement for the ZFE-FD-EXT equals infinity, as reflected by a BER of 0.5 for all SNR values. The MMSE-FD-EXT is also severely impacted by the spectral zero. For moderate SNR values its performance is comparable to that of Fig. 5.5, however, the performance now saturates for high SNR values, as predicted by Eq.(5.32). Indeed all information is lost at the spectral zero and the best strategy is to discard the noise present at this sub-carrier. Roughly speaking this implies that one M^{th} part of the signal power will be lost, resulting in an irreducible error, no matter how high the SNR. This is also apparent from the MSE-curves in Fig. 5.7, for which this limit would be at

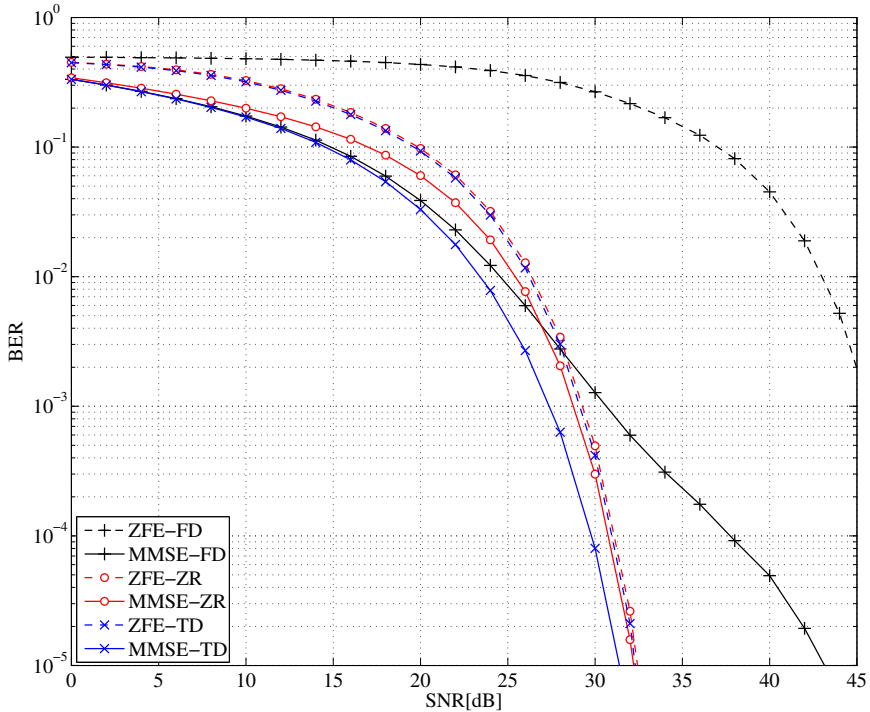


Figure 5.5: Performance comparison for channel $h_1(n)$

64^{-1} or -18 dB. The ZFE-ZR and MMSE-ZR on the other hand assume three spectral (close-to-) zeros ($K = 3$) and reconstruct the information that was stored there. As the SNR levels increase, the estimation of the \mathbf{q} vector in Eq. (5.18) also improves and therefore these equalizers do not show a saturation. They achieve a performance close to the ZFE-TD and the MMSE-TD, which are obviously not at all affected by the spectral zero. These curves also illustrate that the MSE for the two ZFE's is linearly dependent on the noise energy. For low SNR values, the ZFE's are clearly inferior to MMSE-based equalizers that limit the noise enhancement.

The *Rayleigh fading* model is a more realistic description of the wireless channel dominated by multipath ([151], p.705). Such model has been simulated for 10000 randomly generated channels of order $L = 5$, with both the real and imaginary part of the impulse responses following a Gaussian distribution with variance $\sigma_h^2 = 0.5$. For each channel 1000 random blocks using 64-QAM coding have been simulated with $M = 32$, $P = L = 5$, $N = 26$. The threshold to determine which elements of Λ_e are considered as zeros was set at 0.05. The calculated BER is shown in Fig. 5.8. Again

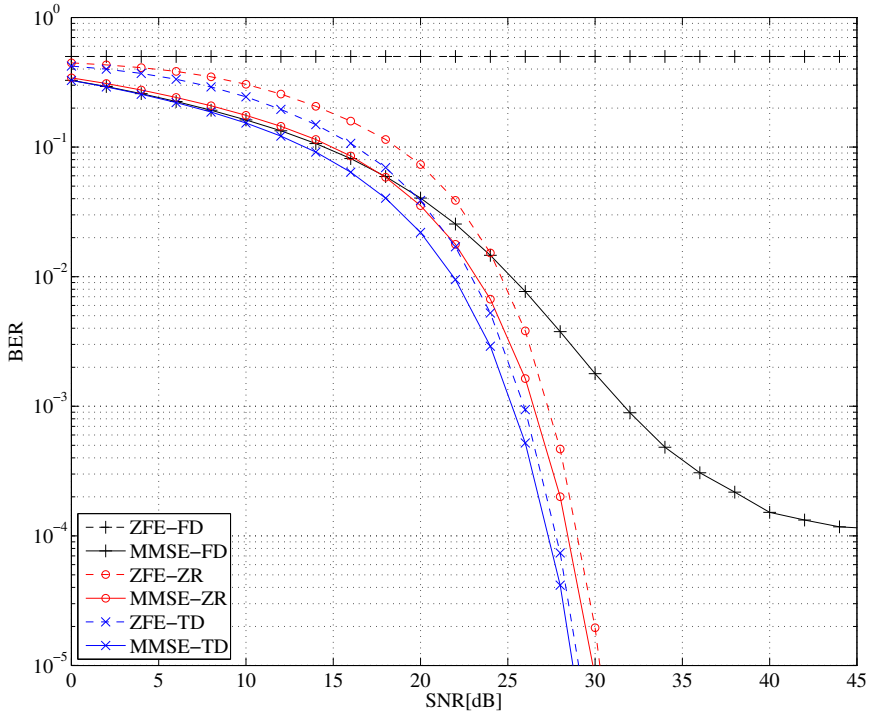


Figure 5.6: Performance comparison for channel $h_2(n)$

the zero-restoration equalizers outperform the classical frequency-domain equalizers, but are inferior to equalization in the time-domain. Note that the zero-restoration mechanism is only triggered for a limited number of channels. The gain is therefore less impressive than for the previous results.

Finally, some more extensive simulations have been done, comparing ZP to CP, SC to OFDM and matrix folding to matrix extension. The dimensions for IEEE 802.11a [93] have been used together with channel models presented by the ITU, more specifically the *Indoor office test environment channel B* [100]. The useful signal length $N=48$ and the padding length $P=16$, be it a ZP or CP. The constellation size for all symbols was QAM64. It is important to note that no coding was used and for OFDM no bit loading was done. The following modulation schemes are compared:

- SC-ZP, using MMSE-TD, ZFE-TD, MMSE-ZR, ZFE-ZR, MMSE-FD-EXT, ZFE-FD-EXT and MMSE-FD-FOLD
- SC-CP, using an MMSE-style FD equalizer

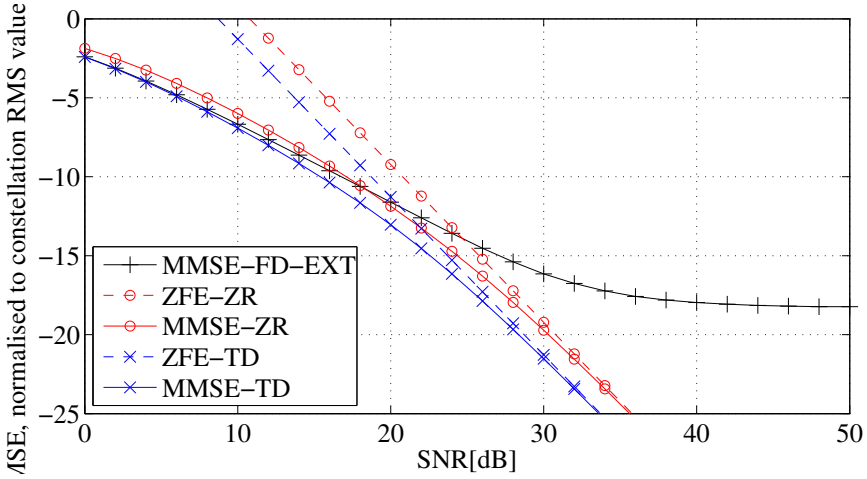


Figure 5.7: Mean square error for channel $h_2(n)$

- OFDM-ZP, using MMSE-FD-EXT and MMSE-ZR.
- OFDM-CP, using an MMSE-style FD equalizer without the final IDFT step. This is the typical OFDM operation.

In total 20000 random channels were generated, for each one 1000 symbols were transmitted. The results are presented in Fig. 5.9. The best performance for SC-ZP systems is again obtained using the MMSE-TD and ZFE-TD, followed by the MMSE-ZR and ZFE-ZR and the other equalizers. It is interesting to see that the SC-ZP with MMSE-FD-FOLD has the same performance as SC-CP, which makes sense because the operations on the useful signal are identical, only the noise distribution is different. The OFDM schemes systematically performs worse than the corresponding SC alternative. This result is pessimistic, though, because no bit-loading is being used. Nevertheless, the OFDM-MMSE-ZR again performs better than the OFDM-MMSE-FD-EXT.

5.6 Conclusion

Two new frequency-domain equalizers have been proposed to equalize zero-padded OFDM and SC-block transmissions over a channel exhibiting spectral zeros or spectral close-to-zeros. Both exploit the redundancy of the ZP to restore the lost information. The first technique is shown to have the zero forcing property, the second one is very similar to an MMSE equalizer. A particularly interesting feature is that

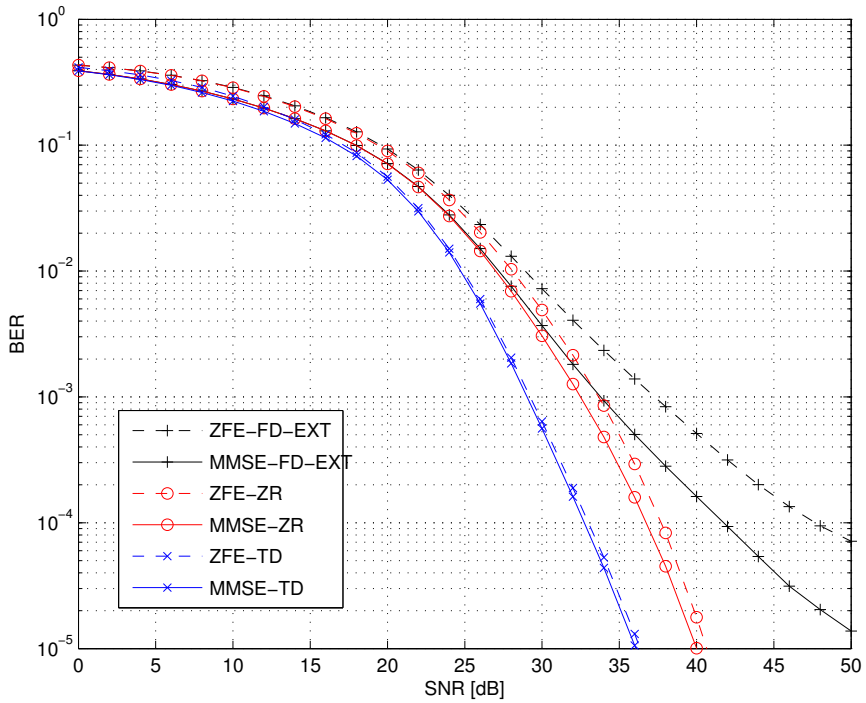


Figure 5.8: Performance comparison for Rayleigh fading channels

these equalizers can be implemented by adding a post-processing to the output of a classical frequency-domain equalizer, typically requiring only very limited additional resources. Simulations show a performance comparable to time-domain equalizers, at a computational complexity comparable to the original frequency-domain equalizers. The equalizers can easily be modified to work with unique wording as well.

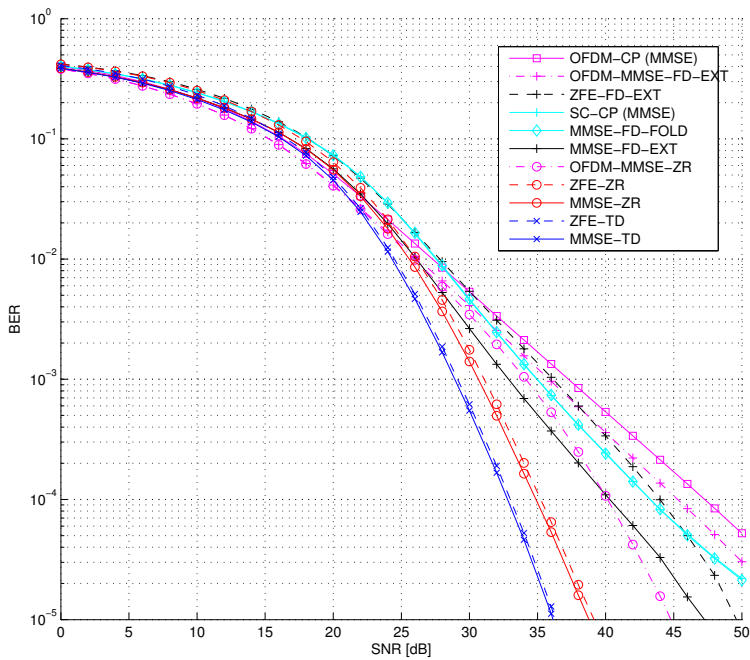


Figure 5.9: Comparing several existing methods for IEEE802.11a dimensions and ITU channels.

Chapter 6

Combining zero restoration and per-tone equalization

This chapter consists of a copy of the article *Combining spectral zero restoration and per-tone equalization in single-carrier block transmissions* [36], as submitted to *Elsevier Signal Processing*. Only the layout and the numbering of the references, equations and figures has been changed to accommodate for the different page size and to improve consistency.

Abstract

A receiver structure for single-carrier block transmission with zero padding is presented, combining per-tone equalization (PTEQ) and spectral zero restoration. The increased resistance against inter carrier interference and inter symbol interference of the PTEQ allows to use a short zero pad. The spectral zero restoration section extends the capacity limits imposed by spectral zeros in the channel frequency response and offers an improved resistance against radio-frequency interference. It can be implemented together with the PTEQ, or as an add-on.

6.1 Introduction

Frequency domain equalizers (FDEs) can be used for both orthogonal frequency division multiplexing (OFDM) and single-carrier (SC) block transmission [163]. In both cases, data at the transmitter is mapped onto individual subsymbols, which are

then grouped into blocks. In case of OFDM, an inverse discrete Fourier transform (IDFT) is applied to the blocks, while in case of SC block transmission the blocks are immediately ready for serialization and transmission over the channel. A discrete Fourier transform (DFT) applied to the vectorized received samples effectively converts the frequency selective fading channel into a number of flat fading subchannels or *tones*, each of which can easily be equalized by multiplication with a complex coefficient, which is referred to as the frequency domain equalizer (FEQ). The two most common FEQs are the zero-forcing equalizer (ZFE) and the minimum mean squared error (MMSE) equalizer. For the ZFE, the FEQ is the inverse of the channel frequency response at the considered tone. For an MMSE equalizer, the FEQ also depends on the noise statistics. After the FEQ, the equalized constellation points of an OFDM receiver can be demapped immediately, while an SC block transmission receiver requires an additional IDFT.

To avoid a loss of orthogonality between the tones, the transmitter inserts a guard interval (GI) in between consecutive blocks. This GI can be chosen in several ways. It can be a copy of the last samples of the block, which is referred to as a cyclic prefix (CP) [145]. The GI can also be a sequence of zeros i.e. a zero pad (ZP) [135]. Alternatively the GI can be a predefined pattern of samples referred to as a known signal pad (KSP) or unique word (UW) [211]. If the order of the channel, modeled as a finite impulse response filter, does not exceed the length of the GI, the linear convolution with the channel can be mathematically described as a circular convolution, preserving the orthogonality between the tones as desired. If the order of the channel does exceed the length of the GI, this results in so-called inter carrier interference (ICI) and inter symbol interference (ISI). Because a long GI lowers the transmission efficiency, a time domain equalizer (TEQ) can be applied before the vectorization of the received samples. The purpose of the TEQ is to shorten the channel impulse response, i.e. the combined impulse response of the channel and the TEQ has a lower spread in time. The TEQ also has some disadvantages, most importantly the non-trivial relation between the TEQ design and the eventual system performance.

The per-tone equalizer (PTEQ) moves the TEQ behind the DFT, offering each tone its own multi-tap equalizer, based on the output of a sliding DFT [196]. Because these multi-tap equalizers now run at the block rate instead of the sample rate and because the sliding DFT can be replaced by only one full DFT and difference terms, the increase in complexity is very modest. The performance is superior to the performance of TEQ+FEQ receivers, especially in combating ISI and ICI [156]. While the original PTEQ was developed for OFDM only, a PTEQ for SC transmission with a CP has also been developed [82]. In this contribution, the use of the PTEQ will be extended to SC transmission with a ZP.

An advantage of ZP systems over CP systems is that the ZFE in the time domain always exists for ZP systems [164], [68]. A frequency-domain implementation of the ZFE, however, can suffer from *spectral zeros* in CP systems as well as in ZP systems. These

spectral zeros are tones where the channel frequency response is zero or close to zero. This can occur e.g. due to destructive interference of alternate paths in a wireless channel. Because a ZFE FEQ inverts the channel response at each tone, a spectral zero will lead to an infinitely large noise amplification. While most implementations deal with this by using a MMSE equalizer instead of a ZFE, the spectral zero restoration (ZR), introduced in [37] makes use of redundancy in the time domain to recover information that is otherwise lost in the spectral zeros.

In this work the ZR is merged with the PTEQ into a *spectral zero restoration PTEQ* (ZR-PTEQ) for use in SC block transmission. This has a wide range of applications, because SC block transmission is becoming increasingly popular, e.g. for the uplink of mobile devices [171]. An advantage of SC block transmission over OFDM is the reduced peak to average power ratio (PAPR) and consequently the lower demands on the linearity of front-end signal amplifiers, and a more constant signal envelope [144]. This is one of the reasons why SC block transmission was selected for the uplink in LTE [1].

The text is organized as follows: section 6.2 provides the system model, section 6.3 describes the PTEQ for zero-padded SC block transmission, section 6.4 introduces the ZR. In section 6.5 the proposed technique is evaluated by means of simulations. Finally, section 6.6 concludes the text.

6.2 System model

The following notation is used: Bold lowercase letters denote vectors and bold uppercase letters denote matrices. Normal uppercase letters denote constants. $(\cdot)^*$, $(\cdot)^T$, $(\cdot)^H$, $(\cdot)^\dagger$ and $\mathcal{E}\{\cdot\}$ denote complex conjugate, transpose, Hermitian transpose, pseudo-inverse and expected value respectively and $\mathbf{A}(k, :)$ selects row k of \mathbf{A} . The DFT, IDFT, zero and identity matrix of size K are represented by \mathcal{F}_K , \mathcal{F}_K^H , $\mathbf{0}_K$, and \mathbf{I}_K respectively. Occasionally, for clarity the dimensions of a matrix are indicated as $[\cdot]_{K \times L}$.

We consider SC block transmission where the blocks have length N and time index k , i.e. $\mathbf{x}^{(k)} = [x_1^{(k)} \ x_2^{(k)} \ \dots \ x_N^{(k)}]^T$. When no confusion is possible, the time index k will be omitted. Without loss of generality it is assumed that the variance of \mathbf{x} equals unity, i.e. $\mathcal{E}\{\mathbf{x}\mathbf{x}^H\} = \mathbf{I}_N$. The zero-padding matrix

$$\mathbf{Z}_{M \times N} = \begin{bmatrix} \mathbf{I}_N \\ \mathbf{0}_{P \times N} \end{bmatrix}, \quad (6.1)$$

with $M = N + P$, adds a ZP of length P to the end of each block so that the effectively transmitted block is $\mathbf{Z}\mathbf{x}$. The channel is modeled as a finite impulse response filter of order L with coefficients stored in reverse order in $\mathbf{h} = [h_L \ h_{L-1} \ \dots \ h_0]$.

6.2.1 Short channels

In case $L \leq P$, the ZP suffices to avoid ISI and the received block of samples can be written as:

$$\mathbf{y} = \underbrace{\begin{bmatrix} h_0 & & & & & \\ & \ddots & & & & \\ & & h_L & & & \\ & & & \ddots & & \\ & & & & h_0 & \\ & & & & & \vdots \\ & & & & & h_L \end{bmatrix}}_{(\mathbf{H}_\ell)_{M \times N}} \mathbf{x} + \mathbf{n}, \tag{6.2}$$

with \mathbf{H}_ℓ the linear convolution matrix of \mathbf{h} and \mathbf{n} additive noise with a variance $\mathcal{E}\{\mathbf{nn}^H\} = \sigma_n \mathbf{I}$. Of the infinite number of possible time-domain ZFEs, the optimal one, which has the minimum-norm and therefore the smallest noise amplification, is \mathbf{H}_ℓ^\dagger , i.e. the pseudo-inverse of \mathbf{H}_ℓ . The equalized block can then be written as:

$$\hat{\mathbf{x}}_{\mathbf{H}_\ell^\dagger} = (\mathbf{H}_\ell^H \mathbf{H}_\ell)^{-1} \mathbf{H}_\ell^H \mathbf{y}. \tag{6.3}$$

Note that the calculation of the pseudoinverse is a complex operation. A computationally cheaper solution is obtained by rewriting Eq.(6.2) as follows

$$\mathbf{y} = \underbrace{\begin{bmatrix} h_0 & & & & h_L & \dots & h_1 \\ & \ddots & & & & \ddots & \vdots \\ & & h_L & & & & h_L \\ & & & \ddots & & & \\ & & & & h_0 & & \\ & & & & \vdots & \ddots & \\ & & & & h_L & h_{L-1} & \dots & h_0 \end{bmatrix}}_{(\mathbf{H}_c)_{M \times M}} \mathbf{z} + \mathbf{n}, \tag{6.4}$$

with \mathbf{H}_c the circular convolution matrix of \mathbf{h} . Because \mathbf{H}_c is a circular matrix, it can be written as $\mathbf{H}_c = \mathcal{F}_M^H \mathbf{\Lambda} \mathcal{F}_M$, with $\mathbf{\Lambda}$ a diagonal matrix. The equalized block can therefore be calculated using a computationally cheap ZFE in the frequency domain,

$$\hat{\mathbf{x}}_{\text{FD}} = \mathbf{Z}^T \mathcal{F}_M^H \mathbf{\Lambda}^{-1} \mathcal{F}_M \mathbf{y}. \tag{6.5}$$

Note that this solution is suboptimal. With some small modifications, however, it is possible to obtain the performance of Eq.(6.3) with a complexity which is only slightly higher than that of Eq.(6.5) [185].

6.2.2 Long channels

In case $L > P$, there will be ISI, and the system model of Eq.(6.2) can no longer be used. The time index (k) is reintroduced and the influence of the preceding block ($k - 1$) and succeeding block ($k + 1$) are also considered, such that the received block of samples can be written as:

$$\mathbf{y}^{(k)} = \underbrace{\begin{bmatrix} \mathbf{O}_{(1)} & \begin{bmatrix} \mathbf{h} & 0 \\ \cdot & \cdot \\ 0 & \mathbf{h} \end{bmatrix} & \mathbf{O}_{(2)} \end{bmatrix}}_{\mathbf{H}} \begin{bmatrix} \mathbf{Z} & \mathbf{O} & \mathbf{O} \\ \mathbf{O} & \mathbf{Z} & \mathbf{O} \\ \mathbf{O} & \mathbf{O} & \mathbf{Z} \end{bmatrix} \begin{bmatrix} \mathbf{x}^{(k-1)} \\ \mathbf{x}^{(k)} \\ \mathbf{x}^{(k+1)} \end{bmatrix} + \mathbf{n}^{(k)}, \quad (6.6)$$

with \mathbf{H} the channel matrix. The dimension of $\mathbf{y}^{(k)}$ is $M + T - 1$, with T the number of TEQ taps (see section 6.3). The size of the zero matrices $\mathbf{O}_{(1)}$ and $\mathbf{O}_{(2)}$ is $(N + T - 1) \times (M - T - L + \delta)$ and $(N + T - 1) \times (M + 1 - \delta)$ respectively, with δ a synchronization parameter which describes the alignment between the transmitter and the receiver, and which should be chosen to maximize the energy of $\mathbf{x}^{(k)}$ in $\mathbf{y}^{(k)}$.

A TEQ+FEQ consists of a TEQ, with coefficients stored in reversed order in $\mathbf{t} = [t_T \ t_{T-1} \ \dots \ t_1]^T$ running at the sample rate and a FEQ $\mathbf{f} = [f_1 \ f_2 \ \dots \ f_M]^T$ running at the block rate. The equalized output can then be written as

$$\hat{\mathbf{x}}_{\text{TEQ+FEQ}}^{(k)} = \mathbf{Z}^T \underbrace{\mathcal{F}_M^H \begin{bmatrix} f_1 & & 0 \\ & \cdot & \\ 0 & & f_M \end{bmatrix}}_{\text{FEQ}} \underbrace{\mathcal{F}_M \begin{bmatrix} \mathbf{t} & 0 \\ \cdot & \cdot \\ 0 & \mathbf{t} \end{bmatrix}}_{\text{TEQ}} \mathbf{y}^{(k)} \quad (6.7)$$

Note that the DFT-size equals M , whereas this would be N in a cyclic-prefix-based system, and that by omitting the multiplication with \mathbf{Z}^T , also the equalized zero-pad would be available. The TEQ+FEQ structure is illustrated in Fig.6.1a.

6.3 Per-tone equalization (PTEQ)

The PTEQ [196] moves the TEQ behind the DFT operation, giving each tone i its individual multi-tap equalizer $\mathbf{w}_i = [w_{i,1} \ w_{i,2} \ \dots \ w_{i,T}]^T$. The equalized time domain block can then be written as

$$\hat{\mathbf{x}}_{\text{PTEQ}}^{(k)} = \mathbf{Z}^T \mathcal{F}_M^H \mathbf{z}^{(k)}, \quad (6.8)$$

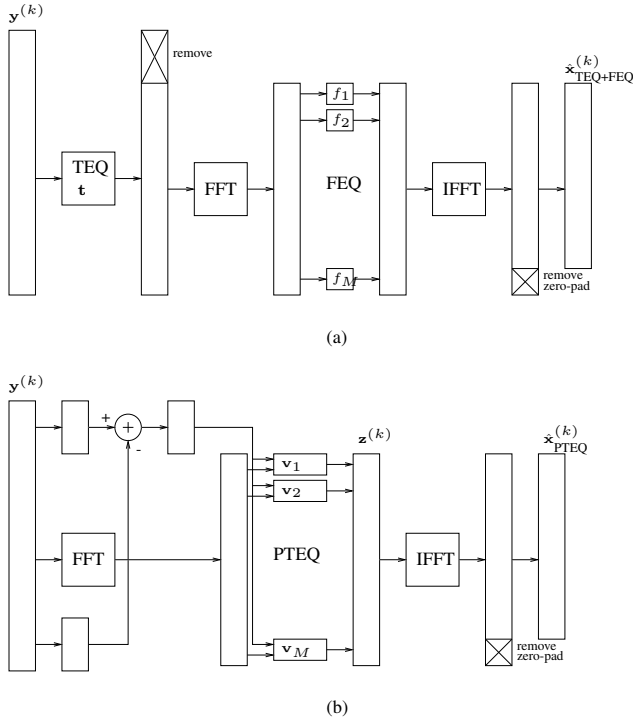


Figure 6.1: The TEQ+FEQ (a) and the PTEQ (b)

with $\mathbf{z}^{(k)} = [z_1^{(k)} \ z_2^{(k)} \ \dots \ z_M^{(k)}]^T$ the equalized block in the frequency domain, that is

$$z_i^{(k)} = \mathbf{w}_i^T \begin{bmatrix} \mathcal{F}_M(i, :) & 0 & \dots \\ \vdots & \ddots & \\ \dots & 0 & \mathcal{F}_M(i, :) \end{bmatrix} \mathbf{y}^{(k)} \quad (6.9)$$

for $i = 1 \dots M$. By choosing $\mathbf{w}_i = f_i \mathbf{t}_i$, Eq.(6.9) yields the same result as Eq.(6.7), so the PTEQ has the freedom to perform at least as good as the TEQ+FEQ.

Unfortunately the formulation of Eq.(6.9) is significantly more complex due to the sliding DFT, even if executed using the fast Fourier transform (FFT). This surplus complexity vanishes, however, when exploiting the structure of the sliding DFT matrix.

Defining

$$\mathbf{v}_i = \begin{bmatrix} v_{i,1} \\ v_{i,2} \\ \vdots \\ v_{i,T} \end{bmatrix} = \begin{bmatrix} 1 & \alpha^{i-1} & \dots & \alpha^{(i-1)(T-1)} \\ 0 & 1 & \ddots & \ddots \\ \vdots & \ddots & \ddots & \alpha^{(i-1)} \\ 0 & \dots & 0 & 1 \end{bmatrix} \mathbf{w}_i, \quad (6.10)$$

with $\alpha = e^{-j2\pi/M}$, Eq.(6.9) can be rewritten in terms of \mathbf{v}_i instead of \mathbf{w}_i , leading to

$$z_i^{(k)} = \mathbf{v}_i^T \underbrace{\begin{bmatrix} \mathbf{I}_{T-1} & \mathbf{O} & -\mathbf{I}_{T-1} \\ \mathbf{O} & \mathcal{F}_M(i, :) \end{bmatrix}}_{\mathbf{D}_i} \mathbf{y}^{(k)}. \quad (6.11)$$

Instead of T DFT's, like in Eq.(6.9), now only one DFT is needed, represented by the last row in the matrix \mathbf{D}_i . The other $T - 1$ rows represent so-called *difference terms*. The PTEQ based on difference terms [196], has a complexity similar to the TEQ+FEQ from Eq.(6.7). After defining

$$\mathbf{V} = \begin{bmatrix} \mathbf{v}_0^T \mathbf{D}_0 \\ \mathbf{v}_1^T \mathbf{D}_1 \\ \vdots \\ \mathbf{v}_M^T \mathbf{D}_M \end{bmatrix}, \quad (6.12)$$

Eq.(6.8) can be written as

$$\hat{\mathbf{x}}_{\text{PTEQ}}^{(k)} = \mathbf{Z}^T \mathcal{F}^H \mathbf{V} \mathbf{y}^{(k)}. \quad (6.13)$$

The PTEQ structure is illustrated in Fig. 6.1b.

To use the PTEQ as such, the filter coefficients \mathbf{v}_i can be determined by minimizing the following mean squared error (MSE) cost function:

$$\begin{aligned} J(\mathbf{V}) &= \mathcal{E} \left\{ \text{tr} \left\{ \left(\hat{\mathbf{x}}_{\text{PTEQ}}^{(k)} - \mathbf{x}^{(k)} \right) \left(\hat{\mathbf{x}}_{\text{PTEQ}}^{(k)} - \mathbf{x}^{(k)} \right)^H \right\} \right\} \\ &= \mathcal{E} \left\{ \text{tr} \left\{ \left(\mathbf{Z}^T \mathcal{F}^H \mathbf{V} \mathbf{y}^{(k)} - \mathbf{x}^{(k)} \right) \left(\mathbf{Z}^T \mathcal{F}^H \mathbf{V} \mathbf{y}^{(k)} - \mathbf{x}^{(k)} \right)^H \right\} \right\} \end{aligned} \quad (6.14)$$

Here, unlike the PTEQ design in the case of OFDM [196], the minimization of Eq.(6.14) is nontrivial because the presence of the \mathbf{Z}^T -matrix inhibits the decoupling between the different tones. This can be avoided by moving the ZP into the equation. The filter coefficients will therefore be determined by minimizing the following MSE cost

function (using an approach similar to [82]):

$$\begin{aligned}
J(\mathbf{V}) &= \mathcal{E} \left\{ \text{tr} \left\{ \left(\mathcal{F}^{\mathcal{H}} \mathbf{V} \mathbf{y}^{(k)} - \begin{bmatrix} \mathbf{x}^{(k)} \\ \mathbf{0} \end{bmatrix} \right) \left(\mathcal{F}^{\mathcal{H}} \mathbf{V} \mathbf{y}^{(k)} - \begin{bmatrix} \mathbf{x}^{(k)} \\ \mathbf{0} \end{bmatrix} \right)^{\mathcal{H}} \right\} \right\} \\
&= \text{tr} \left\{ \mathcal{F}^{\mathcal{H}} \mathbf{V} \mathbf{H} \mathbf{I}_{3N} \mathbf{H}^{\mathcal{H}} \mathbf{V}^{\mathcal{H}} \mathcal{F} + \mathcal{F}^{\mathcal{H}} \mathbf{V} \sigma_n^2 \mathbf{I}_M \mathbf{V}^{\mathcal{H}} \mathcal{F} + \begin{bmatrix} \mathbf{I}_N & \mathbf{0} \\ \mathbf{0} & \mathbf{0} \end{bmatrix} \right. \\
&\quad \left. - \mathcal{F}^{\mathcal{H}} \mathbf{V} \mathbf{H} \begin{bmatrix} \mathbf{0} & \mathbf{0} \\ \mathbf{I} & \mathbf{0} \\ \mathbf{0} & \mathbf{0} \end{bmatrix} - \begin{bmatrix} \mathbf{0} & \mathbf{I} & \mathbf{0} \\ \mathbf{0} & \mathbf{0} & \mathbf{0} \end{bmatrix} \mathbf{H}^{\mathcal{H}} \mathbf{V}^{\mathcal{H}} \mathcal{F} \right\} \\
&= \sum_{i=1}^{N+P} \left(\mathbf{v}_i^T \mathbf{D}_i \mathbf{H} \mathbf{H}^{\mathcal{H}} \mathbf{D}_i^{\mathcal{H}} \mathbf{v}_i^* + \sigma_n^2 \mathbf{v}_i^T \mathbf{D}_i \mathbf{D}_i^{\mathcal{H}} \mathbf{v}_i^* \right. \\
&\quad \left. - \mathbf{v}_i^T \mathbf{D}_i \bar{\mathbf{H}} \begin{bmatrix} \mathbf{I} & \mathbf{0} \end{bmatrix} \mathbf{f}_i^{\mathcal{H}} - \mathbf{f}_i \begin{bmatrix} \mathbf{I} \\ \mathbf{0} \end{bmatrix} \bar{\mathbf{H}}^{\mathcal{H}} \mathbf{D}_i^{\mathcal{H}} \mathbf{v}_i^* \right) + N + P, \quad (6.15)
\end{aligned}$$

with $\bar{\mathbf{H}} = \mathbf{H} \begin{bmatrix} \mathbf{0}_N & \mathbf{I}_N & \mathbf{0}_N \end{bmatrix}^T$, and $\mathbf{f}_i = \mathcal{F}_M(i, :)$.

The optimal \mathbf{v}_i are found by differentiating the MSE cost function with respect to \mathbf{v}_i

$$\begin{aligned}
\frac{\partial J(\mathbf{V})}{\partial \mathbf{v}_i} &= 2\mathbf{D}_i \mathbf{H} \mathbf{H}^{\mathcal{H}} \mathbf{D}_i^{\mathcal{H}} \mathbf{v}_i^* + 2\sigma_n^2 \mathbf{D}_i \mathbf{D}_i^{\mathcal{H}} \mathbf{v}_i^* \\
&\quad - 2\mathbf{D}_i \bar{\mathbf{H}} \begin{bmatrix} \mathbf{I} & \mathbf{0} \end{bmatrix} \mathbf{f}_i^{\mathcal{H}},
\end{aligned}$$

and setting this derivative equal to zero, leading to:

$$\mathbf{v}_{i,\text{opt}}^* = \left(\mathbf{D}_i \mathbf{H} \mathbf{H}^{\mathcal{H}} \mathbf{D}_i^{\mathcal{H}} + \sigma_n^2 \mathbf{D}_i \mathbf{D}_i^{\mathcal{H}} \right)^{-1} \mathbf{D}_i \bar{\mathbf{H}} \begin{bmatrix} \mathbf{I} & \mathbf{0} \end{bmatrix} \mathbf{f}_i^{\mathcal{H}} \quad (6.16)$$

Remember that the PTEQ can be seen as an individual TEQ for each tone. This has two advantages: firstly, this offers more flexibility with regards to the equalization and secondly, with Eq.(6.16) there is an optimal solution for each tone, which minimizes the MSE. It is to be expected that the equivalent channel shortening provided by the PTEQ will allow to decrease the length of the ZP, improving the overall efficiency of the system. In section 6.5 this will be illustrated with simulation results.

6.4 Spectral zero restoration PTEQ (ZR-PTEQ)

6.4.1 Motivation

Although the PTEQ outperforms the TEQ+FEQ, it too is defenseless against *spectral zeros*, i.e. tones where $\mathbf{D}_i \bar{\mathbf{H}}$ is zero or close to zero. From Eqs.(6.11) and (6.16), it is clear that the PTEQ will discard any energy found at these tones, as it only consists of noise. This approach of discarding the tone is common to all MMSE equalizers. A ZFE however, simply inverts the channel response. When confronted with a spectral zero, this leads to severe noise amplification.

The ZR, developed in [37] is based on the observation that a tone exhibiting a spectral zero will also be absent in the time-domain signal. It will reveal itself in the ZP, where it assumes the shape of a complex exponential error, as shown in Fig.6.2.

The frequency of this complex exponential is known -it corresponds to the tone exhibiting the spectral zero- and the amplitude and phase can be estimated using a least-squares fit. Once these have been determined, the complex exponential can be added to the equalized ZP (bringing this closer to zero) and more importantly, also to the useful signal, i.e. the rest of the received block of samples. The information lost in the spectral zero can therefore be restored. Here, the ZR is merged with the PTEQ (ZR-PTEQ).

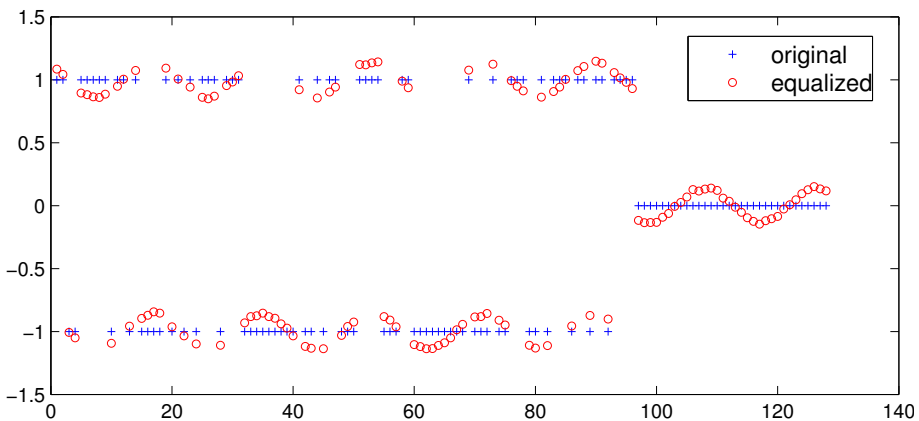


Figure 6.2: A simple example of a binary signal with zero pad, which has been passed through a channel with a spectral zero and through an MMSE equalization. The tone corresponding to the spectral zero is discarded by the equalizer and shows itself as a complex exponential error in the ZP (only real component shown here).

6.4.2 Mathematical derivation

The ZR-PTEQ is based on Eq.(6.13). The equalized block in the time domain (including the ZP), i.e. $\mathcal{F}^H \mathbf{V}_y^{(k)}$, corresponds to a linear combination of the columns of \mathcal{F}^H , the IDFT-matrix, where the coefficients of this linear combination are equal to $\mathbf{V}_y^{(k)}$. In the case of one or more spectral zeros, the coefficients multiplying the corresponding columns of \mathcal{F}^H will be very small or zero, as explained before. This is not desirable, because there is no reason to assume that the contribution of these columns would not be present in the transmitted block. The goal of the ZR is therefore to estimate the true coefficients multiplying the columns corresponding to the spectral zeros. The procedure is as follows: as an intermediate result, the equalized block in the time domain is first constructed by only taking into account the contribution of the other, well-conditioned tones. Note that this intermediate result is equal to the MMSE-solution. The coefficients multiplying the other columns of \mathcal{F}^H , corresponding to the spectral zeros, can then be estimated by solving a least-squares system of equations that minimizes the energy in the ZP. This will now be elaborated mathematically, following an approach similar to that of [37], now merged with the PTEQ.

Assume there are R spectral zeros and $K = M - R$ well-conditioned tones. The columns of \mathcal{F}^H can now be permuted such that the K columns corresponding to the well-conditioned tones are moved to the left and the R columns corresponding to the spectral zeros are moved to the right, resulting in \mathbf{F}^H ,

$$\mathbf{F}^H = \begin{bmatrix} \overset{(K)}{\mathbf{F}_A^H} & \overset{(R)}{\mathbf{F}_C^H} \\ \mathbf{F}_B^H & \mathbf{F}_D^H \end{bmatrix} \begin{matrix} (N) \\ (P) \end{matrix} \quad (6.17)$$

in which $\mathbf{F}_A (K \times N)$, and $\mathbf{F}_B (K \times P)$, $\mathbf{F}_C (R \times N)$ and $\mathbf{F}_D (R \times P)$ are submatrices of \mathbf{F} . Because $\mathbf{F}^H \mathbf{F} = \mathbf{I}$, specific relations hold between these submatrices, e.g. $\mathbf{F}_B^H \mathbf{F}_A = -\mathbf{F}_D^H \mathbf{F}_C$ and $\mathbf{F}_A^H \mathbf{F}_A + \mathbf{F}_C^H \mathbf{F}_C = \mathbf{I}$. The intermediate result, only taking into account the well-conditioned tones, can now be written as:

$$\hat{\mathbf{x}}_{\text{temp}}^{(k)} = \mathbf{Z}^T \mathbf{F}^H \begin{bmatrix} \mathbf{V}_{\text{nz}} \mathbf{y}^{(k)} \\ \mathbf{0} \end{bmatrix}, \quad (6.18)$$

in which the rows of \mathbf{V}_{nz} , corresponding to the well-conditioned tones, are a PTEQ calculated from Eq.(6.16).

The coefficients corresponding to the spectral zeros, \mathbf{q} , can now be obtained by solving a least-squares system of equations to minimize the energy in the equalized ZP,

$$\mathbf{F}_B^H \mathbf{V}_{\text{nz}} \mathbf{y}^{(k)} + \mathbf{F}_D^H \mathbf{q} \stackrel{LS}{=} \mathbf{0}_{R \times 1}, \quad (6.19)$$

leading to

$$\mathbf{q} = -(\mathbf{F}_D \mathbf{F}_D^H)^{-1} \mathbf{F}_D \mathbf{F}_B^H \mathbf{V}_{\text{nz}} \mathbf{y}^{(k)}. \quad (6.20)$$

By adding this contribution to the intermediate result of Eq.(6.18), the final equalizer output is obtained as

$$\begin{aligned} \hat{\mathbf{x}}_{\text{ZR-PTEQ}}^{(k)} &= \mathbf{Z}^T \mathbf{F}^{\mathcal{H}} \left[\frac{\mathbf{V}_{\text{nz}} \mathbf{y}^{(k)}}{\mathbf{q}} \right] \\ &= \begin{bmatrix} \mathbf{F}_A^{\mathcal{H}} & \mathbf{F}_C^{\mathcal{H}} \end{bmatrix} \begin{bmatrix} \mathbf{I} \\ -(\mathbf{F}_D \mathbf{F}_D^{\mathcal{H}})^{-1} \mathbf{F}_D \mathbf{F}_B^{\mathcal{H}} \end{bmatrix} \mathbf{V}_{\text{nz}} \mathbf{y}^{(k)} \end{aligned} \quad (6.21)$$

In practice, the least-squares problem is typically very small, and the multiplication with the matrix $\begin{bmatrix} \mathbf{F}_A^{\mathcal{H}} & \mathbf{F}_C^{\mathcal{H}} \end{bmatrix}$ can be replaced by an IFFT, such that the additional complexity of the ZR is very limited.

While Eq.(6.21) offers a closed-form expression of the ZR-PTEQ, it is also possible to implement ZR as an *add-on* to a PTEQ. A practical implementation could therefore start by evaluating Eq.(6.16) and Eq.(6.11) for all tones. Note that for spectral zeros, the \mathbf{v}_i can be set equal to zero, though the evaluation of Eq.(6.16) will lead to a very low \mathbf{v}_i anyway. After this, the output of the PTEQ is obtained by evaluating Eq.(6.8). It can then be decided whether to use the ZR add-on step or not. To implement the ZR, starting from this point, the least-squares system of equations of Eq.(6.19) can be solved. The contributions of the spectral zeros can then be taken into account by adding the corresponding columns of $\mathbf{F}_D^{\mathcal{H}}$, weighted by \mathbf{q} to the result of the PTEQ.

6.4.3 Selection of the spectral zeros

For practical channels there is a zero probability that $\mathbf{D}_i \bar{\mathbf{H}}$ is a zero matrix. The procedure to label a tone as a spectral zero should therefore use a heuristic, e.g. by comparing the norm of $\mathbf{D}_i \bar{\mathbf{H}}$ to a certain threshold.

In any case the number of spectral zeros R should not exceed the ZP length P . Preferably $R \ll P$, otherwise the least-squares system of equations of Eq.(6.19) is no longer overdetermined, and the elements of \mathbf{q} are no longer an estimate for the information which is lost in the spectral zeros, but also model the white noise and the imperfect equalization of the other tones.

Another guideline is to avoid assigning neighbouring tones as spectral zeros. Otherwise, $\mathbf{F}_D^{\mathcal{H}}$ contains a submatrix corresponding to neighbouring columns of the $\mathcal{F}^{\mathcal{H}}$ -matrix, which is poorly conditioned. In case two neighbouring tones are both potential spectral zeros, it is advisable to assign only one of them as such.

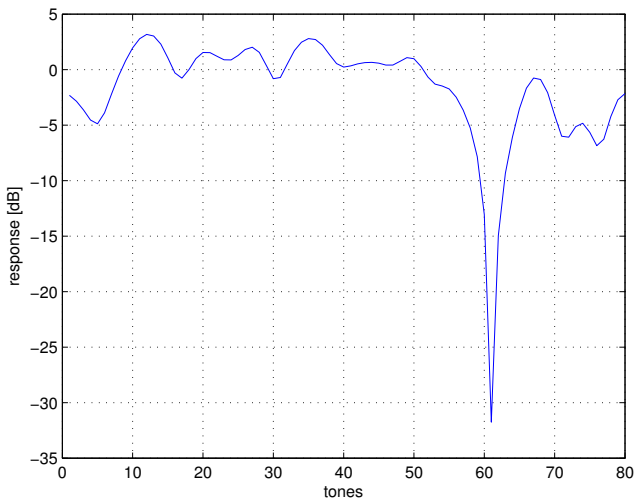


Figure 6.3: Frequency response of a typical Rayleigh fading channel. This example exhibits a spectral zero on tone 61.

6.5 Simulation results

The channel model for the simulations is adopted from the IEEE802.11a [93]. While this system uses OFDM instead of SC block transmission, the simulation parameters are chosen similarly, in particular the DFT-size $M=80$ (IEEE802.11a, uses a DFT size of 64 and CP length of 16, also leading to blocks of length 80). Because the aim of the PTEQ is to optimally shorten the channel impulse response, the length of the ZP is varied, and likewise the number of useful subsymbols is also varied as $N=80-P$. Channels were generated using Matlab's `stdchan` function. These Rayleigh fading channels often exhibit spectral zeros, a typical example is shown in Fig.6.3. This channel of order $L=20$ exhibits a spectral zero at tone 61. The simulations use a typical average signal-to-noise ratio (SNR) of 30dB; Figure 6.4 shows the geometric mean of the SNR of each time-domain subsymbol. The number of coefficients T varies from 1 to 19, and the ZP length P ranges from 0 to 20.

The interpretation of this result is as follows: for small values of P , adding between 2 and 3 coefficients to the equalizer has the same effect as increasing P by one, for both the PTEQ and the ZR-PTEQ. In other words: the ZP length can be shortened in exchange for increased receiver complexity. Because a reduction of the ZP length increases the percentage of the useful payload, this is a very interesting result.

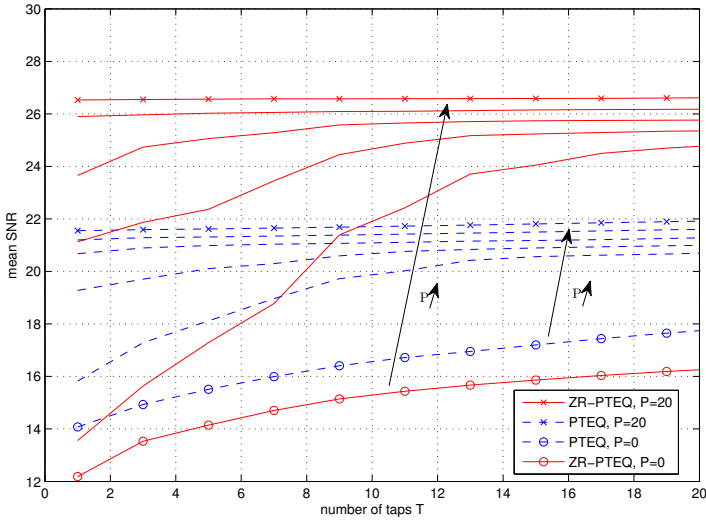


Figure 6.4: The PTEQ and the ZR-PTEQ for the channel from Fig.6.3. The DFT-size $M=80$, the ZP length P is varied from 0 to 20 and the number of coefficients T ranges from 1 to 19.

Moreover, for sufficiently long ZP, or sufficiently large T , which is now known to be equivalent, the ZR adds a significant performance improvement over the PTEQ. For small P and T it performs worse, which makes sense, because in these cases the least-squares system from Eq.(6.19) is poorly conditioned because of the short ZP.

For $P=20(=L)$ the added value of the PTEQ with or without ZR is very limited, which is logical because in this case all ISI and ICI vanish automatically. Still, there remains a large performance difference between the PTEQ and the ZR-PTEQ, which can be attributed to the fact that the PTEQ is missing most of the information from the tone exhibiting the spectral zero.

6.6 Conclusion

We have presented a new equalizer structure for single carrier block transmission with zero padding. The equalization is performed in the frequency domain, using a multi-tap equalizer for each tone. The channel-shortening effect of this equalizer allows to decrease the length of the ZP, leading to an increased transmission efficiency at the

expense of slightly increased receiver complexity. Simulations have shown that for the addition of every 2 to 3 coefficients the ZP can be shortened by one. A spectral zero restoration algorithm is added to recover the information which is otherwise lost in tones exhibiting a spectral zero, where the channel has a very low frequency response. The result, a *zero-restoration per tone equalizer* or ZR-PTEQ allows to go beyond the limits imposed by MMSE-equalizers. The implementation cost of the ZR-PTEQ is only slightly increased with respect to the PTEQ. Moreover, the ZR can be implemented as an add-on to a PTEQ structure

6.7 Acknowledgments

This research was carried out in the frame of KU Leuven Research Council CoE EF/05/006 ‘Optimization in Engineering’ (OPTEC) and PFV/10/002 (OPTEC) and the Belgian Programme on Interuniversity Attraction Poles initiated by the Belgian Federal Science Policy Office IUAP P7/23 ‘Belgian network on stochastic modeling analysis design and optimization of communication systems’ (BESTCOM) 2012-2017. The scientific responsibility is assumed by its authors.

Chapter 7

Chebyshev interpolation for DMT modems

This chapter consists of a copy of the article *Chebyshev interpolation for DMT modems* [43], as published in the proceedings of the *IEEE International Conference on Communications 2004*. Only the layout and the numbering of the references, equations and figures has been changed to accommodate for the different page size and to improve consistency.

Abstract

Sampling clock synchronization in discrete multi tone systems, such as digital subscriber line modems can be done with a phase locked loop. This requires expensive analog hardware, such as a voltage controlled oscillator. However, it is possible to use a cheaper free-running oscillator and tackle the problem in the digital domain. Using resampling or interpolation, the timing correction becomes transparent for subsequent equalizers. This contribution describes a novel resampling technique using Chebyshev polynomials.

7.1 Introduction

Discrete multitone (DMT), a modulation system used in e.g. digital subscriber line (DSL) modems divides the available spectrum into small bands. Carriers in these bands are individually digitally modulated using an inverse discrete Fourier transform

(IDFT). At the receiver, the transmitted information can be restored using the discrete Fourier transform (DFT). To facilitate equalization, a cyclic prefix (CP) is added to each symbol at transmission, and removed again at the receiver. As long as the channel order does not exceed the CP length, equalization can be done using a frequency domain equalizer (FEQ), which is merely a phase rotation and amplitude correction at each tone individually. Otherwise, more sophisticated equalizer structures are needed.

Several levels of synchronization can be discerned. Symbol synchronization between the central office (CO) and the customer premises (CP) is important to maintain the orthogonality between the carriers. Also the users should be synchronized between each other to avoid excessive crosstalk.

At a lower level, synchronization of the sample clocks is important to maintain a good signal to noise ratio. The master clock is generated at the CO, and CP needs to adjust its timing, both in reception and transmission. Usually this is achieved with a voltage controlled oscillator (VCO), adjusted by a phase locked loop (PLL). Timing information (steering the PLL) is usually derived from the data, e.g. using pilot tones. Alternatively, to reduce the cost of analog hardware, one can use a fixed sample clock and correct for it in the digital domain.

A small sample clock offset (delay) leads to a phase error which is linear with the carrier frequency. In the case of a clock frequency mismatch (drift), the phase offset grows from one symbol to the next symbol. When it becomes comparable to the sample duration, a sample is either duplicated or discarded to compensate [31, p.337-352]. While this approach works in practice, these discontinuities of the time axis introduce a non-stationarity at the input of the equalizer, lowering its efficiency.

To circumvent this, a true sample rate convertor is needed. The problem of *interpolation* in communications receivers is well known [127], and is closely related to fractional delay filters. The ideal interpolation filter would be a sampled *sinc* function. Because these extend infinitely in time, they are not useable in practice. However, they can be approximated using a finite impulse response (FIR) filter e.g. having a minimum mean squared error in the frequency band of interest. The *Farrow structure* [61] offers an efficient way to implement variable delays, writing the FIR taps as a polynomial function of the (fractional) delay. However, designing the filters is difficult, especially if the delay compared to the original sample points is small [193]. It may therefore be easier and sufficiently accurate to use *polynomial interpolation* instead of (an approximation of) real Nyquist interpolation.

The text is structured as follows: in section 7.2 we start with a brief review of Chebyshev interpolation theory and the role of Chebyshev polynomials. In section 7.3, two interpolation methods, based on Chebyshev polynomials are described. Some simulation results are given in section 7.4 to prove their validity. Finally, section 7.5 concludes with a short discussion.

7.2 Chebyshev interpolation theory

The polynomial of degree N interpolating the continuous function $f(x)$ at the $N + 1$ distinct points $x_0 \dots x_N$ can be written as:

$$p_N(x) = \sum_{i=0}^N l_i(x) f(x_i), \quad \text{with} \tag{7.1}$$

$$l_i(x) = \prod_{\substack{k=0 \\ k \neq i}}^N \left(\frac{x - x_k}{x_i - x_k} \right), \tag{7.2}$$

the so-called *Lagrange* polynomials. This can also be written in a matrix form,

$$p_N(x) = [f(x_0) \dots f(x_N)] \mathbf{L} \begin{bmatrix} x^N \\ \vdots \\ x^0 \end{bmatrix}, \tag{7.3}$$

where the i^{th} row of the *generating matrix* \mathbf{L} contains the coefficients of $l_i(x)$ in descending powers of x .

There is no restriction on the choice of the points x_i , but in the case of a digital receiver their position is determined by the sample clock, and hence they are equidistant. Unfortunately interpolation on a uniform sampling grid is far from optimal, and leads to a large interpolation error in between the sampling points, especially near the interval edges. This is known as the *Runge phenomenon*, and is comparable to *Gibbs phenomenon* in Fourier series.

We will now look at alternatives to the uniform sampling grid. For the sake of simplicity, but without loss of generality, in the remainder of the text it will be assumed that $|x_i| \leq 1$, i.e. $f(x)$ is interpolated on $[-1, 1]$. Also, for the reader's convenience, we remind that the Chebyshev polynomials of the first kind $T_N(x)$ are given by:

$$T_N(x) = \begin{cases} 1 & N = 0 \\ x & N = 1 \\ 2xT_{N-1}(x) - T_{N-2}(x) & N = 2, 3, \dots \end{cases} \tag{7.4}$$

Another definition is that

$$T_N(x) = T_N(\cos(\theta)) = \cos(N\theta). \tag{7.5}$$

It can now be shown that choosing the interpolation points x_i from (7.1) at the roots z_i of $T_{N+1}(x)$, i.e.

$$z_i = -\cos \frac{\pi(2i + 1)}{2(N + 1)} \tag{7.6}$$

leads to a low maximum interpolation error [138], [157]. These so-called *Chebyshev points* z_i are sparse in the middle, and denser at the edges of the interval $[-1, 1]$. Choosing these points ensures uniform convergence for any continuous function $f(x)$ that satisfies the Dini-Lipschitz condition¹, and convergence in an \mathcal{L}_2 norm for all continuous functions $f(x)$. Moreover, interpolation on these points renders the best \mathcal{L}_2 approximation of $f(x)$ [124] when the inner product is defined as:

$$\langle h, g \rangle = \int_{-1}^1 \frac{h(x)g(x)}{\sqrt{1-x^2}} \tag{7.7}$$

Obviously, it is now possible to calculate $p_N(x)$ in the Lagrange style of eq.(7.1), but for this special choice of sample points, one can also write $p_N(x)$ as a summation of normalized Chebyshev polynomials of the first kind:

$$p_N(x) = \sum_{i=0}^N c_i \tilde{T}_i(x), \text{ with} \tag{7.8}$$

$$\tilde{T}_0(x) = \frac{1}{\sqrt{2}} T_0(x), \tilde{T}_{N>0}(x) = T_{N>0}(x) \tag{7.9}$$

The coefficients c_k of the Chebyshev decomposition can be calculated as the discrete cosine transform (DCT) of the vector of nonuniform samples, taken at z_i [138]. In other words:

$$\begin{bmatrix} c_0 \\ c_1 \\ \vdots \\ c_N \end{bmatrix} = \mathbf{C} \begin{bmatrix} f(z_0) \\ f(z_1) \\ \vdots \\ f(z_N) \end{bmatrix}, \tag{7.10}$$

with the $(m,n)^{th}$ element of \mathbf{C} equal to

$$\mathbf{C}_{m,n} = v_m \cos \frac{m\pi(2n+1)}{2(N+1)}, \tag{7.11}$$

$$v_m = \begin{cases} \frac{\sqrt{2}}{N+1} & m = 0 \\ \frac{2(-1)^m}{N+1} & m = 1, \dots, N \end{cases} \tag{7.12}$$

We can now also write eq. (7.8) in a matrix form as

$$p_N(x) = [f(z_0) \dots f(z_N)] \mathbf{C}^T \mathbf{T} \begin{bmatrix} x^N \\ \vdots \\ x^0 \end{bmatrix}, \tag{7.13}$$

¹The Dini Lipschitz condition is stronger than continuity. If $\omega_f(\delta) = \sup(|f(x_1) - f(x_2)|)$ for $|x_2 - x_1| \leq \delta$, then it requires that $\lim_{\delta \rightarrow 0} \omega_f(\delta) \log(\delta) = 0$.

where the i^{th} row of \mathbf{T} contains the coefficients of $\tilde{T}_i(x)$ in descending powers of x .

It may come as a surprise that these coefficients can be calculated so easily, and that this involves a DCT. However, this result can be understood intuitively if we look at **Figure 7.1**.

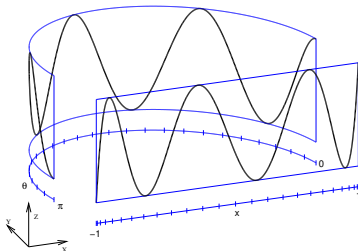


Figure 7.1: Cosines on a uniform grid in the θ -plane correspond to Chebyshev polynomials on a nonuniform grid in the XZ -plane

We can think of signals as being a function of x and z residing in the XZ -plane. Imagine now we construct a new curved plane, which we call the θ -plane, and which is a semicylinder constructed on the unit circle and extending perpendicular from it. Function pairs in the XZ -plane can now be projected (along the Y -axis) to the θ -plane and vice versa. More specifically, the Chebyshev polynomials in the XZ -plane are transformed to cosines in the θ -plane (cfr. formula (7.5)). In figure 7.1, this is shown for $T_7(x)$. Therefore, a decomposition in Chebyshev polynomials in the XZ -plane corresponds to a decomposition into cosines in the θ -plane. Because the non-uniform sampling grid defined in (7.6) is exactly converted to a *uniform* grid in the θ -plane, the coefficients of this cosine decomposition can be calculated with a (slightly modified) DCT. The alternating signs of v_m are due to the fact that x traverses the XZ -plane from left to right, whereas θ traverses the θ -plane from right to left. All Chebyshev polynomials are either symmetric or antisymmetric. For the latter ones, the minus sign is required.

7.3 Implementation

As stated before, although the choice of the Chebyshev points may be interesting for the interpolation, in case of a digital receiver, we are limited to a uniform sampling grid. However, it is possible to think of the received signals as not residing in the XZ -plane, but in the θ -plane! This way, we can do a (numerically interesting) cosine decomposition, and interpolate the function in the θ -plane. This evaluation of the cosine

expansion at an arbitrary point can be done cheaply by calculating the corresponding Chebyshev series in the XZ -plane.

In practice, we need not change the interpolator at every output, but we can do a block-processing where L output samples are reconstructed based on input blocks of size $P = N + 1$, as shown in **Figure 7.2**. The original samples are located at $t_0 \dots t_{P-1}$ and have values $y_0 \dots y_{P-1}$, while the samples to be generated, $\tilde{y}_0 \dots \tilde{y}_{L-1}$ are located at $\tilde{t}_0 \dots \tilde{t}_{L-1}$. After all L samples have been generated, the block is shifted over L samples and the process is repeated.

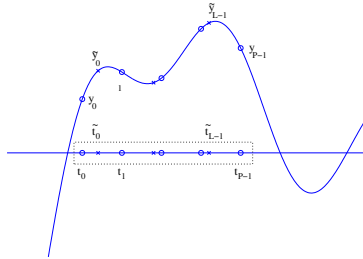


Figure 7.2: L output samples at \tilde{t}_k interpolated from P input samples at t_k

We can now think of the function values $y_0 \dots y_{P-1}$ as in the θ -plane and construct the cosine series there. For each block, P coefficients c_i are generated according to eq. (7.10). In practice, this can be implemented with a fast DCT algorithm. If L is small compared to N , it might be more practical to compute a sliding DCT [213], [107]. Based on these coefficients, we can now evaluate the cosine series at $\tilde{t}_0 \dots \tilde{t}_{L-1}$ by evaluating the corresponding Chebyshev expansion at $\tilde{x}_0 \dots \tilde{x}_{L-1}$,

$$\tilde{x}_k = \cos \left[\pi \left(\frac{1}{2(N+1)} + \frac{\tilde{t}_k - t_0}{t_{p-1} - t_0} \right) \right], \tag{7.14}$$

with $k = 0 \dots L - 1$.

The evaluation of the interpolating polynomial can be done in a numerically interesting way. Using the recurrence relation in eq.(7.4) the summation of Chebyshev polynomials

$$c_N T_N(x) + c_{N-1} T_{N-1}(x) + c_{N-2} T_{N-2}(x) + \dots \tag{7.15}$$

can be written as

$$\underbrace{(2c_N + c_{N-1})}_{b_{N-1}} T_{N-1}(x) + (c_{N-2} - c_N) T_{N-2}(x) + \dots, \tag{7.16}$$

$$\underbrace{(2xb_{N-1} + c_{N-2} - c_N)}_{b_{N-2}} T_{N-2}(x) + (c_{N-3} - b_{N-1})T_{N-3}(x) + \dots \tag{7.17}$$

and eventually

$$b_1 T_1(x) + b_0 T_0(x) = b_1 x + b_0. \tag{7.18}$$

This scheme is depicted in **Figure 7.3**.

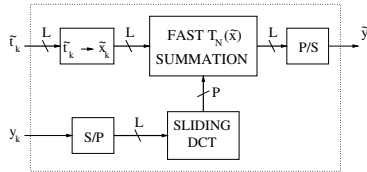


Figure 7.3: The Chebyshev interpolator block diagram

Current interpolation implementations [147], [49],... mostly make use of the so-called *Farrow structure* [61]. This is a known and efficient structure to compute a linear combination of polynomials or alternatively it can be seen as an FIR (interpolation-)filter for which the taps are a polynomial in the fractional delay. It is very suited to implement a Lagrange interpolator [49].

Observing the similarity between eq. (7.3) and eq. (7.13), it is now possible to write our structure as a Lagrange interpolator with generating matrix $\mathbf{G} = \mathbf{C}^T \mathbf{T}$. If we introduce the calculation of a cosine (going from \tilde{t} to \tilde{x}), implemented with a cordic structure [107], we obtain the modified Farrow scheme of **Figure 7.4**.

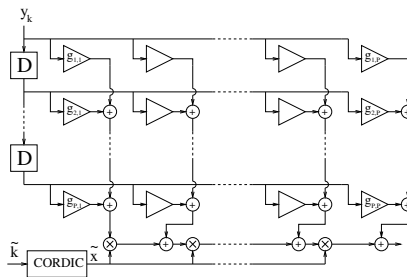


Figure 7.4: The modified Farrow structure

7.4 Simulation results

We have compared the Chebyshev interpolator with the classic Lagrange implementation.

Because of numerical precision, it is very difficult to generate an accurate DSL signal. The most correct way to do so, would be to do true sinc-interpolation. Obviously, the sinc function needs to be truncated in time for practical computations, so that a certain error will be introduced. While increasing the number of sinc-samples will reduce this error, this will on the other hand contribute to roundoff-errors (because more terms are summed).

However, because in practice the clock frequency offsets are small (10^{-5}), the offset between the two clocks will not vary significantly over one symbol period. We have therefore set the frequency offset to zero, while assuming a phase-mismatch of half a sample. This corresponds to the worst-case scenario. As a test signal, we chose an ADSL downstream signal without channel noise. Both the Chebyshev and Lagrange interpolator use $P = 11$ nodes for the interpolation. One sample was interpolated per frame ($L = 1$) and this was chosen in the middle of the frame. The results are shown in **Figure 7.5**. For low frequencies, the Lagrange interpolator is still better than the Chebyshev structure. However, as the frequency increases, the Lagrange structure's performance degrades quickly. This is a general characteristic of interpolators, because they implement an approximation of the ideal sinc filter. Oversampling can solve this problem, and is sometimes used (e.g. [147]), but comes at the cost of increased complexity.

The Chebyshev interpolator also suffers from some degradation at higher frequencies, but manages to keep its performance until very close to the Nyquist frequency.

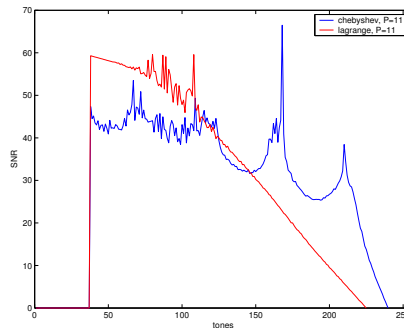


Figure 7.5: Comparison of Chebyshev and Lagrange interpolation. Fractional delay is $1/2$ sample

7.5 Conclusions

A cosine interpolation technique using Chebyshev polynomials was proposed, which does not suffer from the *Runge* phenomenon. Essentially, it is made up by a trigonometric (cosine) series which is converted to a summation of Chebyshev polynomials. The implementation can be done efficiently, using a fast DCT and a special summation scheme for Chebyshev polynomials. However, it can also be molded for use with the Farrow structure, which is a well-known and efficient scheme. Simulation results confirm the useability of the proposed techniques for interpolation in DMT communications system such as DSL. The proposed architectures can also be applied in other areas of signal processing where an interpolation is necessary, e.g. image processing, audio resampling etc.

Chapter 8

Conclusions and future work

In this last chapter, we highlight the relevant results of the thesis in section 8.1, and we also give an indication of where future research could be heading in section 8.2.

8.1 Conclusions

8.1.1 Intruductory material

Multi carrier modulation is an efficient way to use a large bandwidth of a dispersive channel. In chapter 1 we explained the history of MCM, arriving at the implementation using the DFT and the CP. The applications for wireless as well as wireline communication were discussed, with a special emphasis on the case of DSL. The DSL environment and its impairments were covered, including ingress and interference from other users. Most notably, crosstalk from other subscriber loops used to be the limiting factor of DSL performance.

In chapter 2, the mathematics behind MCM are explained. We have shown how the use of DFT-modulation and a CP turns the dispersive channel into a number of flat-fading subchannels. In case the channel order does not exceed the CP length, equalization can be done easily by adjusting the amplitude and phase of each tone by a FEQ. In the case of long channels, a TEQ can be used to shorten the channel. A superior solution is offered by the PTEQ, providing a multi-tap equalizer for each tone individually. We presented ZP and KSP as alternatives for the CP. Special topics such as bit loading, DSM and the PAPR-problem are discussed and we also explained the benefit of windowing functions. Finally, SC-FDE is presented as an alternative for

MCM. This modulation scheme combines the best of both worlds: a cheap equalization in the frequency domain and a low PAPR.

8.1.2 Own contributions

The ever increasing bandwidth occupied by DSL signals makes it overlap more and more with parts of the spectrum where potentially strong narrow-band signals are present e.g. those used by radio amateurs. Theoretically, the twisting of the copper pair should render it immune to pickup of airborne signals. In practice the twisted pair cables work as an antenna, and the DSL signal can be contaminated by strong narrow-band noise. Because of the slow decay of the DFT's side lobes, this noise not only interferes with the overlapping tones, but also with the neighbouring ones. The dual problem also exists: egress, or the radiation of energy in protected frequency bands. Both these problems could be cured by applying a windowing function before the DFT or IDFT. However, this is not straightforward, because we risk to lose the orthogonality between the tones.

In chapter 3 we describe a technique to combine the PTEQ with windowing functions. One of the key elements of the PTEQ is that a sliding DFT can be calculated based on a single DFT and so-called difference terms, just like a moving average can be calculated from the previous average and the difference between new data entering and old data leaving the average. This trick is not straightforward for a windowed DFT, where the corrections are not limited to simple difference terms, but are a tone-dependent linear combination of the samples corresponding to the head of the window and the samples corresponding to the tail of the window. The complexity can be lowered significantly through a judicious choice of the windowing function. It was shown that a linearly tapered window only requires one additional DFT for all tones, and 2 difference terms for each further extension in time. A raised cosine window, which offers much better sidelobe behaviour, can also be implemented efficiently. For each tone, this only requires one additional tap, compared to the case of the linearly tapered window.

Chapter 4 treats the case of egress, which can also be limited by applying a windowing function at the transmitter. To maintain the orthogonality between the tones, the windowing function should respect the cyclic property. We show that the windowing in the time domain can be described as a precoding in the frequency domain. By applying the corresponding decoding at the receiver, the effect of the window is transparent. We present a class of windows that maintains the cyclic property, while only requiring a simple decoder at the receiver. The simplest example is the pointwise-inverse of a raised cosine. The corresponding decoder equalizes each tone using three outputs of the DFT. Interestingly, this special class of windows can also be used to improve the

power efficiency of a simple technique to generate a KSP inside the DFT size of an OFDM symbol.

The work in chapter 5 was done in the context of wireless ZP systems. We have shown how ZFE is always possible in the time domain, though at the cost of a high computational complexity. The ZFE in the frequency domain is less demanding, but can lead to severe noise amplification in the case of spectral zeros, i.e. tones where the channel response is very low. Equalizers based on MMSE avoid this noise amplification, but still have a limited performance, because they discard the spectral zero altogether. We have proposed two ZR-equalizers, a ZFE and an MMSE-like structure which use the redundancy in the time domain to recover the information which was lost in the spectral zeros. They can be implemented standalone, or as an add-on to existing systems.

Chapter 6 links the ZR to the work in earlier chapters, combining it with the PTEQ. We first describe a variant of the PTEQ for ZP-SC transmissions, and combine this with ZR. Again, this can be done in a standalone implementation, or as an add-on to the PTEQ.

Chapter 7 is somewhat of an odd one out. In this chapter we have presented an interpolation technique based on Chebyshev polynomials, which relies on the similarity between these polynomials and trigonometric functions. Though its use is intended for DMT signals, it can also be used for the interpolation of other signals.

8.2 Future work

Just like cold fusion and flying cars, FTTH has always been a technological *nec plus ultra* which is only "a few years away". And just like the other two, the actual implementation has been disappointing. The reason for the limited penetration of fiber is that the largest cost of the deployment of any telecommunication network is not in the active installation, neither the cost of cabling, but in the installation of said cabling in the ground. While twisted pair may not be the easiest transmission medium to work with, neither the one offering the highest possible throughput, it has a distinct advantage of a large deployment. Admittedly, the decoupling point from fiber to copper (including coax) is slowly shifting towards the customer premises, but for the foreseeable future, DSL will continue to play an important role in the *last mile*.

Whereas crosstalk used to be the main limitation on DSL performance, coordination at the signal level allows to use the cable binder like a MIMO network, *exploiting* crosstalk instead of suffering from it. Especially on shorter lines, this leads to impressive data rates. Because this coordination requires a good knowledge of the crosstalk channels, we expect that future work will revolve around (blind) channel identification. Also

channel tracking will become important, to capture events which change the termination impedance of the twisted pair, such as powering off a modem.

We also expect an increased interest in SC-FDE, especially for mobile applications, where the battery life can benefit from the low PAPR. This explains why an SC-FDE-based multiplexing scheme was selected for the uplink of LTE. Because the wireless environment is a fast-changing one, frequent channel identification and tracking are needed. A ZP is not so helpful in this respect, but a KSP could be used for this purpose. Because the repetition of a fixed KSP only offers a limited amount of information about the channel, we expect to see more systems where the KSP is changed periodically, or slowly rotating.

Appendix A

A brief overview of the history of electronic communication

A.1 Nineteenth century: the age of invention

If it is love that makes the world go 'round, it is self induction that makes electromagnetic waves go 'round the world. –Oliver Heaviside

A.1.1 Telegraphy

The history of electronic communication begins in 1837, when William Cook and Charles Wheatstone in Europe, and independently Samuel Morse in the U.S. invent the telegraph [19]. The poor understanding of the transmission medium did not keep the telegraph from spreading widely across the European and American continent, but became apparent at the time of deployment of the first transatlantic cable in 1858. Even before it was put into operation, William Thompson (later Lord Kelvin) showed that the transmission rate would be limited by the resistance of the copper. He also developed his famous mirror galvanometer [20] for the specific purpose of detecting the weak currents at end of the cable, which operated without electronic amplification.

Apart from the attenuation, another major problem for transatlantic communication was the *dispersion*: the frequency dependency of the phase velocity results in a smearing out and overlapping of the received pulses, leading to *inter symbol interference* (ISI). At that time, the only remedy to avoid ISI was to transmit at very low rates, thus allowing the first transatlantic cable to carry only 0.1 words per minute.

On shorter overland lines, the throughput was higher, though not high enough to satisfy the need. To address this need, the so-called *harmonic telegraphy* sent different musical tones simultaneously. This technique, developed by Bell [12], Edison [48] and Gray [74], can be regarded a first implementation of *frequency division multiplexing* (FDM) or MCM.

A.1.2 Telephony

It was realized that if the telegraph line could convey several musical tones, it would also be capable of transmitting human speech [98], leading to the invention of the telephone by Bell in 1876 [13], though it could be argued that Elisha Gray or Phillip Reis deserve the credit more.

The early telephones used only one single telegraph wire with the Earth forming the return path. By the end of the 19th century, this single-ended transmission was increasingly plagued by interference from the emerging electrical tram systems. To avoid this, the single-wire configuration was replaced by a balanced transmission line consisting of two wires, one on each side of the telegraph poles.

With the advent of the electricity distribution, *switching noise* became a new source of electromagnetic interference. To reduce this interference, Bell invented the *twisted pair* cable [14] which is still in use for telephony today. The crosstalk between telephone wires, which caused the signal on one line to be faintly audible on other, was reduced by twisting neighbouring pairs at a different twisting rate.

A.1.3 Dispelling dispersion

The main problems remained, however: dispersion and attenuation in the cables. The first one was tackled by *Oliver Heaviside*. Heaviside was an engineering genius who rewrote Maxwell's laws [125] from a cumbersome quaternion-based formulation to the 4 well-known vector laws [9]. Furthermore, he developed transmission line theory, more specifically the telegraphist's equations.

Heaviside realized that the dispersion in telephony and telegraphy lines was caused by the high line capacitance, and in 1887 he proposed to counteract this by adding series inductances. Initially there was little enthusiasm for this idea, mostly because of Heaviside's controversial nature [137]. It was first practically implemented by Pupin in 1900, by adding series inductors to the twisted pair cables [152]. While this operation had the desired effect of reducing the dispersion and flattening the frequency characteristic of the telephone lines, it also caused an increased attenuation at higher

frequencies. While unimportant at the time, this would prove detrimental for eventual digital communication (see paragraph 1.3.3).

With the invention of the triode in 1908 [45] the problem of amplification was also solved. Meanwhile, *wireless transmissions* had began, with the pioneering work of Hertz in 1888 and the first telegraph by Marconi in 1896 [98].

A.2 Twentieth century: the age of information theory

Now that the work of Heaviside had explained the physics of transmission lines and amplification had become available, the next advances towards digital communication came from the realms of mathematics, and what was to become known as *information theory*.

A.2.1 Bandwidth and sampling

Nowadays it is well known that the minimum sample rate needed to describe a base band signal with band width B is given by the *Nyquist-Shannon sampling theorem*,

$$B \leq \frac{f_s}{2}, \quad (\text{A.1})$$

i.e. the sampling rate f_s should at least be twice the signal band width B . However, this has not always been so obvious. Early telephony designers trying to multiplex signals using mechanical commutators had already discovered a relation between the commutation speed and the intelligibility of the transmitted speech, but their findings were empirical and inconclusive. It took a long time before the theory explaining this was well established.

In 1928 *Nyquist* discovered that the maximum speed at which pulses could be sent independently over a channel was at a rate given by twice the band width [141]. Note that this statement is the dual of the sampling theorem of Eq.(A.1). Later on, this was formalized by Shannon in his landmark papers *A mathematical theory of communication* [168] and *Communication in the presence of noise* [166], where uniform sampling and the subsequent reconstruction of the original signal were explained. Note, however that the first proposal for the interpolation of equidistant functional values using the $\sin(x)/x$ function was published in 1908 by C.-J. de la Vallée Poussin -born in Leuven- in the *Bulletin Academie Royale de Belgique* [120].

A.2.2 Information and channel capacity

The channel capacity is not only dependent on the maximal rate at which one can transmit symbols, but also on the information carried by each of these symbols. In 1924, Nyquist already observed that [140]:

The speed at which intelligence can be transmitted over a telegraph circuit with a given line speed, i.e., a given rate of sending of signal elements, may be determined approximately by the following formula:

$$W = K \log(m),$$

with W is the speed of transmission of "intelligence", m the number of current values, and K a constant.

This concept was expanded by Hartley, who referred to it as *information*

$$H = \log(S^n) \tag{A.2}$$

with S the number of possible symbols, and n the number of symbols in a transmission [80].

Eventually Shannon proposed to represent information in the shape of the now ubiquitous *bits* -based on a base-two instead of base-ten logarithm- which resulted in the well known *Shannon-Hartley theorem* for the *channel capacity*,

$$C = B \log_2 \left(1 + \frac{S}{N} \right), \tag{A.3}$$

with S and N respectively the signal and noise power.

A.3 Voice-band modems

Before the second World War, Shannon had been working on switching circuits [167], which were of great importance in the telephone industry, and subsequently in the development of computers [66]. During the the war he switched to cryptography, and information theory, eventually resulting in *A mathematical theory of communication*. Indeed, the war and its aftermath were a very fruitful time for technological advances. Stimulated by the need for better germanium diode mixers for microwave radars, *Bell labs* invested significantly in the research of solid-state devices. In 1948 this culminated in the invention of the transistor by *Bardeen, Brattain and Shockley* [158].

In the 1950's, the transistor replaced vacuum tubes in the first digital computers, eventually leading to the development of the integrated circuit by *Jack Kilby* [108] and *Robert Noyce* [139]. Around the same time, *pulse code modulation* was developed as a practical digital transmission system for voice communication [73]. Exactly the opposite, the transmission of digital signals over analog voice channels, is done in *modems*.

A.3.1 Early modems: 110-300 bps

The first commercially available modem was developed in the context of the cold war, to connect computers of the Semi-Automatic Ground Environment (SAGE), a system to process radar information. It had a speed of 1200 bits per second (bps) [98].

In 1962 the first civilian commercial modem was developed, operating full-duplex at 300 bps. These modems used binary frequency shift keying (FSK), which only needed a simple timing recovery mechanism. Full-duplex operation was achieved by modulating two different carriers. Later that same year phase shift keying (PSK) and quadrature amplitude modulation (QAM) constellations were proposed [143].

A.3.2 Dispelling dispersion II: 9600 bps

By the mid 1960's, two rivaling approaches emerged to counteract the delay distortion. One was *multi-carrier modulation* -described in more detail in section 1.1-, and the other one was *automatic equalization*. The first such equalizer, adjusting itself using a training sequence was published in 1965 [118]. An adaptive version that operated without training, but could do a decision-based adaptation was developed one year later [119]. Both of these equalizers were optimizing for lowest ISI, not taking into account the noise. Most likely they were prone to *noise enhancement*, i.e. a strong amplification of the thermal noise at frequencies where the equalizer compensates for a dip in the channel response. The issues with noise enhancement play an important role in chapter 5.

Instead of optimizing for the lowest ISI, it is better to optimize for the lowest mean squared error (MSE), including ISI and noise contributions. The first adaptive algorithm to do so was the least-mean-squares (LMS) algorithm [209]. From the end of the 1960's on this was used for tap-gain adjustment. The main problem with LMS is its slow speed of convergence. Different methods were developed to solve this, including memory storage of the coefficients, frequency domain techniques for the initialization e.g. [27] and the recursive least squares (RLS) algorithm.

In case the previously transmitted symbol and the channel impulse response are known, it is possible to generate an artificial ISI and subtract this from the incoming signal, theoretically removing all ISI. In practice, the previously transmitted symbol can only be guessed, or "decided", leading to a *decision feedback equalizer* (DFE) [62]. Obviously this becomes very unstable if one starts making poor decisions. If the channel is known at the transmitter, this instability can be prevented by already subtracting the ISI at the transmitter side. This pre-equalization is now known as *Tomlinson-Harashima precoding*, after Tomlinson [187] and Harashima [77] who developed it independently.

Even though the timing recovery was improved and echo canceling was introduced [109], for a long time the speed of voice modems appeared to be limited to 9600 bps.

A.3.3 Trellis encoding: 33k6 bps

The needed breakthrough appeared in 1982 when *Ungerboeck* published his famous article on (what is now known as) trellis coded modulation [191]. This allowed the transmission rate to evolve from 9600 bps to 14k4, 19k2, eventually culminating in the V.34-standard, offering 33k6 bps [99], which is close to the channel capacity. The V.34 was the *nec plus ultra* of voice-band modems. Any further increase in speed to 56 kbps in the V.90-modem was only possible (in downstream only) by using the same signaling as used in the telephony network itself.

Bibliography

- [1] 3rd generation partnership project; technical specification group radio access network; evolved universal terrestrial radio access (e-utra); physical channels and modulation (release 12), 2014. pages 113
- [2] 3RD GENERATION PARTNERSHIP PROJECT 2 "3GPP2". Physical Layer Standard for CDMA2000 Spread Spectrum Systems. *3GPP2 C.S0002-D* (February 2006). pages 7
- [3] ABRAMSON, N. THE ALOHA SYSTEM: Another Alternative for Computer Communications. In *Proceedings of the November 17-19, 1970, Fall Joint Computer Conference* (New York, NY, USA, 1970), AFIPS '70 (Fall), ACM, pp. 281–285. pages 6
- [4] AKANSU, A., DUHAMEL, P., LIN, X., AND DE COURVILLE, M. Orthogonal transmultiplexers in communication: a review. *Signal Processing, IEEE Transactions on* 46, 4 (Apr 1998), 979–995. pages 33
- [5] AL-DHAHIR, N., AND CIOFFI, J. Optimum finite-length equalization for multicarrier transceivers. *Communications, IEEE Transactions on* 44, 1 (1996), 56–64. pages 36
- [6] ANSI. Spectrum management for loop transmission systems. T1E1.4/2000-002R6 ANSI T1.417, 2000. pages 24
- [7] ARNDT, C. *Information Measures: Information and Its Description in Science and Engineering*, first ed. Engineering online library. Springer, 2001. pages 32
- [8] ARSLAN, G., EVANS, B., AND KIAEI, S. Equalization for discrete multitone transceivers to maximize bit rate. *Signal Processing, IEEE Transactions on* 49, 12 (2001), 3123–3135. pages 28
- [9] ARTHUR, J. The evolution of maxwell's equations from 1862 to the present day. *Antennas and Propagation Magazine, IEEE* 55, 3 (June 2013), 61–81. pages 140

- [10] BAHAI, A. R., AND SALTZBERG, B. R. *Multi-Carrier Digital Communications: Theory and Applications of OFDM*. Plenum Publishing Co., 1999. pages 2
- [11] BAUML, R., FISCHER, R., AND HUBER, J. Reducing the peak-to-average power ratio of multicarrier modulation by selected mapping. *Electronics Letters* 32, 22 (Oct 1996), 2056–2057. pages 27
- [12] BELL, A. Improvement in transmitters and receivers for electric telegraphs, apr 6 1875. US Patent 161,739. pages 140
- [13] BELL, A. G. Improvement in telegraphy, mar 7 1876. US Patent 174,465. pages 140
- [14] BELL, A. G. Telephone-circuit, jul 19 1881. US Patent 244,426. pages 140
- [15] BELL, C., AND WILLIAMS, W. Dab: digital audio broadcasting coverage aspects of a single frequency network. In *Broadcasting Convention, 1992. IBC., International* (Jul 1992), pp. 270–276. pages 5
- [16] BINGHAM, J. Rfi suppression in multicarrier transmission systems. In *Global Telecommunications Conference, 1996. GLOBECOM '96. 'Communications: The Key to Global Prosperity* (Nov 1996), vol. 2, pp. 1026–1030 vol.2. pages 11
- [17] BINGHAM, J. A. C. Multicarrier modulation for data transmission: an idea whose time has come. *Communications Magazine, IEEE* 28, 5 (1990), 5–14. pages 7, 86
- [18] BLUETOOTH SPECIAL INTERESTS GROUP. Bluetooth specification version 1.0 a. pages 6
- [19] BOWERS, B. Cooke and Wheatstone, and Morse: a comparative view. In *Conference on the History of Telecommunications organized by the IEEE History Center and the IEEE History Committee* (2001). pages 139
- [20] BRAY, J., AND OF ELECTRICAL ENGINEERS, I. *Innovation and the Communications Revolution: From the Victorian Pioneers to Broadband Internet*. Institution of Engineering and Technology, 2002. pages 139
- [21] ÇELEBI, S. Interblock interference (IBI) and time of reference (TOR) computation in OFDM systems. *Communications, IEEE Transactions on* 49, 11 (2001), 1895–1900. pages 36
- [22] CENDRILLON, R. *Multi-user signal and spectra co-ordination for digital subscriber lines*. Ph.D. dissertation, KU Leuven, 2004. pages 25

- [23] CENDRILLON, R., AND MOONEN, M. Efficient equalizers for single and multi-carrier environments with known symbol padding. In *Signal Processing and its Applications, Sixth International, Symposium on. 2001* (2001), vol. 2, pp. 607–610 vol.2. pages 80, 81
- [24] CENDRILLON, R., YU, W., MOONEN, M., VERLINDEN, J., AND BOSTOEN, T. Optimal multiuser spectrum balancing for digital subscriber lines. *Communications, IEEE Transactions on* 54, 5 (May 2006), 922–933. pages 25
- [25] CHANG, R. W. Synthesis of band-limited orthogonal signals for multichannel data transmission. *Bell System Technical Journal, The* 45, 10 (Dec 1966), 1775–1796. pages 2
- [26] CHERUBINI, G., ELEFThERIOU, E., AND ÖLÇER, S. Filtered multitone modulation for VDSL. In *Global Telecommunications Conference, 1999. GLOBECOM '99* (1999), vol. 2, pp. 1139–1144 vol.2. pages 65
- [27] CHOQUET, M. Channel equalization apparatus and method using the Fourier transform technique, may 1 1979. US Patent 4,152,649. pages 143
- [28] CHOW, P., CIOFFI, J., AND BINGHAM, J. A. C. A practical discrete multitone transceiver loading algorithm for data transmission over spectrally shaped channels. *Communications, IEEE Transactions on* 43, 234 (1995), 773–775. pages 24
- [29] CIMINI, L. Analysis and simulation of a digital mobile channel using orthogonal frequency division multiplexing. *Communications, IEEE Transactions on* 33, 7 (Jul 1985), 665–675. pages 5
- [30] CIOFFI, J. Lighting up copper [history of communications]. *Communications Magazine, IEEE* 49, 5 (May 2011), 30–43. pages 8
- [31] CIOFFI, J., SILVERMAN, P., AND STARR, T. *Understanding Digital Subscriber Line Technology*, first ed. Prentice Hall, 1999. pages 9, 23, 36, 126
- [32] COOLEY, J., AND TUKEY, J. An algorithm for the machine calculation of complex Fourier series. *Mathematics of Computation* 19, 90 (1965), 297–301. pages 2
- [33] COOMANS, W., MORAES, R., HOOGHE, K., DUQUE, A., GALARO, J., TIMMERS, M., VAN WIJNGAARDEN, A., GUENACH, M., AND MAES, J. Xg-fast: Towards 10 gb/s copper access. In *Globecom Workshops (GC Wkshps), 2014* (Dec 2014), pp. 630–635. pages 26
- [34] COSTAS, J. Phase-shift radio teletype. *Proceedings of the IRE* 45, 1 (Jan 1957), 16–20. pages 6

- [35] CUYPERS, C., MOONEN, M., VANDAELE, P., AND YSEBAERT, G. Multicarrier receiver with a sliding window Fourier transform and a Fourier transform, mar 26 2003. EP Patent App. EP20,010,440,309. pages 12, 35
- [36] CUYPERS, G., AND MOONEN, M. Combining spectral zero restoration and per-tone equalization in single-carrier block transmissions. *Submitted to Elsevier Signal Processing* (2015). pages 111
- [37] CUYPERS, G., AND MOONEN, M. Frequency-domain equalizers with zero restoration for zero-padded block transmission. *Submitted to EURASIP Journal on Wireless Communications and Networking* (2015). pages 85, 113, 119, 120
- [38] CUYPERS, G., MOONEN, M., VANDAELE, P., AND YSEBAERT, G. Multicarrier receiver, aug 14 2003. US Patent App. 10/247,478. pages 12, 35
- [39] CUYPERS, G., VANBLEU, K., YSEBAERT, G., AND MOONEN, M. Egress reduction by intra-symbol windowing in DMT-based transmitters. In *Acoustics, Speech, and Signal Processing, 2003. Proceedings. (ICASSP '03). 2003 IEEE International Conference on* (2003), vol. 4, pp. IV-532-5 vol.4. pages 12
- [40] CUYPERS, G., VANBLEU, K., YSEBAERT, G., AND MOONEN, M. Intra-symbol windowing for egress reduction in DMT transmitters. *EURASIP J. Appl. Signal Process.* 2006 (January 2006), 87-87. pages 63
- [41] CUYPERS, G., VANBLEU, K., YSEBAERT, G., MOONEN, M., AND VANDAELE, P. Combining raised cosine windowing and per tone equalization for RFI mitigation in DMT receivers. In *Communications, 2003. ICC '03. IEEE International Conference on* (2003), vol. 4, pp. 2852-2856 vol.4. pages 37
- [42] CUYPERS, G., VANBLEU, K., YSEBAERT, G., MOONEN, M., AND VANDAELE, P. Combined per tone equalization and receiver windowing in DSL receivers: WiPTEQ. *Elsevier Signal Processing* 85, 10 (2005), 1921-1942. pages 35
- [43] CUYPERS, G., YSEBAERT, G., MOONEN, M., AND PISONI, F. Chebyshev interpolation for DMT modems. In *Communications, 2004 IEEE International Conference on* (June 2004), vol. 5, pp. 2736-2740 Vol.5. pages 125
- [44] CUYPERS, G., YSEBAERT, G., MOONEN, M., AND VANDAELE, P. Combining per tone equalization and windowing in DMT receivers. In *Acoustics, Speech, and Signal Processing (ICASSP), 2002 IEEE International Conference on* (2002), vol. 3, pp. III-2341-III-2344. pages 37, 64
- [45] DE FOREST, L. Space telegraphy., feb 18 1908. US Patent 879,532. pages 141

- [46] DENEIRE, L., GYSELINCKX, B., AND ENGELS, M. Training sequence versus cyclic prefix—a new look on single carrier communication. *Communications Letters, IEEE* 5, 7 (jul 2001), 292–294. pages 20, 32, 80
- [47] DOUFEXI, A., ARMOUR, S., BUTLER, M., NIX, A., BULL, D., MCGEEHAN, J., AND KARLSSON, P. A comparison of the hiperlan/2 and IEEE 802.11a wireless lan standards. *Communications Magazine, IEEE* 40, 5 (May 2002), 172–180. pages 6
- [48] EDISON, T. Improvement in acoustic telegraphs, oct 10 1876. US Patent 182,996. pages 140
- [49] ERUP, L., GARDNER, F. M., AND HARRIS, R. Interpolation in digital modems. ii. implementation and performance. *Communications, IEEE Transactions on* 41, 6 (1993), 998–1008. pages 131
- [50] EUROPEAN TELECOMM. STANDARDS INST. Radio broadcast systems: digital audio broadcasting (DAB) to mobile, portable and fixed receivers. ETS 300 401, RE/JTC-00DAB-4, 1997. pages 5
- [51] EUROPEAN TELECOMM. STANDARDS INST. Transmission and multiplexing (tm); access transmission systems on metallic access cables; very high speed digital subscriber line (VDSL); part 1: Functional requirements. TS 101 270-1 V1.2.1 (1999-10), 1999. pages 65, 76
- [52] EUROPEAN TELECOMM. STANDARDS INST. Broadband Radio Access Networks (BRAN); HIPERLAN Type 2; System Overview. *ETSI TR 101 683 V1.1.1 (2000-02)* (2000). pages 6
- [53] EUROPEAN TELECOMM. STANDARDS INST. Radio Equipment and Systems (RES); HIgh PErformance Radio Local Area Network (HIPERLAN) Type 1; Functional specification. *ETS 300 652* (2000). pages 6
- [54] EUROPEAN TELECOMM. STANDARDS INST. VDSL: Transceiver specification. TS 101 270-2 V1.1.1 (2001-02), 2001. pages 76
- [55] EUROPEAN TELECOMM. STANDARDS INST. Digital Video Broadcasting (DVB); DVB mega-frame for Single Frequency Network (SFN) synchronization. TS 101 191 V1.4.1 (2004-06), 2004. pages 6
- [56] EUROPEAN TELECOMM. STANDARDS INST. Digital Video Broadcasting (DVB); framing structure, channel coding and modulation for digital terrestrial television. EN 300 744 V1.5.1 (2004-06), 2004. pages 6
- [57] EUROPEAN TELECOMM. STANDARDS INST. Digital cellular telecommunications system (Phase 2+); Physical layer on the radio path; General description. ETSI TS 145 001 V10.0.0 (2011-04), 2011. pages 7

- [58] EUROPEAN TELECOMM. STANDARDS INST. LTE; Evolved Universal Terrestrial Radio Access (E-UTRA); Physical channels and modulation. TS 136 211 V10.0.0 (2011-01), 2011. pages 7, 33
- [59] FALCONER, D. History of equalization 1860-1980. *Communications Magazine, IEEE 49*, 10 (Oct 2011), 42–50. pages 18, 28
- [60] FALCONER, D., ARIYAVISITAKUL, S., BENYAMIN-SEYYAR, A., AND EIDSON, B. Frequency domain equalization for single-carrier broadband wireless systems. *Communications Magazine, IEEE 40*, 4 (apr 2002), 58 – 66. pages 32, 86, 87
- [61] FARROW, C. W. A continuously variable digital delay element. In *Circuits and Systems, 1988., IEEE International Symposium on* (1988), pp. 2641–2645 vol.3. pages 126, 131
- [62] FORNEY, G., AND EYUBOGLU, M. Combined equalization and coding using precoding. *Communications Magazine, IEEE 29*, 12 (Dec 1991), 25–34. pages 144
- [63] FORNEY, G. D. 1995 SHANNON LECTURE Performance and Complexity, 1995. pages 23
- [64] FOSCHINI, G., AND GANS, M. J. On limits of wireless communications in a fading environment when using multiple antennas. *Wireless Personal Communications 6* (1998), 311–335. pages 26
- [65] GAGNAIRE, M. An overview of broad-band access technologies. *Proceedings of the IEEE 85*, 12 (Dec 1997), 1958–1972. pages 7
- [66] GALLAGER, R. Claude E. Shannon: a retrospective on his life, work, and impact. *Information Theory, IEEE Transactions on 47*, 7 (Nov 2001), 2681–2695. pages 142
- [67] GALLI, S., VALENTI, C., AND KERPEZ, K. A frequency-domain approach to crosstalk identification in xDSL systems. *Selected Areas in Communications, IEEE Journal on 19*, 8 (Aug 2001), 1497–1506. pages 11
- [68] GIANNAKIS, G. Filterbanks for blind channel identification and equalization. *Signal Processing Letters, IEEE 4*, 6 (1997), 184–187. pages 87, 112
- [69] GIBSON, J. *The Communications Handbook*. The electrical engineering handbook series. CRC Press, 1997. pages 8
- [70] GINIS, G., AND CIOFFI, J. Vectored transmission for digital subscriber line systems. *Selected Areas in Communications, IEEE Journal on 20*, 5 (Jun 2002), 1085–1104. pages 25

- [71] GOLDEN, P., DEDIEU, H., AND JACOBSEN, K. *Fundamentals of DSL Technology*. CRC Press, 2005. pages 30
- [72] GOLUB, G., AND LOAN, C. V. *Matrix computations*, third ed. Johns Hopkins University Press, 1996. pages 102
- [73] GOODALL, W. Telephony by pulse code modulation. *Bell System Technical Journal*, The 26, 3 (July 1947), 395–409. pages 143
- [74] GRAY, E. Improvement in electrical telegraph for transmitting musical tones, jul 27 1875. US Patent 166,095. pages 140
- [75] HAN, S. H., CIOFFI, J., AND LEE, J. H. Tone injection with hexagonal constellation for peak-to-average power ratio reduction in OFDM. *Communications Letters, IEEE* 10, 9 (Sept 2006), 646–648. pages 27
- [76] HAN, S. H., AND LEE, J. H. An overview of peak-to-average power ratio reduction techniques for multicarrier transmission. *Wireless Communications, IEEE* 12, 2 (April 2005), 56–65. pages 27
- [77] HARASHIMA, H., AND MIYAKAWA, H. Matched-transmission technique for channels with intersymbol interference. *Communications, IEEE Transactions on* 20, 4 (Aug 1972), 774–780. pages 144
- [78] HARE, E. *The ARRL RFI book*, first ed. American radio relay league, 1999. pages 11
- [79] HARRIS, F. J. On the use of windows for harmonic analysis with the discrete Fourier transform. *Proceedings of the IEEE* 66, 1 (1978), 51–83. pages 12, 65
- [80] HARTLEY, R. V. L. Transmission of information. *The Bell System Technical Journal* 7 (1928), 535–563. pages 142
- [81] HAUN, R. Laser applications. *Spectrum, IEEE* 5, 5 (May 1968), 82–92. pages 7
- [82] HAYASHI, K., AND SAKAI, H. Per-tone equalization for single carrier block transmission with cyclic prefix. In *Circuits and Systems, 2004. MWSCAS '04. The 2004 47th Midwest Symposium on* (July 2004), vol. 2, pp. II–649–II–652 vol.2. pages 112, 118
- [83] HAYKIN, S. *Adaptive filter theory*, third ed. Prentice-Hall, 1996, pp. 624–628. pages 40, 53
- [84] HEALD, E. T., AND CLABAUGH, R. G. A predicted wave-signalling phase-shift telegraph system. *American Institute of Electrical Engineers, Part I: Communication and Electronics, Transactions of the* 76, 3 (July 1957), 316–319. pages 2

- [85] HEIDEMAN, M., JOHNSON, D., AND BURRUS, C. Gauss and the history of the fast Fourier transform. *ASSP Magazine, IEEE 1*, 4 (October 1984), 14–21. pages 2
- [86] HENKEL, W., OLCER, S., JACOBSEN, K., AND SALTZBERG, B. Guest editorial twisted pair transmission-ever increasing performances on ancient telephone wires. *Selected Areas in Communications, IEEE Journal on 20*, 5 (June 2002), 877–880. pages 8
- [87] HENKEL, W., TAUBÖCK, G., ÖDLING, P., BJÖRESSON, P., PETERSSON, N., AND JOHANSSON, A. The cyclic prefix of OFDM/DMT - an analysis. In *Broadband Communications, 2002. Access, Transmission, Networking. 2002 International Zurich Seminar on* (2002), pp. 22–1–22–3. pages 28, 36
- [88] HOFBAUER, C., HUEMER, M., AND HUBER, J. Coded OFDM by unique word prefix. In *Communication Systems (ICCS), 2010 IEEE International Conference on* (Nov 2010), pp. 426–430. pages 21
- [89] HUBERMAN, S., LEUNG, C., AND LE-NGOC, T. Dynamic spectrum management (dsm) algorithms for multi-user xDSL. *Communications Surveys Tutorials, IEEE 14*, 1 (First 2012), 109–130. pages 25
- [90] HUEMER, M., HOFBAUER, C., AND HUBER, J. Unique word prefix in SC/FDE and OFDM: A comparison. In *GLOBECOM Workshops (GC Wkshps), 2010 IEEE* (dec. 2010), pp. 1296–1301. pages 21, 33, 80
- [91] HUEMER, M., WITSCHNIG, H., AND HAUSNER, J. Unique word based phase tracking algorithms for SC/FDE-systems. In *Global Telecommunications Conference, 2003. GLOBECOM '03. IEEE* (Dec 2003), vol. 1, pp. 70–74 Vol.1. pages 21
- [92] IEEE. Standard for Information Technology- Telecommunications and Information Exchange Between Systems-Local and Metropolitan Area Networks-Specific Requirements-Part 11: Wireless LAN Medium Access Control (MAC) and Physical Layer (PHY) Specifications. *IEEE Std 802.11-1997* (1997), i–445. pages 6
- [93] IEEE. IEEE Std 802.11a-1999(R2003) Part 11: Wireless LAN Medium Access Control (MAC) and Physical Layer (PHY) specifications, High-speed Physical Layer in the 5GHz band, 2003. pages 106, 122
- [94] IEEE. Standard for Information Technology- Telecommunications and Information Exchange Between Systems- Local and Metropolitan Area Networks- Specific Requirements- Part 11: Wireless LAN Medium Access Control (MAC) and Physical Layer (PHY) Specifications. *ANSI/IEEE Std 802.11, 1999 Edition (R2003)* (2003), i–513. pages 6

- [95] IEEE. Standard for Information Technology- Telecommunications and Information Exchange Between Systems- Local and Metropolitan Area Networks- Specific Requirements Part II: Wireless LAN Medium Access Control (MAC) and Physical Layer (PHY) Specifications. *IEEE Std 802.11g-2003 (Amendment to IEEE Std 802.11, 1999 Edn. (Reaff 2003) as amended by IEEE Stds 802.11a-1999, 802.11b-1999, 802.11b-1999/Cor 1-2001, and 802.11d-2001)* (2003), i–67. pages 6
- [96] IEEE. Standard for Local and Metropolitan Area Networks Part 16: Air Interface for Fixed and Mobile Broadband Wireless Access Systems Amendment 2: Physical and Medium Access Control Layers for Combined Fixed and Mobile Operation in Licensed Bands and Corrigendum 1. *IEEE Std 802.16e-2005 and IEEE Std 802.16-2004/Cor 1-2005 (Amendment and Corrigendum to IEEE Std 802.16-2004)* (2006). pages 7
- [97] IEEE. Standard for Information technology– Local and metropolitan area networks– Specific requirements– Part 11: Wireless LAN Medium Access Control (MAC) and Physical Layer (PHY) Specifications Amendment 5: Enhancements for Higher Throughput. *IEEE Std 802.11n-2009 (Amendment to IEEE Std 802.11-2007 as amended by IEEE Std 802.11k-2008, IEEE Std 802.11r-2008, IEEE Std 802.11y-2008, and IEEE Std 802.11w-2009)* (Oct 2009), 1–565. pages 6
- [98] IEEE COMMUNICATIONS SOCIETY. *A Brief History of Communications: IEEE Communications Society - a Fifty-year Foundation for the Future*. The Society, 2002. pages 140, 141, 143
- [99] INTERNATIONAL TELECOMMUNICATIONS UNION (ITU). Rec. ITU-T V.34, a modem operating at data signalling rates of up to 33 600 bit/s for use on the general switched telephone network and on leased point-to-point 2-wire telephone-type circuits, 1996. pages 144
- [100] INTERNATIONAL TELECOMMUNICATIONS UNION (ITU). Rec. ITU-R M.1225, guidelines for evaluation of radio transmission technologies for IMT-2000, 1997. pages 106
- [101] INTERNATIONAL TELECOMMUNICATIONS UNION (ITU). ITU-T G.992.1: Asymmetric digital subscriber line (ADSL) transceivers. pages 10, 24
- [102] JIANG, T., AND WU, Y. An overview: Peak-to-average power ratio reduction techniques for OFDM signals. *Broadcasting, IEEE Transactions on* 54, 2 (June 2008), 257–268. pages 27
- [103] JONES, A., WILKINSON, T., AND BARTON, S. Block coding scheme for reduction of peak to mean envelope power ratio of multicarrier transmission schemes. *Electronics Letters* 30, 25 (Dec 1994), 2098–2099. pages 27

- [104] KAO, K., AND HOCKHAM, G. Dielectric-fibre surface waveguides for optical frequencies. *Electrical Engineers, Proceedings of the Institution of 113*, 7 (July 1966), 1151–1158. pages 7
- [105] KAPOOR, S., AND NEDIC, S. Interference suppression in DMT receivers using windowing. In *Communications, 2000. ICC 2000. 2000 IEEE International Conference on* (2000), vol. 2, pp. 778–782 vol.2. pages 31, 41, 64
- [106] KAPRON, F. P., KECK, D. B., AND MAURER, R. D. Radiation losses in glass optical waveguides. *Applied Physics Letters* 17, 10 (1970), 423–425. pages 7
- [107] KAR, D., AND BAPESWARA RAO, V. A cordic-based unified systolic architecture for sliding window applications of discrete transforms. *Signal Processing, IEEE Transactions on* 44, 2 (1996), 441–444. pages 130, 131
- [108] KILBY, J. Miniaturized electronic circuits, jun 23 1964. US Patent 3,138,743. pages 143
- [109] KOLL, V., AND WEINSTEIN, S. Simultaneous two-way data transmission over a two-wire circuit. *Communications, IEEE Transactions on* 21, 2 (Feb 1973), 143–147. pages 144
- [110] KYEES, P., MCCONNELL, R., AND SISTANIZADEH, K. Adsl: a new twisted-pair access to the information highway. *Communications Magazine, IEEE* 33, 4 (Apr 1995), 52–60. pages 7
- [111] LASORTE, N., BARNES, W., AND REFAI, H. The history of orthogonal frequency division multiplexing. In *Global Telecommunications Conference, 2008. IEEE GLOBECOM 2008. IEEE* (2008), pp. 1–5. pages 86
- [112] LEKE, A., AND CIOFFI, J. A maximum rate loading algorithm for discrete multitone modulation systems. In *Global Telecommunications Conference, 1997. GLOBECOM '97., IEEE* (1997), vol. 3, pp. 1514–1518 vol.3. pages 24
- [113] LEKE, A., AND CIOFFI, J. Transmit optimization for time-invariant wireless channels utilizing a discrete multitone approach. In *Communications, 1997. ICC '97 Montreal, Towards the Knowledge Millennium. 1997 IEEE International Conference on* (Jun 1997), vol. 2, pp. 954–958 vol.2. pages 24
- [114] LIM, D.-W., HEO, S.-J., AND NO, J.-S. An overview of peak-to-average power ratio reduction schemes for OFDM signals. *Communications and Networks, Journal of* 11, 3 (June 2009), 229–239. pages 27
- [115] LIN, Y.-P., AND PHOONG, S.-M. MMSE OFDM and prefixed single carrier systems: BER analysis. In *Acoustics, Speech, and Signal Processing, 2003. Proceedings. (ICASSP '03). 2003 IEEE International Conference on* (6-10 2003), vol. 4, pp. IV – 229–32 vol.4. pages xxii, 87, 103, 104

- [116] LIN, Y.-P., AND PHOONG, S.-M. Window designs for DFT-based multicarrier systems. *Signal Processing, IEEE Transactions on* 53, 3 (2005), 1015–1024. pages 65
- [117] LOWDERMILK, R., AND HARRIS, F. Design and performance of fading insensitive orthogonal frequency division multiplexing (OFDM) using polyphase filtering techniques. In *Signals, Systems and Computers, 1996. Conference Record of the Thirtieth Asilomar Conference on* (Nov 1996), vol. 1, pp. 674–678 vol.1. pages 12
- [118] LUCKY, R. Automatic equalization for digital communication. *Bell System Technical Journal, The* 44, 4 (April 1965), 547–588. pages 143
- [119] LUCKY, R. Techniques for adaptive equalization of digital communication systems. *Bell System Technical Journal, The* 45, 2 (Feb 1966), 255–286. pages 143
- [120] LUKE, H. The origins of the sampling theorem. *Communications Magazine, IEEE* 37, 4 (Apr 1999), 106–108. pages 141
- [121] LYONS, R. G. *Understanding Digital Signal Processing*, first ed. Prentice Hall, 1996, ch. 10, pp. 406–409. pages 49
- [122] MAES, J., AND NUZMAN, C. The past, present, and future of copper access. *Bell Labs Technical Journal* 20 (2015), 1–10. pages 8
- [123] MARTIN, K. Small side-lobe filter design for multitone data-communication applications. *Circuits and Systems II: Analog and Digital Signal Processing, IEEE Transactions on* 45, 8 (1998), 1155–1161. pages 65
- [124] MASON, J., AND HANDSCOMB, D. *Chebyshev polynomials*. Chapman & Hall/CRC, 2003, pp. 145–163. pages 128
- [125] MAXWELL, J. C. *A treatise on electricity and magnetism*. Oxford : Clarendon Press, 1973. pages 140
- [126] MEDEIROS, E., MAGESACHER, T., ERIKSSON, P.-E., LU, C., AND ÖDLING, P. How vectoring in G.fast may cause neighborhood wars. In *Communications (ICC), 2014 IEEE International Conference on* (June 2014), pp. 3859–3864. pages 26
- [127] MEYR, H., MOENECLAËY, M., AND FECHTEL, S. A. *Digital communication receivers*, first ed. Wiley, 1998. pages 126
- [128] MINN, H., TELLAMBURA, C., AND BHARGAVA, V. On the peak factors of sampled and continuous signals. *Communications Letters, IEEE* 5, 4 (2001), 129–131. pages 65

- [129] MORAES, R. *Signal and Spectrum Coordination for Next Generation DSL Networks*. Ph.D. dissertation, KU Leuven, 2014. pages 25
- [130] MOSIER, R. R., AND CLABAUGH, R. G. Kineplex, a bandwidth-efficient binary transmission system. *American Institute of Electrical Engineers, Part I: Communication and Electronics, Transactions of the 76*, 6 (Jan 1958), 723–728. pages 2
- [131] MUCK, M., DE COURVILLE, M., AND DUHAMEL, P. A pseudorandom postfix OFDM modulator - semi-blind channel estimation and equalization. *Signal Processing, IEEE Transactions on 54*, 3 (march 2006), 1005 – 1017. pages 80
- [132] MULLER, S., AND HUBER, J. OFDM with reduced peak-to-average power ratio by optimum combination of partial transmit sequences. *Electronics Letters 33*, 5 (Feb 1997), 368–369. pages 27
- [133] MUQUET, B., DE COURVILLE, M., DUNAMEL, P., AND GIANNAKIS, G. OFDM with trailing zeros versus OFDM with cyclic prefix: links, comparisons and application to the hiperlan/2 system. In *Communications, 2000. ICC 2000. 2000 IEEE International Conference on (2000)*, vol. 2, pp. 1049 –1053 vol.2. pages 90
- [134] MUQUET, B., DE COURVILLE, M., GIANNAKIS, G., WANG, Z., AND DUHAMEL, P. Reduced complexity equalizers for zero-padded OFDM transmissions. In *Acoustics, Speech, and Signal Processing, 2000. ICASSP '00. Proceedings. 2000 IEEE International Conference on (2000)*, vol. 5, pp. 2973–2976 vol.5. pages 90
- [135] MUQUET, B., WANG, Z., GIANNAKIS, G., DE COURVILLE, M., AND DUHAMEL, P. Cyclic-prefixing or zero padding for wireless multicarrier transmissions? *Communications, IEEE Transactions on 50*, 12 (2002), 2136–2148. pages 20, 87, 112
- [136] MURTHY, C. S. R., AND MANOJ, B. *Ad Hoc Wireless Networks: Architectures and Protocols*. Prentice Hall PTR, Upper Saddle River, NJ, USA, 2004. pages 6
- [137] NAHIN, P. J. Among the giants: Oliver heaviside: Genius and curmudgeon. *Spectrum, IEEE 20*, 7 (July 1983), 63–69. pages 140
- [138] NEAGOE, V.-E. Chebyshev nonuniform sampling cascaded with the discrete cosine transform for optimum interpolation. *Acoustics, Speech and Signal Processing, IEEE Transactions on 38*, 10 (1990), 1812–1815. pages 128
- [139] NOYCE, R. Semiconductor device-and-lead structure, apr 25 1961. US Patent 2,981,877. pages 143

- [140] NYQUIST, H. Certain factors affecting telegraph speed. *American Institute of Electrical Engineers, Transactions of the XLIII* (Jan 1924), 412–422. pages 142
- [141] NYQUIST, H. Certain topics in telegraph transmission theory. *American Institute of Electrical Engineers, Transactions of the 47*, 2 (April 1928), 617–644. pages 141
- [142] OPPENHEIM, A. V., SCHAFER, R. W., AND BUCK, J. R. *Discrete-time Signal Processing (2Nd Ed.)*. Prentice-Hall, Inc., Upper Saddle River, NJ, USA, 1999. pages 20
- [143] PAHLAVAN, K., AND HOLSINGER, J. Voice-band data communication modems - a historical review: 1919-1988. *Communications Magazine, IEEE* 26, 1 (Jan 1988), 16–27. pages 143
- [144] PANCALDI, F., VITETTA, G., KALBASI, R., AL-DHAHIR, N., UYSAL, M., AND MHEIDAT, H. Single-carrier frequency domain equalization. *Signal Processing Magazine, IEEE* 25, 5 (september 2008), 37–56. pages 32, 86, 113
- [145] PELED, A., AND RUIZ, A. Frequency domain data transmission using reduced computational complexity algorithms. In *Acoustics, Speech, and Signal Processing, IEEE International Conference on ICASSP '80*. (1980), vol. 5, pp. 964–967. pages 4, 36, 64, 86, 112
- [146] PIESSENS, T., AND STEYAERT, M. Highly efficient xDSL line drivers in 0.35- μm cmos using a self-oscillating power amplifier. *Solid-State Circuits, IEEE Journal of* 38, 1 (Jan 2003), 22–29. pages 27
- [147] POLLET, T., AND PEETERS, M. A new digital timing correction scheme for DMT systems combining temporal and frequential signal properties. In *Communications, 2000. ICC 2000. 2000 IEEE International Conference on* (2000), vol. 3, pp. 1805–1808 vol.3. pages 131, 132
- [148] POLLET, T., PEETERS, M., MOONEN, M., AND VANDENDORPE, L. Equalization for DMT based broadband modems. *Communications Magazine, IEEE* 38, 5 (2000), 106–113. pages 29
- [149] POLLET, T., STEENDAM, H., AND MOENECLAEY, M. Performance degradation of multi-carrier systems caused by an insufficient guard interval duration. In *Proc. Int. Workshop on Copper Wire Access Systems 'Bridging the Last Copper Drop' (CWAS97)* (1997), pp. 265–270. pages 28, 36
- [150] POULARIKAS, A. *The handbook of formulas and tables for signal processing*. CRC Press/IEEE, 1998. pages 30, 67
- [151] PROAKIS, J. G. *Digital communication*, second ed. McGraw-Hill, 1989. pages 105

- [152] PUPIN, M. Art of reducing attenuation of electrical waves., jun 19 1900. US Patent 652,231. pages 140
- [153] RAULT, J., CASTELAIN, D., AND LE FLOCH, B. The coded orthogonal frequency division multiplexing (cOFDM) technique, and its application to digital radio broadcasting towards mobile receivers. In *Global Telecommunications Conference and Exhibition 'Communications Technology for the 1990s and Beyond' (GLOBECOM), 1989. IEEE* (Nov 1989), pp. 428–432 vol.1. pages 5
- [154] REDFERN, A. J. Receiver window design for multicarrier communication systems. *Selected Areas in Communications, IEEE Journal on* 20, 5 (2002), 1029–1036. pages 37, 64
- [155] REEVE, W., AND SOCIETY, I. C. *Subscriber Loop Signaling and Transmission Handbook: Digital*. Telecommunications and Signal Processing Series. IEEE Press, 1995. pages 9
- [156] REZAEI, S., AND PAKRAVAN, M. Per tone equalization analysis in DMT based systems. In *TENCON 2004. 2004 IEEE Region 10 Conference* (Nov 2004), vol. A, pp. 539–542 Vol. 1. pages 112
- [157] RIVLIN, T. J. *The Chebyshev polynomials*. Wiley, 1974, pp. 12–. pages 128
- [158] ROSS, I. The invention of the transistor. *Proceedings of the IEEE* 86, 1 (Jan 1998), 7–28. pages 142
- [159] RUMNEY, M., AND TECHNOLOGIES, A. *LTE and the Evolution to 4G Wireless: Design and Measurement Challenges*. Wiley, 2013. pages 33
- [160] SALTZBERG, B. Performance of an efficient parallel data transmission system. *Communication Technology, IEEE Transactions on* 15, 6 (December 1967), 805–811. pages 2
- [161] SALTZBERG, B. R. Multiply orthogonal system for transmitting data signals through frequency overlapping channels, may 12 1970. US Patent 3,511,936. pages 2
- [162] SALZ, J. Digital transmission over cross-coupled linear channels. *ATT Technical Journal* 64, 6 (July 1985), 1147–1159. pages 11
- [163] SARI, H., KARAM, G., AND JEANCLAUDE, I. Transmission techniques for digital terrestrial tv broadcasting. *Communications Magazine, IEEE* 33, 2 (feb 1995), 100–109. pages 32, 86, 111
- [164] SCAGLIONE, A., GIANNAKIS, G., AND BARBAROSSA, S. Redundant filterbank precoders and equalizers. I. unification and optimal designs. *Signal Processing, IEEE Transactions on* 47, 7 (1999), 1988–2006. pages 21, 87, 112

- [165] SEOANE, J., WILSON, S., AND GELFAND, S. Analysis of intertone and interblock interference in OFDM when the length of the cyclic prefix is shorter than the length of the impulse response of the channel. In *Global Telecommunications Conference, 1997. GLOBECOM '97., IEEE (1997)*, vol. 1, pp. 32–36 vol.1. pages 36
- [166] SHANNON, C. Communication in the presence of noise. *Proceedings of the IRE* 37, 1 (1949), 10–21. pages 24, 141
- [167] SHANNON, C. E. *A Symbolic Analysis of Relay and Switching Circuits*. 1938. pages 142
- [168] SHANNON, C. E. A mathematical theory of communication. *The Bell System Technical Journal* 27 (July, October 1948), 379–423, 623–656. pages 141
- [169] SHUCH, H. P. Indistinguishable from magic (SETI League editorial). <http://www.setileague.org/editor/magic.htm>. Accessed: 2010-09-30. pages 32
- [170] SHYNK, J. Frequency-domain and multirate adaptive filtering. *Signal Processing Magazine, IEEE* 9, 1 (Jan 1992), 14–37. pages 32
- [171] SIVAKUMAR, P., SANGEETHA, S., AND RAJARAM, M. PAPR reduction in OFDM for SC-FDMA channels. In *Signal Processing, Communication, Computing and Networking Technologies (ICSCCN), 2011 International Conference on* (July 2011), pp. 6–9. pages 113
- [172] SJÖBERG, F., NILSSON, R., BÖRJESSON, P., ÖDLING, P., WIESE, B., AND BINGHAM, J. Digital RFI suppression in DMT-based VDSL systems. *Circuits and Systems I: Regular Papers, IEEE Transactions on* 51, 11 (Nov 2004), 2300–2312. pages 31
- [173] SJÖBERG, F., NILSSON, R., ISAKSSON, M., ÖDLING, P., AND BÖRJESSON, O. Asynchronous zipper. In *Communications, 1999. ICC '99. 1999 IEEE International Conference on* (1999), vol. 1, pp. 231–235 vol.1. pages 65
- [174] SONG, K. B., CHUNG, S. T., GINIS, G., AND CIOFFI, J. Dynamic spectrum management for next-generation DSL systems. *Communications Magazine, IEEE* 40, 10 (2002), 101–109. pages 25, 64
- [175] SORENSEN, H., AND BURRUS, C. Efficient computation of the DFT with only a subset of input or output points. *Signal Processing, IEEE Transactions on* 41, 3 (1993), 1184–1200. pages 51
- [176] SPRUYT, P., REUSSENS, P., AND BRAET, S. Performance of improved SMT transceiver for VDSL. In *ANSI Contribution TIE1.4/96-104* (April 1996). pages 31, 41

- [177] STARR, T. *DSL Advances*. Prentice Hall communications engineering and emerging technologies series. Prentice Hall PTR, 2003. pages 25
- [178] STEENDAM, H., MOENECLAEY, M., AND BRUNEEL, H. The Cramer-Rao bound and ML estimate for data-aided channel estimation in KSP-OFDM. In *Personal, Indoor and Mobile Radio Communications, 2007. PIMRC 2007. IEEE 18th International Symposium on* (Sept 2007), pp. 1–5. pages 21
- [179] STOLLE, R. Electromagnetic coupling of twisted pair cables. *Selected Areas in Communications, IEEE Journal on* 20, 5 (2002), 883–892. pages 64
- [180] STORRY, C., ZIVKOVIC, M., VERLINDEN, J., AND DE LIND VAN WIJNGAARDEN, A. J. Aspects of dynamic spectrum management level 3. *Bell Labs Technical Journal* 13, 1 (Spring 2008), 117–127. pages 9, 26
- [181] TANG, S., YANG, F., PENG, K., PAN, C., GONG, K., AND YANG, Z. Iterative channel estimation for block transmission with known symbol padding - a new look at TDS-OFDM. In *Global Telecommunications Conference, 2007. GLOBECOM '07. IEEE* (nov. 2007), pp. 4269–4273. pages 80
- [182] TELLADO, J. *Peak to Average Power Ratio Reduction for Multicarrier Modulation*. Ph.D. dissertation, University of Stanford, 1999. pages 26
- [183] TEPEDELENLIOĞLU, C. Low complexity linear equalizers with maximum multipath diversity for zero-padded transmissions. In *Acoustics, Speech, and Signal Processing, 2003. Proceedings. (ICASSP '03). 2003 IEEE International Conference on* (April 2003), vol. 4, pp. IV–636–9 vol.4. pages 94, 95
- [184] TEPEDELENLIOĞLU, C. Maximum multipath diversity with linear equalization in precoded OFDM systems. *Information Theory, IEEE Transactions on* 50, 1 (Jan 2004), 232–235. pages 95
- [185] TEPEDELENLIOĞLU, C., AND MA, Q. On the performance of linear equalizers for block transmission systems. In *Global Telecommunications Conference, 2005. GLOBECOM '05. IEEE* (Dec 2005), vol. 6, pp. 5 pp.–3896. pages 91, 114
- [186] TIMMERS, M., GUENACH, M., NUZMAN, C., AND MAES, J. G.fast: evolving the copper access network. *Communications Magazine, IEEE* 51, 8 (August 2013), 74–79. pages 8
- [187] TOMLINSON, M. New automatic equaliser employing modulo arithmetic. *Electronics Letters* 7, 5 (March 1971), 138–139. pages 144
- [188] TOSKALA, A., HOLMA, H., AND MUSZYNSKI, P. Etsi WCDMA for UMTS. In *Spread Spectrum Techniques and Applications, 1998. Proceedings., 1998*

- IEEE 5th International Symposium on* (Sep 1998), vol. 2, pp. 616–620 vol.2. pages 7
- [189] TSIAFLAKIS, P. *Resource management and optimization in multi-user DSL systems*. Ph.D. dissertation, KU Leuven, 2009. pages 25
- [190] TUBBAX, J., COME, B., VAN DER PERRE, L., DENEIRE, L., DONNAY, S., AND ENGELS, M. OFDM versus single carrier with cyclic prefix: a system-based comparison. In *Vehicular Technology Conference, 2001. VTC 2001 Fall. IEEE VTS 54th* (2001), vol. 2, pp. 1115–1119 vol.2. pages 32
- [191] UNGERBOECK, G. Channel coding with multilevel/phase signals. *Information Theory, IEEE Transactions on* 28, 1 (Jan 1982), 55–67. pages 144
- [192] VAIDYANATHAN, P. *Multirate systems and filter banks*, first ed. Prentice Hall, 1993, pp. 50–52. pages 72
- [193] VÄLIMÄKI, V., AND LAAKSO, T. Principles of fractional delay filters. In *Acoustics, Speech, and Signal Processing, 2000. ICASSP '00. Proceedings. 2000 IEEE International Conference on* (2000), vol. 6, pp. 3870–3873 vol.6. pages 126
- [194] VAN ACKER, K. *Equalization and echo cancellation for DMT-based DSL modems*. Ph.D. dissertation, KU Leuven, 2001. pages 28
- [195] VAN ACKER, K., LEUS, G., MOONEN, M., AND POLLET, T. RLS-based initialization for per-tone equalizers in DMT receivers. *Communications, IEEE Transactions on* 51, 6 (2003), 885–889. pages 40, 51, 55
- [196] VAN ACKER, K., LEUS, G., MOONEN, M., VAN DE WIEL, O., AND POLLET, T. Per tone equalization for DMT-based systems. *Communications, IEEE Transactions on* 49, 1 (2001), 109–119. pages 36, 38, 39, 40, 64, 74, 112, 115, 117
- [197] VAN ACKER, K., POLLET, T., LEUS, G., AND MOONEN, M. Combination of per tone equalization and windowing in DMT-receivers. *Signal Processing* 81, 8 (2001), 1571–1579. pages 37, 38, 42, 51, 57, 61
- [198] VAN BLADEL, M., AND MOENECLAAY, M. Time-domain equalization for multicarrier communication. In *Global Telecommunications Conference, 1995. Conference record. Communication Theory Mini-Conference, GLOBECOM '95., IEEE* (Nov 1995), pp. 167–171. pages 28
- [199] VAN WELDEN, D., AND STEENDAM, H. Iterative EM based channel estimation for KSP-OFDM. In *Personal, Indoor and Mobile Radio Communications, 2008. PIMRC 2008. IEEE 19th International Symposium on* (sept. 2008), pp. 1–5. pages 80

- [200] VANBLEU, K. *Advanced equalization techniques for DMT-based systems*. Ph.D. dissertation, KU Leuven, 2004. pages 28
- [201] VANBLEU, K., YSEBAERT, G., CUYPERS, G., AND MOONEN, M. Bitrate maximizing time-domain equalizer design for DMT-based systems. In *Communications, 2003. ICC '03. IEEE International Conference on* (2003), vol. 4, pp. 2360–2364 vol.4. pages 36
- [202] VANBLEU, K., YSEBAERT, G., CUYPERS, G., AND MOONEN, M. Adaptive bit rate maximizing time-domain equalizer design for dmt-based systems. *Signal Processing, IEEE Transactions on* 54, 2 (Feb 2006), 483–498. pages 28
- [203] WALZMAN, T., AND SCHWARTZ, M. Automatic equalization using the discrete frequency domain. *Information Theory, IEEE Transactions on* 19, 1 (1973), 59–68. pages 32, 86
- [204] WANG, J., SONG, J., YANG, Z.-X., YANG, L., AND WANG, J. Frames theoretic analysis of zero-padding OFDM over deep fading wireless channels. *Broadcasting, IEEE Transactions on* 52, 2 (june 2006), 252 – 260. pages xxii, 87, 90, 103, 104
- [205] WANG, Z., AND GIANNAKIS, G. Wireless multicarrier communications. *Signal Processing Magazine, IEEE* 17, 3 (May 2000), 29–48. pages 20
- [206] WANG, Z., MA, X., AND GIANNAKIS, G. Optimality of single-carrier zero-padded block transmissions. In *Wireless Communications and Networking Conference, 2002. WCNC2002. 2002 IEEE* (mar 2002), vol. 2, pp. 660 – 664 vol.2. pages 89
- [207] WEINSTEIN, S. The history of orthogonal frequency-division multiplexing [history of communications]. *Communications Magazine, IEEE* 47, 11 (2009), 26–35. pages 8, 86
- [208] WEINSTEIN, S., AND EBERT, P. Data transmission by frequency-division multiplexing using the discrete Fourier transform. *Communication Technology, IEEE Transactions on* 19, 5 (1971), 628–634. pages 3, 64, 86
- [209] WIDROW, B., AND HOFF, M. E. Adaptive switching circuits. In *1960 IRE WESCON Convention Record, Part 4* (New York, 1960), IRE, pp. 96–104. pages 143
- [210] WITSCHNIG, H., MAYER, T., SPRINGER, A., KOPPLER, A., MAURER, L., HUEMER, M., AND WEIGEL, R. A different look on cyclic prefix for SC/FDE. In *Personal, Indoor and Mobile Radio Communications, 2002. The 13th IEEE International Symposium on* (Sept 2002), vol. 2, pp. 824–828 vol.2. pages 32

- [211] WITSCHNIG, H., MAYER, T., SPRINGER, A., MAURER, L., HUEMER, M., AND WEIGEL, R. The advantages of a known sequence versus cyclic prefix in a SC/FDE system. In *Wireless Personal Multimedia Communications, 2002. The 5th International Symposium on* (oct. 2002), vol. 3, pp. 1328 – 1332 vol.3. pages 21, 32, 80, 112
- [212] XIA, X.-G. Precoded and vector OFDM robust to channel spectral nulls and with reduced cyclic prefix length in single transmit antenna systems. *Communications, IEEE Transactions on* 49, 8 (aug 2001), 1363 –1374. pages 87
- [213] YIP, P., AND RAO, K. On the shift property of DCT's and DST's. *Acoustics, Speech and Signal Processing, IEEE Transactions on* 35, 3 (1987), 404–406. pages 130
- [214] YSEBAERT, G. *Equalization and echo cancellation in DMT-based systems*. Ph.D. dissertation, KU Leuven, 2004. pages 30
- [215] YSEBAERT, G., VANBLEU, K., CUYPERS, G., AND MOONEN, M. Joint window and time domain equalizer design for bit rate maximization in dmt-receivers. *Signal Processing, IEEE Transactions on* 53, 3 (March 2005), 1132–1146. pages 31
- [216] YU, W., GINIS, G., AND CIOFFI, J. Distributed multiuser power control for digital subscriber lines. *Selected Areas in Communications, IEEE Journal on* 20, 5 (Jun 2002), 1105–1115. pages 25

Curriculum vitae

Gert Cuypers was born in Leuven, Belgium on the last day of 1975. He received the master degree in electrical engineering (*magna cum laude*) from the Katholieke Universiteit Leuven. In 1999 he started the Ph.D. at the SCD-SISTA (now Stadius) laboratories of the Department of Electrical engineering (Faculty of Applied Sciences) under the supervision of Prof. Marc Moonen. From 1999 to 2003 he was funded by the I.W.T (Flemish Institute for Scientific and Technolgical Research in Industry). He was involved in several research projects in cooperation with Alcatel Bell.

In 2004 he started as a lecturer at Groep T, engineering school of Leuven, teaching courses in electronics and electromagnetic compatibility. In 2006 he started working with the Belgian national railroad company NMBS, where he was responsible for the technical specifications of the fiber optic installation. From 2008 to 2010 he worked at Option Wireless N.V. in the new products introduction (NPI) department, focusing on the development of production test setups. Since 2010 he is an RF design engineer with Septentrio Satellite Navigation, developing hardware for base-band and RF, mainly in the L-band. He has been a free researcher with the KU Leuven since 2004.

List of publications

International journal papers

CUYPERS, G., VANBLEU, K., YSEBAERT, G., MOONEN, M. AND VANDAELE, P. Combined per tone equalization and receiver windowing in DSL receivers: WiPTEQ. *Elsevier Signal Processing* 85, 10 (2005), 1921–1942.

CUYPERS, G., VANBLEU, K., YSEBAERT, G. AND MOONEN, M. Intra-symbol windowing for egress reduction in DMT transmitters. *EURASIP J. Appl. Signal Process. 2006* (January 2006), 87–87.

CUYPERS, G. AND MOONEN, M. Frequency-domain equalizers with zero restoration for zero-padded block transmission. *Submitted to EURASIP Journal on Wireless Communications and Networking* (2015).

CUYPERS, G. AND MOONEN, M. Combining spectral zero restoration and per-tone equalization in single-carrier block transmissions. *Submitted to Elsevier Signal Processing* (2015).

VANBLEU, K., YSEBAERT, G., CUYPERS, G., MOONEN, M. AND VAN ACKER, K. Bitrate-maximizing time-domain equalizer design for DMT-based systems. *Communications, IEEE Transactions on* 52, 6 (June 2004), 871–876.

VANBLEU, K., YSEBAERT, G., CUYPERS, G. AND MOONEN, M. On time-domain and frequency-domain MMSE-based TEQ design for DMT transmission. *Signal Processing, IEEE Transactions on* 53, 8 (Aug 2005), 3311–3324.

VANBLEU, K., YSEBAERT, G., CUYPERS, G. AND MOONEN, M. Adaptive bit rate maximizing time-domain equalizer design for DMT-based systems. *Signal Processing, IEEE Transactions on* 54, 2 (Feb 2006), 483–498.

VANBLEU K., YSEBAERT G., CUYPERS G. AND MOONEN M. Bitrate Maximizing Per Group Equalization for DMT-based Systems *Elsevier Signal Processing* 86, 10

(2006), 1433–1445.

YSEBAERT, G., VANBLEU, K., CUYPERS, G., MOONEN, M. AND POLLET, T. Combined RLS-LMS initialization for per tone equalizers in DMT-receivers. *Signal Processing, IEEE Transactions on* 51, 7 (July 2003), 1916–1927.

YSEBAERT, G., VANBLEU, K., CUYPERS, G. AND MOONEN, M. Split SR-RLS for the joint initialization of the per-tone equalizers and per-tone echo cancelers in DMT-based receivers. *EURASIP J. Appl. Signal Process.* 2004 (jan 2004), 1433–1445.

YSEBAERT, G., VANBLEU, K., CUYPERS, G. AND MOONEN, M. Joint window and time domain equalizer design for bit rate maximization in dmt-receivers. *Signal Processing, IEEE Transactions on* 53, 3 (March 2005), 1132–1146.

International conference papers

CUYPERS, G., YSEBAERT, G., MOONEN, M. AND VANDAELE, P. Combining per tone equalization and windowing in DMT receivers. In *Acoustics, Speech and Signal Processing (ICASSP), 2002 IEEE International Conference on* (2002), vol. 3, pp. III–2341–III–2344.

CUYPERS, G., VANBLEU, K., YSEBAERT, G. AND MOONEN, M. Combining per tone equalization and windowing in DMT receivers. In *Proc. of Signal Processing Symposium (SPS) (2002)*, pp. 173–176.

CUYPERS, G., VANBLEU, K., YSEBAERT, G., MOONEN, M. AND VANDAELE, P. Combining raised cosine windowing and per tone equalization for RFI mitigation in DMT receivers. In *Communications, 2003. ICC '03. IEEE International Conference on* (2003), vol. 4, pp. 2852–2856 vol.4.

CUYPERS, G., VANBLEU, K., YSEBAERT, G. AND MOONEN, M. Egress reduction by intra-symbol windowing in DMT-based transmitters. In *Acoustics, Speech and Signal Processing, 2003. Proceedings. (ICASSP '03). 2003 IEEE International Conference on* (2003), vol. 4, pp. IV–532–5 vol.4.

CUYPERS, G., YSEBAERT, G., MOONEN, M. AND PISONI, F. Chebyshev interpolation for DMT modems. In *Communications, 2004 IEEE International Conference on* (June 2004), vol. 5, pp. 2736–2740 Vol.5.

YSEBAERT, G., VANBLEU, K., CUYPERS, G., MOONEN, M. AND VAN ACKER, K. Double talk cancellation in echo cancelled DMT-systems. In *Signal Processing Conference, 2002 11th European* (Sept 2002), pp. 1–4.

YSEBAERT G., VANBLEU K., CUYPERS G., MOONEN M. AND VAN ACKER K.

Double Talk Cancellation in Echo Cancelled DMT-systems In *Proc. of Signal Processing Symposium (SPS)* (2002), pp. 169-172.

VANBLEU, K., YSEBAERT, G., CUYPERS, G. AND MOONEN, M. Bitrate maximizing time-domain equalizer design for DMT-based systems. In *Communications, 2003. ICC '03. IEEE International Conference on* (May 2003), vol. 4, pp. 2360–2364 vol.4.

YSEBAERT, G., VANBLEU, K., CUYPERS, G., MOONEN, M. AND VERLINDEN, J. Echo cancellation for discrete multitone frame-asynchronous ADSL transceivers. In *Communications, 2003. ICC '03. IEEE International Conference on* (May 2003), vol. 4, pp. 2421–2425 vol.4.

YSEBAERT, G., VANBLEU, K., CUYPERS, G. AND MOONEN, M. ADSL per-tone/per-group optimal equalizer and windowing design. In *Signals, Systems and Computers, 2002. Conference Record of the Thirty-Sixth Asilomar Conference on* (Nov 2002), vol. 1, pp. 383–387 vol.1.

VANBLEU, K., YSEBAERT, G., CUYPERS, G. AND LEUS, G. Adaptive bitrate maximizing TEQ design for DMT-based systems. In *Acoustics, Speech and Signal Processing, 2004. Proceedings. (ICASSP '04). IEEE International Conference on* (May 2004), vol. 4, pp. iv–1057–60 vol.4.

VANBLEU, K., YSEBAERT, G., CUYPERS, G. AND MOONEN, M. On time-domain and frequency-domain MMSE-based TEQ designs for DMT transmission. In *Signal Processing Conference, 2004 12th European* (Sept 2004), pp. 1927–1930.

VANBLEU K., YSEBAERT G., CUYPERS G. AND MOONEN M. On the relation between time-domain equalizers and per-tone equalizers for DMT-based systems In *Proc. of Signal Processing Symposium (SPS)* (2004)

YSEBAERT, G., VANBLEU, K., CUYPERS, G. AND MOONEN, M. Bit rate maximizing window and equalizer design for DMT-systems. In *Signal Processing Conference, 2004 12th European* (Sept 2004), pp. 1923–1926.

Patents

CUYPERS, G., MOONEN, M., VANDAELE, P. AND YSEBAERT, G. Multicarrier receiver, aug 14 2003. US Patent App. 10/247,478.

CUYPERS, C., MOONEN, M., VANDAELE, P. AND YSEBAERT, G. Multicarrier receiver with a sliding window Fourier transform and a Fourier transform, mar 26 2003. EP Patent App. EP20,010,440,309.

This chapter gives an introduction to *multi-carrier modulation* (MCM) and its application to *digital subscriber line* (DSL) technology. While different implementations have been proposed over time, the distinguishing property of MCM is that the available spectrum is divided into a large number of narrow sub-bands, which are individually modulated. Because the symbol rate in these sub-bands is lower and the dispersion is smaller, the equalization can be much simpler than for the original large band. The idea of dividing the band into smaller sub-bands is naturally associated with an individual modulation of each sub-band, but can also be beneficial for the equalization of a wide-band signal, referred to as *single-carrier frequency domain equalization* (SC-FDE). The chapter is organized as follows: in section 1.1 we provide a brief overview of MCM. The application to wireless communication is highlighted in section 1.2. The application of MCM to DSL, and the challenges faced in the DSL-environment are treated in section 1.3. Finally, section 1.4 provides an overview of the contributions in this work. In this chapter we have avoided formulas. For a more rigorous description of the mathematics involved, we refer to chapter 2, which also explains SC-FDE in more detail. For a short history of telecommunications prior to MCM, and an overview of how the current twisted pair infrastructure came to be, we refer to Appendix A. There are two approaches for the utilization of a dispersive channel with large bandwidth. One approach fills the complete band with a *single-carrier* (SC) transmission at high symbol rate and relies on equalization to avoid *symbol interference* (ISI). The other approach, now known as *multi-carrier modulation* (MCM), divides the large band into a number of narrower sub-channels or sub-bands or *tones*. As a result, the symbol period increases, leading to a relatively lower ISI. Dividing the available bandwidth into multiple channels incurs the risk of *inter-channel interference* (ICI). This can be prevented by avoiding spectral overlap of adjacent channels using strong filtering and a large spectral distance between the carriers. Unfortunately, this leads to a less efficient spectrum use. A first implementation which allowed the bands to *overlap*, while avoiding ICI, was the 1958 *Collins Kineplex system* -so called because it combines kinematic filters at the receiver and used multiplexing. This wireless system operated in the HF-band and had a carrier spacing of 110 Hz. Each of 20 tones is modulated by differential *phase shift keying* (PSK) without filtering. The spectra of the sub-bands are therefore *sinc-shaped* and strongly overlap. However, similar to modern MCM-implementations, the tones are spaced at frequency intervals almost equal to the signaling rate and can be separated at the receiver. While the Kineplex system had some remarkably modern properties, it also had disadvantages. First of all, it was very complex and bulky. Secondly, some spectrum was lost above the highest tone and below the lowest, to allow for a proper roll-off of their slowly decaying sinc spectrum. It would be interesting to have at least some filtering to limit the overlap to the nearest neighbours, while maintaining the orthogonality between the tones. In the 1960's it was realized that it is possible to shape filters such that the transmitted signals are still orthogonal to each other. Later on *Saltzberg* proposed a system with base band signals meeting this condition, and deemed it promising enough to be patented. A drawback of these early systems was their complexity, resulting from the analog implementation using individual oscillators, mixers and the shaping filters for each tone. The discovery of the *fast Fourier transform* (FFT) algorithm in 1965 (which was actually already conceived by *Gauss* in 1805) opened up a completely new approach. Considering that the Fourier transform of a complex exponential in the frequency domain (FD), and the inverse Fourier transform of a single pulse yields a complex exponential in the time domain (TD), it is obvious that the inverse Fourier transform of a superposition of impulses yields a superposition of complex exponentials. Applied to the *discrete Fourier transform* (DFT), this means that the sum of a large number of modulated carriers can be obtained through the *inverse DFT* (IDFT) of a complex vector representing the phases and magnitudes of the individual carriers, as shown in Fig. 1.1. This coding scheme is called *orthogonal frequency division multiplexing* (OFDM). The first DFT-based system was proposed by *Weinstein and Ebert* in 1971. A fully digital implementation has the significant benefit that the design is much simpler and cheaper because there is no need for individual

FACULTY OF ENGINEERING SCIENCE
ESAT: DEPARTMENT OF ELECTRICAL ENGINEERING
STADIUS

Kasteelpark Arenberg 10
B-3001 Heverlee

gert.cuyper@esat.kuleuven.be
<http://www.esat.kuleuven.be/stadius>

